FUNCTIONAL CHARACTERIZATION OF NOVEL *RHOT1* VARIANTS, WHICH ARE ASSOCIATED WITH PARKINSON'S DISEASE

DISSERTATION

zur Erlangung des Grades eines

DOKTORS DER NATURWISSENSCHAFTEN

DER MATHEMATISCH-NATURWISSENSCHAFTLICHEN FAKULTÄT

und

DER MEDIZINISCHEN FAKULTÄT

DER EBERHARD-KARLS-UNIVERSITÄT TÜBINGEN

vorgelegt

von

DAJANA GROßMANN

aus Wismar, Deutschland

Mai 2016

PhD-FSTC-2016-15
The Faculty of Sciences, Technology and Communication

The Faculty of Science and Medicine and
The Graduate Training Centre of Neuroscience

DISSERTATION

Defense held on 13/05/2016 in Luxembourg

to obtain the degree of

DOCTEUR DE L'UNIVERSITÉ DU LUXEMBOURG EN BIOLOGIE

AND

DOKTOR DER EBERHARD-KARLS-UNIVERISTÄT TÜBINGEN

IN NATURWISSENSCHAFTEN

by

Dajana GROßMANN

Born on 14 August 1985 in Wismar (Germany)

FUNCTIONAL CHARACTERIZATION OF NOVEL *RHOT1* VARIANTS, WHICH ARE ASSOCIATED WITH PARKINSON'S DISEASE.

Date of oral exam: 13th of May 2016

President of the University of Tübingen: Prof. Dr. Bernd Engler

……

Chairmen of the Doctorate Board of the University of Tübingen: Prof. Dr. Bernd Wissinger

……

Dekan der Math.-Nat. Fakultät: Prof. Dr. W. Rosenstiel

……

Dekan der Medizinischen Fakultät: Prof. Dr. I. B. Autenrieth

.....

President of the University of Luxembourg: Prof. Dr. Rainer Klump

……

Supervisor from Luxembourg: Prof. Dr. Rejko Krüger

……

Supervisor from Tübingen: Prof. Dr. Olaf Rieß

……

Dissertation Defence Committee:

Committee members: Dr. Alexander Skupin ……...

Prof. Dr. Olaf Rieß ……..……..…..

Prof. Dr. Rejko Krüger ……..……..……...

Prof. Dr. Enza Maria Valente ……..…..…..…

Prof. Dr. Daniela Vogt-Weisenhorn ……..…..

Prof. Dr. Bernd Wissinger ……..…..…..

Affidavit / Declaration

I hereby declare that I have produced the work entitled “Miro1 mutations cause mitochondrial dysfunction and are associated with Parkinson’s disease ”, submitted for the award of a doctorate, on my own (without external help), have used only the sources and aids indicated and have marked passages included from other works, whether verbatim or in content, as such. I swear upon oath that these statements are true and that I have not concealed anything. I am aware that making a false declaration under oath is punishable by a term of imprisonment of up to three years or by a fine.

Luxembourg, the 10.06.2016 ……

Signature

Acknowledgements

The work for this dissertation was carried out in the "**Functional Neurogenomics group**" at the **Hertie Institute for Clinical Brain Research** (HIH) at the **University of Tübingen** and in the "**Clinical and Experimental Neuroscience group**" at the **Luxembourg Centre for Systems Biomedicine** (LCSB) at the **University of Luxembourg** between June 2012 and May 2016.

In the first place, I would like to thank the supervisor of my thesis, **Prof. Dr. Rejko Krüger**, for giving me the chance to work on this exciting project within his group. Furthermore, I would like to thank you for all the advice and supervision throughout the recent years and for the challenging tasks that helped me to learn and improve skills. Thank you for the everything-is-possible-spirit and for the support and encouragement for starting a career in science.

Furthermore, I thank the members of my advisory board, **Prof. Dr. Olaf Rieß** and **Prof. Dr. Bernd Wissinger**, for taking time and for the profound advice and the interest in this project.

I would like to acknowledge the funding source for this work. The project was funded by a **Fortüne Grant** awarded to **Dr. Lena Brubulla** by the **Fortune program of the University of Tübingen**.

I also want to acknowledge the **Graduate School for Cellular and Molecular Neuroscience of the University of Tübingen** for offering an excellent doctoral training program with a manifold of diverse courses.

In the present project I had the opportunity to work in collaboration with many very helpful and supporting people. Thank you **Prof. Dr. Doron Rapaport** and **Dr. Kai-Stefan Dimmer** (Interfakultäres Institut für Biochemie, IFIB, University of Tübingen, Germany), **Dr. Peter Lichtner** (Helmholtz Centre, Munich, Germany), **Dr. Patrick May** (LCSB, University of Luxembourg, Belvaux, Luxembourg), **Dr. Enrico Glaab** (LCSB, University of Luxembourg, Belvaux, Luxembourg), **Dr. Simon Lehle** (DNA Damage & Repair Unit Tübingen, Tübingen, Germany) and **Dr. Manu Sharma** (Hertie-Institute for Brain Research, University of Tübingen, Tübingen) for the prolific collaboration and the interest in the project topic.

Also thank you very much to **Dr. Alexander Skupin** and **Dr. Aymeric Fouquier D'Herouël** (LCSB, University of Luxembourg, Belvaux, Luxembourg) for introducing me to calcium imaging as well as to **Prof. Dr. Daniela Vogt-Weisenhorn** and **Annerose Kurz-Drexler**

(Institute of Developmental Genetics, Helmholtz Zentrum München, Germany) for help and advice on the immortalization of fibroblasts.

I would like to thank the members of the laboratory of "**Functional Neurogenomics**" (HIH, University of Tübingen): **Daniela**, **Katharina**, **David**, **Lena** and especially **Brigitte** (I will always miss our lunch conversations). I also want to thank **Dr. Lena Burbulla** for supervising.

A very warm thank you to the whole **LCSB team** for the nice welcome and the support of our move from Tübingen to Luxembourg, in particular **Nicolas** and **Christophe**.

Thank you to the **CEN group**: **Mary**, **Gérald**, **Francois**, **Yvonne**, **Marie**, **Zoé**, **Bruno**, **Pete** and **Nicole**. Thank you very much **Caro** for being the best fellow PhD student (CEN group is not the same without you) and **Jill** for treating my fibroblasts with so much care (you are the best fibroblast technician). I very much appreciated the spirit of helping and having fun at work.

I owe special thanks to **Julia** and **Dr. Ibo**, who provided very valuable support and advice for my project. Your interest in the project and your patience allowed me to learn and improve so much. Thanks to your guidance I didn't felt lost during my work.

I also want to thank my **mum** and my grandparents **Manfred** and **Wanda**. You always believed in me and supported my academic ambitions. Although you do not fully understand what I am doing you understand that this work is so important for me. Special thanks to **Maja**, who is the best sister ever, for always listening and cheering me up.

Finally I cannot express how grateful I am to my husband **Alex**. During the recent years you showed more patience and support than one could ask for. Your strength and support is most precious to me. I really owe this work to you.

Table of Contents

Figures

Tables

Abbreviations

Abbreviation	
5' UTR	5' untranslated region
Abs	absorbance
a.u.	area unit
cDNA	complementary DNA
C-terminal	carboxy terminal
Ctrl	control
DA neuron	dopaminergic neuron
dMiro	*drosophila* Miro
DNA	deoxyribonucleic acid
E. coli	*Escherichia coli*
EF hand	embryonic fibroblast hand
ER	endoplasmic reticulum
ERMES	ER-mitochondrial encounter structure
FACS	fluorescence-activated cell sorting
FBS	fetal bovine serum
GAP	GTPase-activating protein
***gem1*Δ**	*gem1* knockout
GEP	guanine nucleotide exchange factor
KD	knockdown
MCU	mitochondrial calcium uniporter
MIB buffer	Mitochondrial isolation buffer
Miro	mitochondrial Rho GTPase
min	minute

miRNA	micro RNA
MMP	mitochondrial membrane potential
MnSOD	manganese superoxide dismutase (SOD2)
mRNA	messenger RNA
mtDNA	mitochondrial DNA
MTS	mitochondrial targeting sequence
NeEMO	Network Enthalpic Modelling
N-terminal	amino terminal
OCR	oxygen consumption rate
OMM	outer mitochondrial membrane
ORF	open reading frame
PCR	polymerase chain reaction
PD	Parkinson's disease
pDNA	plasmid DNA
prot. conc.	protein concentration
RNA	ribonucleic acid
ROS	reactive oxygen species
rpm	rotation per minute
rtPCR	reverse transcription PCR
SERCA	sarco-endoplasmic reticulum calcium-ATPase
TCA	tricarboxylic acid cycle
TMD	transmembrane domain
(Ub)n-Miro1	ubiquitinated Miro1
WT	wild type
LM 1/2	Ligand mimic motif 1/2

Summary/ Abstract

Parkinson's disease (PD) is a common neurodegenerative disease affecting up to 2 % of the population older than 65 years. Most PD cases are sporadic with unknown cause, and about 10 % are familial inherited. PD is a progressive neurodegenerative disease characterized by loss of predominantly dopaminergic neurons, leading to typical symptoms like rigidity and tremor. Commonly involved pathogenic pathways are linked to mitochondrial dysfunction, e.g. increased oxidative stress, disruption of calcium homeostasis, decreased energy supply and mitochondrial-controlled apoptosis. The mitochondrial outer membrane protein Miro1 is important for mitochondrial distribution, quality control and maintenance. To date Miro1 is not established as risk factor for PD.

Using a comprehensive mutation screening of *RhoT1* in German PD patients we dissected the role of the first PD-associated mutations in *RhoT1*, the gene encoding for Miro1. Three mutations in *RhoT1* have been identified in three PD patients with positive family history for PD. For analysis of mitochondrial phenotypes patient-derived fibroblasts from two of the three patients were available. As independent cell model served the neuroblastoma cell line M17 with stable knockdown of endogenous *RhoT1* and transiently overexpression of the *RhoT1* mutant variants.

Investigation of yeast with knockout of endogenous Gem1 (the yeast orthologue of Miro1) and overexpression of Gem1-R298Q (the orthologue of Miro1-R272Q) revealed that growth on non-fermentable carbon source was impaired. These findings suggest that Miro1-R272Q is a loss of function mutation. Interestingly, the Miro1 protein amount was significantly reduced in Miro1-R272Q and Miro1-R450C mutant fibroblast lines compared to controls. Functional analysis revealed that mitochondrial mass was decreased in Miro1-R450C, but not in Miro1-R272Q fibroblasts, whereas mitochondrial biogenesis was increased in Miro1-R450C fibroblasts, as indicated by elevation of PGC1α. A similar phenotype with reduction of mitochondrial mass was also observed in M17 cells overexpressing Miro1-R272Q or Miro1-R450C. Additionally, spare respiratory capacity was reduced in Miro1-R272Q fibroblasts compared to Ctrl 1 fibroblasts. In contrast, Miro1-R450C fibroblasts showed increased respiratory activity compared to Ctrl 1, despite citrate synthase activity was significantly reduced. Both alterations of respiratory activity lead to mitochondrial membrane hyperpolarization in Miro1-R272Q and Miro1-R450C fibroblasts, a phenotype which was also found in M17 cells with knockdown of *RhoT1*. Both Miro1 mutant fibroblasts lines displayed different problems with cytosolic calcium buffering: in Miro1-R272Q fibroblasts histamine treatment increased cytosolic calcium concentration significantly

compared to Ctrl 1 fibroblasts, indicating that calcium homeostasis was impaired, whereas in Miro1-R450C fibroblasts the buffering capacity for cytosolic calcium was impaired.

The results indicate that mutations in Miro1 cause significant mitochondrial dysfunction, which are likely contributing to neurodegeneration in PD and underline the importance of Miro1 for mitochondrial maintenance.

1 Introduction

1.1 Parkinson's disease (PD)

Parkinson's disease is a progressive neurodegenerative disease that affects approximately 1-2 % of the population older than 65 years worldwide (von Campenhausen, Bornschein et al. 2005). The symptoms are very heterogeneous and can be classified in motor symptoms and non-motor symptoms. Already years before PD is diagnosed the patients suffer from non-motor symptoms like depression, constipation, sleep disturbances, anxiety and disturbance of the olfactory sense (Jankovic 2008). PD typically is diagnosed at a mean age of 65 years (de Rijk, Launer et al. 2000) when motor symptoms become more obvious. The cardinal motor symptoms of PD are tremor, hyperkinesia, rigidity, postural instability and a mask-like facial expression. Although the motor symptoms are more prominent it seems that PD patients suffer more from the non-motor symptoms (Breen and Drutyte 2013) as they severely affect the quality of life.

The emergence of the clinical symptoms correlates with the progression of the disease. In 2004 Braak and colleagues presented the stages of PD pathology (Braak, Ghebremedhin et al. 2004). They found that Lewy bodies and Lewy neurites, which are intraneuronal inclusion bodies of aggregated fibrillar α-synuclein (Spillantini, Schmidt et al. 1997) and represent the pathological hallmark of PD, start their spreading throughout the nervous system from specific sites in a predictable pattern. In early stages of PD, before the diagnosis, Lewy bodies are first present in the medulla oblongata/ pontine tegmentum, the olfactory bulb and the anterior olfactory nucleus. From there the pathology spreads further to the substantia nigra and other regions of the midbrain and forebrain. At this stage first motor symptoms occur. The neocortex gets affected in the late stages of PD, leading to the full clinical manifestation (Braak, Ghebremedhin et al. 2004).

PD motor symptoms arise from loss of dopaminergic neurons (DA neurons), predominantly in the substantia nigra pars compacta. When approximately 30 % of the DA neurons are gone clinical symptoms start to manifest (Bernheimer, Birkmayer et al. 1973). The resulting loss of the inhibitory dopaminergic innervation leads to an over-activity of the subthalamic nucleus and the globus pallius, which triggers the motor symptoms (Obeso, Rodriguez-Oroz et al. 2000). To date there is no causative or preventive treatment for PD available because the exact mechanisms leading to the underlying neurodegeneration are not fully understood. Therefore it is of great interest to identify involved genes and pathways that contribute to the progression of PD.

1.2 Aetiology of PD

PD can be divided in idiopathic forms, where the underlying cause of the disease is unknown, and familial forms, caused by genetic mutations or genetic risk factors. The major risk factor for the development of idiopathic, or sporadic PD is aging (Bowling and Beal 1995). With about 11 % only a small portion of all PD patients have a positive family history (Shino, McGuire et al. 2010). Nevertheless it is of great interest to understand the disease causing mechanism of familial PD because these mechanisms are likely to be involved in the development of sporadic PD as well.

To date, there have been 21 genes identified, which can cause PD (http://www.omim.org/entry/616361) and about 28 risk factors that are involved in the pathogenesis of PD (Nalls, Pankratz et al. 2014), amongst them α-synuclein, Parkin, PINK1, DJ-1, LRRK2 and Omi/HtrA2.

1.2.1 α-synuclein – PARK1

Aggregates of α-synuclein are the main component of Lewy bodies (Anderson, Walker et al. 2006) (Fujiwara, Hasegawa et al. 2002) (Spillantini, Schmidt et al. 1997) and so far it is still obscure whether the formation of those aggregates is toxic or protective in PD. Several mutations in α-synuclein are known to cause PD. The missense mutations A53T and A30P have been shown to enhance the formation of α-synuclein protofibrils (Caughey and Lansbury 2003). To date the function of α-synuclein is still not fully understood. The protein has been shown to affect mitochondrial morphology and to bind specifically to the mitochondrial membrane (Li, Yang et al. 2007) (Nakamura, Nemani et al. 2011) (Nakamura, Nemani et al. 2008). Other functions have been indicated in the ubiquitin-proteasome system, the maintenance of synaptic function and response to oxidative stress (Clayton and George 1998) (Greten-Harrison, Polydoro et al. 2010) (Nemani, Lu et al. 2010) (Tompa 2005). Its ability to modulate the activity of tyrosine hydroxylase raises the possibility that α-synuclein might also be involved in dopamine metabolism (Perez, Waymire et al. 2002) (Tabrizi, Orth et al. 2000).

1.2.2 Parkin – PARK2 and PINK1 – PARK6

Together with mutations in PINK1 (phosphatase and tensin homologue (PTEN)-induced putative kinase 1), Parkin mutations are the most frequent causes of early onset PD (Valente, Salvi et al. 2004) (Abou-Sleiman, Muqit et al. 2006). Furthermore heterozygous mutations in the parkin gene with reduced penetrance represent a risk factor for sporadic PD and are therefore likely to contribute to typical late-onset PD (Klein, Lohmann-Hedrich et al. 2007) (Hedrich, Kann et al. 2001) (West, Maraganore et al. 2002). PINK1 and Parkin have major roles in mitochondrial quality control and subsequent degradation. PINK1 accumulates at depolarized membranes of dysfunctional mitochondria and recruits Parkin from the cytosol (Geisler, Holmstrom et al. 2010). Subsequently, Parkin ubiquitinates proteins at the outer mitochondrial membrane to label them for proteasomal degradation (Wang, Winter et al. 2011), which is possibly the first step to initiate degradation of dysfunctional mitochondria via the autophagosom-lysosomal pathway, so called mitophagy (Weihofen, Thomas et al. 2009). Parkin also has an anti-apoptotic function independent of its interaction with PINK1, as it decreases the location of the pro-apoptotic protein Bax at the mitochondrial membrane (Johnson, Berger et al. 2012) and increases the threshold for release of cytochrome c from mitochondria (Berger, Cortese et al. 2009).

1.2.3 DJ-1 – PARK7

Mutations in DJ-1 are rare and cause autosomal recessive early-onset Parkinsonism (van Duijn, Dekker et al. 2001). Several studies suggested multiple functions for DJ-1, amongst them chaperone activity (Shendelman, Jonason et al. 2004), protease activity (Koide-Yoshida, Niki et al. 2007) (Olzmann, Brown et al. 2004), influence of transcription (Taira, Iguchi-Ariga et al. 2004), e.g. for tyrosine hydroxylase (Xu, Zhong et al. 2005), changing dopamine receptor transmission (Goldberg, Pisani et al. 2005), suppression of apoptosis (Junn, Taniguchi et al. 2005) (Sekito, Koide-Yoshida et al. 2006) (Kim, Peters et al. 2005) and peroxiredoxin function (Andres-Mateos, Perier et al. 2007). Furthermore, DJ-1 was found to interact with PINK1 (Tang, Xiong et al. 2006) and Parkin (Moore, Zhang et al. 2005) and to be involved in the regulation of mitochondrial fusion (Krebiehl, Ruckerbauer et al. 2010). DJ-1 plays an important role in mitochondrial maintenance as it acts as sensor for oxidative stress via the highly conserved cysteine 106, which gets oxidized to form sulfinic acid (Honbou, Suzuki et al. 2003) (Lee, Kim et al. 2003) (Wilson, Collins et al. 2003). Oxidized DJ-1 is translocated to mitochondria to accomplish its mitoprotective activity (Canet-Aviles, Wilson et al. 2004) in a proposed parallel pathway to the PINK1/Parkin

pathway (Thomas, McCoy et al. 2011). This activity probably explains the neuroprotective function of DJ-1, which is mediated by cysteine 106 (Meulener, Xu et al. 2006).

1.2.4 LRRK2 – PARK8

Mutations in the Leucine-rich repeat kinase 2 (LRRK2) have been identified in up to 5-6 % of PD cases with positive family history. This makes mutations in LRRK2 the most common cause for hereditary PD (Singleton, Farrer et al. 2013). Most interestingly, variants in LRRK2 are also found in 1.6 % of sporadic PD cases (Gilks, Abou-Sleiman et al. 2005), because polymorphisms in LRRK2 are associated with an increased PD risk (Nalls, Pankratz et al. 2014). LRRK2 encodes a kinase, which is likely to be associated with the outer mitochondrial membrane (OMM) (West, Moore et al. 2005) and was found to interact with Parkin (Smith, Pei et al. 2005). The physiological function of LRRK2 remains unknown, but the protein was associated with different pathways, amongst them the Mitogen Activated Protein Kinase pathways (MAPK). Within these pathways LRRK2 was found to activate MAP2K 3-4-6 and 7 (Hsu, Chan et al. 2010) (Gloeckner, Schumacher et al. 2009), sequentially leading to the activation of JNK and p38, which in turn regulate cell proliferation and differentiation, apoptosis, inflammation and immune responses (Milosevic, Giovedi et al. 2011). LRRK2 is also involved in the Wingless signalling pathway (wnt), which activates the transcription of β-Catenin, a transcription factor that is regulating about 400 genes (Milosevic, Giovedi et al. 2011) responsible for cell growth, apoptosis, immune response, inflammation, synaptic development and synaptic maintenance. Amongst other suggested functions, LRRK2 seems to be involved in mitochondrial maintenance as well (Wang, Yan et al. 2012) (Niu, Yu et al. 2012) (Su and Qi 2013), with overexpression of the pathogenic G2019S mutant LRRK2 causing mitochondrial uncoupling and depolarization of the mitochondrial membrane in SH-SY5Y cells (Papkovskaia, Chau et al. 2012) and increased mitophagy in primary mouse neurons (Cherra, Steer et al. 2013), while wild type LRRK2 protected HEK293 and SH-SY5Y cells against H_2O_2 induced cell-death (Liou, Leak et al. 2008).

1.2.5 Omi/HtrA2 – PARK13

Loss of function mutations or knockout of the mitochondrial protease Omi/ high temperature requirement A2 (HtrA2) leads to neurodegeneration in mice, which causes a remarkable parkinsonian phenotype, including trembling and early death (Martins, Morrison et al. 2004) (Jones, Datta et al. 2003). In PD patients six different heterozygous mutations in the 5' and 3' regulatory region of the *Omi/HtrA2* gene have been found, which suggests a crucial role of transcriptional regulation of Omi/HtrA2 in neurodegeneration (Bogaerts, Nuytemans et al. 2008). In 2005 a genetic screen for mutations in the *Omi/HtrA2* gene identified German PD patients with the heterozygous mutation G399S and furthermore the risk allele A141S, which resulted in impaired protease activity and subsequent mitochondrial dysfunction, ultimately leading to neurodegeneration (Strauss, Martins et al. 2005). Later, the same mutation was found in a large Turkish family with inherited PD and essential tremor (Unal Gulsuner, Gulsuner et al. 2014). Omi/HtrA2 is a serine protease (Strauss, Martins et al. 2005), which is localized in the mitochondrial intermembrane space. Upon mitochondrial damage Omi/HtrA2 is localized to the cytosol where it activates proapoptotic proteins (Hegde, Srinivasula et al. 2002) (van Loo, van Gurp et al. 2002). Still, Omi/HtrA2 is not considered as proapoptotic driver, as deletion of Omi/HtrA2 in mice caused loss of DA neurons and severe motor dysfunction (Martins, Morrison et al. 2004). These findings suggest that Omi/HtrA2 has pro-survival as well as pro-apoptotic functions, depending on its localization inside mitochondria or in the cytosol (Dagda and Chu 2009).

1.3 Mitochondria and PD

In 1983 Langston and colleagues described cases of drug abusers that developed an irreversible parkinsonian syndrome upon exposure to 1-methyl-4-phenyl-1,2,3,4-tetrahydropyridine (MPTP) (Langston, Ballard et al. 1983). The active metabolite of MPTP, MPP^+, inhibits complex I of the respiratory chain and is further more able to enter DA neurons via the dopamine transporter (DAT). Inhibition of complex I causes neurotoxicity and finally cell death (Nicklas, Vyas et al. 1985) by subsequent increased production of ROS and decreased ATP supply. Additionally MPP^+ leads to enhanced release of dopamine, which causes more oxidative damage (Fiskum, Starkov et al. 2003). These findings provided the first evidences for an involvement of mitochondrial dysfunction in the development of PD.

Interestingly, many of the genes involved in the development of familial PD are associated with mitochondrial function, like intramitochondrial production of reactive oxygen species

(ROS), mitochondrial membrane potential (MMP) and mitochondrial oxygen consumption, e.g. PINK1, Parkin, DJ-1 or Omi/HtrA2.

Mitochondria are important organelles not only as main source to provide ATP, but they are also involved in supplying intermediates for metabolic pathways, they are the main source for ROS production in cells, they are involved in cell differentiation, control of the cell cycle and cell growth and can initiate apoptosis (McBride, Neuspiel et al. 2006), serve as major calcium buffer and regulate lipid metabolism (Karbowski and Youle 2003). Therefore mitochondrial integrity is crucial for neurons, and mitochondrial dysfunction easily results in neurodegeneration (Mandemakers, Morais et al. 2007), as neurons have a need of constant ATP supply at synapses (DiMauro 2004) for the release and recycling of neurotransmitters (Hollenbeck 2005). Due to this energy demand the brain uses up ~20 % of the resting energy production of the whole body (Attwell and Laughlin 2001).

1.3.1 Mitochondrial electron transport chain

A number of studies showed a decrease of complex I in substantia nigra, skeletal muscle and platelets of PD patients (Mizuno, Ohta et al. 1989) (Parker, Boyson et al. 1989) (Schapira, Cooper et al. 1989) (Orth and Schapira 2002). Betarbet et al. treated rats with the specific complex I inhibitor rotenone. The rats subsequently developed a syndrome resembling typical features of PD, including neurodegeneration and inclusion bodies of aggregated α-synuclein (Betarbet, Sherer et al. 2000).

Complex I and III of the respiratory chain produce ROS, which damages proteins, lipids and DNA (Van Houten, Woshner et al. 2006). Damage of mtDNA in turn leads to malfunctioning of complex I and III, in turn generating more ROS and leading to increased oxidative stress (Van Houten, Woshner et al. 2006) (Voets, Huigsloot et al. 2012) (Alexeyev 2009). Finally ROS damage leads to inhibition of the respiratory chain complexes and the tricarboxylic acid cycle (TCA) and in consequence to a collapse of mitochondrial metabolism (Ghezzi and Zeviani 2012).

Thirteen proteins of the respiratory chain are encoded by the mitochondrial DNA (mtDNA), meaning that most mitochondrial proteins are encoded by nuclear genes and therefore need to be transported across the mitochondrial membranes after translation in the cytosol. A study in 2000 identified mtDNA mutations, e.g. in the *12SrRNA* gene, which cause maternally-inherited Parkinsonism (Thyagarajan, Bressman et al. 2000). It was hypothesized that DA neurons have higher levels of oxidative stress, probably caused by auto-oxidized dopamine, making DA neurons in the substantia nigra pars compacta more

prone to accumulate mtDNA mutations. In line with this hypothesis, a higher load of mtDNA deletions was found in PD patients compared to age-matched controls (Bender, Krishnan et al. 2006) (Kraytsberg, Kudryavtseva et al. 2006). Cell death of DA neurons probably increases when a critical threshold of about 60 % mutated mtDNA accumulates over time (Rossignol, Faustin et al. 2003). Once this threshold is reached the remaining intact mtDNA cannot compensate the impairment of mitochondrial function by producing enough proteins to sustain the function of the electron transport chain.

Overexpression of Parkin had a protective effect on mitochondria by either directly or indirectly enhancing complex I activity. In this way the overexpression of Parkin decreased the formation of ROS and increased the MMP (Kuroda, Mitsui et al. 2006). On the other side, parkin deficient mice showed a reduction of complex I and complex IV subunits with subsequent increase of protein oxidation and lipid-peroxidation due to increased ROS formation (Palacino, Sagi et al. 2004).

Another PD-related gene with connection to the respiratory chain is DJ-1. In mouse embryonic fibroblasts (MEFs) of DJ-1 knockout mice the observed reduction of complex I activity was sufficient to cause an impairment of the energy metabolism (Krebiehl, Ruckerbauer et al. 2010). Therefore DJ-1 was implicated to be involved in the integrity of complex I, further supported by studies that showed an intramitochondrial localization of DJ-1 (Zhang, Shimoji et al. 2005) (Hayashi, Ishimori et al. 2009).

The displayed studies implicate that dysfunction of the respiratory chain plays a significant role in the development of PD, by depleting neurons from energy supply and by increasing the load of oxidative stress.

1.3.2 Oxidative stress

Although the brain has a very high metabolic activity due to its high energy demand, its resources for ROS defence, e.g. by superoxide dismutase (SOD), are limited. Therefore vulnerability to oxidative stress is increased, as the brain also contains high amounts of polyunsaturated fatty acids which are highly vulnerable to ROS damage (reviewed by (Bhat, Dar et al. 2015)). Oxidative stress seems to cause specific damage to areas that are affected in neurodegeneration, that is in Alzheimer's disease the cortex and hippocampus and in PD the substantia nigra (Hensley, Maidt et al. 1998) (Butterfield, Castegna et al. 2002) (Dexter, Carter et al. 1989) (Good, Hsu et al. 1998) (Aoyama, Matsubara et al. 2000).

PD is characterized by a loss of DA neurons in the substancia nigra. This type of neurons is especially susceptible to oxidative stress because of the dopamine metabolism. The

unstable dopamine undergoes auto-oxidation very easily and thereby produces ROS (Slivka and Cohen 1985). Enzyme-dependent [e.g. by cyclooxygenase (Hastings 1995), cytochrome C (Rosei, Blarzino et al. 1998), xanthine oxidase (Foppoli, Coccia et al. 1997), monoamine oxidase and peroxidase (d'Ischia and Prota 1997)] or enzyme-independent degradation of dopamine in the cytosol also produces ROS as by-products (Fasano, Bergamasco et al. 2006) (Sulzer and Zecca 2000).

Impairment of the electron transport chain, like inhibition of complex I, leads to increased ROS production, exposing cells to increased oxidative stress. Several PD-associated genes have been identified, which influence pathways involved in oxidative stress.

One of these genes encodes for α-synuclein. It was found that oxidative stress is closely related to aggregation of α-synuclein in PD (Spillantini, Schmidt et al. 1997) (Conway, Rochet et al. 2001). Protofibrils of α-synuclein bind to synaptic vesicles and may form pores that release dopamine into the cytosol (Lashuel, Hartley et al. 2002). The formation and stability of protofibril pores is enhanced by dopamine quinones, which result from the oxidation of dopamine. This mechanism is one possible explanation for the specific toxicity of α-synuclein in the substantia nigra (Conway, Rochet et al. 2001). It was also found that the function of neuronal mitochondria was indirectly affected by dysfunctional α-synuclein. When mutant α-synuclein was over expressed, neurons became more prone to oxidative stress induced by dopamine and MPP^+, causing enhanced protein carbonylation and peroxidation of lipids (Orth and Tabrizi 2003) (Tabrizi, Orth et al. 2000).

Cultured primary neurons of PINK1 knockout mice showed a depolarization of the mitochondrial membrane with increased ROS levels and the same phenotype was observed in human midbrain neurons derived from fetal mesencephalon stem cells with knockdown of *PINK1* (Wood-Kaczmar, Gandhi et al. 2008). The phenotype was caused by a dysregulation of the mitochondrial Na+/Ca+ exchanger and subsequent intramitochondrial calcium overload, which resulted in enhanced formation of ROS via the NADPH oxidase (Gandhi, Wood-Kaczmar et al. 2009).

DJ-1 is involved in oxidative stress response. Mutations in DJ-1 are rare and cause eraly-onset, autosomal recessive forms of PD (Bonifati, Rizzu et al. 2003). After oxidative stress overexpressed DJ-1 was found to be recruited from the cytosol to the OMM (Canet-Aviles, Wilson et al. 2004). There, DJ-1 functions as a scavenger of ROS, by preventing the accumulation of ROS produced by the respiratory chain (Kim, Smith et al. 2005). Loss of DJ-1 function causes mitochondrial impairment and increased vulnerability to complex I inhibition (Meulener, Xu et al. 2006) (Kim, Smith et al. 2005) (Andres-Mateos, Perier et al.

2007). Furthermore, DJ-1 knockout mice showed a higher susceptibility to MPP^+ neurotoxicity (Kim, Smith et al. 2005).

The numerous studies showing a link between PD-associated genes and oxidative stress suggest that this could be a common mechanism involved in various PD-related pathways (Abou-Sleiman, Muqit et al. 2006). Oxidative damage of proteins, lipids and DNA is increased in idiopathic and in familial PD patients, indicating that oxidative stress is a major cause for the development of PD (Bosco, Fowler et al. 2006) (Nakabeppu, Tsuchimoto et al. 2007) (Zeevalk, Razmpour et al. 2008).

1.3.3 Ubiquitin-proteasome system (UPS)

Additionally, results of several studies implicated a link between mitochondrial function and the ubiquitin-proteasome system (UPS).

For example it was shown that decreased proteasome activity can result from defects of complex I (Hoglinger, Carrard et al. 2003) (Sullivan, Dragicevic et al. 2004). One possible reason for this link is the fact that the UPS needs ATP for proper function. In this regard it is likely that impaired mitochondrial function and decreased ATP supply also cause dysfunction of the UPS (Abou-Sleiman, Muqit et al. 2006). This hypothesis was supported by a study of Shamoto-Nagai et al., in which the neuroblastoma cell line SH-SY5Y was treated with the specific complex I inhibitor rotenone. The cells consequently not only displayed an increase in ROS production and accumulation of oxidized proteins, but also a depletion of ATP of about 20 % and a significant decrease of proteasome activity (Shamoto-Nagai, Maruyama et al. 2003).

Another link between mitochondrial function and the UPS was provided by Valente et al., who showed that inhibition of the proteasome induced depolarization of the MMP and apoptosis in SH-SY5Y cells transfected with G309D-mutant PINK1, a phenotype that was not observed in cells transfected with wild-type PINK1 (Valente, Abou-Sleiman et al. 2004).

Moreover, UPS impairment can induce secondary dysfunction and damage of mitochondria. This was shown in primary rat cortical neurons treated with proteasome inhibitors. In these cells the MMP was depolarized, resulting in release of cytochrome c from mitochondria to the cytosol and subsequent apoptotic cell death (Qiu, Asai et al. 2000). The observed link between UPS inhibition and mitochondrial induced apoptosis could be due to the fact that pro-apoptotic proteins, like p53 and members of the BCL2 protein family are degraded by the UPS under normal conditions (Jesenberger and Jentsch 2002). Inhibition of the proteasome leads to the accumulation of pro-apoptotic proteins, which

cause opening of the mitochondrial permeability transition pore, depolarization of the mitochondrial membrane and induction of apoptosis (Jesenberger and Jentsch 2002).

PD-associated DJ-1 is a multi-functional protein, which is also implicated in the link between mitochondria and UPS. It was shown that RNAi induced knockdown of DJ-1 increased susceptibility of neurons to inhibition of the proteasome (Yokota, Sugawara et al. 2003). DJ-1 was identified as a regulator of the transcription of the pro-apoptotic protein p53 and in this way might be able to connect UPS and mitochondrial stress response (Shinbo, Taira et al. 2005).

1.3.4 Mitochondrial quality control via PINK1 and Parkin

Many cell types contain a large network of interconnected mitochondria. This is not the case in neuronal processes because mitochondria have to be transported into distal parts of axons and dendrites. Therefore mitochondria in axons typically are discrete organelles with a size of 1 - 3 µm (Chang, Honick et al. 2006). These peripheral mitochondria need to be supplied with mitochondrial proteins that are synthesized in the soma. Mitochondrial maintenance occurs by fission and fusion events to mix and exchange mitochondrial content (Amiri and Hollenbeck 2008). The importance of mitochondrial fission and fusion for the maintenance of healthy mitochondria was underlined by studies showing that disruption of mitochondrial fusion causes peripheral neuropathy (Zuchner, Mersiyanova et al. 2004) and progressive loss of mtDNA integrity and depolarization of the MMP (Chen, McCaffery et al. 2007).

When maintenance of aged mitochondria cannot be obtained or mitochondria get damaged due to pathological insults, they need to be degraded. One possible mechanism for degradation proposed that depolarized mitochondria are transported back to the soma for degradation (Miller and Sheetz 2004) (Cai, Zakaria et al. 2012). However, other studies failed to verify a link between MMP and direction of mitochondrial transport (Verburg and Hollenbeck 2008), indicating that depolarized mitochondria are not preferentially transported to the soma. Instead, there is growing evidence supporting the idea that mitochondrial degradation by the lysosomal pathway also occurs in axons and dendrites: i) different studies were able to show functional mature lysosomes in axons (Lee, Sato et al. 2011) (Maday, Wallace et al. 2012) and ii) aged mitochondrial proteins were found to remain in neuronal processes, likely for local degradation instead of being transported back to the soma (Ferree, Trudeau et al. 2013). Recently, Ashrafi and colleagues showed that mitophagy of damaged mitochondria in axons depends on the PINK1/ Parkin pathway (Ashrafi, Schlehe et al. 2014). Local degradation prevents fusion of damaged mitochondria

with the healthy network and the spreading of oxidative damage throughout the cell (Wang, Winter et al. 2011).

PINK1 is constantly recruited from the cytosol to healthy mitochondria where it gets cleaved (Greene, Grenier et al. 2012). However, when the membrane of damaged mitochondria gets depolarized PINK1 is stabilized at the OMM. PINK1 then recruits Parkin to the mitochondrial surface (Geisler, Holmstrom et al. 2010). Subsequently PINK1 and Parkin bind to the target protein and Parkin is phosphorylated by PINK1 to activate its function as E3 ubiquitin ligase (Wang, Winter et al. 2011). As a result, ubiquitination of the target proteins at the OMM leads to proteasomal degradation, which likely is the initial step for mitophagy (Wang, Winter et al. 2011).

Studies in *drosophila* showed that due to their close interplay in the mitophagy-inducing pathway PINK1 and Parkin knockout flies display a very similar phenotype of mitochondrial dysfunction, including flight muscle degeneration, reduced ATP levels, male sterility and, most interestingly, loss of DA neurons (Clark, Dodson et al. 2006) (Park, Lee et al. 2006).

1.3.5 Mitochondrial transport

Neurons have a highly polarized morphology with extended dendritic and axonal processes. As mitochondrial biogenesis occurs mainly in the cell soma, mitochondria have to be transported to distal sites of the cell (Hollenbeck and Saxton 2005). Therefore, transport of mitochondria is crucial for neuronal maintenance and function. For this reason it is not surprising that mutations in motor proteins cause neurological diseases in humans (Baloh 2008) (De Vos, Grierson et al. 2008).

Experimental work on mitochondrial trafficking revealed that in axons approximately the same fraction of 15 % of mitochondria are moving in the anterograde and in the retrograde direction and ~70 % of mitochondria are stationary for a certain time (Wang and Schwarz 2009).

Impaired mitochondrial transport was observed in loss of function PINK1 mutants in *drosophila*, which lead to selective loss of DA neurons (Liu, Sawada et al. 2012). In this regard impaired mitochondrial trafficking could play a significant role in the development of PD.

1.3.6 Mitochondrial membrane potential and calcium homeostasis control cell death

Calcium is an important secondary messenger involved in many cell mechanisms. Therefore tight regulation of calcium concentration in the cytosol is crucial. Mitochondria provide an important calcium buffering capacity (Starkov 2010). Calcium enters the mitochondrial matrix through the mitochondrial calcium uniporter (MCU), driven by the mitochondrial membrane potential (MMP) (reviewed by (Rizzuto, De Stefani et al. 2012).

The MMP is generated when protons are pumped through the proton pumps of the respiratory chain (complexes I, III, IV and V) across the inner mitochondrial membrane from the matrix into the intermembrane space. The re-entry of protons through complex V provides the energy necessary to convert ADP to ATP. The MMP fluctuates under normal conditions between -108 and -159 mV (Li, Fang et al. 2013) (Valko, Leibfritz et al. 2007) (Radak, Chung et al. 2008). Low MMP values normally are associated with high ATP production and oxygen consumption, because the MMP is discharged by ATP synthesis. In contrast, high MMP values under normal conditions arise from a reduction of respiratory activity and a low oxygen consumption and ATP production (Arvier, Lagoutte et al. 2007) (Bagkos, Koufopoulos et al. 2014).

Both, MMP and mitochondrial calcium uptake are closely linked and under certain conditions related to dysregulation of homeostasis, thereby inducing necrotic and/ or apoptotic cell death. It was found that staurosporine induces cell death dependent on calcium influx into mitochondria and mitochondrial membrane hyperpolarization. Staurosporine leads to calcium over-load of mitochondria (Kruman and Mattson 1999), thereby most likely increasing the activity of the respiratory chain and subsequently increasing MMP (Poppe, Reimertz et al. 2001). Hyperpolarization of the mitochondrial membrane was sufficient to cause release of cytochrome c from mitochondria, finally inducing apoptosis (Poppe, Reimertz et al. 2001) (Vander Heiden, Chandel et al. 1997).

Cell death was also induced by depolarization of MMP. Treatment with the potassium-ionophore Valinomycin caused depolarisation of the mitochondrial membrane and increased the influx of potassium ions into the mitochondrial matrix, causing the entry of anions and water. Therefore mitochondria swell until the membrane gets ruptured (Poppe, Reimertz et al. 2001) (Vander Heiden, Chandel et al. 1997). Subsequently, cytochrome c was released into the cytosol, but without activation of the caspase cascade that induces apoptosis. The resulting cell death therefore was characterized as necrotic instead of apoptotic (Poppe, Reimertz et al. 2001).

Poppe et al. concluded that mitochondrial membrane hyperpolarization likely is the active physiological trigger for release of cytochrome c, whereas depolarization of the mitochondrial membrane leads to a passive release of cytochrome c due to rupture of the membrane (Poppe, Reimertz et al. 2001).

However, the mechanisms behind the regulation of MMP, calcium homeostasis and apoptosis remain not fully clarified. A decrease in MMP can also cause opening of the mitochondrial transition pore (Zoratti and Szabo 1995), which enables the release of pro-apoptotic proteins (Zamzami, Susin et al. 1996) (Lemasters, Nieminen et al. 1998). On the other hand, other groups reported that MMP depolarization prevented apoptosis by inhibiting calcium uptake through the mitochondrial calcium uniporter (MCU) (Nicholls and Akerman 1982) (Andreyev, Fahy et al. 1998), thereby preventing calcium over-load and ROS production (Castilho, Hansson et al. 1998) (Stout, Raphael et al. 1998). Iijima proposed that hyperpolarization of the mitochondrial membrane could be an intermediate state when the mitochondrial transition pore is not jet opened and calcium influx into the mitochondrial matrix has not started (Iijima 2006).

To date it is still not clear which intrinsic, physiological signals trigger mitochondria-induced apoptosis. A number of studies generated contradicting results regarding the involvement of depolarization or hyperpolarization of the mitochondrial membrane in different cell types, but it is apparent that pathological changes of MMP and mitochondrial calcium concentration are involved in cell death.

1.4 Miro – more than just an adaptor for mitochondrial transport

Miro is present in nearly all eukaryotes, except of Micosporidia, *Entamoeba* spp., *Giardia intestinalis* and *Trichomonas vaginalis* which have either mitosomes or hydrogenosomes instead of classical mitochondria. Furthermore, Miro is absent from Myzozoa, green algae of the order Mamiellales, the haptophyte *Emiliania huxleyi* and the stramenopile alga *Aureococcus anophagefferens*, which do have aerobic mitochondria, but probably lost Miro during the course of their evolutionary development (Vlahou, Elias et al. 2011). The fact that most eukaryotes possess Miro proteins underlines the importance of this protein for the functionality of mitochondria.

Miro was classified as mitochondrial Rho GTPase, giving the protein its name, because the N-terminal GTPase domain of Miro shows sequence similarity to small Rho GTPases (Fransson, Ruusala et al. 2003). Typically Rho GTPases are involved in the organization of the actin cytoskeleton (Takai, Sasaki et al. 2001), but several studies failed to

demonstrate a role of Miro in the organization of the actin or microtubule cytoskeleton (Fransson, Ruusala et al. 2003) (Aspenstrom, Fransson et al. 2004).

Miro is ubiquitously expressed in vertebrate tissue. The expression level varies, depending on mitochondrial density and energy demand, for example high expression levels were observed in heart, brain and skeletal muscle (Fransson, Ruusala et al. 2003). In yeast and *drosophila* only one Miro protein exists (Guo, Macleod et al. 2005), but in mammals two isoforms, called Miro1 and Miro2, have been identified. Both proteins are 60 % identical, are co-expressed in most tissue and localized at the OMM (Fransson, Ruusala et al. 2003).

Experimental work suggested significant differences in Miro1 and Miro2 function. In yeast overexpression of Miro1 or Miro2 caused mitochondrial clustering, but only in Miro1 over-expressing yeast mitochondria were interconnected, which was not observed in Miro2 over-expressing yeast (Fransson, Ruusala et al. 2006). In T cells mitochondrial redistribution was affected by knockdown of Miro1, although endogenous expression of Miro2 remained unchanged (Morlino, Barreiro et al. 2014). Even Miro1 knockout mice showed a severe neurological phenotype including neurodegeneration and premature death, although Miro2 expression was intact (Nguyen, Oh et al. 2014). However, still to date the different functions of Miro1 and Miro2 are not exactly defined.

Overexpression of *drosophila* Miro (dMiro) in *drosophila* caused a specific loss of DA neurons (Liu, Sawada et al. 2012). A knockout on the other hand lead to slimness and lethality of the third instar larvae. Furthermore, synaptic boutons were found to have abnormal morphology and tend to cluster together in big cauliflower-like structures, while axons and presynaptic synapses were devoid of mitochondria (Guo, Macleod et al. 2005) (Tsai, Course et al. 2014). Similar results were obtained in studies with mutations in mammalian Miro and dMiro that caused defective transport of mitochondria into neuronal axons and dendrites of *drosophila* (Fransson, Ruusala et al. 2003) (Fransson, Ruusala et al. 2006) (Guo, Macleod et al. 2005).

Miro is involved in many mitochondrial pathways that have already been introduced in the pathology of PD, which are not only mitochondrial transport, but also cellular calcium homeostasis and mitochondrial dynamics and quality control.

1.4.1 The structure of Miro proteins

The first description of a Miro protein was the one of the yeast orthologue Gem1, which was identified as open reading frame (ORF) YAL048c on chromosome 1 of *saccharomyces cerevisiae* (Bussey, Kaback et al. 1995), and already in 1986 two studies, by Woolford et al. and Ammerer et al. described the protein encoded by YAL048c as polypeptide of 662 amino acids with a molecular mass of 75,137 kDa. The polypeptide was predicted to contain two putative ATP/GTP-binding site motifs with weak similarity to small GTPases and a transmembrane domain at the carboxyterminal (C-terminal) end (Woolford, Daniels et al. 1986) (Ammerer, Hunter et al. 1986).

The first study on the 3D structure of Miro protein, including the crystal structure was described in 2013 (Klosowiak, Focia et al. 2013). In this study dMiro was described as monomeric protein, with a compact linear conformation.

Miro proteins contain a N-terminal GTPase domain, followed by the two EF hand domains, a second C-terminal GTPase domain and the transmembrane domain (TMD) (Figure 1).

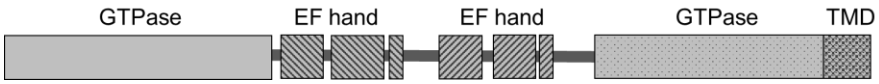

Figure 1: Structure of Miro protein

Protein structure of Miro proteins showing the N-terminal GTPase domain, both EF hand domains, the C-terminal GTPase domain and the C-terminal transmembrane domain (TMD).

The GTPase domains have been reported to be involved in the organisation of mitochondrial trafficking. Whereas loss of function mutations of both GTPase domains did not affect the recruitment of TRAK2, an important binding partner of Miro for mitochondrial transport, constitutively active mutations of the N-terminal GTPase disrupted the recruitment of TRAK2 to Miro, thereby affecting mitochondrial transport (MacAskill, Brickley et al. 2009). The C-terminal GTPase domain was found to rather modulate the retrograde transport of mitochondria in axons, whereas the functionality of the N-terminal GTPase domain was more crucial for cell survival, because loss of function mutations in this domain disrupted the kinesin- as well as dynein-driven axonal transport of mitochondria and subsequently the proper distribution of mitochondria in axons and dendrites (Babic, Russo et al. 2015). The N-terminal GTPase domain was supposed to accomplish this function by driving the shift from immobile to mobile mitochondria (Babic, Russo et al. 2015).

Miro's GTPase domains are unique, because they lack the typical CAAX-box motif that targets Rho GTPases to membranes (McTaggart 2006). Instead Miro possesses a C-terminal TMD which anchors the protein in the outer mitochondrial membrane and exposes it to the cytosol (Fransson, Ruusala et al. 2006) (Frederick, McCaffery et al. 2004). In COS-7 cells deletion of the TMD of Miro1 and Miro2 caused a mislocalization of Miro proteins from mitochondria to the cytoplasm, indicating that the TMD indeed is required for proper mitochondrial targeting (Fransson, Ruusala et al. 2006). The TMD is composed of hydrophobic amino acid residues, flanked by positively charged amino acids, which is a common feature of TMDs of OMM proteins (Wattenberg and Lithgow 2001).

A rather unusual feature of Miro proteins is the presence of calcium binding embryonic fibroblast (EF) hand domains. These domains are highly conserved calcium binding motifs, which are also present in other calcium buffering proteins (Gifford, Walsh et al. 2007). The EF hand domain contains a helix-loop-helix motif that exposes the calcium-binding amino acids on the protein surface (Gifford, Walsh et al. 2007). Calcium binding to EF hand domains typically leads to a conformational shift of the protein structure to initiate a certain function (Hoeflich and Ikura 2002). The EF hand domains of Miro were found to be highly conserved amongst Miro proteins of different species and are unique to the Miro protein family (Finn, Mistry et al. 2010), because each of the both canonical EF hand motifs is accompanied by a non-canonical EF hand domain, which are in turn followed by a helix that mimics a ligand (ligand mimic, LM1 and LM2) for the EF hand motif and a linker region (Klosowiak, Focia et al. 2013). Due to the linker regions the canonical EF hands are positioned side-by-side with the C-terminal GTPase domain, creating a unique direct interaction of EF hand and GTPase, which was reported for the first time in Miro (Klosowiak, Focia et al. 2013).

Surprisingly, nucleotide or ion binding at the GTPase or EF hand domains did not cause a great conformational shift of the protein structure, nor was an oligomerization of Miro observed (Klosowiak, Focia et al. 2013).

1.4.2 Miro as adaptor for mitochondrial transport

Miro protein functions as adaptor for mitochondrial transport by connecting the OMM via a second adaptor protein called Milton to motor proteins (Wang and Schwarz 2009) (Koutsopoulos, Laine et al. 2010). In mammals two isoforms of Milton homologues are known: O-GlcNAC-transferase (OGT)-interacting proteins 106 and 98 (OIP106 and OIP98) (Iyer, Akimoto et al. 2003), which are also called huMilt1 or TRAK1 (refers to OIP106) and huMilt2 or TRAK2 or $GABA_A$ receptor-interacting factor (GRIF-1) (Beck, Brickley et al. 2002) (refers to OIP98), respectively (in the following text summarized as Milton proteins). In contrast to the mitochondria restricted localization of Miro, the Milton proteins are also localized in the cytosol and on other organellar cargo (MacAskill, Brickley et al. 2009). Milton proteins bind at the N-terminal GTPase domain of Miro (Fransson, Ruusala et al. 2006), an interaction that is regulated by the GTP-loading of the GTPase domain (MacAskill, Brickley et al. 2009). The Miro/Milton complex recruits both, kinesin (Wang and Schwarz 2009) and dynein motors (Morlino, Barreiro et al. 2014) for retrograde as well as anterograde transport of mitochondria. Whereas huMilt1 was found to interact with both, kinesin and dynein (van Spronsen, Mikhaylova et al. 2013) and is found predominantly in axons for anterograde and retrograde mitochondrial transport, huMilt2 preferentially binds to dynein to mediate retrograde transport in dendrites (van Spronsen, Mikhaylova et al. 2013). The observation that most mitochondria are able to change direction quickly indicates that different motor proteins are tethered to the OMM at the same time (Miller and Sheetz 2004) (Pilling, Horiuchi et al. 2006) (Russo, Louie et al. 2009). To date it is not fully understood how mitochondrial transport is regulated in terms of directionality. Several interaction partner of the Miro/ Milton complex have been found to influence mitochondrial transport, e.g. Alex3, Mitofusin2, HUMMR and DISC1.

Alex3 and Miro – Nucleus-dependent control of mitochondrial distribution?

Recently, members of the *Armcx* gene family have been identified to interact with Miro and huMilt2 (Lopez-Domenech, Serrat et al. 2012). The *Armcx* genes encode for Alex1, 2 and 3 (arm-containing protein lost in epithelial cancers linked to the X chromosome). Alex3 is expressed mainly in the nervous system and interacts with the transcription factor Sox10 (Mou, Tapper et al. 2009). Furthermore, Alex3 localizes to mitochondria and increases Sox10 association to mitochondria, which raises the possibility of a yet undescribed Sox10/Alex3-mediated signalling cascade between mitochondria and the nucleus (Mou, Tapper et al. 2009). Alex3 was found in three cellular compartments of neurons: at the outer mitochondrial membrane, in the nucleus and in the cytosol (Lopez-Domenech, Serrat et al. 2012). Overexpression of Alex3 in HEK293T cells caused an aggregation of the

mitochondrial network, which was independent of Miro1 function, but also a severe impairment of mitochondrial trafficking. Downregulation of Alex3 expression caused a reduction of mitochondrial transport as well (Lopez-Domenech, Serrat et al. 2012). The reason for the alteration of mitochondrial trafficking is likely caused by the direct interaction of Alex3 with Miro1, Miro2 and huMilt2 (Lopez-Domenech, Serrat et al. 2012). Similar to the regulation of Miro/Milton interaction via calcium binding to the EF hand domains, the interaction with Alex3 is also regulated by calcium: 2 mM calcium was found to reduce the interaction of Alex3 with the Miro proteins and with huMilt2 (Lopez-Domenech, Serrat et al. 2012). Further investigations will reveal whether the interaction of Alex3 with Miro is sufficient to mediate regulation of mitochondrial distribution by signalling from the nucleus.

Mitofusin2 and Miro – Co-regulation of mitochondrial fusion and transport

Mitochondrial fusion is mediated by a protein complex of the Mitofusins1 and 2 on the OMM and Opa1 on the inner mitochondrial membrane (IMM) (Rojo, Legros et al. 2002) (Chen, Detmer et al. 2003) (Eura, Ishihara et al. 2003) (Cipolat, Martins de Brito et al. 2004). All involved proteins belong to the dynamin GTPase family and work together to tether membranes of two mitochondria to promote their fusion. Studies with Mitofusin2 mutations, which are associated with Charcot-Marie-Tooth Neuropathy Type 2A, 0showed impaired mitochondrial transport in cultured neurons (Baloh, Schmidt et al. 2007) and abnormal mitochondrial distribution in motor neurons (Detmer, Vande Velde et al. 2008). Misko et al. were able to demonstrate an interaction of Mitofusin2 with the Miro/Milton complex and even declared Mitofusin2 to a key component of the complex (Misko, Jiang et al. 2010). This hypothesis was supported by the observation that loss of Mitofusin2 function caused impaired mitochondrial transport, a phenotype that was independent of the role of Mitofusin2 in mitochondrial fusion and that was not rescued by overexpression of Miro2 (Misko, Jiang et al. 2010). The interplay of Mitofusin2 and Miro seems to be important to adapt the recruitment of anterograde moving kinesin and retrograde moving dynein to the cell requirements (Russo, Louie et al. 2009). Moreover, the interaction of Mitofusin2 and Miro could partially explain the frequently observed influence of Miro on mitochondrial morphology (Fransson, Ruusala et al. 2006) (MacAskill, Brickley et al. 2009) (Saotome, Safiulina et al. 2008). As mitochondrial transport requires distinct, single organelles and as moving increases the likelihood for mitochondria to fuse (Liu, Weaver et al. 2009) it is reasonable to conclude that mitochondrial fusion and transport are closely linked for a coordinated regulation (Misko, Jiang et al. 2010).

HIF-1α, HUMMR and Miro

Hypoxia-inducible factor 1 α (HIF-1α) is a transcription factor that is predominantly activated and stabilized during hypoxic conditions, which require a fast cellular response to increase oxygen and energy supply (Semenza 2000). This cellular response involves HIF-1α-induced alteration of mitochondrial respiration in a way that reduces mitochondrial ROS production (Kim, Tchernyshyov et al. 2006) (Papandreou, Cairns et al. 2006) and modulates the electron transport (Fukuda, Zhang et al. 2007). In 2009 a study identified a new protein involved in the HIF-1α-mediated mitochondrial response to hypoxia: hypoxia up-regulated mitochondrial movement regulator (HUMMR) (Li, Lim et al. 2009). HUMMR protein expression in neurons and astrocytes was strongly induced by HIF-1α during hypoxia. The protein consists of an N-terminal TMD and a following mitochondrial targeting sequence (MTS) and is localized at mitochondria (Li, Lim et al. 2009). HUMMR appeared to be anchored with its TMD in the OMM, positioning the C-terminus of the protein in the intermembrane space. The same study established an interaction between HUMMR and Miro, as well as a HUMMR-facilitated recruitment of huMilt2 to mitochondria (Li, Lim et al. 2009). HUMMR and Miro most likely interact at their TMDs (Li, Lim et al. 2009). The results of the study indicate that HUMMR promotes mitochondrial transport in the anterograde direction by recruiting preferentially huMilt2 to mitochondria, which in turn facilitates the engagement of kinesin (Li, Lim et al. 2009). This hypothesis is supported by another study showing that mitochondria are enriched in synapses after ischemia (Briones, Suh et al. 2005), which is important for neuronal and synaptic plasticity that is observed in brains after stroke-induced ischemia (Carmichael 2003). But HUMMR-expression is also regulated by HIF-1α under normoxia conditions, e.g. in testes, ovary and corneal epithelium (Kinouchi, Kinouchi et al. 2006), but also in Alzheimer's disease (Soucek, Cumming et al. 2003), probably as compensatory mechanism in neurodegeneration (Li, Lim et al. 2009). These findings suggest that the directionality of mitochondrial transport is likely regulated according to the cell needs by additional binding and interaction partner of the Miro/Milton protein complex.

DISC1 and Miro

Mitochondria are not only known to be involved in the pathophysiology of PD, but also in many other neurological disorders, one of them being schizophrenia (Ben-Shachar and Laifenfeld 2004). Analysis of post-mortem brains of schizophrenia patients revealed impaired oxidative phosphorylation (Maurer, Zierz et al. 2001) and alteration of mitochondrial morphology and quantity (Kung and Roberts 1999). About 80 % of schizophrenia cases are familial inherited (Cardno and Gottesman 2000). One of the genes

causing inherited schizophrenia is Disrupted-in-schizophrenia 1 (DISC1) (Mackie, Millar et al. 2007). The protein DISC1 is related to neurodevelopment, neurite outgrowth, neuronal migration, neurogenesis (Kamiya, Kubo et al. 2005) (Ozeki, Tomoda et al. 2003) (Duan, Chang et al. 2007) (Mao, Ge et al. 2009) and cAMP signalling (Millar, Pickard et al. 2005). DISC1 was also linked to mitochondrial function by a study that showed localization of DISC1 at the inner mitochondrial membrane, as well as a reduction of mitochondrial NADH dehydrogenase activity and ATP production and impaired calcium dynamics induced by DISC1 disruption (Park, Jeong et al. 2010). The same study established a direct interaction of DISC1 and the inner mitochondrial membrane protein Mitofilin (Park, Jeong et al. 2010). Furthermore, DISC1 was shown to regulate axonal transport of mitochondria (Atkin, MacAskill et al. 2011), an interesting result that was confirmed by establishing an interaction of DISC1 with Miro1/huMilt1 (Ogawa, Malavasi et al. 2014). In this study huMilt1 was shown to influence the recruitment of DISC1 to mitochondria. Additionally, overexpression of DISC1 caused an increase of anterograde mitochondrial movement (Ogawa, Malavasi et al. 2014). These findings support the idea that additional binding partner of the Miro/Milton complex influence mitochondrial transport according to current needs of the cell.

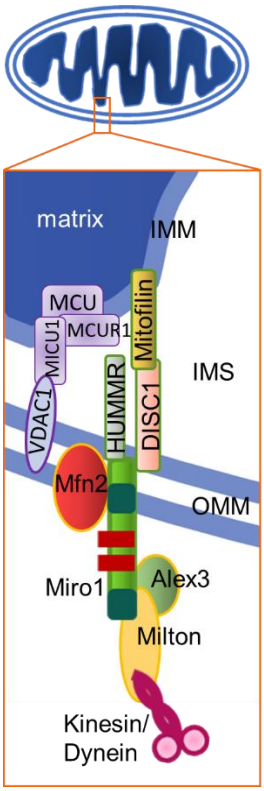

Schematic overview of the multiple protein interactions involved in mitochondrial transport. Miro interacts with Milton and the motor proteins Kinesin or Dynein. The interaction with Mfn2 allows for coordinated regulation of mitochondrial fusion and transport. The interaction of the Miro/ Milton complex with Alex3 probably facilitates control of mitochondrial distribution. HUMMR likely promotes mitochondrial transport into the anterograde direction. The same function was proposed for DISC1. Interestingly, DISC1 and HUMMR are located in the intermembrane space, therefore raising the possibility of intramitochondrial signals in regulating mitochondrial transport.

IMM: inner mitochondrial membrane. **IMS**: intermembrane space. **OMM**: outer mitochondrial membrane. **Mfn2**: Mitofusin2. **MCU**: mitochondrial calcium uniporter. **MICU**: mitochondrial calcium uptake (Perocchi, Gohil et al. 2010). **MCU**: mitochondrial calcium uniporter (Baughman, Perocchi et al. 2011) (De Stefani, Raffaello et al. 2011). **MCUR1**: mitochondrial calcium uniporter regulator 1 (Mallilankaraman, Cardenas et al. 2012).

Figure 2: Schematic overview of the mitochondrial transport protein complex

In summary, it seems that mitochondrial transport is facilitated by a multi-protein complex, with a set of different proteins, which are required for regulation of transport. Miro is a core component of this complex and it is likely to assume that in future more interaction partner will be identified. Furthermore, it seems that mitochondrial transport is not only regulated by signals outside of mitochondria, but also by intrinsic mitochondrial signals. Miro seems to be located at the centre of the complex, connecting the complex members of the OMM (e.g. Mfn2, Alex3, Milton, Kinesin/Dynein) to proteins in the intermembrane space (HUMMR, DISC1) and the IMM (Mitofilin, MCU).

1.4.3 Miro as calcium binding protein

Proper distribution of mitochondria to sites of high energy consumption is most important for the function and maintenance of cells and especially of highly polarized and big neurons. Therefore, mitochondrial transport requires a switch to turn off transport at the destination site where mitochondria are currently needed. Confirmed by the observations of a number of different studies, the signal to switch off mitochondrial transport most likely is an increase of cytosolic calcium concentration (Chang, Honick et al. 2006) (Hollenbeck and Saxton 2005) (Szabadkai, Simoni et al. 2006). Calcium enters the cell at sites of high energy demands like synapses where ATP is needed for transmitter release and recycling. The protein that mediates the calcium-dependent transport stop is Miro. Interestingly, it seems that the molecular mechanism by which Miro mediates the arrest of transport is different in *drosophila* and vertebrates:

The group of Wang and Schwarz investigated mitochondrial motility in *drosophila* and found that calcium binding to Miro leads to a direct interaction of Miro with kinesin heavy chain, causing the motor protein to disconnect from microtubules and in this way stopping mitochondrial transport, while the Miro/Milton/kinesin complex remains intact at the OMM (Wang and Schwarz 2009).

In contrast to the *drosophila* model, it seems that in vertebrates kinesin is not interacting with Milton, but binds directly to Miro (Macaskill, Rinholm et al. 2009). As soon as calcium binds to the EF hands of Miro, kinesin disconnects from Miro and in this way mitochondria are derailed from the microtubule tracks (Macaskill, Rinholm et al. 2009).

Calcium binding to the EF hand domains was only sufficient to mediate arrest of transport when both EF hand domains and both GTPase domains were intact (Saotome, Safiulina et al. 2008). Calcium-mediated stop of mitochondrial transport is dose dependent, with a calcium concentration of ~1 µM (Macaskill, Rinholm et al. 2009) to 50 µM (Wang and

Schwarz 2009) inhibiting ~50 % of mitochondrial movement. These concentrations are within the physiological range as calcium influx into synapses through NMDA receptors can increase calcium concentration to 6 µM and more at repeated stimuli (Noguchi, Matsuzaki et al. 2005). The calcium-dependent arrest of mitochondrial transport is especially important to protect neurons from glutamate excitotoxicity as shown in a study in *drosophila* expressing loss of function mutants of Miro in which neuronal survival was significantly impaired due to excitotoxicity (Wang and Schwarz 2009).

One recent study suggested that not only cytosolic calcium regulates mitochondrial traffic but also calcium influx into the mitochondrial matrix through the MCU (Chang, Niescier et al. 2011). The speed of mitochondrial movement was negatively correlated to mitochondrial matrix calcium concentration. Additionally, influx of calcium into mitochondria required functional EF hand domains of Miro (Chang, Niescier et al. 2011). Chang and colleagues proposed a model, in which elevated cytosolic calcium concentration leads to rapid increase of mitochondrial matrix calcium via the MCU, controlled by Miro, which in turn leads to stop of mitochondrial transport (Chang, Niescier et al. 2011).

1.4.4 Miro is involved in ER-mitochondrial interaction

Single mitochondria and the endoplasmic reticulum (ER) are tethered by a big protein complex called ER-mitochondrial encounter structure (ERMES) in yeast (Kornmann and Walter 2010). The yeast orthologue of Miro, Gem1 was identified as regulatory component of the ERMES complex, meaning Gem1 is not crucial for the assembly and stability of the complex, but for its proper organization and function (Kornmann, Osman et al. 2011). Localization of Gem1 to ERMES requires the second EF hand domain and the first GTPase domain, whereas the second GTPase domain controls ERMES function (Kornmann, Osman et al. 2011). Because the affinity of Miro to bind calcium was relatively low (K_d ~50 µM) (Wang and Schwarz 2009) it is possible that the ER-mitochondria connection sites create a sub-compartement in which local calcium concentration can reach much higher concentrations, enabling calcium to bind to the EF hands and mediate exchange of metabolites, calcium and signalling between both organelles (Kornmann, Osman et al. 2011).

ERMES foci are mostly located at mitochondrial restriction sites, where mitochondrial DNA (mtDNA) is replicated (Hobbs, Srinivasan et al. 2001) (Hanekamp, Thorsness et al. 2002) and mitochondria are subsequently dividing (Murley, Lackner et al. 2013). Gem1 plays an important role to separate the newly divided mitochondrial tips and distribute the synthesized mtDNA alongside with the mitochondria (Murley, Lackner et al. 2013). These

findings may explain the observation why *gem1*Δ yeast lines lose mtDNA over time (Frederick, McCaffery et al. 2004), because the co-transport of newly synthesized mtDNA to the newly divided mitochondrial tips is disrupted in *gem1*Δ yeast. In mammalian cells Miro1 was also observed to localize in discrete puncta at ER-mitochondrial contact sites (Kornmann, Osman et al. 2011). To date some members of a potential ER-mitochondrial encounter structure are identified in mammalian cells, amongst them are Mitofusin2 (de Brito and Scorrano 2008), VDAC1 and Grp75 (Rapizzi, Pinton et al. 2002) (Szabadkai, Bianchi et al. 2006) and Miro (Kornmann, Osman et al. 2011), which is interesting because the interaction of Miro and Mitofusin2 was also suggested to be important for a co-ordinated regulation of mitochondrial fusion and transport.

1.4.5 Miro is targeted by the PINK1/Parkin pathway for mitochondrial quality control

In 2009 Weihofen and colleagues identified PINK1 and Parkin as interaction partner of the Miro/Milton complex (Weihofen, Thomas et al. 2009). This interaction was initiated by depolarization of the mitochondrial membrane (Wang, Winter et al. 2011). Weihofen and colleagues further proposed that ubiquitination by Parkin and subsequent proteasomal degradation of Miro and mitofusin might be the initial step to isolate damaged mitochondria from the mitochondrial network and to prevent the fusion and subsequent spreading of the toxic insult, e.g. oxidative stress, to other healthy mitochondria. The resulting immobile and fragmented mitochondria are ready for autophagosomal uptake and lysosomal clearance (Weihofen, Thomas et al. 2009). The quarantine of damaged mitochondria for subsequent degradation seems to be very important for the maintenance of neuronal integrity. As mentioned before, disruption of the PINK1/ Parkin-induced clearance of dysfunctional mitochondria in PINK1 or Parkin knockout flies lead to loss of DA neurons (Park, Lee et al. 2006) (Clark, Dodson et al. 2006). On the other hand, disruption of Miro, Milton or kinesin heavy chain (KHC) function was able to rescue PINK1 mutant phenotypes, whereas overexpression of Miro1 caused a similar phenotype, including enlargement of mitochondria and loss of DA neurons (Liu, Sawada et al. 2012), supporting the idea that the arrest of mitochondrial movement is necessary for mitophagy. These findings support the relevance of mitochondrial quality control for neurons and the important interaction of PINK1/ Parkin and Miro within this mechanism.

1.4.6 BDNF and Miro – Synaptic maintenance and plasticity

The brain-derived neurotrophic factor (BDNF) is crucial for neuronal survival and the development and plasticity of synapses. BDNF signalling is operated via two different cell membrane receptors: TrkB and p75. TrkB receptor activation in turn drives the activation of the MAPK-PI3K-pathway that ultimately leads to release of calcium from internal stores (Numakawa, Suzuki et al. 2010). Beyond that, BDNF was reported to increase mitochondrial respiration in the brain, but the mechanism behind this function remained elusive (Markham, Cameron et al. 2004). The idea of a possible link between BDNF and Miro protein arose from the observation that BDNF activity causes an impairment of retrograde and anterograde axonal transport (Su, Ji et al. 2014). This BDNF-mediated influence on mitochondrial transport seems to be operated by the activation of PI3K and PLCγ via the TrkB receptor. This pathway ultimately leads to release of calcium from intracellular stores through IP3 receptors (Su, Ji et al. 2014). Subsequently, increased cytosolic calcium concentration enables calcium to bind to the EF hands of Miro and stops moving mitochondria at synapses. In this way the interplay of BDNF with Miro causes the accumulation of mitochondria at presynaptic sites, which is required for BDNF-induced release of neurotransmitters (Su, Ji et al. 2014).

1.4.7 VopE and Miro – Mitochondria-mediated immune response

A recent study linked Miro1 and Miro2 to the innate immune response. Mitochondria are already known to contribute to the innate immune response (Cloonan and Choi 2013), as many bacterial infection pathways target mitochondria (Arnoult, Carneiro et al. 2009). An important effector of the *Vibrio cholera* type III secretion system (T3SS) is VopE. (Alam, Miller et al. 2011). A recent study identified a mitochondrial targeting sequence (MTS) at the N-terminus and a toxic GTPase-activating protein (ToxGAP) domain at the C-terminus of VopE (Suzuki, Danilchanka et al. 2014). ToxGAP domains are often found in bacterial T3SS effector proteins, like SptP and ExoS, and have been reported to cause the collapse of the actin cytoskeleton of infected cells (Aktories, Schmidt et al. 2000). In contrast, the ToxGAP domain of VopE was found to influence mitochondrial morphology (Suzuki, Danilchanka et al. 2014). This function was mediated by the direct binding of VopE to the N-terminal GTPase domain of Miro1, which caused a 5-fold increase of the GTPase activity of Miro1 (Suzuki, Danilchanka et al. 2014). The results of this study suggest that VopE inhibits the calcium-dependend regulation of mitochondrial transport by increasing Miro's GTPase activity. In this way VopE is able to influence the mitochondrial-mediated innate immune response (Suzuki, Danilchanka et al. 2014). Moreover, VopE is the first described

GAP that regulates Miro GTPase activity. As the GTP hydrolysis rate of Miro is relatively low, it is likely that Miro GTPase activity is regulated by GAPs and guanine nucleotide exchange factors (GEFs) (Kornmann, Osman et al. 2011) (Koshiba, Holman et al. 2011), but still to date endogenous GAPs and GEFs that influence Miro proteins remain unknown.

The combined information of studies throughout the recent years suggests that Miro is not simply an adaptor protein to link mitochondria to motor proteins for regulation of mitochondrial transport. Instead, Miro's ability to interact with kinesin and dynein to mediate transport along microtubules likely developed in metazoans, because other interaction partners of that complex, like Milton or PINK1 are not existent in *D. discoideum* (Vlahou, Elias et al. 2011), yeast or plants (Yamaoka and Leaver 2008). The primary function of Miro proteins could therefore be involved in mitochondrial homeostasis rather than transport (Vlahou, Elias et al. 2011). All eukaryotic lineages possess Miro proteins, whereas no homologs could be identified in prokaryotes (Vlahou, Elias et al. 2011). These findings suggest that Miro evolved very early in the evolution of eukaryotes, most likely together with the development of mitochondria (Vlahou, Elias et al. 2011).

While summarizing the obtainable information about Miro proteins, it is striking in how many pathways Miro is involved around mitochondrial maintenance. Taking together the available pieces of the puzzle most of the numerous functions of Miro can be boiled down to the following:

i) Miro regulates mitochondrial transport by multiple direct or indirect interactions of its N-terminal GTPase domain with different other adaptor proteins like Milton, Mitofusin, kinesin, dynein, HUMMR, DISC1, Alex3;

ii) Miro's interaction with other proteins, like Milton, Mitofusin, Alex3 and kinesin is regulated by calcium binding to the EF hand domains and at least in part by the C-terminal GTPase domain.

However, it remains elusive how many other direct and indirect interaction partner of Miro proteins exist, which differential functions Miro1 and Miro2 exactly have and how the different interplays are executed in a stress-response and tissue specific manner.

1.5 Patient-derived fibroblasts as cell model

Patient-derived fibroblasts are a cell model that is frequently used in PD research. The cells harbour the whole genetic background of the PD patient and express the disease-relevant protein at endogenous levels. This is an advantage compared to other cell models, in which the protein of interest is artificially over-expressed to an extent that does not always reflect the situation in the patient cells. This was for example the case in a study investigating the E64D mutation in DJ-1 by Krebiehl and colleagues (Krebiehl, Ruckerbauer et al. 2010). Fibroblasts from the homozygous mutation carrier revealed that DJ-1 protein was actually significantly decreased *in vivo*. The mitochondrial phenotype therefore arose from the loss of DJ-1 protein rather than from the DJ-1-E64D mutant protein itself (Krebiehl, Ruckerbauer et al. 2010).

Although energy production in fibroblasts is based mainly on glycolysis rather than on mitochondrial respiration, still mitochondrial phenotypes can be robustly assessed in fibroblasts as shown by a number of different studies throughout the last years.

Patient-derived fibroblasts harbouring the homozygous nonsense mutation W437X in PINK1 displayed a reduction in respiratory activity and increase in mitochondrial ROS production (Piccoli, Sardanelli et al. 2008).

Another study characterized the effects of homozygous PINK1 mutations Q456X and V170G. Interestingly, the mutations caused different phenotypes on mitochondrial function and morphology: PINK1-V170G caused an increased ROS production in enlarged and swollen mitochondria, whereas PINK1-Q456X caused reduction of ATP production (Grunewald, Gegg et al. 2009).

Parkin mutations were found to cause mitochondrial phenotypes in patient-derived fibroblasts as well. Mortiboys et al. found a reduction of complex I activity and ATP-production, accompanied by an alteration of mitochondrial morphology (Mortiboys, Thomas et al. 2008). The same workgroup applied the Parkin mutant fibroblasts on a screen for compounds that might improve the mitochondrial phenotype and were able to identify ursocholanic acid and ursodeoxycholic acid, which markedly rescued the phenotypes and are therefore regarded as promising compounds for neuroprotective treatment (Mortiboys, Aasly et al. 2013).

In another study it was also possible to detect severe mitochondrial phenotypes in Parkin mutant fibroblasts, like structural changes of mitochondria, disruption of the energy

metabolism and increase of mitochondrial ROS production, a phenotype caused by deletion of exon 2-3 in Parkin (Pacelli, De Rasmo et al. 2011).

Impaired mitochondrial function, reflected by decreased mitochondrial membrane potential, increased oxygen consumption and decreased ATP-production was also a phenotype observed in LRRK2-G2019S mutant fibroblasts (Papkovskaia, Chau et al. 2012).

Taken together, fibroblasts represent a good cellular model that display relevant mitochondrial phenotypes, which are involved in the pathological development of PD, including decreased complex I activity, lack of ATP, increased oxidative stress and depolarization of mitochondrial membrane potential. These changes in mitochondrial function are often accompanied by alteration of mitochondrial morphology, which also can be robustly assessed in fibroblasts.

Fibroblasts from PD patients with mutations in mitochondria-related genes therefore represent a good model for first characterization of the effects of mutations on mitochondrial function.

1.6 Aim of the study

Of all PD cases only about 11 % are familial inherited (Shino, McGuire et al. 2010), meaning that the majority of PD cases are sporadic with unknown cause for the disease. Still, mitochondrial pathways, e.g. dysfunction of the mitochondrial respiratory chain, oxidative stress, dysfunction of mitochondrial quality control and transport, or disruption of calcium homeostasis, play an important role in the pathogenesis of both, sporadic and familial cases of PD. Investigation of the underlying mechanisms in PD patients with specific mutations allows insight into the development of the disease. This knowledge supports also the investigation of the disease causing mechanisms in sporadic PD as the same cellular pathways seem to be involved.

Although during recent years numerous studies underlined the importance of the Miro protein family for mitochondrial maintenance and distribution, especially for the health and integrity of neuronal function, a first effort to establish an association between *RhoT1* or *RhoT2*, the genes encoding for Miro1 and Miro2, and the development of PD in 2012 by Anvret and colleagues failed (Anvret, Ran et al. 2012). In this study, a Swedish case-control cohort was screened for single nucleotide polymorphisms (SNP) in order to assess, whether they were associated with PD or the age of onset of PD. No association was established, however, the authors admitted that their study cannot rule out the presence of

rare disease-associated mutations not captured by the SNPs and therefore Miro1 or Miro2 are still promising candidates to cause PD.

For the present study the first PD-associated Miro1 mutations were investigated with regard to their pathogenic potential. The main aim of the study was the characterization of mitochondrial phenotypes in patient-derived fibroblasts to investigate whether mutations in Miro1 can lead to mitochondrial dysfunction that is sufficient to cause neurodegeneration in PD. The results of the investigations emphasize the important role of Miro1 for mitochondrial maintenance and function and adds Miro1 as potential novel risk gene to the pathogenic pathways leading to PD.

2 Materials and Methods

2.1 Chemicals, Kits, Equipment and Software

2.1.1 Chemicals and reagents

Table 1: Chemicals and reagents

Chemical	Supplier	Order number
10x buffer red for restriction enzymes	Thermo Fisher Scientific, Braunschweig, Germany	BR5
4',6-Diamidino-2-phenylindole dihydrochloride (**DAPI**)	Thermo Fisher Scientific, Braunschweig, Germany	D3571
5,5'-Dithiobis(2-nitrobenzoic) acid (**DNTB**)	Sigma Aldrich Chemie GmbH, Munich, Germany	D8130
Acetyl-CoA	Sigma Aldrich Chemie GmbH, Munich, Germany	A2056-25MG
Acrylamide/ Bis-acrylamide 30 % solution	Sigma Aldrich Chemie GmbH, Munich, Germany	A3699-100ML
Agarose	Sigma Aldrich Chemie GmbH, Munich, Germany	A9539
Amersham™ ECL™ Prime Western Blotting Detection Reagent	GE Healthcare, Freiburg, Germany	RPN 2232
Amersham™ ECL™ Select Western Blotting Detection Reagent	GE Healthcare, Freiburg, Germany	RPN 2235
Amonium persulfate (**APS**)	Sigma Aldrich Chemie GmbH, Munich, Germany	A3678
Ampicillin sodium salt	Sigma Aldrich Chemie GmbH, Munich, Germany	A9518-25G
Annexin V, Alexa Fluor® 568 conjugate	Thermo Fisher Scientific, Braunschweig, Germany	A13202
Antimycin A	Sigma Aldrich Chemie GmbH, Munich, Germany	A8674-25MG

bicarbonate-free basal DMEM powder	Sigma Aldrich Chemie GmbH, Munich, Germany	D5030
Blasticidin S HCl	Invitrogen GmbH, Karlsruhe, Germany	R210-01
Bovine serum albumin (**BSA**)	AppliChem GmbH, Darmstadt, Germany	A6588,0100
Bradford solution	Bio-Rad Laboratories, Munich, Germany	5000201
Bromphenole blue	Sigma Aldrich Chemie GmbH, Munich, Germany	B0126-25G
Carbonyl cyanide 4-(trifluoromethoxy) phenylhydrazone (**FCCP**)	Sigma Aldrich Chemie GmbH, Munich, Germany	C2920-10MG
Complete Protease Inhibitor	Roche Applied Science, Mannheim, Germany	04693124001
D(+)-Sucrose	Sigma Aldrich Chemie GmbH, Munich, Germany	84100
D-Glucose	Sigma Aldrich Chemie GmbH, Munich, Germany	D8375
Dimethyl sulfoxide (**DMSO**)	Sigma Aldrich Chemie GmbH, Munich, Germany	D8418
DL-Dithiothreitol (**DTT**)	Sigma Aldrich Chemie GmbH, Munich, Germany	D-9163-25G
DMEM without Glucose	Thermo Fisher Scientific, Braunschweig, Germany	11966-025
DMEM/Ham's-F12 [-] L-Glutamine	Thermo Fisher Scientific, Braunschweig, Germany	21331-046
DNA T4 ligase	New England Biolabs GmbH, Frankfurt, Germany	M0202T
DPBS/ Modified [+] Ca^{2+}, [+] Mg^{2+} (**DPBS+/+**)	Thermo Fisher Scientific, Braunschweig, Germany	SH30264.01
Dulbeco's modified Eagle medium (**DMEM**) [+] 4,5 g/L D-Glucose, [+] L-Glutamine, [-] Pyruvate	Thermo Fisher Scientific, Braunschweig, Germany	41965-062

EcoRI restriction enzyme	Thermo Fisher Scientific, Braunschweig, Germany	ER0271
Ethylene Glycol-bis(2-aminoethylether)-N,N,N',N'-tetraacetic acid (**EGTA**)	Sigma Aldrich Chemie GmbH, Munich, Germany	E3889
Fetal bovine serum (**FBS**)	Thermo Fisher Scientific, Braunschweig, Germany	10270106
Glycerin	Sigma Aldrich Chemie GmbH, Munich, Germany	G6279
Glycine	AppliChem GmbH, Darmstadt, Germany	A3707,1000
Goat Serum	Sigma Aldrich Chemie GmbH, Munich, Germany	G9023
HEPES	Sigma Aldrich Chemie GmbH, Munich, Germany	H3375
Histamine	Sigma Aldrich Chemie GmbH, Munich, Germany	H7125-1G
Hydrogen peroxide (**H_2O_2**)	AppliChem GmbH, Darmstadt, Germany	A1134,0250
LB broth	Sigma Aldrich Chemie GmbH, Munich, Germany	L7275
LB broth with agar	Sigma Aldrich Chemie GmbH, Munich, Germany	L7025
L-Glutamine	Thermo Fisher Scientific, Braunschweig, Germany	35050-038
LysoTracker® red	Thermo Fisher Scientific, Braunschweig, Germany	L-7528
LysoTracker® yellow HCK-123	Thermo Fisher Scientific, Braunschweig, Germany	L-12491
Magnesium chloride (**$MgCl_2$**)	Sigma Aldrich Chemie GmbH, Munich, Germany	M8266
Mannitol	Sigma Aldrich Chemie GmbH, Munich, Germany	M4125
Midori Green Advance DNA stain	Biozym Scientific, Hessisch Oldendorf, Germany	617004

MitoSOX™ Red Mitochondrial Superoxide Indicator	Thermo Fisher Scientific, Braunschweig, Germany	M36008
MitoTracker® green FM	Thermo Fisher Scientific, Braunschweig, Germany	M-7514
MitTracker® deep red FM	Thermo Fisher Scientific, Braunschweig, Germany	M224426
N,N,N',N'-Tetramethyl-ethylenediamine (**TEMED**)	Sigma Aldrich Chemie GmbH, Munich, Germany	T9281-25ML
Non-essential amino acids	Thermo Fisher Scientific, Braunschweig, Germany	K0293
Nonidet P 40 substitute (**NP40**)	VWR International, Pennsylvania, USA	492016-100
nuclease-free water	Qiagen GmbH, Hilden, Germany	
Oligomycin A	Sigma Aldrich Chemie GmbH, Munich, Germany	75351-5MG
One Shot® TOP10 Chemically competent E. coli	Thermo Fisher Scientific, Braunschweig, Germany	c4040-03
OPTI-MEM [+] HEPES, [+] 2,4 g/L Sodium Bicarbonate, [+] L-Glutamine	Thermo Fisher Scientific, Braunschweig, Germany	31985-062
Oxaloacetic acid	Sigma Aldrich Chemie GmbH, Munich, Germany	O7753
PageRuler Plus Prestained Protein Ladder	Thermo Fisher Scientific, Braunschweig, Germany	26620
Paraformaldehyde (**PFA**)	Sigma Aldrich Chemie GmbH, Munich, Germany	1.04005.1000
Penicillin-Streptomycin	Thermo Fisher Scientific, Braunschweig, Germany	15140-122
Phosphate buffered saline (**PBS**)	Thermo Fisher Scientific, Braunschweig, Germany	14190-169
Piericidin A	Santa Cruz, Dallas, Texas	sc-202287
Polybrene®	Sigma Aldrich Chemie GmbH, Munich, Germany	107689
Potassium bicarbonate (**$KHCO_3$**)	Sigma Aldrich Chemie GmbH, Munich, Germany	60339

Potassium chloride (**KCl**)	Sigma Aldrich Chemie GmbH, Munich, Germany	P9541
Rotenone	Sigma Aldrich Chemie GmbH, Munich, Germany	R8875-5G
Skim Milk Powder	Sigma Aldrich Chemie GmbH, Munich, Germany	70166-500G
Sodium chloride (**NaCl**)	Sigma Aldrich Chemie GmbH, Munich, Germany	S3014
Sodium dodecyl sulfate (**SDS**) solution	Sigma Aldrich Chemie GmbH, Munich, Germany	71736
Staurosporine	Sigma Aldrich Chemie GmbH, Munich, Germany	S5927-1MG
SV 40 large T antigene lentivirus	Applied Biological Materials Inc., Richmond, Canada (Biocat)	G203 EVOAMB
Tetramethylrhodamine methyl ester (**TMRE**)	Thermo Fisher Scientific, Braunschweig, Germany	T-669
TransIT®-2020 transfection reagent	Mirus Bio LLC, Madison, USA	MIR 5400
Triton X-100	Sigma Aldrich Chemie GmbH, Munich, Germany	X100
Trizma base	Sigma Aldrich Chemie GmbH, Munich, Germany	T1503
Trizma hydrochloride	Sigma Aldrich Chemie GmbH, Munich, Germany	5941
Trypsin-EDTA (0,05 %), phenol red	Thermo Fisher Scientific, Braunschweig, Germany	25300-054
Trypsin-EDTA (0,25 %), phenol red	Thermo Fisher Scientific, Braunschweig, Germany	25200-056
Tween-20	Sigma Aldrich Chemie GmbH, Munich, Germany	P1379
Valinomycin	Sigma Aldrich Chemie GmbH, Munich, Germany	V0627-25MG
Vectashield	Vector Laboratories Inc., Burlingame, USA	H-1000
XF-calibrant solution	Seahorse Bioscience, Massachusetts, USA	

XhoI restriction enzyme	Thermo Fisher Scientific, Braunschweig, Germany	ER0695
β-Mercaptoethanol	Thermo Fisher Scientific, Braunschweig, Germany	31350-010

2.1.2 Kits

Table 2: Kits

Kit	Supplier	Order number
BLOCK-iT Inducible Pol II miR RNAi Expression Vector Kit with EmGFP	Invitrogen GmbH, Karlsruhe, Germany	K4939
Complex I Enzyme Activity Dipstick Assay Kit	Abcam, Cambridge, UK	ab109720
Fluo-4 Direct™ Calcium Assay Kit	Thermo Fisher Scientific, Braunschweig, Germany	F10471
High Fidelity complimentary DNA Synthesis Kit	Roche Applied Science, Mannheim, Germany	PE-401-4001
High pure RNA isolation Kit	Roche Applied Science, Mannheim, Germany	11828665001
LookOUT® Mycoplasma PCR Detection Kit	Sigma Aldrich Chemie GmbH, Munich, Germany	MP0035-1KT
QIA Blood and Tissue DNA kit	Qiagen GmbH, Hilden, Germany	69506
Qiagen Plasmid Midi/Maxi Kit	Qiagen GmbH, Hilden, Germany	12143 / 12663
QIAprep spin MiniPrep Kit	Qiagen GmbH, Hilden, Germany	27106
QIAquick Gel Extraction Kit	Qiagen GmbH, Hilden, Germany	28704
QIAquick PCR purification Kit	Qiagen GmbH, Hilden, Germany	28104

2.1.3 Equipment

Table 3: Equipment

Equipment	Supplier
Agarosegel tank	VWR International, Pennsylvania, USA
Bacterial incubator	Binder, Tuttlingen, Germany
BD LSR Fortessa	Becton, Dickinson and Company©, Erembodegem, Belgium
Biofuge pico and fresco	Thermo Fisher Heraeus, Hanau, Germany
Centrifuge 5810R	Eppendorf, Hamburg, Germany
Centrifuge Evolution Rc	Thermo Fisher Sorvall, Hamburg, Germany
Centrifuge Micro 22R	Hettich, Tuttlingen, Germany
Confocal microscope Axiovert 2000, with ApoTome, CO_2 humidifier, plan-apochromate objectives, AxioCam MRc	Carl Zeiss Microimaging GmbH, Jena, Germany
Confocal microscope Axiovert 2000, with spinning disc, CO_2 humidifier, plan-apochromate objectives, Hamamatsu camera C11440	Carl Zeiss Microimaging GmbH, Jena, Germany
Countess II cell counter	Life Technologies/ Thermo Fisher Scientific, Braunschweig, Germany
CyAn ADP Analyzer	Beckman Coulter, California, USA
Geldoc system T:Genius	Syngene, Cambridge, UK
iBlot 2	Invitrogen GmbH, Karlsruhe, Germany
Incubator	Panasonic Biomedical, London, UK
Microtiter plate reader	Bio-Rad laboratories GmbH, Munich, Germany
Milli-Q Synthesis	Millipore Corporation, Darmstadt, Germany
NanoDrop (ND1000)	Peqlab, Erlangen, Germany
ODYSSEY chemiluminescence 2800 Fc	LI-COR, Lincoln, USA
Pipetboy Integra	Bioscience, Fernwald, Germany
Power pack	Bio-Rad Laboratories, Munich, Germany
Spectrophotometer SPECORD 210Plus	Analytic Jena AG, Jena, Germany
Stereo microscope MZ7	Leica, Solms, Germany
Sterile bench Herasafe	Thermo Fisher Heraeus, Hanau, Germany

Synergy Mx microplate Reader	BioTek Instruments, Inc., Bad Friedrichshall, Germany
Thermocycler TP Professional standard gradient 96	Biometra, Analytic Jena AG, Jena, Germany
Thermomixer comfort	Eppendorf, Hamburg, Germany
WB TANK	Bio-Rad Laboratories, Munich, Germany
XF^{e}96 extracellular flux Analyzer	Seahorse Bioscience, Massachusetts, USA

2.1.4 Consumables

Table 4: Plastic ware

Plastic ware	**Supplier**	**Order number**
cell culture consumables	BD Biosciences, Heidelberg, Germany; Corning, Kaiserslautern, Germany; Greiner Bio-One GmbH, Frickenhausen, Germany; Thermo Fisher Scientific, Braunschweig, Germany	
coverslips	Carl Rhoth GmbH, Karlsruhe, Germany	
iBlot 2 NC Regular/ Mini Stacks (Nitrocellulose membrane)	Invitrogen GmbH, Karlsruhe, Germany	IB23001 / IB23002
Nunc™ Lab-Tek™ Chamber slides	Thermo Fisher Scientific, Braunschweig, Germany	155382 / 155409
PCR reaction tubes	Eppendorf, Hamburg, Germany	
pipette tips	Eppendorf, Hamburg, Germany	
reaction tubes	Eppendorf, Hamburg, Germany	
XF^{e}96 assay cartridge	Seahorse Bioscience, Massachusetts, USA	102416-100
XF^{e}96 cell culture microplate	Seahorse Bioscience, Massachusetts, USA	101085-004

2.1.5 Software

Table 5: Software

Software	Purpose	Supplier
Flowjo 10	evaluation of FACS data	Flowjo LLC, Oregon, USA
ImageJ	evaluation of microscopy images	Wayne Rasband, NIH
Primer3	primer design	freeware
Prism 6	statistical analysis	GraphPad Software, Inc., La Jolla, USA
Summit 4.3.02b2451	evaluation of FACS data	Beckman Coulter, California, USA
ZEN Blue	evaluation of microscopy images	Carl Zeiss Microimaging GmbH, Jena, Germany
FinchTV	visualization of DNA chromatograms	Geospiza Inc., Seattle, USA

2.2 *In silico* prediction of pathogenic effects of *RhoT1* mutations

In silico prediction of the pathogenic effects of the identified *RhoT1* mutations was performed by Patrick May (LCSB, University of Luxembourg, Belvaux, Luxembourg). The *RhoT1* mutations were analysed with the analysis tools shown in (Table 6).

Table 6: Applied analysis tools for in silico prediction of pathogenic effects of RhoT1 mutations

Analysis tool	**Database/ source**
SIFT (Sorting Intolerant from Tolerant), sift.jcvi.org **Polyphen2** (Polymorphism Phenotyping v2), genetics.bwh.harvard.edu/pph2/ **Mutation taster**, www.mutationtaster.org **Mutation assessor**, www.mutationassessor.org **FATHMM** (Functional Analysis through Hidden Markov Models), fathmm.biocompute.org.uk	http://www.ncbi.nlm.nih.gov/pubmed/21520341 http://annovar.openbioinformatics.org/en/latest/ http://sites.google.com/site/jpopgen/dbNSFP
LRT pred. (Likelihood ratio test)	http://www.genetics.wustl.edu/jflab/lrt_query.html (Chun and Fay 2009)
radial SVM pred. **LR pred.**	(Dong, Wei et al. 2015)

2.3 Homology modelling of Miro1

To date, there is no crystal structure for human Miro1 available. Klosowiak et al. established the first partial crystal structure for the *drosophila* ortholog dMiro (Klosowiak, Focia et al. 2013). Based on the crystal structure of dMiro a homology model for human Miro1 was created by Enrico Glaab (LCSB, University of Luxembourg, Belvaux, Luxembourg).

A multiple sequence alignment for the amino acid sequences of human Miro1 (Swiss-Prot accession: Q8IXI2) and dMiro (Swiss-Prot accession: Q8IMX7) was performed using the Clustal Omega software (Sievers, Wilm et al. 2011) and SIAS software (http://imed.med.ucm.es/Tools/sias.html), with BLOSUM62 substitution matrix for similarity estimation. The alignment revealed a sequence similarity of 60.51 % of both orthologs.

I-TASSER software for protein structure prediction with default parameters (Zhang 2008) was then used to derive the crystal structure of human Miro1 from the dMiro structure (PDB: 4COJ).

The resulting model was used to determine the amino acid sequence conservation scores by ConSurf software (UNIREF90 database and MAFFT program) (Ashkenazy, Erez et al. 2010).

Protein stability of the Miro1 mutant proteins were calculated for physiological conditions of 37°C and a pH of 7 with the neural-network based Network Enthalpic Modelling (NeEMO) prediction method (Giollo, Martin et al. 2014) and the support vector machine approach I-MUTANT 2.0 (Capriotti, Fariselli et al. 2005).

2.4 Genotyping of cohorts for *RhoT1* mutations

Existing genetic databases including 1500 genomes available on a whole exome server were analyzed by Manu Sharma (Hertie-Institute for Brain Research, University of Tübingen, Tübingen).

Further analysis of 61486 unrelated individuals available from different databases (snp138, Avsnp138, cosmic70, cosmic68wgs, nci60, esp6500si, esp6500siv2, cg46, cg69, 1000g2014oct, exac02, exac alleles, popfreq) were done by Peter Lichtner (Helmholtz Centre, Munich, Germany).

A large independent cohort of DNA samples of 1238 German PD patients and 662 healthy controls from the KORA cohort (KORA-Study Group consists of A. Peters, J. Heinrich, R. Holle, R. Leidl, C. Meisinger, K. Strauch, and their co-workers, who are responsible for the design and conduct of the KORAstudies) was genotyped by the laboratory of Peter Lichtner (Helmholtz Centre, Munich, Germany) as well.

2.5 Cell Culture

All fibroblast and M17 cells were grown in cell culture approved flasks and dishes (BD Bioscience, Heidelberg, Germany; Corning, Kaiserslautern, Germany; Greiner Bio-One GmbH, Frickenhausen, Germany; Thermo Fisher Scientific, Braunschweig, Germany). The cells were incubated at 37°C and 5 % CO_2. For long term storage stocks were frozen in freezing medium (Table 7) and stored in liquid nitrogen or at -150°C. When thawed, cells were resuspended in medium and plated into appropriate cell culture flasks. The medium containing DMSO (Sigma Aldrich Chemie GmbH, Munich, Germany) was replaced with fresh medium on the next day.

All cells were tested regularly for contamination with Mycoplasma using the LookOUT® Mycoplasma PCR Detection Kit (Sigma Aldrich Chemie GmbH, Munich, Germany) according to manufacturer's instructions.

Table 7: Freezing medium

Cell line	Proportion	Chemical
Native fibroblasts	90 %	FBS
	10 %	DMSO
Immortalized fibroblasts	50 %	DMEM +/+
	40 %	FBS
	10 %	DMSO
M17 cells	50 %	DMEM/Ham´s-F12 +/+
	40 %	FBS
	10 %	DMSO

2.5.1 Fibroblast cell culture

2.5.1.1 Skin biopsy for cultivation of fibroblasts

Prior to the skin biopsies, informed consent was obtained from each patient in this study (Table 8). The informed consent was approved by the Ethics Committee of the Medical faculty and the University Hospital Tübingen, Germany.

Skin biopsy was taken from patients, transferred to a 50 mL falcon containing DMEM+/+ (Table 9) and processed immediately. First, the biopsy was transferred to a 6 cm dish and washed 3x in PBS (Thermo Fisher Scientific, Braunschweig, Germany). Fatty tissue and hair was removed from the skin. Skin biopsy was then cut into 8 – 12 pieces and 3 – 4 of these biopsy pieces were placed into a T25 flask with 2 mL DMEM+/+ (Table 9). By shaking gently the skin pieces were distributed equally inside the flask, not too close to the edges. The flasks were incubated for at least one week without moving them to allow cells to attach and grow. After one week, half of the medium was replaced with fresh medium. From this point on, medium was changed twice every week. When fibroblasts started growing out from the skin samples and were confluent in the flask, cells were trypsinated and stocks were frozen. This procedure was repeated several times.

Table 8: Healthy control and patient-derived fibroblasts

Name	Internal ID	Gender	Year of birth	Age at biopsy
Ctrl 1	18156	female	1954	57
Ctrl 2	15243	male	1956	55
Ctrl 3	18075	female	1939	72
Miro1-R272Q		female	1935	78
Miro1-R450C		female	1958	54

2.5.1.2 Immortalization of fibroblasts

Fibroblasts were immortalized with a pLenti-III-SV40 construct (Applied Biological Materials Inc., Richmond, Canada), expressing the Large T Antigen of SV40, to be able to maintain cells to higher passage numbers and to expand cells more easily.

For immortalization 100.000 cells per well were seeded into 6 well plates and allowed to attach to the well surface overnight. The medium was replaced with 1 mL of fresh DMEM+/+ (Table 9) per well. Prior to transduction Polybrene® (Thermo Fisher Scientific, Braunschweig, Germany) was diluted in medium to a concentration of 10 µg/ mL and added to the cells. Then, 1 mL of SV40 lentiviral vector solution was added drop wise to the cells. Fibroblasts were incubated for 14 hours at 37°C, 5 % CO_2. After the incubation time medium was changed and cells were grown until they reached confluency. Successfully immortalized fibroblasts were selected from non-immortalized fibroblasts by serial splitting of 1:10 and monitored based on cell morphology. After successful immortalization stocks of fibroblasts were frozen down and maintained further for experiments.

2.5.1.3 Cell Culture maintenance of native and immortalized fibroblasts

Native and immortalized fibroblasts were grown in DMEM+/+ medium (Table 9). For splitting fibroblasts were washed with PBS once and Trypsin-EDTA (0,25 %), phenol red (Thermo Fisher Scientific, Braunschweig, Germany) was added for 2 min at room temperature. When cells were detached DMEM+/+ medium was added to inactivate the Trypsin and the cell suspension was collected. The cell number was determined with the Countess II automated cell counter (Life Technologies/ Thermo Fisher Scientific, Braunschweig, Germany) and the appropriate cell number was seeded into cell culture flasks or dishes. Native fibroblasts were used until passage number 10 – 12, whereas immortalized fibroblasts were used until passage number 30 – 35.

2.5.2 M17 cell culture

2.5.2.1 Cell Culture maintenance of M17 cells

The human neuroblastoma M17 cell line was grown in DMEM/F12 +/+ medium (Table 9). For splitting, cells were washed once with PBS and Trypsin-EDTA (0,05 %), phenol red (Thermo Fisher Scientific, Braunschweig, Germany) was added for 2 min at room temperature. Detached cells were resuspended in medium to inactivate the Trypsin. The cell suspension was collected and seeded into appropriate cell culture flasks or dishes.

Table 9: Cell culture media

Medium	Cell line	Amount	Chemical
DMEM +/+	Fibroblasts	84 %	DMEM + 4,5 g/L D-Glucose + L-Glutamine - Pyruvate
		15 %	FBS
		1 %	Penicillin-Streptomycin
DMEM/Ham´s-F12 +/+	M17 cells	82 %	DMEM/F12 - L-Glutamine
		15 %	FBS
		1 %	L-Glutamine
		1 %	non-essential amino acids
		1 %	Penicillin-Streptomycin

2.5.2.2 Generation of M17 cells with stable knockdown of RhoT1

In the M17 cell line a stable knockdown of *RhoT1* was introduced using the BLOCK-iT Inducible Pol II miR RNAi Expression Vector Kit with EmGFP (Invitrogen GmbH, Karlsruhe, Germany) according to the manufacturer's instructions. The single-stranded nucleotide oligos were designed to target different regions of *RhoT1* (Table 10) and cloned into the pcDNA6.2-GW/EmGFP-miR vector provided by the kit. The EmGFP tag was removed according to the kit protocol. One Shot® TOP10 Chemically competent *E. coli* (Thermo Fisher Scientific, Braunschweig, Germany) were transformed (see 2.4.1.) with either pcDNA6.2-GW/EmGFP-miR vector containing one of the *RhoT1*-targeting miRNA's or the

pcDNA6.2-GW/EmGFP-miR-neg control plasmid, also provided by the kit. The plasmids were purified from the bacteria (see 2.4.2.) and used to transfect the M17 cells (see 2.6.). Positively transfected M17 cells were then selected with DMEM-F12 +/+ medium containing 6 µg/mL Blasticidin S HCl (Invitrogen GmbH, Karlsruhe, Germany). After successful selection the knockdown of *RhoT1* was verified by Western Blot analysis and the miRNA construct with the most efficient knockdown was selected for further experiments.

Table 10: Targeting sequences of nucleotide oligos

Oligo name	**Sequence 5' to 3'**	**target region**
524_top	TGCTGTTTATGAGAGGAATCCATCGAGTTTTGGCCACTG ACTGACTCGATGGACCTCTCATAAA	ORF
524_bottom	CCTGTTTATGAGAGGTCCATCGAGTCAGTCAGTGGCCA AAACTCGATGGATTCCTCTCATAAAC	
1335_top	TGCTGTAAATAAGTCGTGAGCGTCCAGTTTTGGCCACT GACTGACTGGACGCTCGACTTATTTA	ORF
1335_bottom	CCTGTAAATAAGTCGAGCGTCCAGTCAGTCAGTGGCCA AAACTGGACGCTCACGACTTATTTAC	
2471_top	TGCTGTATGCTAGCCAATACTGCAGTGTTTTGGCCACTG ACTGACACTGCAGTTGGCTAGCATA	5' UTR
2471_bottom	CCTGTATGCTAGCCAACTGCAGTGTCAGTCAGTGGCCA AAACACTGCAGTATTGGCTAGCATAC	

2.6 Deoxyribonucleic acid (DNA) and Ribonucleic acid (RNA) analysis

2.6.1 Quantification of DNA and RNA samples

DNA and RNA samples were quantified using the NanoDrop ND1000 (Peqlab, Erlangen, Germany).

2.6.2 Isolation of DNA from eukaryotic cells

Genomic DNA was isolated from cultured fibroblasts using the QIA Blood and Tissue DNA kit (Qiagen GmbH, Hilden, Germany) according to the manufacturer's instructions.

2.6.3 Measurement of mitochondrial DNA (mtDNA) damage and mtDNA copy number

Native Fibroblasts were grown in 6 well plates under standard conditions until they were confluent. Cells were then either treated with 5 mM H_2O_2 for 5 min, 10 µM Rotenone for 20 min or a combination of 5 mM H_2O_2 (for 5 min) and 10 µM Rotenone (for 20 min) to induced ROS-mediated mtDNA damage.

Total DNA and mtDNA was isolated from cell pellets of fibroblasts with the QIA Blood and Tissue DNA kit (Qiagen GmbH, Hilden, Germany) according to the manufacturer's instructions. The elution step was performed twice with 30 µL of Elution buffer to obtain a minimum concentration of 10 ng/µL of total DNA.

Mitochondrial DNA damage and copy number were measured at the DNA Damage & Repair Unit Tübingen (Tübingen, Germany), using a high-sensitivity long-run real-time PCR technique for DNA-damage quantification (LORD-Q). While undamaged DNA is successfully amplified, different types of DNA modification or lesions result in delayed or disrupted PCR elongation, which can be detected as reduction of fluorescence intensity (Lehle, Hildebrand et al. 2014).

2.6.4 Isolation of RNA

For semi-quantitative measurement of *RhoT1* mRNA levels fibroblasts were grown in appropriate dishes and harvested by trypsinizing. The cell pellet was washed twice with PBS and stored at -80°C until RNA was isolated.

RNA isolation from the cell pellets was performed with the High pure RNA isolation Kit (Roche Applied Science, Mannheim, Germany) following the manufacturer's instructions. RNA samples were stored at -80°C until further processing.

2.6.5 Reverse transcription PCR for cDNA synthesis

The High Fidelity complimentary DNA (cDNA) Synthesis Kit (Roche Applied Science, Mannheim, Germany) was used for reverse transcription of isolated RNA from fibroblasts (2.6.4). Complementary DNA was synthesised using 200 ng of RNA per reaction and with anchored-oligo(dT) primers provided by the kit. As negative control served a reaction without reverse transcriptase. For the reaction mix see (Table 11) and for polymerase chain reaction (PCR) program (Table 12). Complementary DNA samples were stored at -20°C until the semi-quantitative measurement of cDNA was performed using rtPCR.

Table 11: Reaction mix for cDNA synthesis

Reagent	Volume
reaction buffer	4 µL
RNAse inhibitor	0.5 µL
dNTPs	2 µL
DTT	1 µL
reverse transcriptase	1.1 µL
RNA	→ 200 ng

Table 12: PCR program for cDNA synthesis

Temperature	Time
29°C	10 min
42°C	60 sec
85°C	5 min
4°C	60 min

2.6.6 Semi-quantitative measurement of RhoT1 mRNA level by rtPCR

The level of *RhoT1* mRNA was measured by rtPCR using the cDNA synthesized from isolated RNA (2.6.4). Primers were designed with Primer3 software (freeware) (Table 13). *TBP* was used as housekeeping gene to quantify *RhoT1* mRNA level. The reaction mix is shown in (Table 14) and the PCR programme is shown in (Table 15). The PCR product was loaded on a 2 % agarose gel (Biozym Scientific, Hessisch Oldendorf, Germany) containing 7 µL/100 mL Midori Green Advance DNA stain (Biozym Scientific, Hessisch Oldendorf, Germany) to visualize the results. Intensity of the cDNA bands were measured using ImageJ (Wayne Rasband, NIH) and the results were used to quantify the relative mRNA amounts.

Table 13: Primer sequences for rtPCR

Primer	**Sequence (5' – 3')**	**Supplier**
***RhoT1*-1 forward**	CTGCTTTCCATGCCCGGTT	Metabion international AG (Steinkirchen, Germany)
***RhoT1*-1 reverse**	ACTGCAAAAACAGTAGCACCAA	
***TBP* forward**	GAAGTTGGGTTTTCCAGCTAA	
***TBP* reverse**	GGAGAACAATTCTGGGTTTGA	

Table 14: Reaction mix for rtPCR

Reagent	**Volume**
5x buffer	5 µL
dNTP mix	1 µL
$MgCl_2$	2 µL
forward primer	0.5 µL
reverse primer	0.5 µL
H_2O	5.9 µL
Taq polymerase	1 µL

Table 15: PCR program for rtPCR

Temperature	Time	Cycles
94°C	1 min	
94°C	10 sec	25 x
56°C	5 sec	
60°C	10 sec	
60°C	4 min	
4°C	∞	

2.6.7 Sequencing of RhoT1 cDNA

RNA was isolated from immortalized fibroblasts (2.6.4) and used for cDNA synthesis (2.6.5). The cDNA was further used to amplify the *RhoT1* gene containing the nucleotides at positions c.815 and c.1348 by PCR (Table 18). The resulting PCR product was purified with QIAquick PCR purification Kit (Qiagen GmbH, Hilden, Germany). Sanger sequencing of the purified cDNA PCR product was performed by Seqlab (Seqlab Sequence Laboratories Göttingen GmbH, Göttingen, Germany), using the same primers (Table 17) as for PCR amplification of *RhoT1*. The chromatograms from sequencing results were visualized using FinchTV software (Geospiza Inc., Seattle, USA).

Table 16: PCR reaction mix for RhoT1 amplification from cDNA

Reagent	Volume
5x buffer	5 µL
dNTP mix (10 mM)	1 µL
$MgCl_2$ (25 mM)	2 µL
forward primer (Table 17)	1 µL
reverse primer (Table 17)	1 µL
H_2O	12.9 µL
Taq polymerase	0.1 µL
sample	3 µL

Table 17: Primer for RhoT1 amplification of cDNA and sequencing

Primer	Primer sequence (5' – 3')	Supplier
RhoT1 cDNA - forward	TGATGGTGTGGCTGACAGTG	Eurogentec (Liège, Belgium)
RhoT1 cDNA - reverse	CCGATTCTGAGATATCATGCAACA	

Table 18: PCR program for RhoT1 amplification from cDNA

Temperature	Time	Cycles
95°C	2 min	
95°C	30 sec	30 x
60°C	30 sec	
72°C	1:30 min	
72°C	6 min	
10°C	∞	

2.7 Cloning

2.7.1 Transformation of bacteria

One Shot® TOP10 Chemically competent *E. coli* (Thermo Fisher Scientific, Braunschweig, Germany) were transformed using plasmid DNA (pDNA) as instructed by the manufacturer.

2.7.2 Plasmid DNA (pDNA) purification

Plasmid DNA was isolated using the QIAprep spin MiniPrep Kit or Qiagen Plasmid Midi/ Maxi Kit (Qiagen GmbH, Hilden, Germany), according to the needed amount of pDNA, following the manufacturers' protocol. The pDNA was eluted in elution buffer and stored at -20°C.

2.7.3 Cloning of RhoT1 into pcDNA3.1/V5-HisA

For the study the *RhoT1* gene was purchased as TrueORF cDNA clone in a pCMV6-Entry vector from Origene Technologies (Rockville, USA) and subcloned into a pcDNA3.1/V5-HisA vector (Invitrogen GmbH, Karlsruhe, Germany).

One Shot® TOP10 Chemically competent *E. coli* were transformed with the pCMV6-Entry vector, containing *RhoT1* as described before (2.4.1.). *E. coli* containing the empty vector

pcDNA3.1/V5-HisA were grown from a frozen glycerol stock in sterilized LB medium (Sigma Aldrich Chemie GmnH, Munich, Germany), containing the appropriate concentration of antibiotics. Both pDNAs were isolated from *E. coli* as described before (2.4.2.).

Both purified pDNAs were digested for 3 hours at 37°C with the restrictions enzymes EcoRI and XhoI (Thermo Fisher Scientific, Braunschweig, Germany) following the manufacturers protocol to linearize the pcDNA3.1/V5-HisA vector and to cut out the *RhoT1* insert from the pCMV6-Entry vector (Table 19). The digested pDNA was separated in a 1 % agarose gel containing 7 µL/100 mL Midori Green Advance DNA stain. The linearized pcDNA3.1/V5-HisA vector and the *RhoT1* insert were cut out from the agarose gel. The DNA was purified from the gel using the QIAquick Gel Extraction Kit (Qiagen GmbH, Hilden, Germany) according to manufacturer's protocol.

The *RhoT1* insert was then ligated into the pcDNA3.1/V5-HisA vector using DNA T4 ligase (New England Biolabs GmbH, Frankfurt, Germany) over night at 16°C as instructed by the manufacturer. The amount of *RhoT1* insert and linearized pcDNA3.1/V5-HisA vector was calculated with the equation shown below.

Table 19: Restriction digest reaction

Amount	Reagent	Supplier
10 U/ µg DNA	restriction enzyme EcoRI/ XhoI	Thermo Fisher Scientific (Braunschweig, Germany)
1x	10 x buffer red	Thermo Fisher Scientific (Braunschweig, Germany)
add to 25 µL	nuclease-free water	Qiagen GmbH (Hilden, Germany)
2 µg	*RhoT1*-pCMV6-Entry	Origene Technologies (Rockville, USA)
2 µg	pcDNA3.1/V5-HisA	Invitrogen GmbH (Karlsruhe, Germany)

$$\frac{ng\ insert \times bp\ vector}{bp\ insert \times 3} = ng\ vector$$

Equation for calculation of insert and vector ratio for ligation

Table 20: Ligation reaction for cloning RhoT1 into pcDNA3.1/V5-HisA

Amount	Reagent	Supplier
5 ng	RhoT1 insert	Origene Technologies (Rockville, USA)

1 ng	pcDNA3.1/V5-HisA	Invitrogen GmbH (Karlsruhe, Germany)
0.33 µL	DNA T4 ligase	New England Biolabs GmbH (Frankfurt, Germany)
1x	10x buffer	New England Biolabs GmbH (Frankfurt, Germany)

The ligation reaction was used to transform One Shot® TOP10 Chemically competent *E. coli* as described before (2.4.1.). *E. coli* were subsequently plated on LB agar (Sigma Aldrich Chemie GmnH, Munich, Germany) plates containing the appropriate amount of Ampicillin (Sigma Aldrich Chemie GmnH, Munich, Germany) and grown over night at 37°C in a CO_2-free incubator. Colonies were picked and grown in 8 mL LB medium containing Ampicillin over night at 37°C in a CO_2-free incubator at 300 rpm agitation. Plasmid DNA was isolated using the QIAprep spin MiniPrep Kit as described before (2.4.2.).

To verify the successful ligation of insert and vector an analytical restriction digestion with EcoRI and XhoI was performed for 1 hour at 37°C and the fragments were separated and visualized on a 1 % agarose gel containing 7 µL/100 mL Midori Green Advance DNA stain.

The successfully generated pcDNA3.1/V5-HisA vector containing the *RhoT1* insert was then used for transformation of One Shot® TOP10 Chemically competent *E. coli* as described before (2.4.1.) to purify larger amounts of pDNA using the Qiagen Plasmid Midi Kit as described before (2.4.2.) for further use.

2.8 Mutagenesis of *RhoT1* in pcDNA3.1/V5-HisA

For analysis of the previously identified *RhoT1* mutations mutagenesis of the *RhoT1* insert in the pcDNA3.1/V5-HisA vector was performed by GenScript (Hong Kong) to obtain pcDNA3.1/V5 constructs expressing Miro1-R272Q, Miro1-R450C or Miro1-F676V, respectively.

2.9 Transfection of M17 cells

For transfection with *RhoT1* constructs (Table 21) M17 cells with stable knockdown of *RhoT1* were seeded in appropriate cell culture plates under standard growth conditions. Cells were then transfected with *RhoT1* constructs (Table 21) using TransIT®-2020 transfection reagent (Mirus Bio LLC, Madison, USA) according to the manufacturers' protocol.

Table 21: RhoT1 constructs

Construct name	Vector	Supplier
	pcDNA3.1/V5-HisA	Invitrogen GmbH, Karlsruhe, Germany
Miro1-WT	pcDNA3.1/V5-HisA	self-made
Miro1-R272Q	pcDNA3.1/V5-HisA	GenScript (Hong Kong)
Miro1-R450C	pcDNA3.1/V5-HisA	GenScript (Hong Kong)
Miro1-F676V	pcDNA3.1/V5-HisA	GenScript (Hong Kong)
Miro1-WT-myc	pRK-5 myc	kind gift from Prof. P. Aspenström (Karolinska Institute, Stockholm, Schweden); (NCBI: AJ517412.1) (Fransson et al., 2003)

2.10 Microscopy

2.10.1 Live cell imaging

Native human fibroblasts were cultured under standard growth conditions and seeded into Nunc™ Lab-Tek™ Chamber slides (Thermo Fisher Scientific, Braunschweig, Germany) for imaging. Live cell imaging was performed with the Live Cell Microscope Axiovert 2000 (Carl Zeiss Microimaging GmbH, Jena, Germany) or a Live Cell Microscope Axiovert 2000 with spinning disc (Carl Zeiss Microimaging GmbH, Jena, Germany) in a humidified atmosphere containing 5 % CO_2 at 37°C.

2.10.2 MitoTracker staining for analysis of mitochondrial morphology and mitochondrial mass

To visualize mitochondria irrespective of their membrane potential, native human fibroblasts were stained with 0.1 nM MitoTracker® green FM for 20 min (Thermo Fisher Scientific, Braunschweig, Germany) and 0.5 µg/mL DAPI for 5 min (Thermo Fisher Scientific, Braunschweig, Germany) in DMEM +/+ at 37°C and 5 % CO_2. Then, fibroblasts were washed 3x with PBS and fresh DMEM +/+ was added for imaging.

Mitochondrial morphology was analysed on single cell level. Therefore mitochondria were defined with ImageJ software (Wayne Rasband, NIH) and automatically analysed for the parameters perimeter, area, major axis and minor axis using the “analyse particles” tool of ImageJ. These parameters were used to calculate Form Factor, indicating mitochondrial

branching, and Aspect Ratio which is an indicator for mitochondrial length as described below:

$$\frac{perimeter\text{^}2}{4 * PI * area} = Form\ Factor$$

$$\frac{major\ axis}{minor\ axis} = Aspect\ Ratio$$

Mitochondrial mass was assessed using the same staining. For this measurement images of stained mitochondria and bright field images were obtained from the same cells. Cell size was measured from bright field images and mitochondrial area from MitoTracker images using ImageJ software (Wayne Rasband, NIH). To calculate mitochondrial mass, mitochondrial area was normalized to cell size (ratio of mitochondrial area to cell size).

2.10.3 Co-staining of MitoTracker and LysoTracker for co-localization analysis of mitochondria and lysosomes

Native human fibroblasts were stained with 0.1 nM MitoTracker® green FM or MitoTracker® deep red (Thermo Fisher Scientific, Braunschweig, Germany) and 0.1 nM LysoTracker® red or LysoTracker® yellow (Thermo Fisher Scientific, Braunschweig, Germany) for 20 min and 0.5 µg/mL DAPI for 5 min in DMEM +/+ at 37°C and 5 % CO_2. Fibroblasts were washed 3x with PBS and fresh DMEM +/+ was added for imaging. Co-localization of mitochondria and lysosomes was automatically analysed on single cell level using the JACoP plugin of ImageJ software (Wayne Rasband, NIH).

2.10.4 Co-staining of Fluo4 and MitoTracker for analysis of cytosolic calcium flux

Native human fibroblasts were stained with 0.1 nM MitoTracker® deep red FM (Thermo Fisher Scientific, Braunschweig, Germany) for 20 min and 0.5 µg/mL DAPI for 5 min in DMEM +/+ at 37°C and 5 % CO_2. Fibroblasts were washed 3x with PBS and fresh DMEM +/+ was added. Then, Fluo-4 (Thermo Fisher Scientific, Braunschweig, Germany) was added to the cells according to manufacturer's instructions. Baseline fluorescence intensity of Fluo4 was measured for 5 min with an interval of 700 ms between each image using a Live cell imaging microscope (Axiovert with spinning disc, Carl Zeiss Microimaging GmbH, Jena, Germany). Fluorescence of Fluo4 and MitoTracker® deep red FM were measured using the 488 nm and the 638 nm laser, respectively. A 1 mM Histamine (Sigma Aldrich Chemie GmbH, Munich, Germany) solution was diluted in DMEM +/+ to a

concentration of 60 µM. The 60 µM Histamine solution, prewarmed to 37°C was added to the chamber slide to obtain a final concentration of 30 µM to release calcium from intracellular calcium stores. The cell response was measured for 5 min with an interval of 700 ms between each image.

The fluorescence intensity of Fluo4 was analysed with ZEN Blue software (Carl Zeiss Microimaging GmbH, Jena, Germany). Therefore, regions of interest (ROI) were defined in each cell within one field of view. Fluorescence intensity data were calculated for each time point. The fluorescence of each ROI at time point 1 was defined as 1 and used to normalize all other values. The resulting relative fluorescence data were plotted in a curve over time using Graph Pad Prism 6 software.

2.10.5 Immunofluorescence (IF)

For immunofluorescence staining M17 cells were grown under standard conditions and seeded into Chamber slides. Cells were transfected with pcDNA3.1/V5-HisA-*RhoT1* constructs using TransIT®-2020 transfection reagent (Mirus Bio LLC, Madison, USA) as described before (2.9) and incubated for 24 hours. After this incubation time the medium was aspirated and cells were washed with PBS. Cells were fixed in 4 % Paraformaldehyde (PFA; in PBS) (Sigma Aldrich Chemie GmbH, Munich, Germany) over night at 4°C. The fixed cells were washed 3x in DPBS+/+ (Thermo Fisher Scientific, Braunschweig, Germany) and permeabilised in permeabilisation buffer (Table 22) for 1 hour at room temperature. Then, cells were washed 3x with DPBS+/+ and incubated in primary antibody solution (Table 22) over night at 4°C.

The primary antibody solution was washed off 3x with DPBS+/+ and afterwards cells were incubated in secondary antibody solution (Table 22) for 3 hours at room temperature. The secondary antibody solution was then washed off 3x with DPBS+/+ and cells were stained with 0.5 µg/mL DAPI in PBS for 15 min at room temperature. DAPI was then washed off 3x with PBS and the fixed and stained cells were mounted with a coverslip in a drop of Vectashield mounting medium (Vector Laboratories Inc., Burlingame, USA).

Automated co-localization analysis were done using the “JACoP” plugin of ImageJ.

Table 22: Solutions for Immunofluorescence staining

Solution	Amount	Chemical
permeabilisation buffer		DPBS+/+
	0.4 %	Triton X-100
	10 %	Goat Serum
	2 %	BSA
primary antibody solution		DPBS+/+
	1:500	primary antibody
	0.1 %	Triton X-100
	1 %	Goat Serum
	0.2 %	BSA
secondary antibody solution		DPBS+/+
	1:1000	secondary antibody
	0.1 %	Triton X-100
	1 %	Goat Serum
	0.2 %	BSA

2.11 Western Blot (WB) analysis

Immortalized fibroblasts and M17 cells for Western Blot analysis were grown under standard conditions and treated as appropriate for the readout. Lysis of all applied cell types was done in lysis buffer (Table 23). Cells were harvested by trypsination and washed once with PBS. Cells were spined down at 1500 rpm for 5 min at 4°C. The cell pellet was mixed with an appropriate volume of lysis buffer and incubated on ice for 30 min. The cell debris was centrifuged at 3000x g for 10 min at 4°C. The supernatant was transferred to a new 1.5 mL tube. The protein concentration of the lysate was measured with Bradford solution (Bio-Rad Laboratories, Munich, Germany) according to manufacturer's instructions. The lysate was mixed with 5x Laemmli buffer (Table 23), heated to 96°C for 6 min and afterwards cooled on ice prior to loading on the acrylamide gel.

For detection of intact complexes of the respiratory chain with the OXPHOS antibody cocktail (Abcam, Cambridge, UK) (Table 24) the cell lysate was not heated to 96°C, but mixed with 5x Laemmli buffer and incubated for 15 min at room temperature.

The appropriate amount of lysate was loaded on a self-made 10 % polyacrylamide-SDS gel with a 4 % stacking gel (Table 23) (Bio-Rad Laboratories, GmbH, Munich, Germany)

together with PageRuler Plus Prestained Protein Ladder (Thermo Fisher Scientific, Braunschweig, Germany) as size standard. Samples were resolved by one-dimensional discontinuous sodium dodecyl sulfate polyacrylamide gel electrophoresis (SDS-PAGE), running at 80 V in the stacking gel and at 120 V in the running gel. Proteins were blotted from the gel on nitrocellulose membrane (Invitrogen GmbH, Karlsruhe, Germany) with the iBlot 2 device (Invitrogen GmbH, Karlsruhe, Germany) for 7 min at 20 V.

The membrane was blocked in 5 % Milk (Table 23) for 1 hour at room temperature and subsequently incubated in primary antibody solution (Table 24) either for 1 hour at room temperature or overnight at 4°C under agitation. The membrane was then washed 3x for 10 min in TBS-T (Table 23) and subsequently incubated in secondary antibody (Table 24) either for 1 hour at room temperature or overnight at 4°C under agitation. The membrane was then washed for 3x in TBS-T for 10 min and the labelled proteins were visualized with Amersham ECL Western Blotting Detection Reagent (GE Healthcare, Freiburg, Germany) according to the protocol of the manufacturer. Luminescence was detected with ODYSSEY chemiluminescence 2800 Fc (Li-COR, Lincoln, USA).

Table 23: Composition of buffers required for Western Blot

Buffer	Chemical	Amount
lysis buffer	HEPES	10 mM
	$MgCl_2$	1,5 mM
	KCl	10 mM
	DTT	0,5 mM
	NP40	0,05 %
	Complete Protease inhibitor	add fresh
	Triton X-100	add fresh 1 %
10x TBS pH 7.5	Tris	50 mM
	NaCl	150 mM
1x TBS-T	1x TBS in VE water	
	Tween 20	1 %
5 % Milk	Skim Milk powder	5 g
	TBS-T	100 mL
5 % BSA	BSA	5 g
	TBS-T	100 mL

5x running buffer	Tris	45 g
	Glycine	216 g
	SDS	150 mL (10 %)
	VE water	add to 3 L
4 % polyacrylamide-SDS stacking gel	VE water	1,15 mL
	Acrylamide/ Bis-acrylamide 30 % solution	0,33 mL
	0,5 M Tris	0,5 mL
	10 % SDS	0,02 mL
	TEMED	0,002 mL
	10 % APS	0,02 mL
10 % polyacrylamide-SDS running gel	VE water	2 mL
	Acrylamide/ Bis-acrylamide 30 % solution	1,7 mL
	0,5 M Tris	1,3 mL
	10 % SDS	0,05 mL
	TEMED	0,002 mL
	10 % APS	0,05 mL
5x Laemmli buffer	Trizma hydrochloride	62.5 mM, pH 6.8
	β-mercaptoethanol	5 %
	Glycerin	10 %
	SDS	2 %
	Bromphenol blue	1 spatula tip
	DTT	50 µM

Table 24: Antibodies for WB and IF

Antibody	Species reactivity	Dilution	Solution	Supplier	Order number
Anti-RhoT1	mouse	1:500	5 % Milk	Sigma Aldrich	WH0055 288M1
Anti-RhoT1	rabbit	1:500	5 % Milk	Sigma Aldrich	HPA010687
V5	mouse	1:1000	5 % Milk	Sigma Aldrich	R960-25
β-Actin	mouse	1:3000	5 % Milk	Thermo Scientific	MA1-744
LC3I/II	rabbit	1:1000	5 % BSA	Cell Signalling	2775
Tom20	rabbit	1:1000	5 % BSA	Santa Cruz	sc-11415
Total OXPHOS Rodent WB Antibody cocktail	mouse	1:1000	5 % Milk	Abcam	ab110413
Citrate Synthase	rabbit	1:1000	5 % Milk	Gene Tex	GTX110624
MnSOD (SOD 2)	rabbit	1:1000	5 % Milk	Abcam	ab13533
Mitofusin1 (Mfn1)	mouse	1:1000	5 % Milk	Abcam	ab57602
PGC1α	rabbit	1:1000	5 % Milk	Novus Biologicals	NBP1-04676
Goat anti-mouse IgG, horseradish peroxidase conjugate		1:10000	TBS-T	Novex	A24524
Goat anti-rabbit IgG, horseradish peroxidase conjugate		1:5000	TBS-T	Novex	A24537
Alexa Fluor 488 Goat anti-mouse IgG		1:1000	2nd antibody solution (Table 22)	Life Techn.	A-11029
Alexa Fluor 568 Goat anti-rabbit IgG		1:1000		Life Techn.	A11036

The antibodies for detection of Miro1 have been chosen to bind at epitopes which are located distinct from the amino acids R272 and R450 (Figure 3). Therefore it can be excluded that the mutations R272Q and R450C interfere with antibody binding so that the antibodies also detect mutant proteins.

```
        10         20         30         40         50         60
MKKDVRILLV GEPRVGKTSL IMSLVSEEFP EEVPPRAEEI TIPADVTPER VPTHIVDYSE

        70         80         90        100        110        120
AEQSDEQLHQ EISQANVICI VYAVNNKHSI DKVTSRWIPL INERTDKDSR LPLILVGNKS

       130        140        150        160        170        180
DLVEYSSMET ILPIMNQYTE IETCVECSAK NLKNISELFY YAQKAVLHPT GPLYCPEEKE

       190        200        210        220        230        240
MKPACIKALT RIFKISDQDN DGTLNDAELN FFQRICFNTP LAPQALEDVK NVVRKHISDG

       250        260        270        280        290        300
VADSGLTLKG FLFLHTLFIQ RGRHETTWTV LRRFGYDDDL DLTPEYLFPL LKIPPDCTTE

       310        320        330        340        350        360
LNHHAYLFLQ STFDKHDLDR DCALSPDELK DLFKVFPYIP WGPDVNNTVC TNERGWITYQ

       370        380        390        400        410        420
GFLSQWTLTT YLDVQRCLEY LGYLGYSILT EQESQASAVT VTRDKKIDLQ KKQTQRNVFR

       430        440        450        460        470        480
CNVIGVKNCG KSGVLQALLG RNLMRQKKIR EDHKSYYAIN TVYVYGQEKY LLLHDISESE

       490        500        510        520        530        540
FLTEAEIICD VVCLVYDVSN PKSFEYCARI FKQHFMDSRI PCLIVAAKSD LHEVKQEYSI

       550        560        570        580        590        600
SPTDFCRKHK MPPPQAFTCN TADAPSKDIF VKLTTMAMYP HVTQADLKSS TFWLRASFGA

       610        620
TVFAVLGFAM YKALLKQR
```

Figure 3: Epitopes of Miro1 antibodies

Amino acid sequence of Miro1 protein. The amino acids R272 and R450 are highlighted in red. The epitope for the Miro1 antibody anti-RhoT1 (Sigma Aldrich, produced in rabbit, HPA010687) is highlighted in green. The epitope for the Miro1 antibody anti-RhoT1 (Sigma Aldrich, produced in mouse, WH0055 288M1) is highlighted in yellow. The epitopes of both antibodies are located distant of both mutations R272Q and R450C. Therefore the mutations are not likely to interfere with antibody binding.

2.12 Flow cytometry

Flow cytometry measurement was performed to functionally analyse mitochondrial membrane potential, mitochondrial production of reactive oxygen species (ROS) and early apoptosis of cells.

Flow cytometry measurement was performed with the CyAn ADP Analyzer (Beckman Coulter, California, USA) or with the BD LSRFortessa (Becton, Dickinson and Company©, Erembodegem, Belgium). At least 10000 events per sample were measured and analysed using the Summit 4.3.02b2451 software (Beckman Coulter, California, USA) or the Flowjo software (Flowjo LLC, Oregon, USA).

2.12.1 MitoSOX staining

MitoSOX™ Red Mitochondrial Superoxide Indicator (Thermo Fisher Scientific, Braunschweig, Germany) specifically stains mitochondria in living cells and gets oxidised by superoxide, which results in an increase of fluorescence signal.

Immortalized fibroblasts were grown under standard conditions. For the experiment 200000 cells per well were seeded into 6 well plates and grown for 24 hours. Cells were either treated with 20 nM Piericidin A (Santa Cruz, Dallas, Texas), a specific inhibitor of the ubiquitin acceptor site of Complex I, which increases mitochondrial ROS production, or with low Glucose medium (DMEM + 1g/L D-Glucose, 15 % FBS, 1 % P/S) for 14 hours.

Cells were harvested with 0.25 % Trypsin-EDTA. Then, cells were stained with 2,25 µM MitoSOX™ Red and 0.1 nM MitoTracker® green FM in PBS for 20 min at 37°C in a CO_2-free incubator. Cells were centrifuged for 5 min at 900 rpm, 4°C, the cell pellet was washed in PBS and resuspended in 500 µL PBS containing 1 % FBS for the measurement. Fluorescence of MitoSOX™ Red and MitoTracker® green FM were measured using the 561 nm and the 488 nm laser, respectively.

The relative level of mitochondrial superoxide was calculated as ratio of MitoSOX™ Red fluorescence intensity to MitoTracker® green FM fluorescence intensity to take the mitochondrial mass into account.

2.12.2 Tetramethylrhodamine methyl ester (TMRE) staining

Active mitochondria are able to sequester TMRE (Thermo Fisher Scientific, Braunschweig, Germany) which results in a membrane potential-dependent fluorescence signal.

For measurement of mitochondrial membrane potential (MMP) cells were grown under standard conditions. One day before the measurement, 200000 cells per well were seeded into 6 well plates. After one day of growing, immortalized fibroblasts were treated with 5 nM Valinomycin (Sigma Aldrich Chemie GmbH, Munich, Germany) for 14 hours and M17 cells were treated with 10 µM CCCP (Abcam, Cambridge, UK) for 20 min. Valinomycin and CCCP were used to decrease the MMP to verify that changes in MMP can be observed using the applied method.

Cells were harvested with Trypsin-EDTA and stained with 20 µM TMRE and 0.1 nM MitoTracker® green FM for 20 min at 37°C, 5 % CO_2. Cells were centrifuged for 5 min at 900 rpm, 4°C, the cell pellet was washed in PBS and afterwards the pellet was resuspended in 500 µL PBS containing 1 % FBS for measurement. Fluorescence of TMRE and MitoTracker® green FM were measured using the 561 nm and the 488 nm laser, respectively.

The relative MMP level was calculated as ratio of TMRE fluorescence intensity to MitoTracker fluorescence intensity to include the mitochondrial mass into the results.

2.12.3 Annexin V staining

Annexin V is a phospholipid-binding protein that specifically binds phosphatidyl serine (PS) when PS is present at the outer leaflet of the plasma membrane during apoptosis (Koopman, Reutelingsperger et al. 1994).

To assess early apoptosis and cell death, immortalized fibroblasts were grown under standard conditions. For each cell line 200000 cells per well were seeded into 6 well plates. After two days of growth cells were treated with 1 µM Staurosporine (Sigma Aldrich Chemie GmbH, Munich, Germany) for 2 hours. Cells were harvested by thrypsination and stained with Annexin V, Alexa Fluor® 568 conjugate (Thermo Fisher Scientific, Braunschweig, Germany) for apoptosis detection according to the protocol of the manufacturer. When cells were resuspended in annexin-binding buffer (provided by the Annexin V kit) after staining, 0.5 µg/mL of DAPI was added to each sample to discriminate living and dead cells.

Samples were kept on ice and measured immediately on the BD LSRFortessa (Becton, Dickinson and Company©, Erembodegem, Belgium) using the 561 nm and the 405 nm laser.

2.13 Biochemical measurement of Citrate Synthase activity

Citrate Synthase is the key enzyme of the tricarboxylic acid cycle (TCA) in the mitochondrial matrix, catalysing the reaction of oxaloacetate and acetyl CoA. The formed free Coenzyme A reacts with DTNB. The resulting colour change was measured at 412 nm using the monochromatic spectrophotometer SPECORD 210Plus (Analytic Jena AG, Jena, Germany).

The described method was primarily published by (Janssen, Trijbels et al. 2007) and further adapted by Iain Hargreaves (Neurometabolic Unit, The National Hospital for Neurology and Neurosurgery, Queen Square, London, UK) and Julia Fitzgerald (Hertie-Institute for Clinical Brain Research, University of Tübingen, Tübingen, Germany) in collaboration with Boehringer Ingelheim GmbH (Ingelheim am Rhein, Germany).

2.13.1 Subfractionation of mitochondria from immortalized fibroblasts

Immortalized fibroblasts were grown under standard conditions in 10 cm dishes until they reached confluency. Cells were harvested using 0.25 % Trypsin/EDTA and centrifuged for 5 min at 1200 rpm, 4°C. The resulting cell pellet was homogenized in 100 µL mitochondrial isolation buffer (MIB) (Table 25). Additional 900 µL of MIB buffer were added and the lysate was centrifuged for 10 min at 1000x g, 4°C. The supernatant was transferred to a new 1.5 mL tube. The supernatant was centrifuged again at 9000x g for 15 min at 4°C. The resulting supernatant of this centrifugation step was separated from the pellet into a new 1.5 mL tube. The pellet was resuspended in 50 µL of MIB buffer and 5 µL of this lysate were used to measure the protein concentration of the lysate with Bradford solution. The remaining lysate was centrifuged again at 10000x g for 10 min, 4°C. The resulting pellet was resuspended in 50 µL of MIB buffer containing 0.5 % BSA. All samples were kept on ice and used immediately for measurement of citrate synthase activity (see 2.13.2).

Table 25: Composition of mitochondrial isolation buffer (MIB)

Mitochondrial isolation buffer (MIB)	
Chemical	**Concentration**
Sucrose	70 nM
Mannitol	210 mM
HEPES	5 mM
EGTA	1 mM
BSA	(add fresh after protein estimation) 0.5 %

2.13.2 Citrate Synthase activity assay

For measurement of Citrate Synthase activity the reagents shown in (Table 26) were prepared prior to the experiment and used to prepare the reaction mix as shown in (Table 27). The stable baseline activity was measured on the spectrophotometer SPECORD 210Plus (Analytic Jena AG, Jena, Germany) at 412 nm for 2 min. To initiate the reaction 10 µL of 10 mM Oxaloacetate (Table 26) were added to each sample and measured for 2 min. Finally, 10 µL of 10 % Triton X-100 (Table 26) were mixed in the sample and the reaction was measured for 2 min. Triton X-100 permeabilized the mitochondrial membrane and leads to release of citrate synthase, thereby allowing to measure the total enzyme activity.

Table 26: Composition of Reagents for Citrate Synthase activity assay

Chemical	**Concentration**	**Preparation**
Tris	200 mM	in $Aqua_{dd}$, pH 8.0
Acetyl-CoA	100 mM	in $Aqua_{dd}$
DNTB	100 mM (4 mg/ mL)	add pinch of $KHCO_3$ to dissolve in $Aqua_{dd}$
Oxaloacetate	10 mM	adjust pH to 7.0 with Tris, in $Aqua_{dd}$
Triton X-100	10 %	in PBS

Table 27: Reaction mix per sample for Citrate Synthase activity assay

Reagent	Amount
Tris	500 µL
Acetyl-CoA	20 µL
DNTB	20 µL
mitochondrial protein	50 µg
$Aqua_{dd}$	add to 1 mL

2.13.3 Calculation of Citrate Synthase activity

Citrate Synthase activity was calculated from the optical density (OD) measured on the Spectrophotometer SPECORD 210Plus (Analytic Jena AG, Jena, Germany) (2.10.2.) using the formula as described below. Values of OD were displayed on a scatter blot using Excel. For the calculation OD values were used from the beginning (OD1) and the end (OD2) of the linear increase of optical density over time.

$$\frac{OD2 - OD1}{time} = \Delta\, Abs/min$$

$$\frac{\Delta Abs/min}{extinction\, coefficient} = mole/min/L$$

(extinction coefficient = 13600)

$$\frac{mole/min/L}{1000} = mole/min/mL$$

$$\frac{mole/min/mL}{prot.conc.} = enzyme\ activity\ (mole/min/mL/\mu g)$$

2.14 Measurement of complex I activity

Complex I activity was measured in immortalized fibroblasts using the complex I Enzyme Activity Dipstick Assay Kit (Abcam, Cambridge, UK). The active Complex I gets immune-precipitated from the cell lysate on the Dipstick. The activity buffer, provided by the kit, contains NADH as substrate for complex I and nitrotetrazolium blue (NBT) as electron acceptor. When NADH gets oxidized by complex I NBT, gets reduced by the resulting H^+ and turns into a blue-purple form. The intensity of the colour reaction is directly correlated to complex I activity (User Manual: ab109720 – Complex I Enzyme Activity Dipstick Assay Kit, Abcam, Cambridge, UK).

For measuring complex I activity immortalized fibroblasts were grown in 10 cm dishes under standard conditions until they reached confluency in the dish. Half of the cells were lysed for Western Blot (2.8.) and the other half of the cells from the same dish was used to measure complex I activity as instructed by the kit protocol. The intensity of reduced purple NBT on the dipsticks was quantified with ImageJ software.

Western Blot was performed to assess the citrate synthase (Table 24) protein level (see 2.8.) from the same sample. The Citrate synthase protein level was used to normalize complex I activity to mitochondrial abundance.

2.15 Measurement of oxygen consumption rate (OCR)

Mitochondrial oxygen consumption rate (OCR) in immortalized fibroblasts was analysed using the XF^{e}96 extracellular flux assay kit measured on the XF^{e}96 extracellular flux Analyzer (Seahorse Bioscience, Massachusetts, USA). The XF^{e}96 extracellular flux Analyzer allows real-time measurement of the concentration of dissolved oxygen in the medium, which is a direct result of cellular oxygen consumption and correlates with the activity of the respiratory chain.

Immortalized fibroblasts were grown under standard conditions and one day prior to measurement cells were seeded into XF96 cell culture microplates (Seahorse Bioscience, Massachusetts, USA) at an appropriate cell density to obtain an even cell monolayer. Freshly seeded cells were kept at room temperature for 30 min before incubation at 37°C, 5 % CO_2 overnight.

The assay cartridge (Seahorse Bioscience, Massachusetts, USA) was hydrated with 200 µL of XF-calibrant solution (Seahorse Bioscience, Massachusetts, USA) per well and incubated at 37°C in a CO_2-free incubator, 24 hours prior to the experiment.

On the day of the measurement, Seahorse assay media, composed of bicarbonate-free basal DMEM (Sigma Aldrich Chemie GmbH, Munich, Germany), 1 % L-Glutamine (Sigma Aldrich Chemie GmbH, Munich, Germany) and 4.5 g/L D–Glucose (Sigma Aldrich Chemie GmbH, Munich, Germany), was incubated at 37°C in a non-CO_2 incubator for at least 1 hour. Then, the DMEM+/+ was removed from the cells, without scratching the cell monolayer, and cells were rinsed twice with Seahorse assay media. The XF96 cell culture microplate was then filled with 175 µL Seahorse assay media and incubated in a non-CO_2 incubator for at least 1 hour to equilibrate.

The ports of the Seahorse utility plate (Seahorse Bioscience, Massachusetts, USA) were loaded with 25 µL per well of Oligomycin (Sigma Aldrich Chemie GmbH, Munich, Germany), FCCP (Sigma Aldrich Chemie GmbH, Munich, Germany) or a mixture of Rotenone (Sigma Aldrich Chemie GmbH, Munich, Germany) and Antimycin A (Sigma Aldrich Chemie GmbH, Munich, Germany), each at appropriate concentrations prepared in Seahorse assay media [for optimization of the compound concentrations see (Figure 35)].

The Seahorse utility plate, loaded with Oligomycin, FCCP and Rotenone/ Antimycin A, and the equilibrated XF96 cell culture microplate were loaded to the XF^{e}96 extracellular flux Analyzer and OCR was measured as shown in (Table 28).

Table 28: Program for measurement of OCR

Basal			**Injection 1 (Oligomycin)**			**Injection 2 (FCCP)**			**Injection 3 (rot. + antim.A)**		
cycles	mix	measure	cycles	mix	measure	cycles	mix	measure	cycles	mix	measure
5	3	3	3	3	3	3	3	3	3	3	3
30 min			18 min			18 min			18 min		

After measurement was finished, total protein concentration in each well of the XF96 cell culture microplate was determined using the Bradford assay (Bio-Rad Laboratories, Munich, Germany). Therefore, medium was aspirated from the wells and cells were incubated with 10 µL of lysis buffer (Table 23) for 10 min at room temperature. 200 µL per well of Bradford buffer was added and optical density was measured on the Synergy Mx microplate reader. The calculated protein concentration was used to normalize the OCR raw data to total protein amount. The obtained OCR data were used to calculate the levels of basal respiration, ATP production, proton leak, maximal respiration, spare respiratory capacity and non-mitochondrial respiration as shown in (Table 29; Figure 4).

Table 29: Equations for calculation of OCR parameters

parameter	**equation**
non-mitochondrial respiration	minimum rate measurement after rotenone/antimycin A injection
basal respiration	(last rate measurement before first injection) – (non-mitochondrial respiration)
ATP production	(last rate measurement before oligomycin injection) – (minimum rate measurement after oligomycin injection)
proton leak	(minimum rate measurement after oligomycin injection) – (non-mitochondrial respiration)
maximal respiration	(maximum rate measurement after FCCP injection) – (non-mitochondrial respiration)
spare respiratory capacity	(maximal respiration) – (basal respiration)

A)

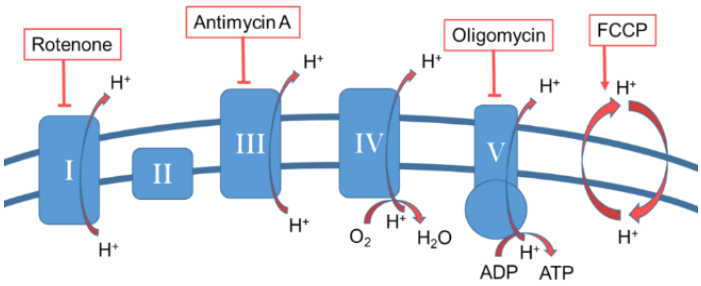

B)

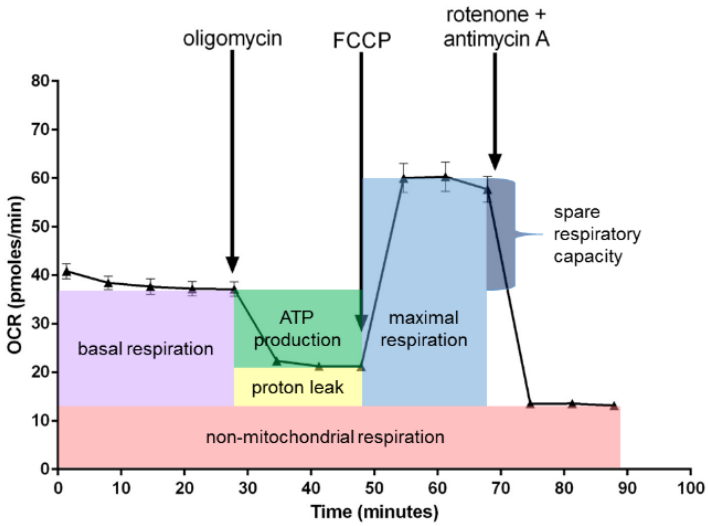

Figure 4:Schematic overview of OCR measurement

A) Overview of inhibition of respiratory chain complexes by Rotenone, Antimycin A and Oligomycin and uncoupling of respiration by FCCP. Rotenone inhibits complex I and Antimycin A inhibits complex III, which leads to a complete inhibition of mitochondrial respiration. The remaining respiratory activity is the non-mitochondrial respiration resulting from side reatcions. Oligomycin inhibits ATP production by complex V, which enables calculation of the capacity for ATP production by complex V. The remaining OCR arises from the proton leak. FCCP uncoupling enables measurement of maximal respiration and calculation of spare respiratory capacity **B)** Schematic overview of OCR measurement and the calculation of basal respiration, ATP production, proton leak, maximal respiration, spare respiratory capacity and non-mitochondrial respiration.

2.16 Growth assay of Gem1 deficient yeast

A yeast strain deficient of Gem1 (*gem1*Δ) was generated in collaboration with Doron Rapaport and Kai Dimmer (Interfakultäres Institut für Biochemie, IFIB, University of Tübingen, Germany). The *gem1*Δ strain was transfected with wild type *gem1* or gem1-R298Q and the cells applied to a drop dilution assay on YPD and YPG media at 30°C or 35°C. YPD medium contains dextrose and peptose for optimal growing. YPG medium in contrast contains glycerol as non-fermentable carbon source. This assay allows to assess the ability of yeast to grow when energy production by fermentation is inhibited due to lack of a fermentable substrate. Growth on a non-fermentable carbon source then relies on energy production by mitochondrial respiration.

3 Results

3.1 PD patients with mutations in *RhoT1* have a positive family history

In direct preparation of the present study a German cohort of 760 PD patients and 280 healthy, age matched controls was screened for mutations in *RhoT1*, the gene encoding for Miro1, using SNaPshot technology (done by David Scheibner) in our laboratory. Three PD patients were identified carrying novel heterozygous mutations in *RhoT1* (Figure 6).

All three patients have a positive family history for PD. The fathers of the patients carrying the Miro1-R272Q and the Miro1-R450C mutations had tremor dominant PD and the brother of the patient carrying the Miro1-F676V mutation was diagnosed with PD (Figure 5). All three PD patients with mutations in *RhoT1* displayed a tremor dominant clinical phenotype. Due to their positive family history, the patients also have been tested for mutations in GBA (N370S, L444P) and LRRK2 (exon 7 and 41, which covers the mutations G2019S and I2020T), and the patient with the mutation F676V was furthermore tested for mutations in Parkin, PINK1, DJ-1 and SNCA. All three PD patients were negative for the mentioned mutations, indicating that mutations in these genes can be excluded as PD-causing.

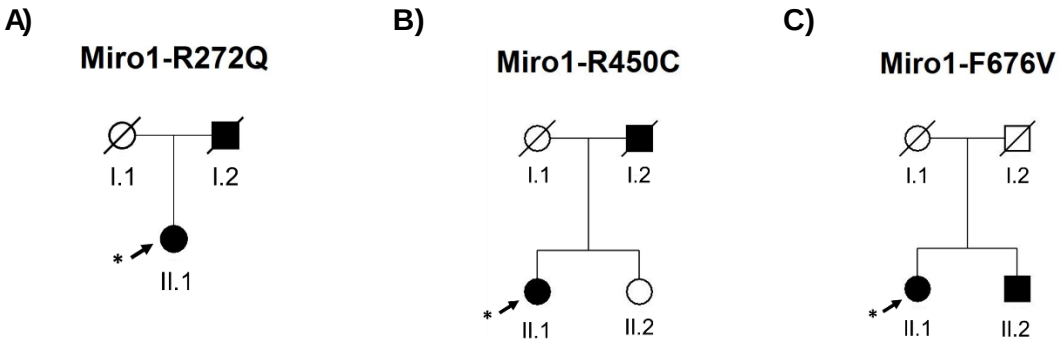

Figure 5: Family pattern of PD patients with mutations in RhoT1

The family patterns of three identified PD patients carrying mutations in *RhoT1*. Individuals with motor symptoms and individuals that have been diagnosed with PD are highlighted in black. Arrows indicate the index patients identified with mutations in *RhoT1*. All three PD patients have a positive family history for PD-related symptoms.

The PD-associated mutations of *RhoT1* are located in different exons, encoding for different conserved functional domains of the Miro1 protein (Figure 6). The mutation R272Q is located within the ligand mimic motif of the first EF hand domain (Klosowiak, Focia et al.

2013), R450C is found in the C-terminal GTPase domain and F676V lies within the transmembrane domain of Miro1.

Nucleotide change	Exon	Amino acid change	Location
c.815 G > A	11	**p.R272Q**	first EF hand
c.1348 C > T	16	**p.R450C**	second GTPase
c.2026 T > G	21	**p.F676V**	TMD

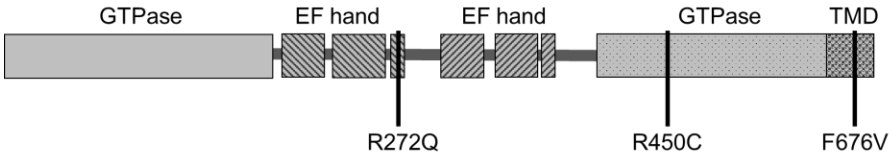

Figure 6: PD-associated mutants of Miro1

Protein structure of Miro proteins showing the N-terminal GTPase domain, both EF hand domains, the C-terminal GTPase domain and the C-terminal transmembrane domain (TMD). The mutations R272Q, R450C and F676V are indicated at their respective locations within the protein domains.

As the proper function of the domains is essential to ensure the full functionality of Miro1 protein and as Miro1 function is essential for mitochondrial homeostasis, mutations in or close to the functional domains are likely to cause mitochondrial dysfunction.

Fibroblasts were obtained from the patients carrying the mutations R272Q and R450C. The fibroblasts were used for characterization of mitochondrial phenotypes.

3.2 In silico analysis predict pathogenic effects of *RhoT1* mutations

The identified PD patients with mutations in *RhoT1* had a positiv family history. In order to assess the pathogenic relevance *in silico* analysis of the Miro1 variants were done by Patric May. Miro1-R272Q was predicted to be disease causing by eight out of the nine applied analysis tools. Miro1-R450C was predicted to be disease causing by SIFT, Polyphen2 HDIV, LRT, and Mutation taster prediction tool, whereas Polyphen2 HVAR and Mutation assessor prediction tools predicted that the mutation was probably disease causing. Miro1-F676V was predicted to be disease causing by LRT and Mutation taster.

All three mutations have a score of 0.164 for haplo-insufficiency, refelcting a medium likelihood (with a score of 0.3 predicting a high likelihood). All three mutations are expressed in the brain.

Variant	SIFT pred.	Polyphen2 HDIV pred.	Polyphen2 HVAR pred.	LRT pred.	Mutation taster pred.	Mutation assessor pred.	FATHMM pred.	RadialSVM pred.	LR pred.	Haplo-insufficincy
R272Q	D	D	D	D	D	H	T	D	D	0.164
R450C	D	D	P	D	D	M	T	T	T	0.164
F676V	T	B	B	D	D	N	T	T	T	0.164

Figure 7: In silico prediction of pathogenic effects of Miro1 mutations

Summary of *in silico* prediction of the pathogenic effects of the Miro1 mutations R272Q, R450C and F676V.

Legend: D = disease causing. H = high. P = probably disease causing. M = medium. B = benign. T = tolerable. N = normal.

Miro1-R272Q was predicted to be disease causing by eight of the nine applied analysing tools, whereas the prediction was less clear for Miro1-R450C and Miro1-F676V. The role of Haplo insufficiency in all three Miro1 variants was predicted with a medium score of 0.164 (a value of ≥ 0.3 predicts a high likelihood of haplo-insufficiency).

3.3 A homology model of human Miro1 shows that amino acids R272 and R450 are highly conserved and exposed at the protein surface

A homology model of the protein was computerized by Enrico Glaab (LCSB, University of Luxembourg, Esch-sur-Alzette) to further assess the effect of the identified mutations on the protein structure. Do date there was only part of the crystal structure of dMiro published by Klosowiak et al. (2013). This crystal structure (Figure 8 A) was used to construct a homology model of the human Miro1 protein (Figure 8 B). Sequence alignment with BLOSUM62 substitution matrix software revealed a sequence similarity of dMiro and human Miro1 protein of ~60.51 %. The amino acid F676 is not conserved in *drosophila* and was therefore not included in the homology model for human Miro1 (Figure 10). Analysis showed that both amino acids R272 and R450 are highly conserved and exposed to the cytosol on the protein surface (Figure 8).

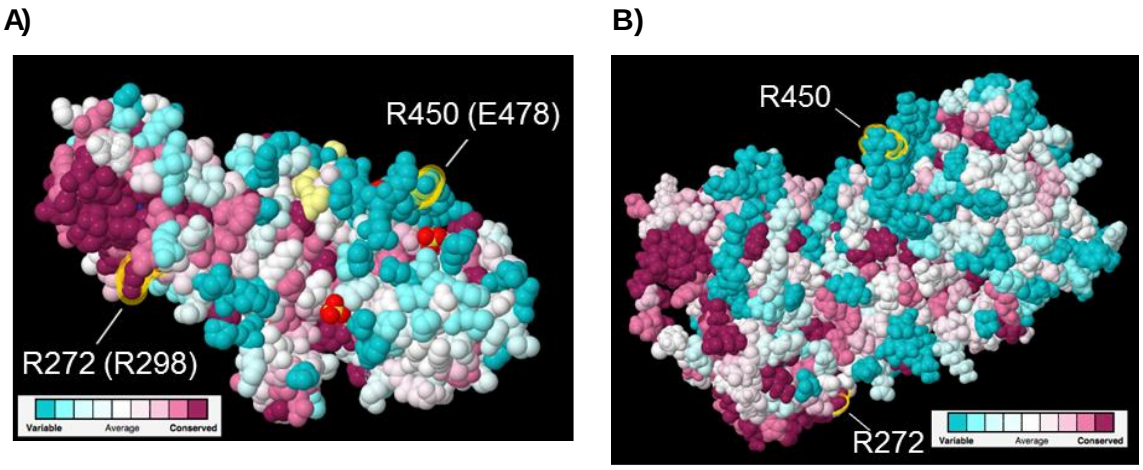

Figure 8: Crystal structure of dMiro and homology model of Miro1

Based on the crystal structure of dMiro (**A**) a homology model of human Miro1 (**B**) was constructed. The colour scale indicates the protein surface conservation scores from a multiple sequence alignment.

The influence of the mutations on the protein stability was predicted with NeEMO and I-MUTANT 2.0 methods. Both mutations R272Q and R450C cause only a slight decrease of protein stability:

Miro1 variant	NeEMO	I-MUTANT 2.0
R272Q	0.32 Kcal/mol	0.4 Kcal/mol
R450C	0.39 Kcal/mol	0.07 Kcal/mol

Figure 9: Impact of mutations on Miro1 protein stability

PhosphoSitePlus analysis showed that the closest phosphorylation sites to R272Q and R450C are residues T298 and Y463, both phosphorylation sites are not located adjacent to the mutations in the 3D structure that was predicted by I-TASSER.

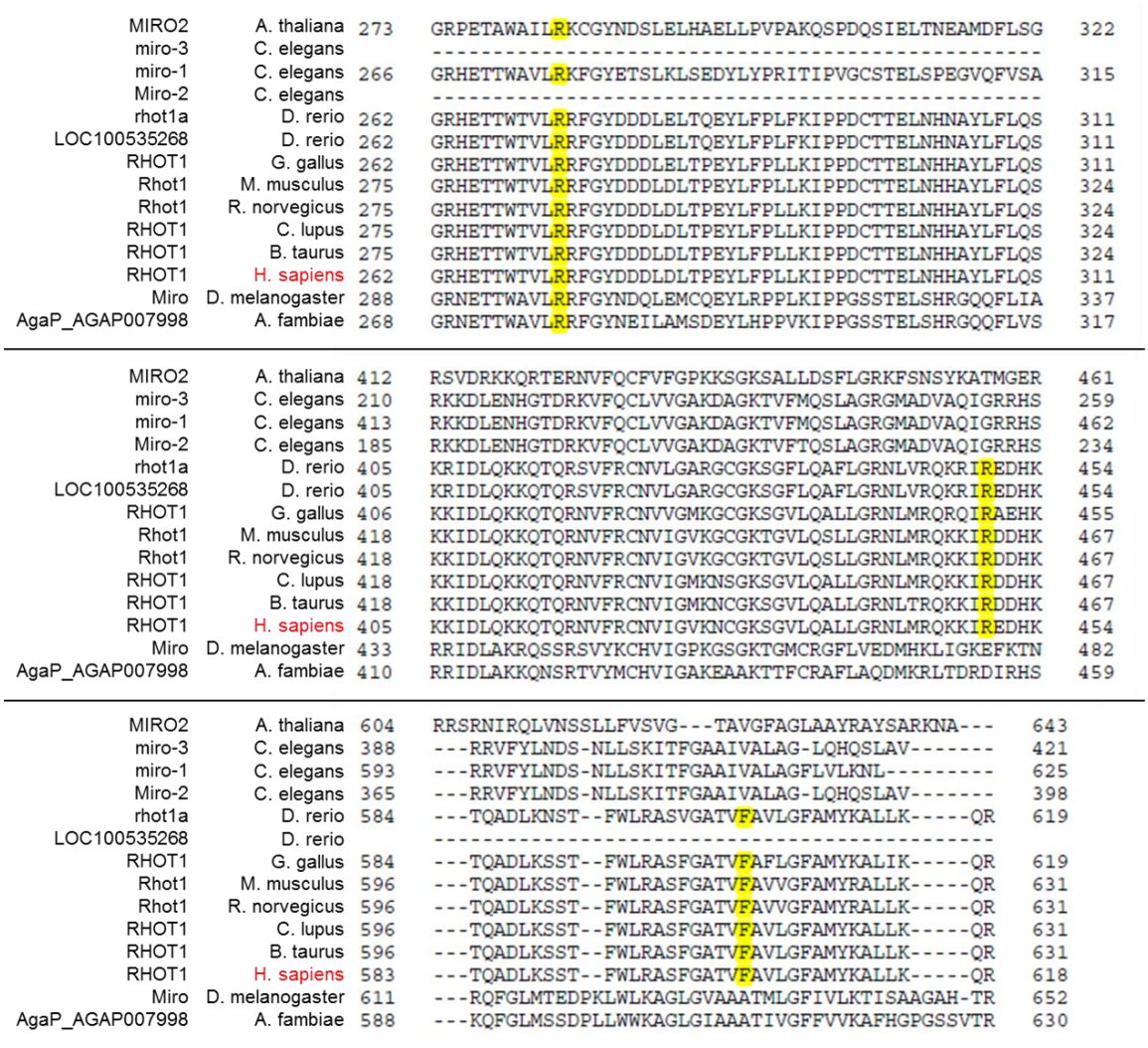

Figure 10: Multiple alignment for mutated Miro1 sites in different species

The multiple sequence alignment was created with NCBI. Sections of the amino acid sequence of Miro1 containing the amino acids R272, R450 and F676 are highlighted in yellow. The amino acid R272 is highly conserved in all shown species and R450 and F676 are conserved in vertebrates.

(http://www.ncbi.nlm.nih.gov/homologene?cmd=Retrieve&dopt=MultipleAlignment&list_uids=56803)

3.4 Data mining and genotyping of cohorts reveals the rareness of PD-associated *RhoT1* mutants

Analysis of existing genetic databases was performed by Manu Sharma and Peter Lichtner to further substantiate the association of the Miro1 variants R272Q, R450C or F676V with PD. On the whole exome server which includes 1500 genomes these Miro1 variants were not found. Furthermore the R272Q and F676V variant were not found in genetic information of a total of 67486 unrelated individuals available from the following databases: snp138, avsnp138, cosmic70, cosmic68wgs, nci60, esp6500si, esp6500siv2, cg46, cg69, 1000g2014oct, exac02, exac alleles, popfreq. Only the R450C variant was found in cosmic70, a database for somatic cancer mutations. There was no further information available about neurological diagnosis of this individual (Table 30).

To further validate the genetic data another genotyping of an independent cohort with DNA samples of 1238 German PD patients and 662 healthy unrelated individuals (KORA-Study) was done by the laboratory of Peter Lichtner. In this cohort the F676V variant was identified in one healthy control sample of a 63 year old male without PD diagnosis (Table 30).

Based on these results it is likely that the identified Miro1 mutantions R272Q and R450C are rare pathogenic variants.

Table 30: Screen for Miro1 variants

Data origin	Sample size	Type of analysis	Variants
Whole Exome Server on neurodegenerative diseases (Tübingen, Munich)	1500 genomes	database	--
662 healthy controls (KORA cohort) 1238 German PD patients	1900 samples	genotyping	F676V in control
different databases*	67486 unrelated individuals	database	R450C in cosmic70

***)** different databases: snp138, avsnp138, cosmic70, cosmic68wgs, nci60, esp6500si, esp6500siv2, cg46, cg69, 1000g2014oct, exac02, exac alleles, popfreq

3.5 Gem1-R298Q is not sufficient to rescue the growth defect of *gem1*Δ yeast on a non-fermentable carbon source

Several studies reported a growth defect of yeast, which was devoid of Gem1, the yeast orthologue of Miro, on medium containing a non-fermentable carbon source (Frederick, McCaffery et al. 2004) (Kornmann, Osman et al. 2011). Therefore it was of great interest whether the Miro mutants display the same phenotype. The residue R272 is conserved in yeast on position R298, whereas residues R450 and F676 are not conserved in yeast (Figure 11).

Gem1p [Saccharomyces cerevisiae S288c]
Sequence ID: **ref|NP_009351.1|** Length: 662 Number of Matches: 1

See 3 more title(s)
Range 1: 3 to 612

Score	Expect	Method	Identities	Positives	Gaps	Frame
294 bits(753)	8e-94()	Compositional matrix adjust.	199/623(32%)	319/623(51%)	57/623(9%)	

Features:

```
Query  2    KKDVRILLVGEPRVGKTSLIMSLVSEEFPEEVPPRAEEITIPADVT--PERVPTHIVDYS  59
            K+ +R+++ G+  VGK+SLI+SL   EF   +      I+IP D +  P   P + V
Sbjct  3    KETIRVVICGDEGVGKSSLIVSLTKAEFIPTIQDVLPPISIPRDFSSSPTYSPKNTVLID  62

Query  60   EAEQSDEQLHQEISQANVICIVYAVNNKHSIDKVTSRWIPLINERTDKDSRLPLILVGNK  119
             ++     L  E+  A+VI +VY   +  S D V+  W+P           +P+IL  NK
Sbjct  63   TSDSDLIALDHELKSADVIWLVYC--DHESYDHVSLFWLPHFRSLG---LNIPVILCKNK  117

Query  120  SDL---VEYSSM----------------ETILPIMNQYTEIETCVECSAKNLKNISELFY  160
             D    V  ++M                E  +PI+ ++ EI+TC++ SAK   ++++ FY
Sbjct  118  CDSISNVNANAMVVSENSDDDIDTKVEDEEFIPILMEFKEIDTCIKTSAKTQFDLNQAFY  177

Query  161  YAQKAVLHPTGPLYCPEEKEMKPACIKALTRIFKISDQDNDGTLNDAELNFFQRICFNTP  220
              Q+A+ HP  PL+     E+KP  + AL RIF +SD + D  L+D E+   Q+ CFN
Sbjct  178  LCQRAITHPISPLFDAMVGELKPLAVMALKRIFLLSDLNQDSYLDDNEILGLQKKCFNKS  237

Query  221  LAPQALEDVKNV---VRKHISDG------VADSGLTLKGFLFLHTLFIQRGRHETTWTVL  271
             +    L  +K++   + KH  +       V   G+T  GFL L+ ++ +RGRHETTW +L
Sbjct  238  IDVNELNFIKDLLLDISKHDQEYINRKLYVPGKGITKDGFLVLNKIYAERGRHETTWAIL  297

Query  272  RRFGYDDDLDLTPEYLFPLLKIPPDCTTELNHHAYLFLQSTFDKHDLDRDCALSPDELKD  331
             R F Y D L +  + L P L +P   + EL+   Y FL   F K D+D D  L+  EL
Sbjct  298  RTFHYTDSLCINDKILHPRLVVPDTSSVELSPKGYRFLVDIFLKFDIDNDGGLNNQELHR  357

Query  332  LFKVFPYIP--W-GPDVNNTVCTNERGWITYQGFLSQWTLTTYLDVQRCLEYLGYLGYSI  388
             LFK  P +P  W   +   +   N +G IT QG+L+QW++TT+L+      YL Y G+
Sbjct  358  LFKCTPGLPKLWTSTNFPFSTVVNNKGCITLQGWLAQWSMTTFLNYSTTTAYLVYFGF--  415

Query  389  LTEQESQASAVTVTRDKKIDLQKKQ------TQRNVFRCNVIGVKNCGKSGVLQALLGRN  442
              QE    A+ VT+ +K+  +  +        R VF C VIG   CGKS +L+A LGR+
Sbjct  416  ---QEDARLALQVTKPRKMRRRSGKLYRSNINDRKVFNCFVIGKPCCGKSSLLEAFLGRS  472

Query  443  LMRQKKIREDHKSYYAINTVYVY-GQEKYLLLHDISESEF--LTEAEII--CDVVCLVYD  497
              ++     K   A+N++ +  G++ YL+L ++ E E+  L   + +  CDV+CL YD
Sbjct  473  F--SEEYSPTIKPRIAVNSLELKGGKQYYLILQELGEQEYAILENKDKLKECDVICLTYD  530

Query  498  VSNPKSFEYCARIFKQHFMDSRIPCLIVAAKSDLHEVKQEYSISPTDFCRKHKMPPPQAF  557
              S+P+SF Y   +  +      +P + VA+K+DL + +Q   I P +   +  +  P
Sbjct  531  SSDPESFSYLVSLLDKFTHLQDLPLVFVASKADLDKQQQRCQIQPDELADELFVNHPLHI  590

Query  558  TCNTADAPSKDIFVKLTTMAMYP  580
             +     + + ++F+K+T  A+ P
Sbjct  591  SSRWLSSLN-ELFIKITEAALDP  612
```

Figure 11: Alignment of human RhoT1 and yeast gem1 sequence

Alignment of human Miro1 sequence and yeast Gem1p sequence using the blast tool of NCBI. Amino acids R272 (R298 in yeast) and R450C are highlighted in yellow. R272 is conserved in yeast at position R298, whereas R450 and F676V are not conserved in yeast.

On YPD medium containing a fermentable carbon source the *gem1*Δ yeast and *gem1*Δ yeast transfected with Gem1-R298Q showed similar growth as the wild type strain at 30° as well as at 35°C.

Consistent with previous studies (Frederick, McCaffery et al. 2004) (Kornmann, Osman et al. 2011) the *gem1*Δ yeast strain generated by the laboratory of Prof. Doron Rapaport (Interfakultäres Iinstitut für Biochemie, IFIB, University of Tübingen, Germany) showed poor growth on non-fermentable YPG medium (Figure 12). Transfection of *gem1*Δ yeast with wild type *gem1* (WT) successfully rescued the growth defect (Figure 12 B).

Interestingly, transfection with Gem1-R298Q was not sufficient to rescue the growth defect of *gem1*Δ yeast (Figure 12 B).

Wild type Gem1 and Gem1-R298Q constructs with HA tag displayed similar growth patterns as the untagged proteins (Figure 12 A).

The results indicate that *gem1*Δ causes a deficiency of oxidative phosphorylation in yeast and that Gem1-R298Q causes a similar phenotype, which argues for a loss of function of Gem1-R298Q.

A)

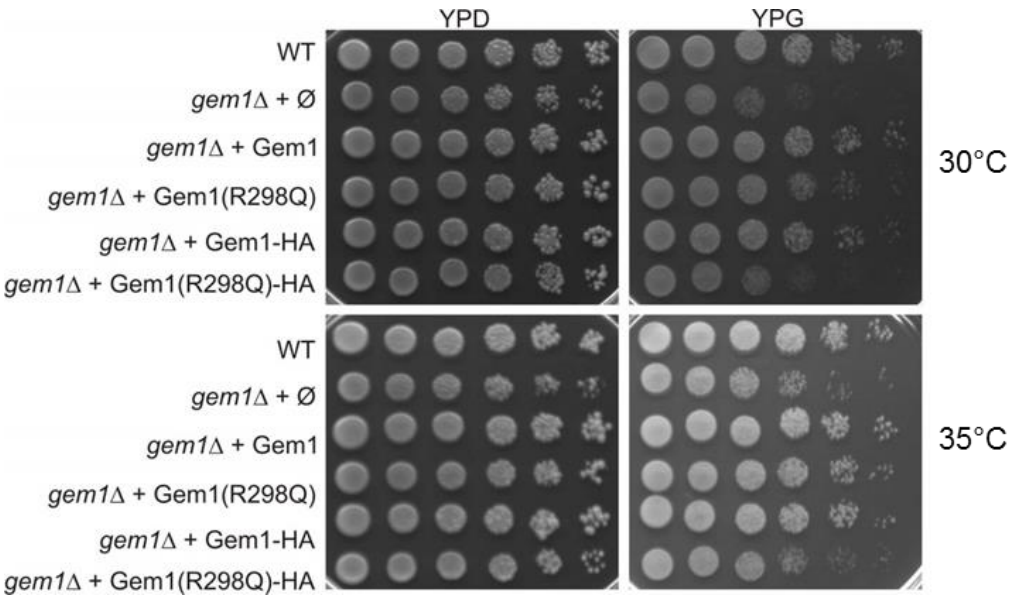

B)

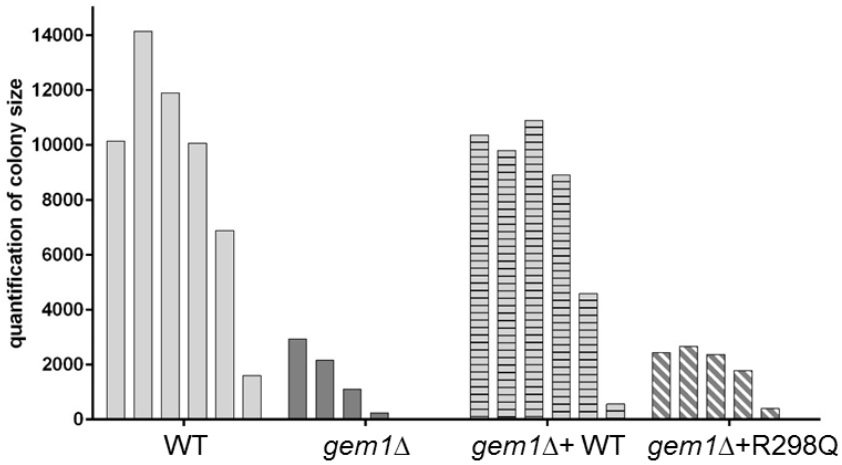

Figure 12: Yeast growing on different media at 30°C and 35°C

A) Drop dilution assay of a yeast *Saccharomyces cerevisiae* strain with deletion of *gem1* (*gem1*Δ) on YPD medium and YPG medium at 30°C and at 35°C.

B) Densitometry quantification of colony size of yeast grown on non-fermentable YPG medium at 30°C. The *gem1*Δ yeast strain grows less efficient on non-fermentable YPG medium, whereas a transfection of Gem1-WT sufficiently rescues the growth phenotype. In contrast, retransfection of the *gem1*Δ yeast strain with Gem1-R298Q is not sufficient to restore the growth.

Legend: **WT** = wild type yeast strain. ***gem1*Δ** = *gem1* deficient yeast strain. ***gem1*Δ + Gem1** = *gem1* deficient strain retransfected with wild type *gem1*. ***gem1*Δ + Gem1(R298Q)** = *gem1* deficient strain retransfected with Gem1-R298Q.

3.6 Miro1 protein level is reduced in Miro1 mutant fibroblasts

Analysis of the homology model of Miro1 revealed a slightly decreased protein stability caused by the mutations (Figure 8). Furthermore, results of *gem1*Δ yeast transfected with Gem1-R298Q (Figure 12) indicated that at least Miro1-R272Q could be a loss of function mutation. Therefore first interest was focused on the protein level of Miro1 in patient-derived fibroblasts.

The mitochondrial membrane protein Tom20 served as marker for mitochondrial mass. As Miro1 is anchored in the outer mitochondrial membrane (Fransson, Ruusala et al. 2006), Miro1 protein level was normalized to Tom20 protein.

The applied Miro1 antibodies bind at epitopes, which are located distinct from the amino acids R272 and R450C (Figure 3), therefore avoiding the possibility that mutant Miro1 was not detected due to impaired antibody binding.

The data revealed that Miro1 protein level was significantly reduced to less than half in both patient-derived immortalized fibroblast lines compared to Ctrl 1 fibroblasts. In Miro1-R272Q fibroblasts Miro1 protein level was reduced to ~0,2 fold and in Miro1-R450C fibroblasts to ~0,4 fold of Miro1 protein level in the Ctrl 1 fibroblast line (Figure 13).

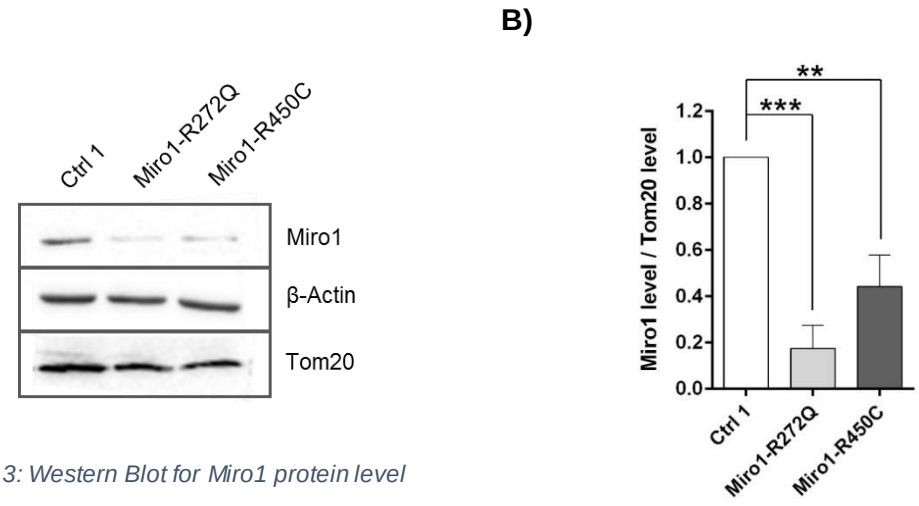

Figure 13: Western Blot for Miro1 protein level

A) Representative image of Western Blot showing Miro1 and Tom20 protein. **B)** Densitometry evaluation of Western Blot analysis. Miro1 protein level normalized to Tom20 protein, relative to Control 1, is significantly reduced in both Miro1 mutant fibroblast lines. Data indicated as mean ± SEM. * $p \leq 0.05$ ** $p \leq 0.01$ *** $p \leq 0.001$ by multiple t-test, Holm-Sidak multiple comparison correction. n = 4

3.6.1 RhoT1 mRNA level is decreased in Miro1-R450C mutant fibroblasts

Miro1 protein level was significantly decreased in Miro1-R272Q and Miro1-R450C mutant fibroblasts (Figure 13). Therefore, semi-quantitative rtPCR was used to shed light on the possible reason behind the reduced protein level.

Evaluation of semi-quantitative rtPCR results obtained from mRNA showed that *RhoT1* mRNA level was significantly reduced in Miro1-R450C fibroblasts to ~0.5 fold of the level of *RhoT1* mRNA in Ctrl 1 fibroblasts. Although Miro1 protein level was significantly reduced in Miro1-R272Q fibroblasts as well (Figure 13), *RhoT1* mRNA level was not changed in this cell line.

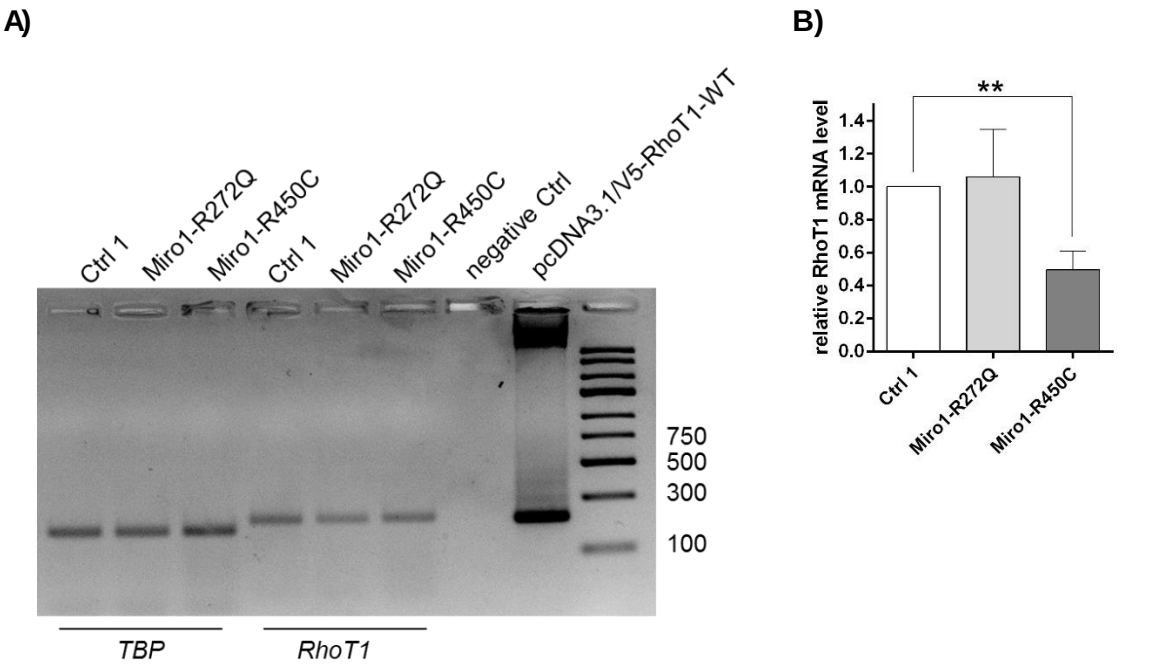

Figure 14: semi quantitative measurement of RhoT1 mRNA level

A) Representative image of agarose gel of semi quantitative rtPCR. Bands are visible for the house-keeping gene *TBP* and for *RhoT1* cDNA level. *RhoT1* bands were normalized to *TBP* bands. The primers for *RhoT1* were also applied on the pcDNA3.1/V5-*RhoT1*-WT construct to verify the primer specificity for *RhoT1*. The DNA ladder indicates bands ranging from 100 to 750 bp. **B)** Quantification of *RhoT1* mRNA level. Signal intensity of bands of *RhoT1* were normalized to the signal of TBP bands. The mRNA level of *RhoT1* was significantly reduced in Miro1-R450C fibroblasts compared to Ctrl 1 and Miro1-R272Q fibroblasts. Data indicated as mean ± SEM, * $p \leq 0.05$ ** $p \leq 0.01$ *** $p \leq 0.001$ by multiple t-test, Holm-Sidak multiple comparison correction. n = 5.

3.6.2 *RhoT1 mutant RNA is expressed in Miro1-R272Q and Miro1-R450C fibroblasts*

The amount of Miro1 protein was significantly reduced in both Miro1 mutant fibroblast lines (Figure 13) and semi-quantitative PCR revealed that mRNA levels of *RhoT1* were reduced in Miro1-R450C fibroblasts (Figure 14). These findings lead to the question whether the heterozygous *RhoT1* variants leading to Miro1 mutant protein are expressed in Miro1 mutant fibroblast lines.

Sequencing of cDNA synthesized from mRNA of Ctrl 1 fibroblasts confirmed that these fibroblasts are homozygous wild type for the nucleotides at position c.815 and at position c.1348 of the cDNA (Figure 15 A, B).

In contrast, the chromatogram of cDNA from Miro1-R272Q fibroblasts showed the heterozygous expression of Guanine (G) and Adenine (A) at position c.815 (Figure 15 C). The exchange of G>A at position c.815 leads to the exchange of the amino acid Arginine (R) to Glutamine (Q).

In Miro1-R450C fibroblasts sequencing of *RhoT1* cDNA revealed the heterozygous expression of Cytosine (C) and Thymine (T) at position c.1348 (Figure 15 D). The substitution of C>T at position c.1348 leads to a change of the amino acid Arginine (R) to Cysteine (C).

Thus, sequencing of *RhoT1* cDNA showed that heterozygous *RhoT1* variants are expressed on mRNA level in Miro1-R272Q fibroblasts and in Miro1-R450C fibroblasts.

A) Chromatogram of *RhoT1* cDNA at position c.815 – Ctrl 1 fibroblasts

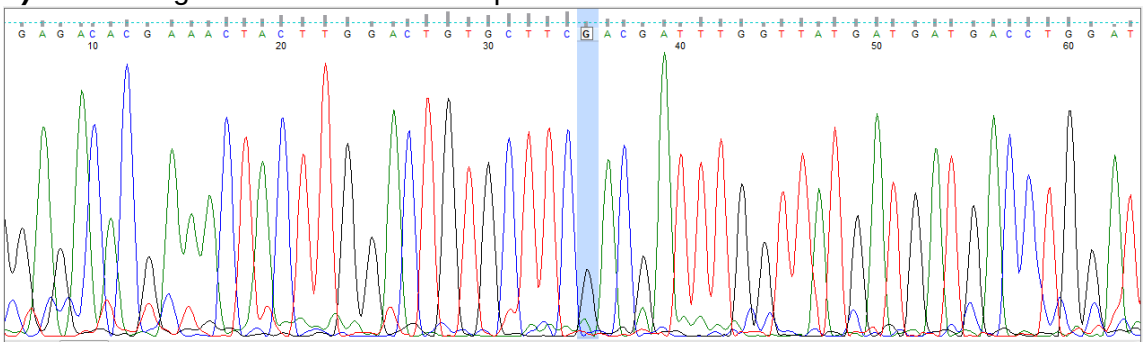

B) Chromatogram of *RhoT1* cDNA at position c.1348 – Ctrl 1 fibroblasts

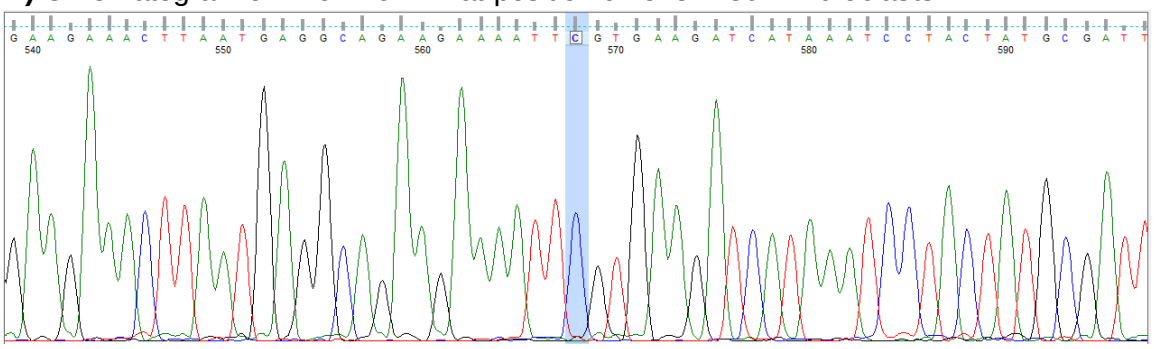

C) Chromatogram of *RhoT1* cDNA at position c.815 – Miro1-R272Q fibroblasts

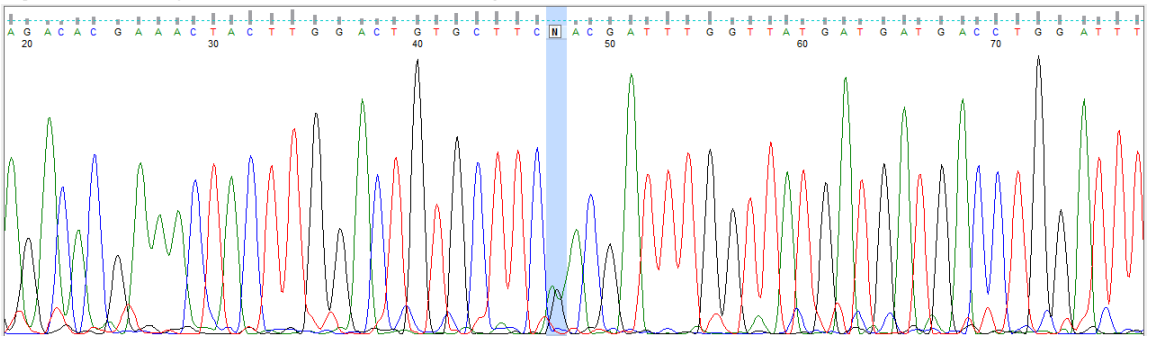

D) Chromatogram of *RhoT1* cDNA at position c.1348 – Miro1-R450C fibroblasts

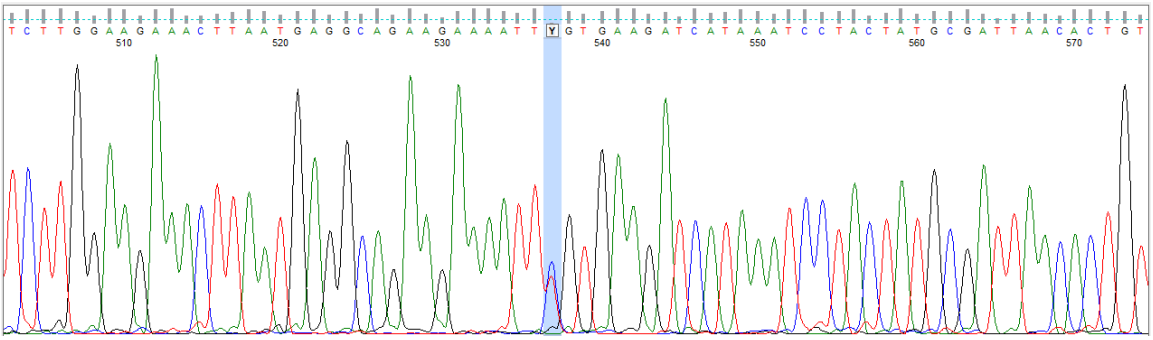

Figure 15: Chromatograms of RhoT1 cDNA

Chromatograms of cDNA from fibroblast lines. RNA was isolated from all three fibroblast lines and subsequently used to synthesize cDNA. Sanger sequencing was performed on cDNA and the resulting chromatograms were visualized with FinchTV software. **A) B)** Chromatograms of *RhoT1* cDNA from Ctrl 1 fibroblasts. Nucleotides at position c.815 and c.1348 are highlighted in blue. Ctrl 1 fibroblasts are homozygous wild type for both positions. **C)** Chromatogram of *RhoT1* cDNA from Miro1-R272Q fibroblasts showed that the cells were heterozygous at position c.815, expressing wild type Guanine (G) as well as mutant Adenine (A). **D)** Chromatogram of *RhoT1* cDNA from Miro1-R450C fibroblasts revealed heterozygous expression of wild type Cytosine (C) and mutant Thymine (T) at position c.1348.

3.6.3 Rescue of Miro1 protein by inhibition of the proteasome

Due to the observation that reduction of Miro1 protein in Miro1-R272Q fibroblasts was apparently not accompanied by decreased *RhoT1* mRNA levels, we wondered whether it was possible to rescue Miro1 protein levels by specific inhibition of proteasomal degradation using 10 µM MG132. Previous studies reported that Miro1 is degraded predominantly via the proteasomal pathway rather than by the lysosomal pathway (Wang, Winter et al. 2011) (Birsa, Norkett et al. 2014). Immortalized fibroblasts were treated with 10 µM MG132 for 14 h and afterwards protein levels were analysed by Western Blot. Miro1 bands running at ¬75 kDa were considered to be not ubiquitinated, whereas bands running higher were considered as ubiquitinated Miro1 ((Ub)n-Miro1) (Birsa, Norkett et al. 2014).

Analysis showed that MG132 treatment increased Miro1 protein in Ctrl 1 fibroblasts as well as in Miro1-R272Q and Miro1-R450C fibroblasts (Figure 16 A, B). However, only in Ctrl 1 fibroblasts the Miro1 protein level after MG132 treatment was significantly higher compared to Miro1 protein in untreated cells.

Mean values of Miro1 protein were used to calculate the ~fold increase of Miro1 protein after inhibition of the proteasome, expressed as ratio of Miro1 protein after MG132 treatment/ Miro1 amount in untreated cells. In Ctrl 1 fibroblasts inhibition of the proteasome increased Miro1 protein levels to ~3 fold, whereas in Miro1-R272Q and Miro1-R450C fibroblasts Miro1 was increased to ~4.6 - 4.7 fold. This revealed that inhibition of the proteasome increased Miro1 protein ~1.6 fold more in Miro1 mutant fibroblasts lines compared to Ctrl 1 fibroblasts.

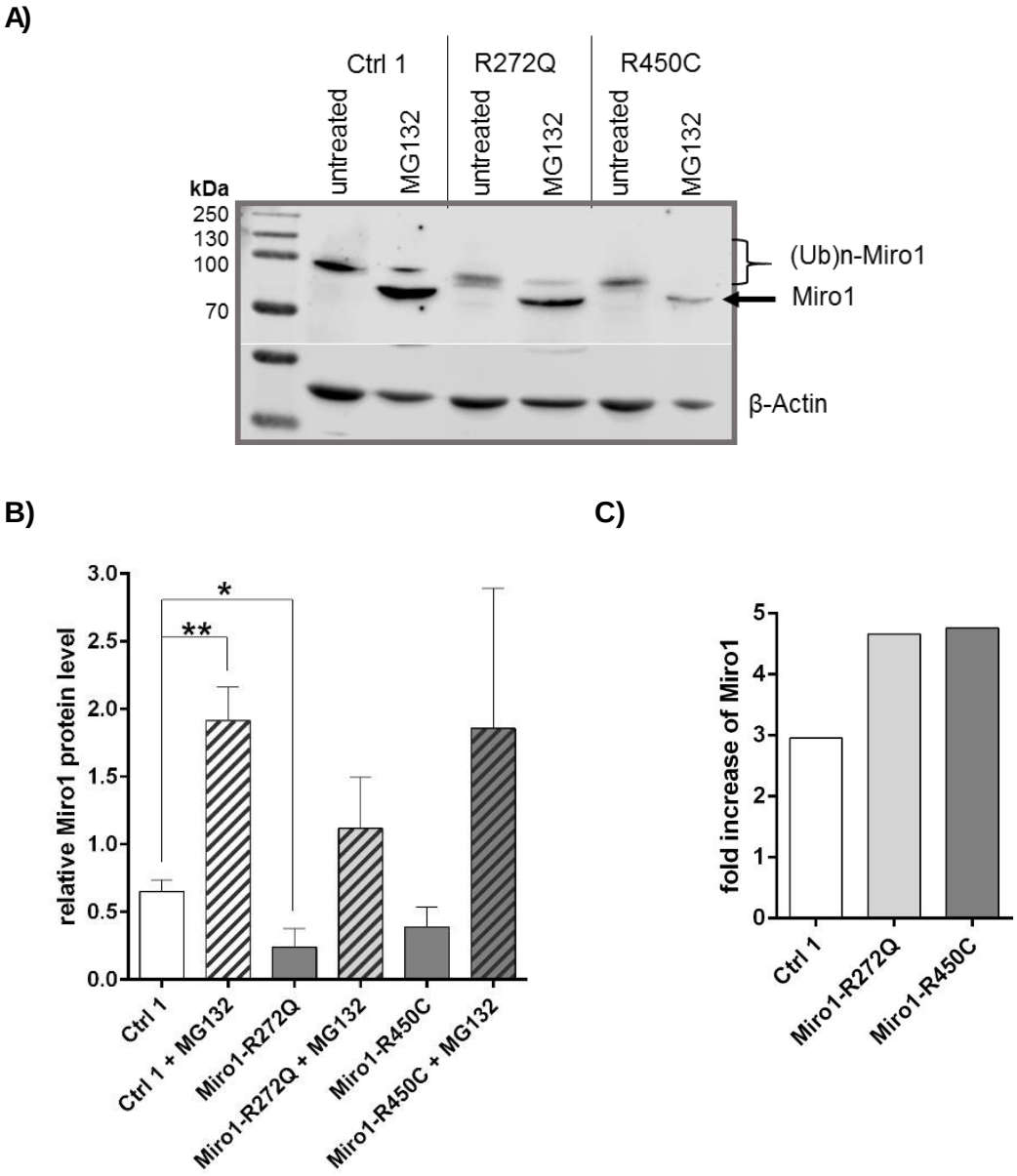

Figure 16: Rescue of Miro1 protein by inhibition of the proteasome

A) Representative Western Blot showing Miro1 protein in lysates from immortalized fibroblasts treated with 10 µM MG132 for 14 h. Inhibition of the proteasome leads to increase of Miro1 protein of ¬75 kDa. Higher molecular bands of Miro1 were considered to be ubiquitinated Miro1 ((Ub)n-Miro1). **B)** Densitometry evaluation of total Miro1 protein amount showed that inhibition of the proteasome rescues Miro1 protein level in all three fibroblast lines. **C)** Ratio of Miro1 protein after MG132 treatment to Miro1 protein in untreated cells indicates ~fold increase of Miro1 protein amount upon proteasome inhibition. The increase of Miro1 protein is higher in Miro1-R272Q and Miro1-R450C fibroblasts compared to Ctrl 1 fibroblasts. Data indicated as mean ± SEM. * $p \leq 0.05$ ** $p \leq 0.01$ *** $p \leq 0.001$ by multiple t-test, Holm-Sidak multiple comparison correction. n = 5

3.7 Miro1-R450C causes reduction of mitochondrial mass in fibroblasts

Miro1 protein level was assessed together with Tom20 protein, which served as marker for mitochondrial mass. Interestingly, the Western Blot analysis of Tom20 protein revealed that mitochondrial mass was significantly reduced in Miro1-R450C fibroblasts to ~0,4 fold of the mitochondrial mass of Ctrl 1 fibroblasts (Figure 17). Also mitochondrial mass in Miro1-R450C fibroblasts was significantly lower compared to Miro1-R272Q fibroblasts.

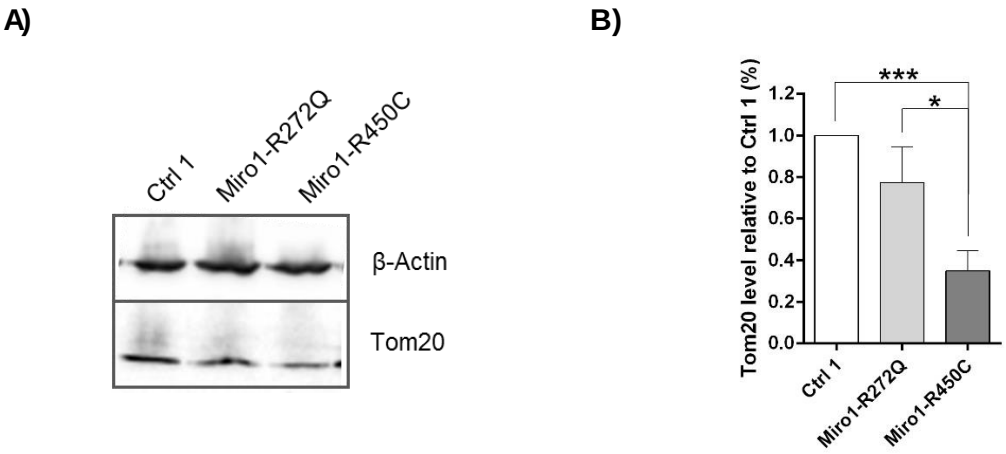

Figure 17: Western Blot for Tom20 protein level

A) Representative image of Western Blot showing Tom20 protein. **B)** Densitometry evaluation of Western Blot analysis. Tom20 protein level normalized to β-Actin protein. Tom20 protein level is significantly reduced in Miro1-R450C mutant fibroblast lines compared to Control 1. Data indicated as mean ± SEM. * $p \leq 0.05$ ** $p \leq 0.01$ *** $p \leq 0.001$ by multiple t-test, Holm-Sidak multiple comparison correction. n = 9

To verify that Tom20 was a reliable marker for mitochondrial mass and not reduced independently of mitochondrial content, live cell imaging microscopy was used as independent approach to assess mitochondrial mass. Therefore, native fibroblasts were stained with MitoTracker green FM to analyse mitochondrial content. Bright field images of the same cells were used to measure the cell size for normalization of mitochondrial area. The resulting ratio of mitochondrial area to cell size served to indicate mitochondrial mass.

Evaluation of the obtained microscopy data showed that mitochondrial mass was indeed significantly reduced in Miro1-R450C fibroblasts compared to Ctrl 1 fibroblasts (Figure 18), thereby verifying Tom20 as indicator for mitochondrial mass.

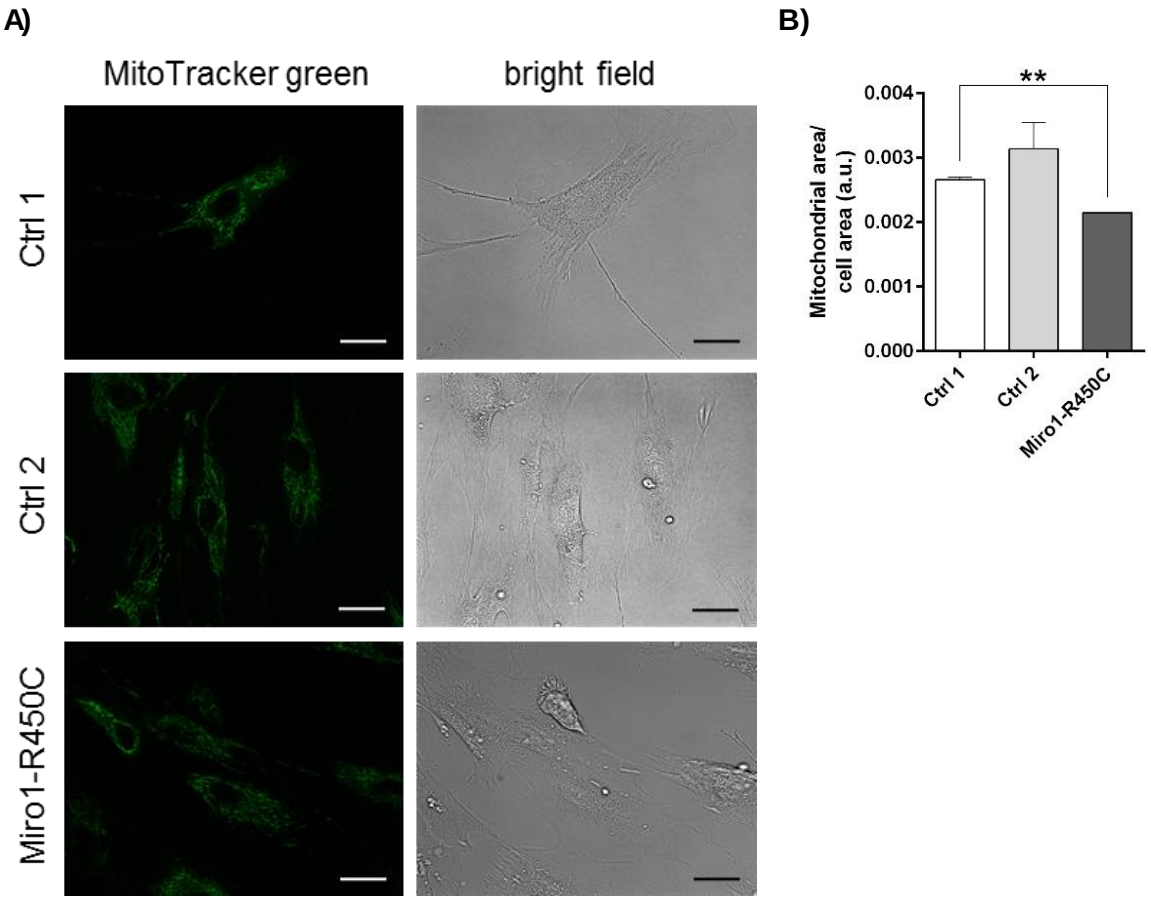

Figure 18: Live cell imaging of native fibroblasts for mitochondrial mass

Live cell imaging of native fibroblasts to analyse mitochondrial mass. **A)** Representative images of native fibroblasts stained with MitoTracker green to assess mitochondrial area. Bright field images were used to assess the cell size. Mitochondrial mass was calculated as ratio of mitochondrial area normalized to cell size. Miro1-R450C fibroblasts were compared to two age matched control fibroblast lines (Ctrl 1 and Ctrl 2). Images taken at x40 magnification. Scale bars indicate 20 µm. **B)** Evaluation of mitochondrial area normalized to cell size in native fibroblasts revealed that mitochondrial mass in Miro1-R450C fibroblasts was significantly lower compared to Ctrl 1 fibroblasts. Data indicated as mean ± SEM. * $p \leq 0.05$ ** $p \leq 0.01$ *** $p \leq 0.001$ by multiple t-test, Holm-Sidak multiple comparison correction. n = 2

3.7.1 Miro1 mutants cause reduction of mitochondrial mass in M17 cells

An independent cell model was established to investigate whether the Miro1 mutants are causative for the phenotypes observed in patient-derived fibroblasts. For this purpose a stable knockdown of endogenous *RhoT1* was established in the human neuroblastoma cell line M17.

3.7.1.1 Characterisation of M17 cells with stable knockdown of endogenous RhoT1 and overexpression of RhoT1 constructs

The knockdown of *RhoT1* was introduced using the BLOCK-iT Inducible Pol II miR RNAi Expression Vector Kit with EmGFP (Invitrogen GmbH, Karlsruhe, Germany). Different miRNA constructs were generated and transfected into M17 cells. After subsequent selection of positively transfected cells with Blasticidin S HCl (Invitrogen GmbH, Karlsruhe, Germany), the knockdown of *RhoT1* was verified by Western Blot analysis for Miro1 protein.

Western Blot showed that the miRNA-2471 construct in the 5'UTR of *RhoT1* induced the strongest downregulation of Miro1 protein to ~50 % compared to cells transfected with miRNA-Ctrl.

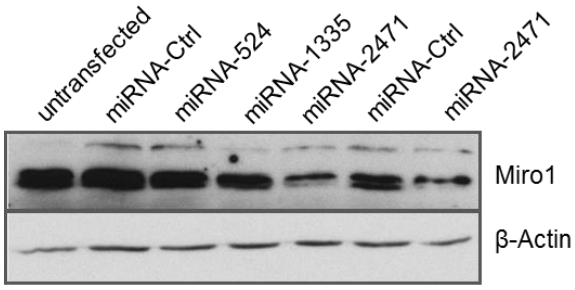

Figure 19: Western Blot analysis for RhoT1 knockdown in M17 cells

Western Bot analysis for Miro1 protein in M17 cells transfected with miRNA-Ctrl, miRNA-524, miRNA-1335 and miRNA-2471. The negative control miRNA-Ctrl caused no downregulation of Miro1 protein. The miRNA-2471 in the 5'ÚTR of *RhoT1* caused a significant reduction of Miro1 protein.

3.7.1.2 *M17 cells with stable knockdown of endogenous RhoT1 successfully express Miro1-V5 constructs*

For further analysis M17 cells were transfected with the miRNA-2471 construct and subsequently maintained under constant selection with 6 µg/ mL Blasticidin S HCl to generate a polyclonal M17 cell line with stable knockdown of endogenous *RhoT1*. The miRNA-2471 targets the 5'UTR of *RhoT1* and therefore allows the overexpression of *RhoT1*/V5 constructs while expression of the endogenous *RhoT1* is down regulated. This cell line was transfected with Miro1-V5 constructs overexpressing Miro1-WT, Miro1-R272Q, Miro1-R450C or Miro1-F676V with a V5 tag, respectively, for subsequent experimental analysis.

Western Blot showed that M17 cells with stable knockdown of endogenous *RhoT1* successfully overexpressed Miro1/V5 protein from the different applied constructs (Figure 20).

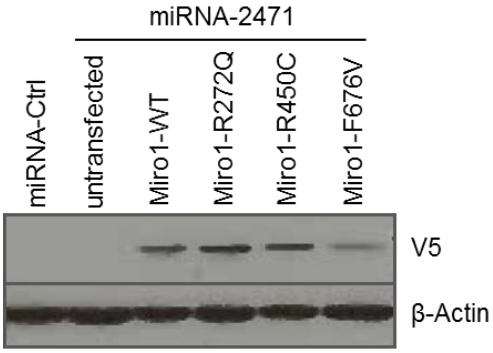

Figure 20: Western Blot for over expressed Miro1-V5 protein in M17 cells with knock down of endogenous Miro1

M17 cells with stable knockdown of endogenous *RhoT1* were transfected with the Miro1/V5 constructs Miro1-WT, Miro1-R272Q, Miro1-R450C or Miro1-F676V. Western Blot analysis showed the overexpression of the Miro1 protein with V5 tag.

3.7.1.3 *Over expressed Miro1/V5 protein is localized at mitochondria*

M17 cells with stable knockdown of endogenous *RhoT1* were transfected with Miro1-WT, Miro1-R272Q, Miro1-R450C or Miro1-F676V in pcDNA3.1/V5-HisA constructs, respectively (see 2.9). Cells were fixed and immunostained for microscopy (see 2.10.5) to verify the expression of Miro1/V5 constructs and the localization of the overexpressed protein on mitochondria.

Microscopy of fixed M17 cells stained with V5-antibody (Sigma Aldrich Chemie GmbH, Munich, Germany) and anti-RhoT1 antibody (Sigma Aldrich Chemie GmbH, Munich,

Germany) showed a clear overlap of V5 signal and Miro1 signal, proofing the specificity of Miro1 antibody (Figure 21).

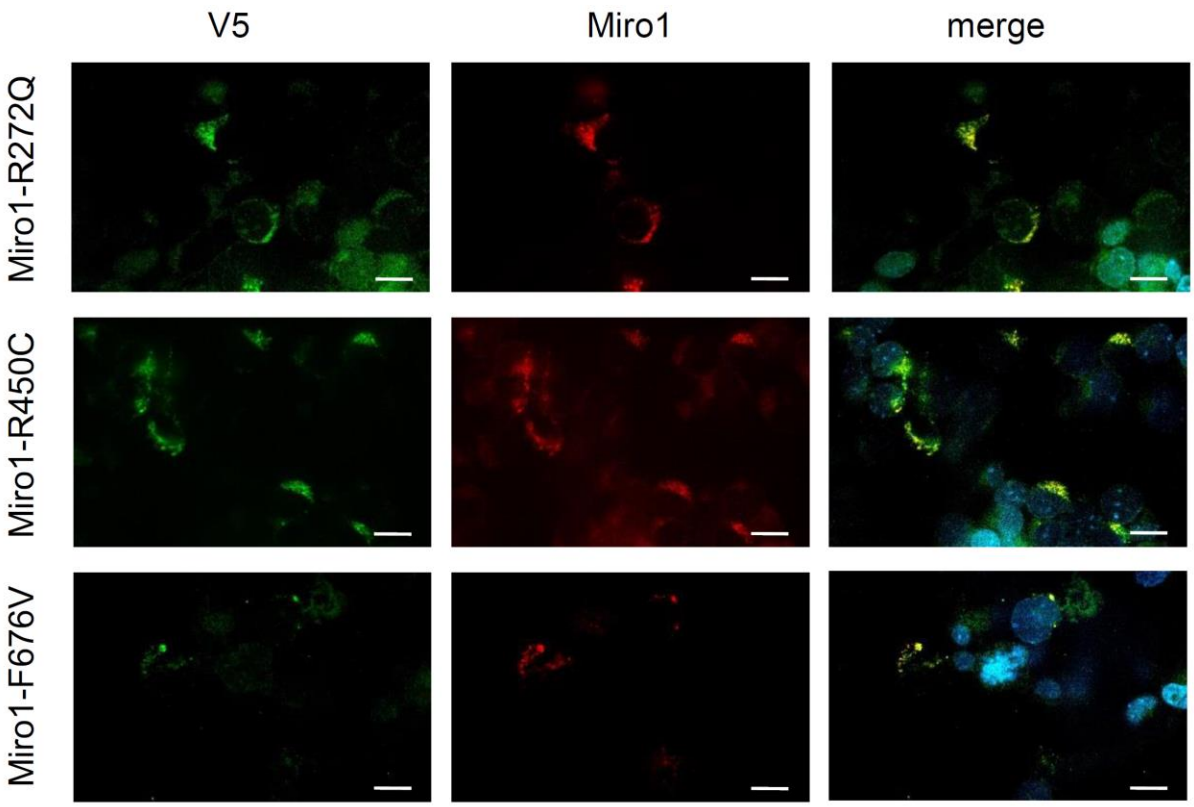

Figure 21: Expression of Miro1-V5 in M17 cells

M17 cells with stable knockdown of endogenous *RhoT1* were transfected with Miro1-R272Q, Miro1-R450C and Miro1-F676V constructs. Cells were fixed and stained with V5-antibody and Miro1-antibody and subsequently imaged. Microscopy analysis showed an overlap of V5-antibody stain and Miro1-antibody stain, indicating the specific targeting of both antibodies. Images taken at x63 magnification. Scale bars indicate 20 µm.

Microscopy images of fixed M17 cells stained with V5-antibody (Sigma Aldrich Chemie GmbH, Munich, Germany) and Tom20 antibody (Santa Cruz, Dallas, Texas, USA) (Figure 22 A) were furtheron used to analyse the co-localization of overexpressed Miro1 protein and mitochondria. The Pearson's coefficient for Miro1/V5 and Tom20 signal was calculated with approximately 0,6 for all Miro1/V5 proteins (Figure 22 B). This value indicates a partially overlap of Miro1/V5 and mitochondria, indicating that Miro1-WT/V5, Miro1-R272Q/V5, Miro1-R450C/V5 and Miro1-F676V/V5 are all partially localized to mitochondria.

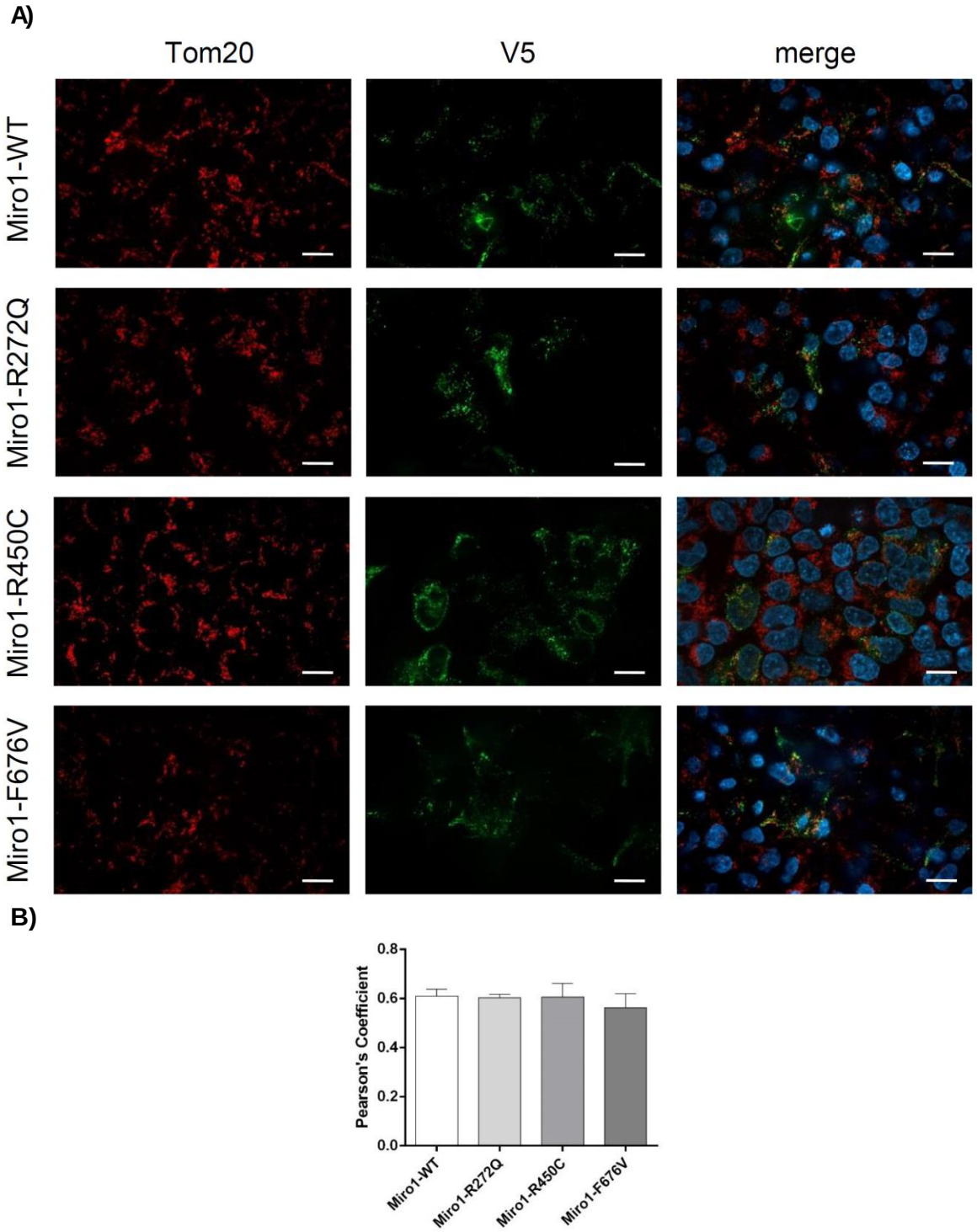

Figure 22: Co-localization of Miro1/V5 protein and mitochondria

A) M17 cells with stable knockdown of *RhoT1* were transfected with the Miro1/V5 constructs Miro1-WT, Miro1-R272Q, Miro1-R450C and Miro1-F676V. Cells were fixed and stained with V5-antibody and Tom20 antibody, which served as mitochondrial marker. Immunofluorescence signals were analysed with microscopy. Images taken at x63 magnification. **B)** Co-localization analysis of Miro1/V5 and Tom20 with ImageJ software revealed a Pearson's coefficient of approximately 0,6 for all Miro1-V5 constructs, indicating a partially overlap of Miro1 and mitochondria. Scale bars indicate 20 µm. Data indicated as mean ± SEM. * $p \leq 0.05$ ** $p \leq 0.01$ *** $p \leq 0.001$ by Students t-Test. n = 3

3.7.2 Overexpression of Miro1 mutant protein causes reduction of mitochondrial mass in M17 cells

M17 cells with stable knockdown of endogenous *RhoT1* were transiently transfected with pcDNA3.1/V5-HisA constructs overexpressing Miro1-WT, Miro1-R272Q, Miro1-R450C or Miro1-F676V. Cells were then used for Western Blot analysis of Tom20 protein to assess mitochondrial mass. Analysis of three independent experiments revealed that knockdown of *RhoT1* (*RhoT1*-KD) had no effect on Tom20 protein level. Overexpression of Miro1-WT likewise did not result in reduced Tom20 protein level. In contrast, overexpression of Miro1-R272Q, Miro1-R450C or Miro1-F676V resulted in significantly reduced Tom20 protein amount compared to M17 cells without knockdown of *RhoT1* (miRNA-Ctrl) (Figure 23), indicating that Miro1 mutations cause reduction of mitochondrial mass.

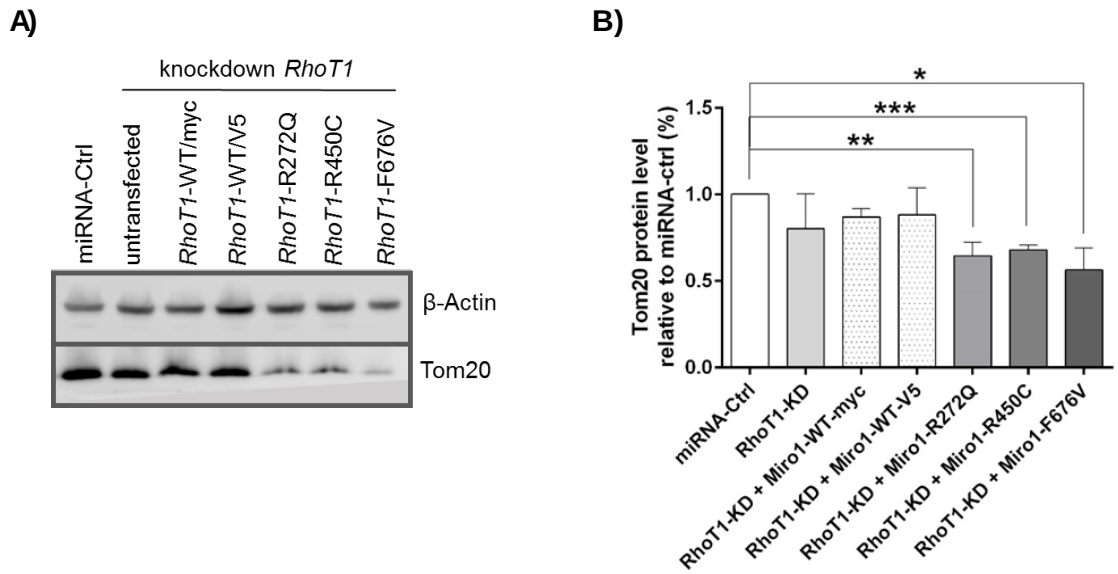

Figure 23: Western Blot for Tom20 protein level in M17 cells with RhoT1-KD

A) Representative Western Blot of M17 cells with stable knockdown of endogenous *RhoT1* (RhoT1-KD) and overexpression of Miro1-WT, Miro1-R272Q, Miro1-R450C or Miro1-F676V protein. **B)** Densitometry evaluation of Western Blot for Tom20 protein level. M17 cells with stable knockdown of endogenous *RhoT1* (*RhoT1*-KD), over-expressing Miro1-R272Q, Miro1-R450C or Miro1-F676V showed significantly less levels of Tom20 protein compared to M17 cells without knockdown of *RhoT1* (miRNA-Ctrl). Data indicated as mean ± SEM. * $p \leq 0.05$ ** $p \leq 0.01$ *** $p \leq 0.001$ by multiple t-test, Holm-Sidak multiple comparison correction. n = 3

3.8 Mitochondrial morphology is not changed in Miro1 mutant fibroblasts

Mitochondrial mass was found to be significantly reduced in Miro1 mutant fibroblasts. One possible reason could be an increased clearance of damaged mitochondria via mitophagy. Mitochondrial dysfunction can influence mitochondrial morphology as fusion with other mitochondria is an important factor for mitochondria maintenance (Amiri and Hollenbeck 2008) (Chen, McCaffery et al. 2007), whereas fission serves as initial step towards clearance (Weihofen, Thomas et al. 2009).

For analysis of mitochondrial morphology native fibroblasts were stained with the MMP-independent mitochondrial dye MitoTracker green FM (Figure 24) and analysed for Form Factor as indicator of mitochondrial branching and Aspect Ratio, which indicates mitochondrial length.

Analysis revealed that mitochondrial morphology was not altered in both mutant fibroblasts lines under standard growth conditions (Figure 25). Mitochondria showed neither a hyper fusion, nor a fragmentation phenotype, as assessed by From Factor and Aspect Ratio.

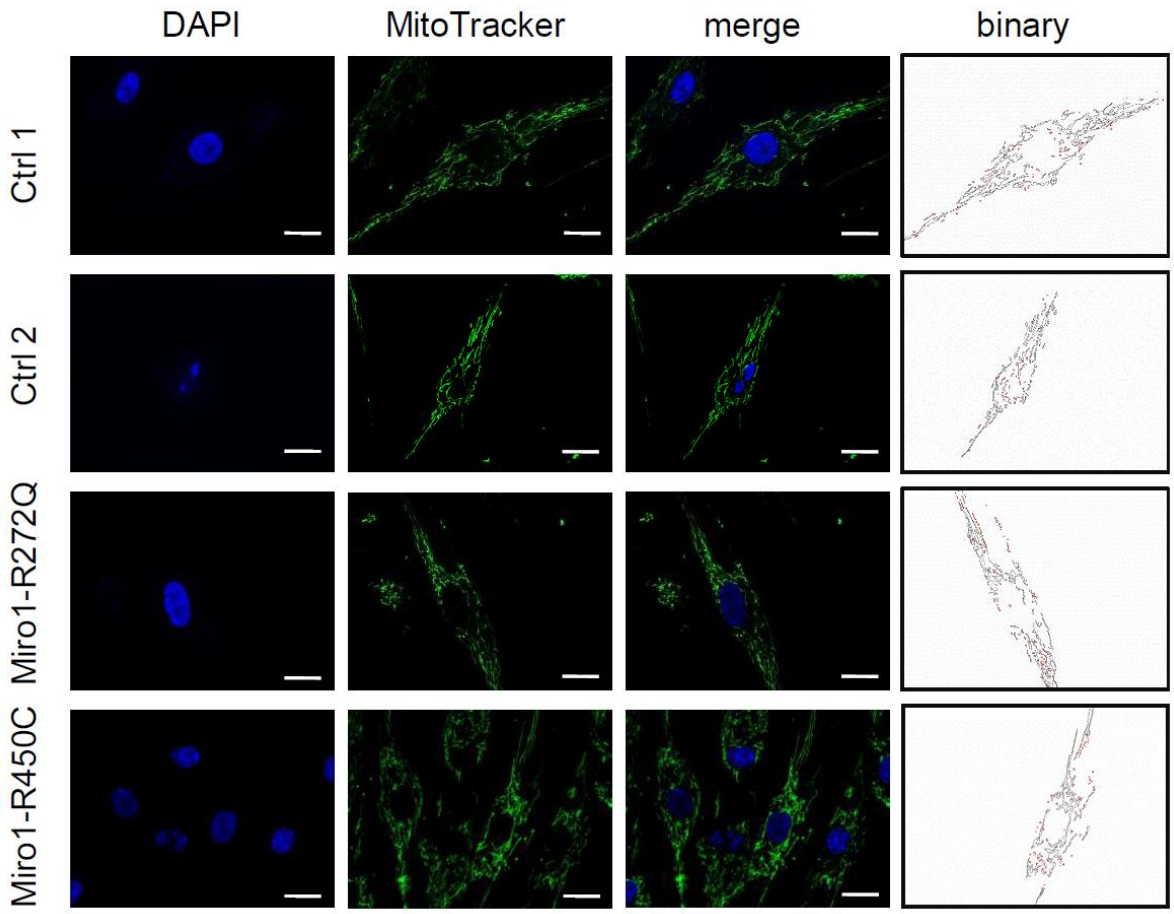

Figure 24: Live cell imaging of patient derived fibroblasts

Representative images of Live cell microscopy of native fibroblasts. Fibroblasts were stained with DAPI and MitoTracker green FM. Images taken at x40 magnification. Scale bars indicate 20 µm.

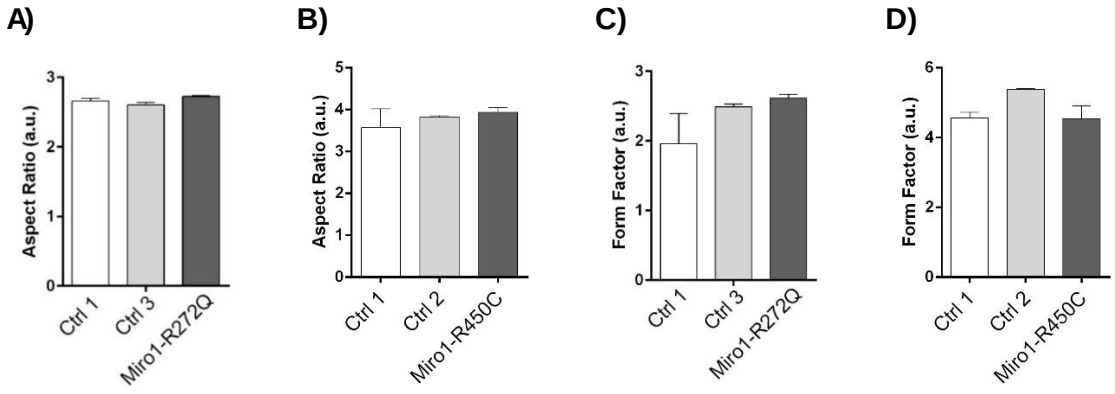

Figure 25: Mitochondrial morphology in patient-derived native fibroblasts

The Live cell microscopy images of native fibroblasts were analysed with ImageJ software for the parameters perimeter, area, major axis and minor axis of the defined mitochondria, which were used to calculate Form Factor and Aspect Ratio. Mitochondrial morphology was not altered in Miro1-R272Q and Miro1-R450C fibroblasts. n = 3-4

3.9 Mitophagy is impaired in Miro1 mutant fibroblasts

3.9.1 Co-localization of mitochondria and lysosomes is not increased in Miro1 mutant fibroblasts

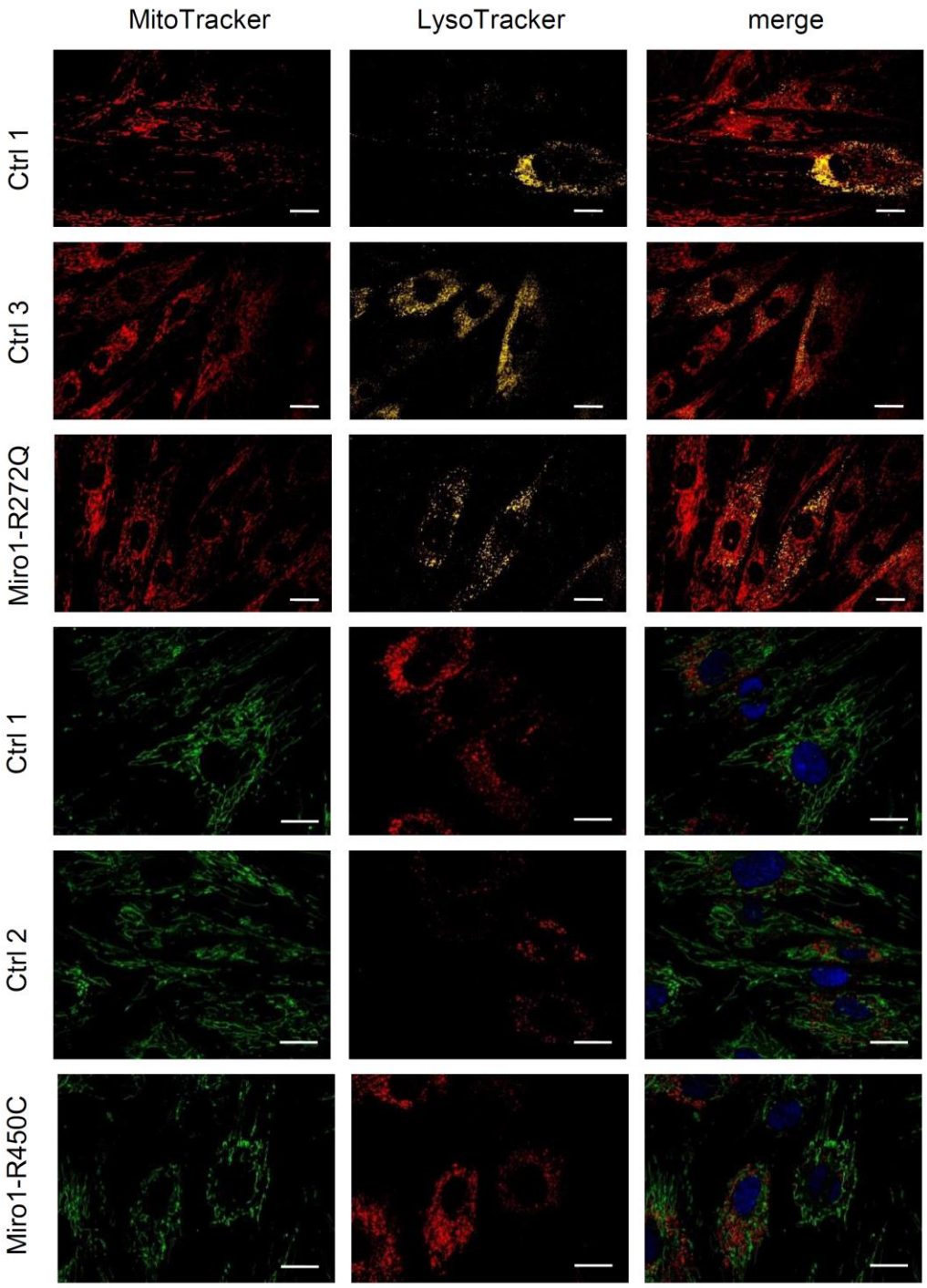

Figure 26: Live cell imaging of native fibroblasts for mitochondria and lysosomes

Representative images of Live cell microscopy of native fibroblasts. Fibroblasts were stained with MitoTracker and LysoTracker. Images taken at x40 magnification. Scale bars indicate 20 µm.

One approach to analyse mitophagy was done by live cell imaging of native fibroblasts stained with MitoTracker and LysoTracker (Figure 26) and subsequent co-localization analysis of mitochondria and lysosomes (Figure 27). An increased co-localization indicates higher levels of mitophagy. Co-localization of mitochondria and lysosomes was not increased in Miro1-R272Q and Miro1-R450C fibroblast lines under standard growth conditions, as assessed by Pearson's Coefficient (Figure 27).

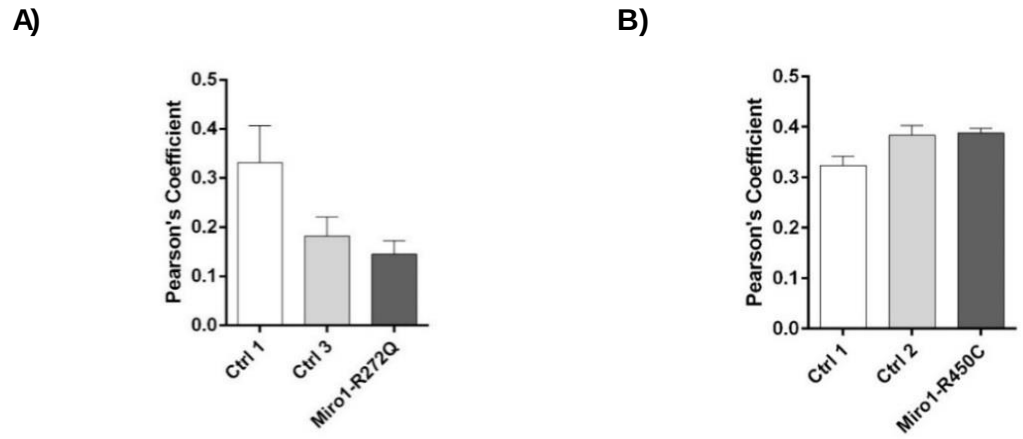

Figure 27: Co-localization of mitochondria and lysosomes

The Live cell microscopy images of native fibroblasts were analysed with ImageJ software. Co-localisation of mitochondria and lysosomes was not altered in **A)** Miro1-R272Q and **B)** Miro1-R450C fibroblasts compared to their respective age matched controls. Data indicated as mean ± SEM. n = 3 – 4

3.9.2 Analysis of LC3II protein levels revealed impaired autophagic flux in Miro1 mutant fibroblasts

Mitophagy is a form of autophagy, specifically degrading mitochondria via the lysosomal pathway. Proteins and organelles are engulfed by autophagosomes, which fuse with lysosomes for subsequent degradation. Microtubule-associated protein 1A/1B-light chain 3 (LC3) exists as soluble isoform LC3 I in the cytosol and gets recruited to autophagosome membranes, where it forms the LC3-phosphatidylethanolamine conjugate LC3 II. LC3 II is degraded in autolysosomes together with the other engulfed proteins and/ or organelles. Therefore, LC3 II turnover is considered as marker to monitor autophagic flux (Tanida, Ueno et al. 2008).

Immortalized fibroblasts were treated with 10 nM Bafilomycin A_1, a specific inhibitor of autophagy, for 24 h. Samples were taken after 3 h, 6 h and 24 h of treatment and the LC3 II turnover investigated using Western Blot analysis. In Ctrl 1 fibroblasts LC3 II accumulated

significantly after 3 h, 6 h and 24 h (Figure 28 A, D). In contrast, LC3 II did not significantly increase in Miro1-R272Q fibroblasts after 3 h or 6 h treatment. Only after 24 h treatment LC3 II protein level increased significantly compared to the untreated control, but this value was significantly lower compared to 24 h treatment in Ctrl 1 fibroblasts (Figure 28 B, D). In Miro1-R450C a significant accumulation of LC3 II was not observed (Figure 28 C, D). To induce autophagy, cells were starved in medium without FBS. This treatment resulted in no obvious increase of LC3 II over time in Ctrl 1 fibroblasts, likely because LC3 II is constantly degraded (Figure 28 A, E). In Miro1-R272Q and Miro1-R450C LC3 II protein did not increased upon FBS starvation as well (Figure 28 B, C, E). The results indicate that autophagy, and therefore most likely mitophagy as well, is impaired in Miro1-R272Q and Miro1-R450C mutant fibroblasts.

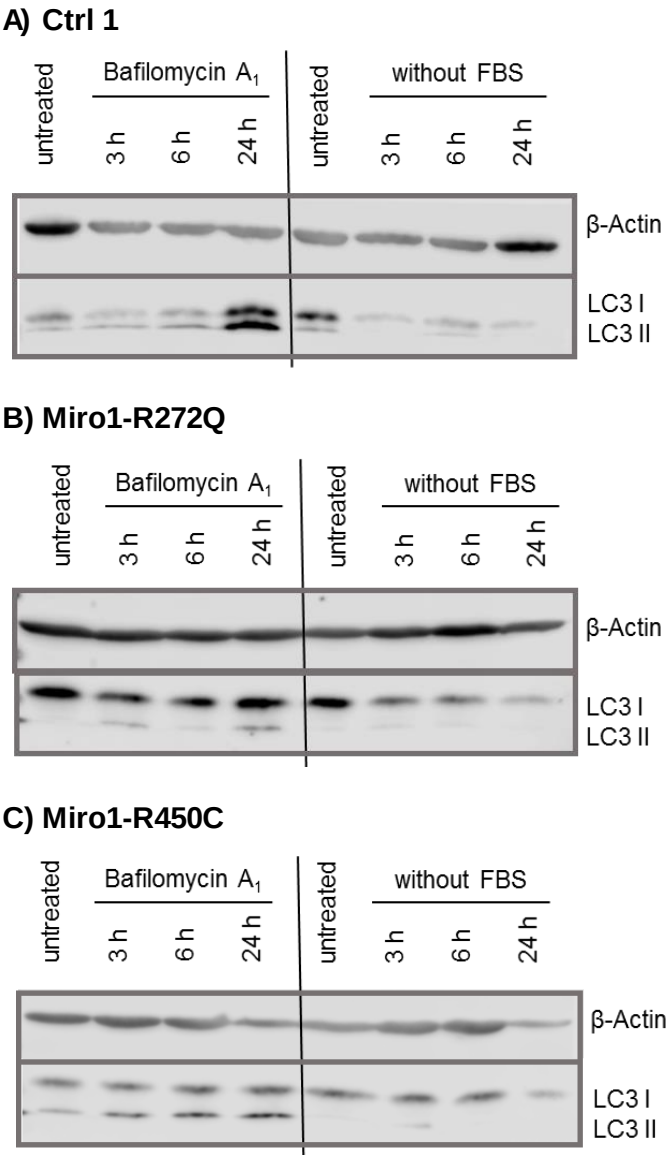

Representative Western Blot image of immortalized fibroblasts treated with 10 nM Bafilomycin A_1 to inhibit autophagy and with FBS-starvation to induce autophagy. Treatment was done over a time course of 24 h, samples were collected after 3 h, 6 h and 24 h.

A) In **Ctrl 1** fibroblasts LC3 II significantly increased over a time course of 24 h treatment with Bafilomycin A_1, indicating that autophagy was successfully blocked. Starvation of immortalized fibroblasts in medium without FBS did not result in LC3 II accumulation, indicating that autophagy turnover occurs.

In **B) Miro1-R272Q** and **C) Miro1-R450C** fibroblasts accumulation of LC3 II upon inhibition of autophagy was not observed, suggesting that mitophagy might be impaired.

D) LC3 II protein under Bafilomycin A_1 treatment

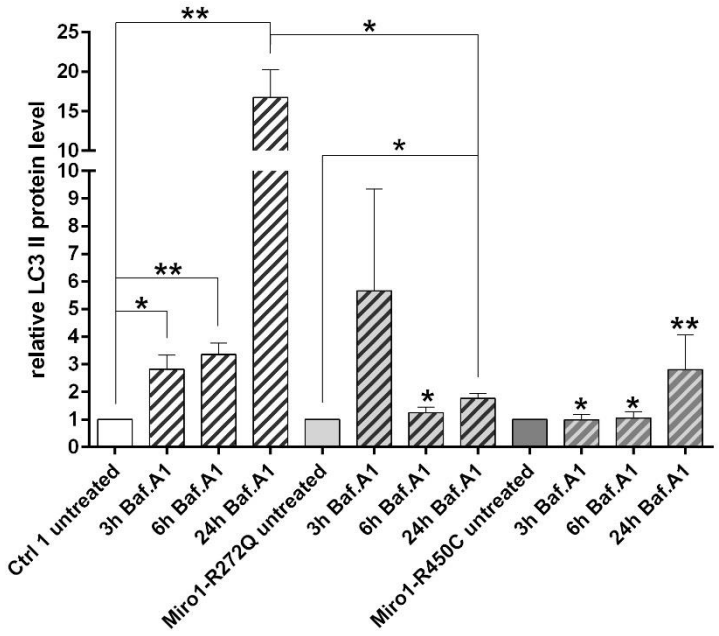

E) LC3 II protein under FBS starvation

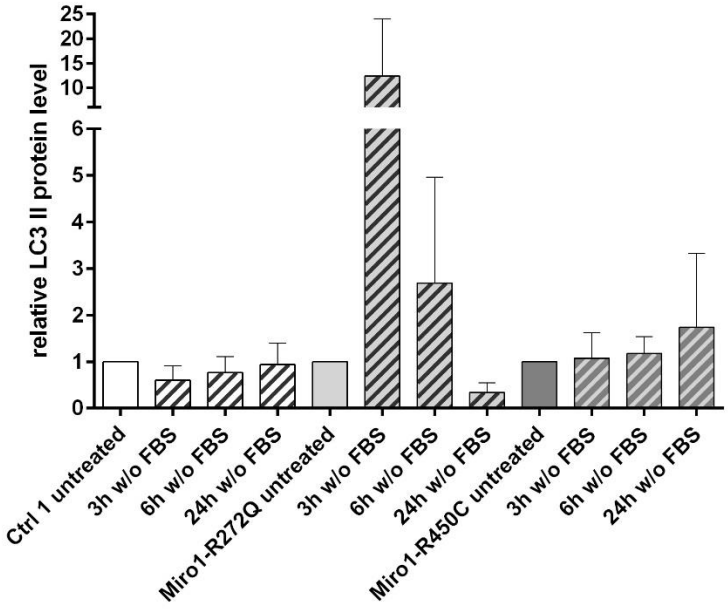

Figure 28: Western Blot for autophagy marker LC3 II

D) Densitometry evaluation of Western Blot for LC3 II protein under inhibition of autophagy using Bafilomycin A1. In **Ctrl 1** fibroblasts LC3 II accumulated significantly after 3 h, 6 h and 24 h of treatment. In **Miro1-R272Q** fibroblasts LC3 II was significantly increased after 24 h of Bafilomycin A1 treatment, but the value was much lower compared to 24 h treatment in Ctrl 1 fibroblasts. In **Miro1-R450C** fibroblasts LC3 II did not accumulate even after 24 h treatment, indicating that autophagic flux was impaired in Miro1 mutant fibroblasts.

E) Densitometry evaluation of Western Blot for LC3 II protein under FBS starvation. In **Ctrl 1** fibroblasts LC3 II levels did not change, indicating a turnover of LC3 II by lysosomal degradation. In **Miro1-R272Q** and **Miro1-R450C** fibroblasts a slightly increase of LC3 II upon FBS starvation was observed, indicating that lysosomal clearance might be affected.

Data indicated as mean ± SEM. * $p \leq 0.05$ ** $p \leq 0.01$ *** $p \leq 0.001$ by multiple t-test, Holm-Sidak multiple comparison correction. n = 3 - 4

3.10 Mitochondrial biogenesis is increased in Miro1-R450C fibroblasts

Western Blot analysis for Tom20 revealed a significantly reduced mitochondrial mass in Miro1-R450C fibroblasts. Mitophagy analysis of the autophagy marker LC3 II in patient-derived Miro1 mutant fibroblasts indicated that mitochondrial degradation via the lysosomal pathway might be impaired (Figure 28). To further investigate the reason for the reduced mitochondrial mass mitochondrial biogenesis was analysed with two different approaches, Western Blot analysis of PGC1α and analysis of mtDNA copy number.

3.10.1 Protein level of PGC1α is increased in Miro1-R450C fibroblasts

One of the applied approaches to analyse mitochondrial biogenesis was the assessment of PGC1α protein level. PGC1α is a co-activator for transcription, which induces mitochondrial biogenesis and is therefore upregulated prior to biogenesis (Kelly and Scarpulla 2004) (Lin, Handschin et al. 2005). Western Blot analysis showed that PGC1α protein level in Miro1-R272Q was comparable to Ctrl 1 fibroblasts (Figure 29). Miro1-R450C fibroblasts, that have a significantly reduced mitochondrial mass (Figure 17), showed a significant increase of PGC1α protein level to the ~3,5 fold of PGC1α protein in Ctrl 1 fibroblasts (Figure 29).

A) **B)**

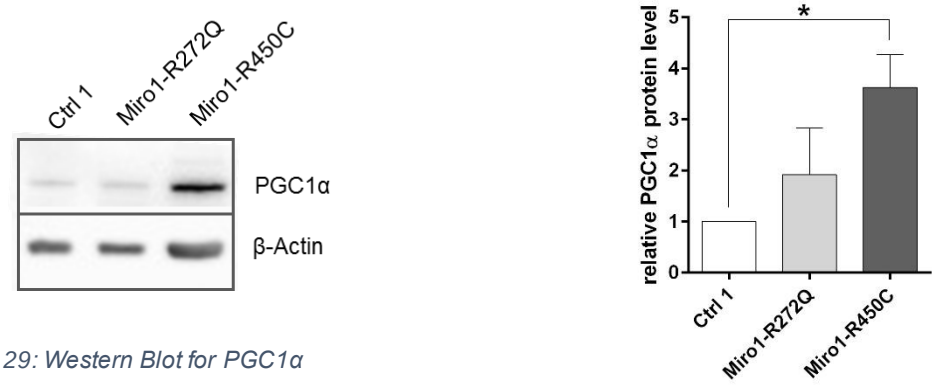

Figure 29: Western Blot for PGC1α

A) Representative image of Western Blot showing PGC1α and β-Actin protein. **B)** Densitometry evaluation of Western Blot analysis. PGC1α protein level normalized to β-Actin protein, relative to Control 1, was significantly increased in Miro1-R450C mutant fibroblast lines. Data indicated as mean ± SEM. * $p \leq 0.05$ ** $p \leq 0.01$ *** $p \leq 0.001$ by multiple t-test, Holm-Sidak multiple comparison correction. n = 8

3.10.2 mtDNA copy number is not changed in Miro1-R450C fibroblasts

Analysing mtDNA copy number in the patient-derived fibroblasts was used as additional approach to investigate mitochondrial biogenesis. Amongst other functions PGC1α induces the replication of mtDNA, an important requirement for mitochondrial biogenesis (Kelly and Scarpulla 2004) (Lin, Handschin et al. 2005).

Under basal conditions mtDNA copy number of Miro1-R272Q and Miro1R450C was indistinguishable from the mtDNA copy number of three different control fibroblast lines. Induction of oxidative stress by treatment with H_2O_2, Rotenone or a combination of both induced a tendency for an increase of mtDNA copy number in Miro1-R272Q and Miro1-R450C fibroblasts, but not in the control fibroblast lines from healthy donors. The slightly increased mtDNA copy number under oxidative stress did not reach statistical significance.

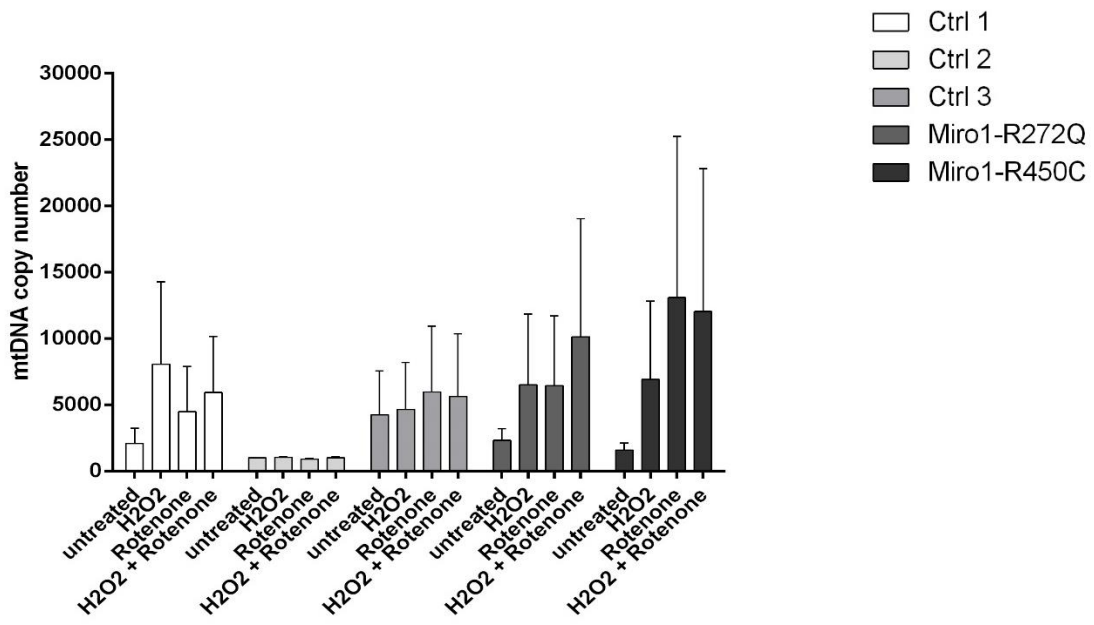

Figure 30: mtDNA copy number in native fibroblasts

Analysis of mtDNA copy number in native fibroblasts under standard growth conditions and after treatment with H_2O_2 and Rotenone to induce oxidative stress. Mitochondrial DNA copy number was statistically not significant increased in fibroblasts carrying the Miro1-R450C mutation, whereas in three control lines mtDNA copy number was not increased by induction of oxidative stress. Data indicated as mean ± SEM. n = 2 - 3

3.11 Mitochondrial respiration is altered in Miro1 mutant fibroblasts

Mitochondrial respiratory function is immensely important for the functionality of neurons as mitochondria provide ATP, that is needed at synapses (DiMauro 2004) for the release and recycling of neurotransmitters (Hollenbeck 2005). Investigation of the respiratory function in Miro1 mutant fibroblasts therefore was of great interest, because the reduced mitochondrial mass in Miro1-R450C fibroblasts (Figure 17) and the growth defect of *gem1*Δ and *gem1*Δ+R298Q yeast strains observed on medium containing a non-fermentable carbon source (Figure 12) provided first evidence for a possible impairment of energy metabolism or energy supply.

3.11.1 Citrate synthase activity is reduced in Miro1-R450C mutant fibroblasts

Citrate synthase is the key enzyme of the tricarboxylic acid cycle (TCA) that provides NADH and $FADH_2$ as proton donors for the enzymes of the respiratory chain. Measuring the activity of citrate synthase therefore was the first approach to assess the functionality of mitochondrial respiration in patient-derived fibroblasts.

Citrate synthase activity was measured in mitochondrial fractions of immortalized fibroblasts under standard growth conditions. The enzyme activity of citrate synthase was significantly reduced in Miro1-R450C fibroblasts and not changed in Miro1-R272Q fibroblasts compared to Ctrl 1 fibroblasts (Figure 31 A).

To further analyse the reason for the altered activity, Western Blot for citrate synthase protein was done. Citrate synthase protein amount was normalized to Tom20 protein amount. Analysis revealed a significant increase of citrate synthase protein level in Miro1-R450C fibroblasts compared to Ctrl 1 fibroblasts, which was not observed in Miro1-R272Q fibroblasts (Figure 31 B).

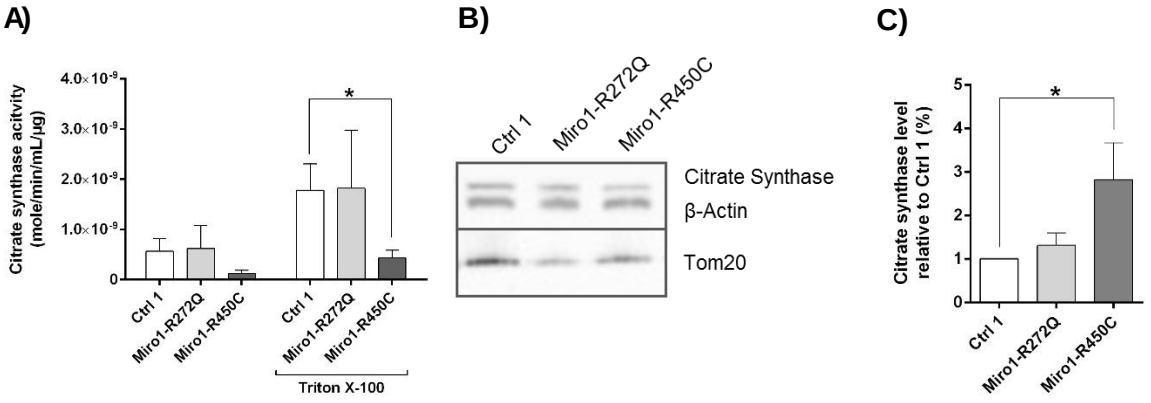

Figure 31: Citrate synthase activity and protein level

A) Biochemical measurement of citrate synthase activity in immortalized fibroblasts. Citrate synthase activity was significantly reduced in Miro1-R450C fibroblasts. Data indicated as mean ± SEM. * p ≤ 0.05 ** p ≤ 0.01 *** p ≤ 0.001 by multiple t-test, Holm-Sidak multiple comparison correction. n = 3 **B)** Representative image of Western Blot showing citrate synthase, β-Actin and Tom20 protein. **C)** Densitometry evaluation of citrate synthase protein level. Citrate synthase protein level was normalized to mitochondrial mass. Citrate synthase protein level was significantly increased in Miro1-R450C fibroblasts, compared to Ctrl 1 fibroblasts. Data indicated as mean ± SEM. * p ≤ 0.05 ** p ≤ 0.01 *** p ≤ 0.001 by multiple t-test, Holm-Sidak multiple comparison correction. n = 8

3.11.2 Complex I activity is not changed in Miro1 mutant fibroblasts

Due to the observed alteration of citrate synthase activity and protein level in Miro1-R450C fibroblasts the function of the mitochondrial respiratory chain was further investigated in patient-derived fibroblasts.

The activity of the respiratory chain complex I was measured in immortalized fibroblasts with the Complex I Enzyme Activity Dipstick Assay Kit (Abcam, Cambridge, UK).

Citrate synthase protein level (Figure 31 C) was used for normalization to indicate complex I activity on mitochondria level. The results obtained showed that complex I activity was only slightly, but not statistically significant increased in Miro1-R272Q and not changed in Miro1-R450C fibroblasts (Figure 32).

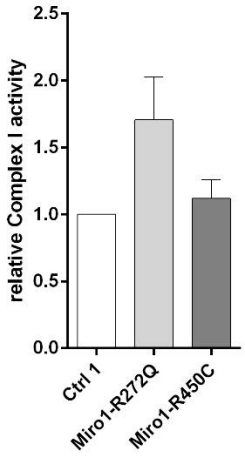

Figure 32: Complex I activity in immortalized fibroblasts

ComplexI activity was measured using the ComplexI Enzyme Activity Dipstick Assay Kit. Densitometry data from the ComplexI Enzyme Activity Dipstick Assay Kit were normalized to citrate synthase protein level. ComplexI activity was not changed in Miro1-R272Q and in Miro1-R450C fibroblasts compared to Ctrl 1 fibroblasts. Data indicated as mean ± SEM. * $p \leq 0.05$ ** $p \leq 0.01$ *** $p \leq 0.001$ by multiple t-test, Holm-Sidak multiple comparison correction. n = 3

3.11.3 Abundance of complex V is increased in Miro1-R272Q mutant fibroblasts

Complex I activity was found to be only moderately increased in Miro1-R272Q fibroblasts. As a result analysing the protein amounts of the complexes of the respiratory chain was the next step in characterizing mitochondrial respiratory function.

The amount of intact protein complexes of the respiratory chain was measured in immortalized fibroblasts under standard growth conditions by Western Blot analysis using the Total OXPHOS antibody cocktail (Abcam, Cambridge, UK). Normalized to mitochondrial mass, complex II was slightly increased in Miro1-R272Q and complex IV was moderately increased in Miro1-R272Q and Miro1-R450C fibroblasts. Complex V was significantly increased in Miro1-R272Q fibroblasts to ~4,5 fold compared to Ctrl 1 fibroblasts (Figure 33).

A)

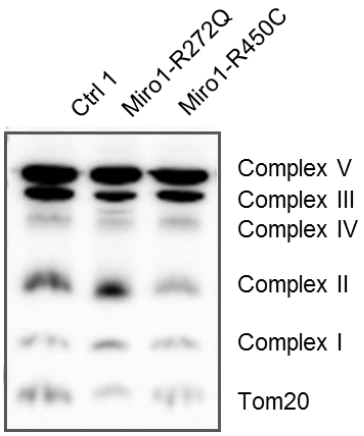

B)

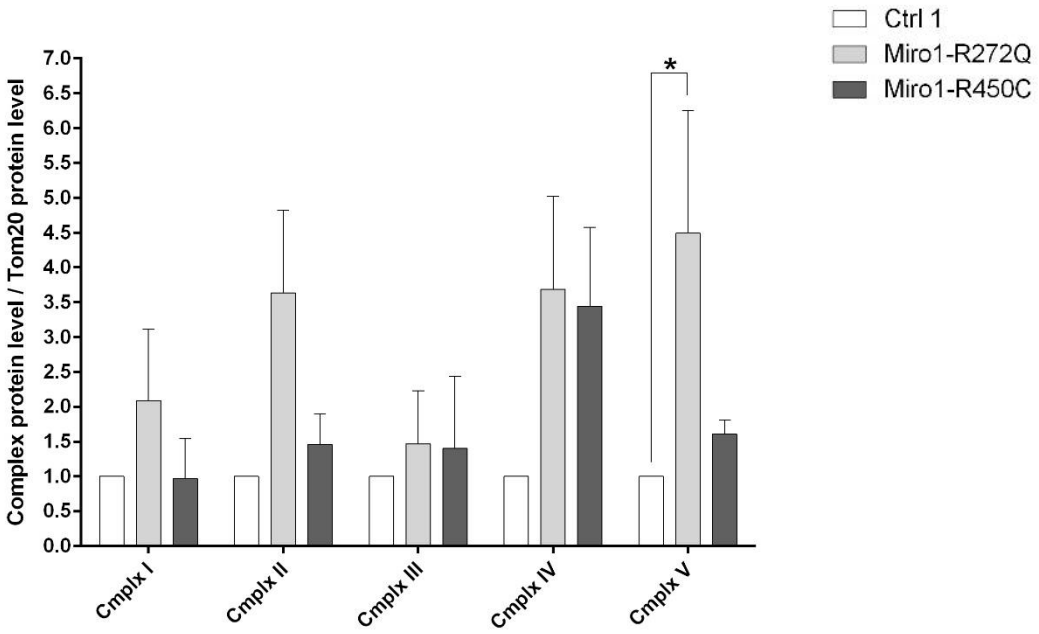

Figure 33: Protein level of respiratory chain complexes

Protein abundance of respiratory chain complexes was measured with Western Blot analysis using the Total OXPHOS antibody cocktail (Abcam, Cambridge, UK) which detects only intact protein complexes. **A)** Representative image of Western Blot showing the Complexes I, II, III, IV and V of the respiratory chain, and Tom20 protein. **B)** Densitometry analysis of Western Blot results, normalized to Tom20 showed that complex IV was tendentially increased in Miro1-R272Q and Miro1-R450C fibroblasts and complex V was significantly increased in Miro1-R272Q fibroblasts compared to the control fibroblast line.

Data indicated as mean ± SEM. * $p \leq 0.05$ ** $p \leq 0.01$ *** $p \leq 0.001$ by multiple t-test, Holm-Sidak multiple comparison correction. n = 4

3.11.4 Mitochondrial respiration is different in Miro1-R450C and in Miro1-R272Q mutant fibroblasts

Citrate synthase activity was decreased in Miro1-R450C fibroblasts, whereas complex I activity was not changed in Miro1-R272Q or Miro-R450C fibroblasts (Figure 32, Figure 33). Measuring the oxygen consumption rate (OCR) with the XF^{e}96 extracellular flux Analyzer is a powerful tool to further assess the functionality of the respiratory chain.

3.11.4.1 Optimization of cell density for OCR measurement

To measure the OCR with the XF^{e}96 extracellular flux Analyzer cells are required to grow in a monolayer that evenly covers the bottom of the well of the XF^{e}96 cell culture microplate. Therefore immortalized Ctrl 1 fibroblasts were seeded into a XF^{e}96 cell culture microplate at different cell densities to establish the optimal cell density. Analysis of the obtained OCR data showed that a cell density of 16000 cells per well produces most robust data (Figure 34). All other measurements of OCR were therefore done using this cell density.

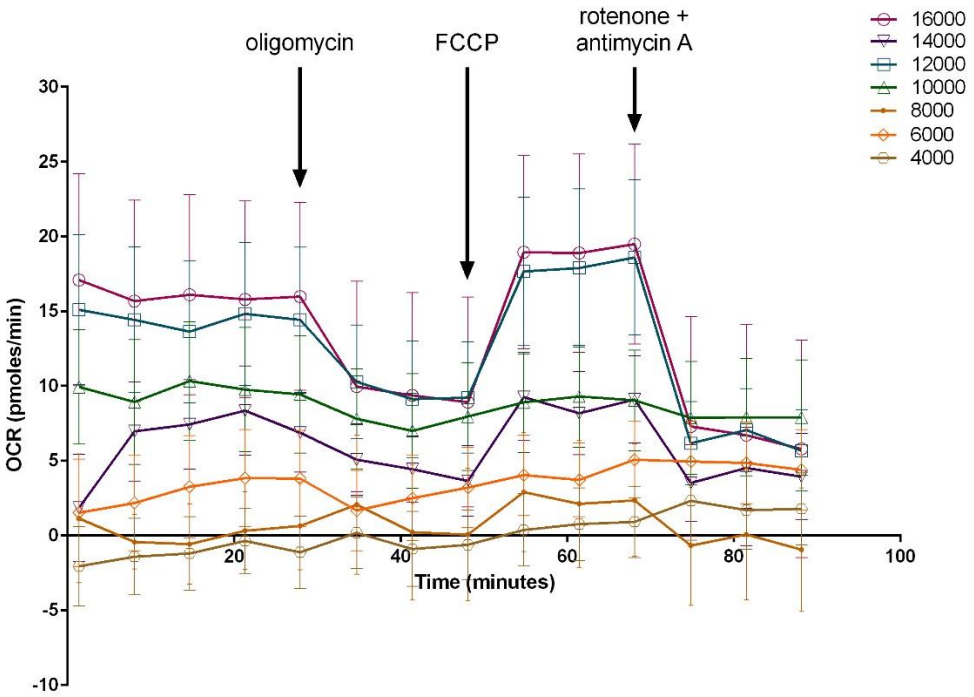

Figure 34: Optimization of cell density for OCR measurement

OCR data for the immortalized fibroblast line Ctrl 1 seeded at different cell densities. Best results were obtained at a cell density of 16000 cells per well. Data indicated as mean ± SEM. n = 5

3.11.4.2 Optimization of Oligomycin and FCCP concentration for OCR measurement

To measure the extracellular oxygen flux with the XF^{e}96 extracellular flux Analyzer cells were treated with oligomycin to inhibit the ATP synthase complex of the respiratory chain. The resulting decrease of OCR allows conclusions on ATP production and proton leak of the respiratory chain. Following treatment with FCCP leads to uncoupling of the respiratory chain. The subsequent increase of OCR is used to calculate the maximal respiration. For establishing the optimal concentrations of oligomycin and FCCP cells were treated with different concentrations of the respective compounds. OCR measurement showed that 2 µM of Oligomycin resulted in decrease of OCR below the basal OCR, indicating inhibition of complex V (Figure 35 A, B). Uncoupling of the respiratory chain using 250 nM of FCCP caused an increase of OCR above the basal OCR (Figure 35 C, D). The optimal concentrations were used for further analysis of OCR of immortalized fibroblasts.

A) Ctrl 1 + different concentrations of Oligomycin

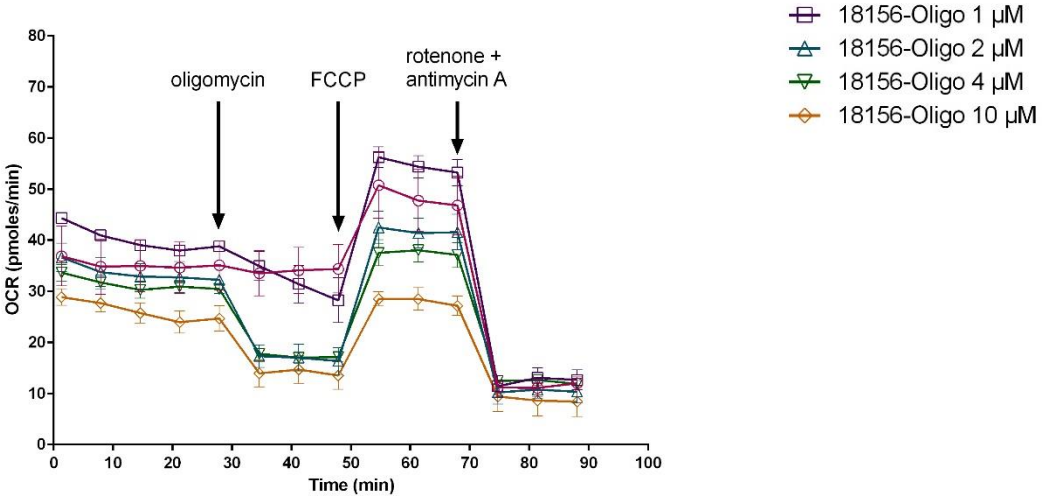

B) Miro1-R450C + different concentrations of Oligomycin

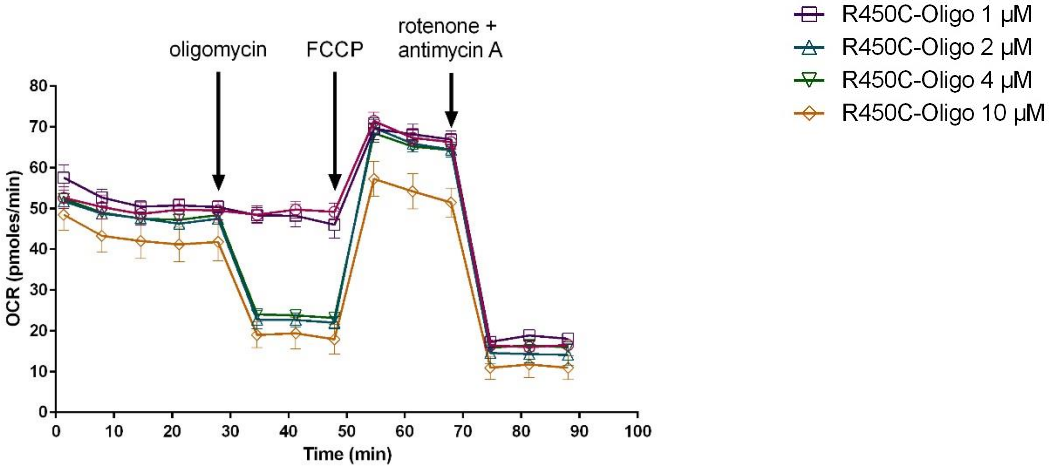

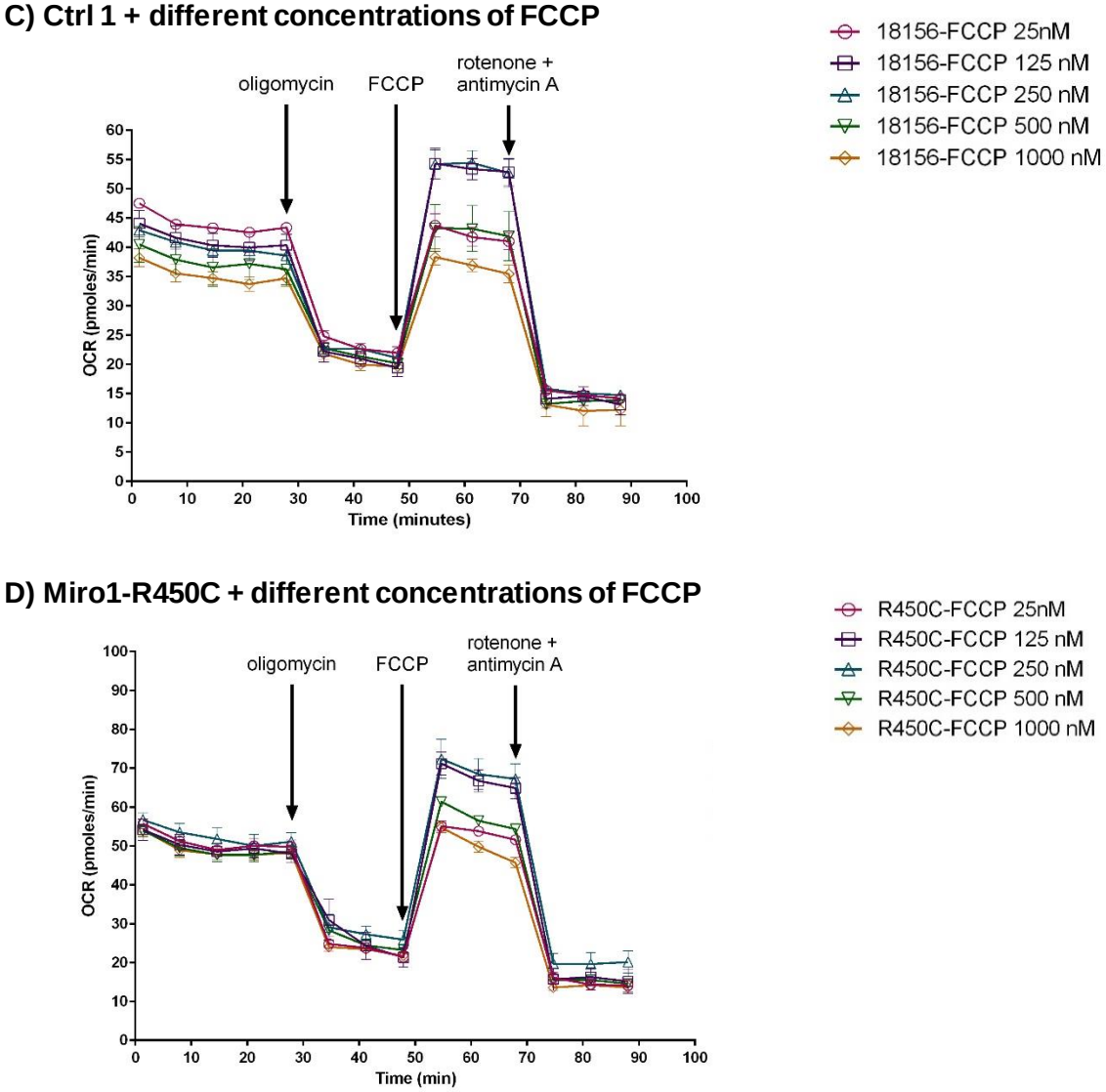

Figure 35: Optimization of Oligomycin and FCCP concentration for OCR measurement

OCR data for the immortalized fibroblast lines Ctrl 1 and Miro1-R450C. Cells were treated with different concentrations of Oligomycin (**A**, **B**) and different concentrations of FCCP (**C**, **D**) to establish the optimal concentrations. **A) B)** For Oligomycin a concentration of 2 µM was optimal to inhibit ATP synthase of the respiratory cahin. **C) D)** FCCP was most efficient to uncouple the respiratory chain at a concentration of 250 nM. Data indicated as mean ± SEM. n = 3

3.11.4.3 *The oxygen consumption rate was changed in Miro1 mutant fibroblasts*

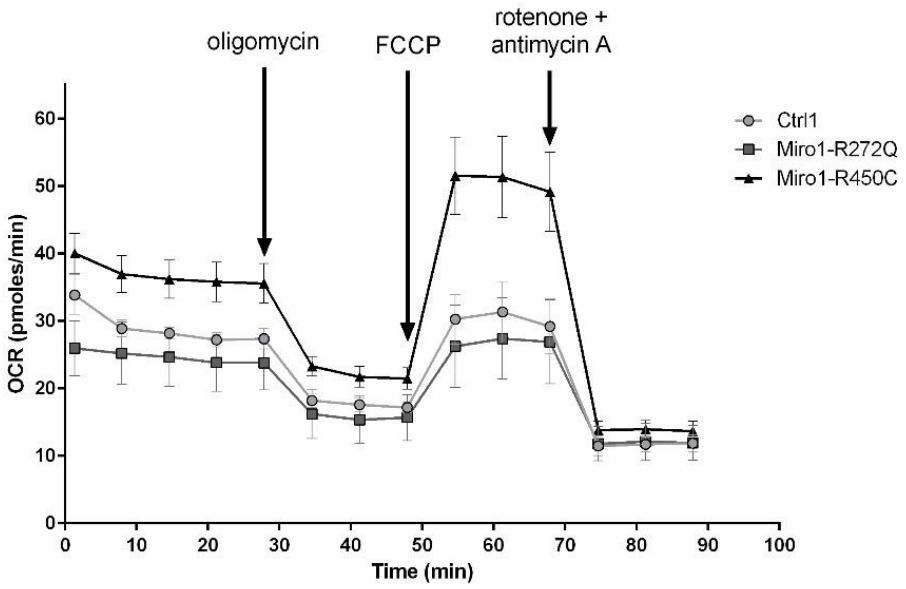

Figure 36: Oxygen consumption rate of patient-derived fibroblasts

OCR data of immortalized fibroblasts. Basal respiration is increased in Miro1-R450C fibroblasts compared to Ctrl 1 and Miro1-R272Q fibroblasts, as well as maximal respiration. Data indicated as mean ± SEM. n = 5 - 6

The OCR data (Figure 36) were used to calculate different parameters to assess mitochondrial respiratory function (Figure 4). Respiration was found to be significantly different between Miro1-R272Q and Miro1-R450C fibroblasts: Basal respiration (Figure 37 A), capacity for ATP production (Figure 37 B) and maximal respiration (Figure 37 D) were significantly increased in Miro1-R450C fibroblasts compared to Miro1-R272Q fibroblasts. Proton leak was significantly decreased in Miro1-R272Q fibroblasts compared to Ctrl 1, and slightly but not significantly increased in Miro1-R450C fibroblasts (Figure 37 C). Spare respiratory capacity was significantly decreased in Miro1-R272Q and significantly increased in Miro1-R450C fibroblasts compared to Ctrl 1 fibroblasts (Figure 37 E). Non-mitochondrial respiration, which arises from oxygen consumption caused by side reactions of substrates in the cell, was increased in Miro1-R450C fibroblasts compared to Ctrl 1 and Miro1-R272Q fibroblasts (Figure 37 F).

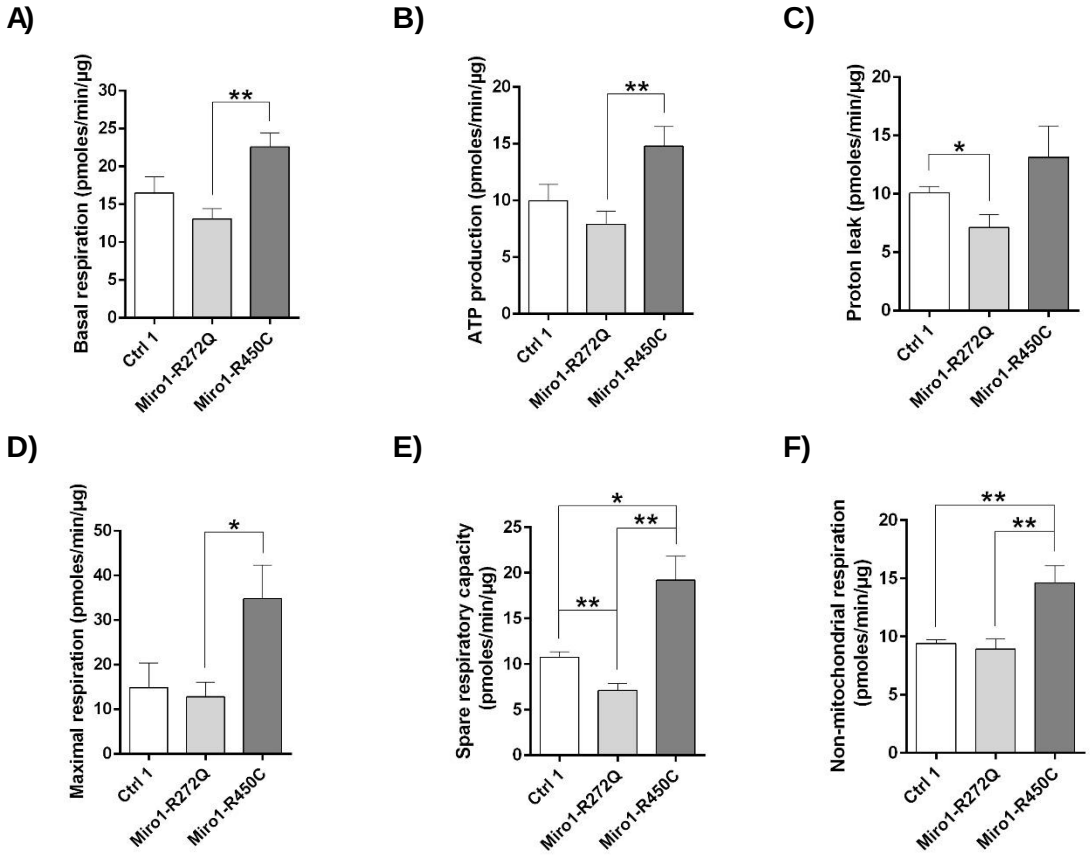

Figure 37: Evaluation of respiratiory function of immortalized fibroblasts

A) Basal respiration was significantly higher in Miro1-R450C fibroblasts compared to Miro1-R272Q. **B)** Capacity for ATP production was significantly higher in Miro1-R450C compared to Miro1-R272Q. **C)** Proton leak in Miro1-R272Q fibroblasts was significantly lower compared to Ctrl 1. **D)** Maximal respiration was significantly increased in Miro1-R450C fibroblasts compared to Miro1-R272Q. **E)** Spare respiratory capacity in Miro1-R272Q fibroblasts was significantly decreased and in Miro1-R450C fibroblasts significantly higher than in Ctrl 1 fibroblasts. **F)** Non-mitochondrial respiration was increased in Miro1-R450C fibroblasts. Data indicated as mean ± SEM. * $p \leq 0.05$ ** $p \leq 0.01$ *** $p \leq 0.001$ by multiple t-test, Holm-Sidak multiple comparison correction. n = 5

3.12 Mitochondrial membrane potential is increased in Miro1 mutant fibroblasts

The mitochondrial membrane potential arises from complexes I, III, IV and V that pump protons from the mitochondrial matrix across the inner membrane into the intermembrane space. The resulting proton gradient is subsequently used to produce ATP. In this regard the mitochondrial membrane potential is an important indicator for mitochondrial function. Immortalized fibroblasts were treated with 5 nM Valinomycin for 14 hours to decrease MMP. Cells were afterwards stained with the MMP-dependent dye TMRE and the MMP-independent dye MitoTracker green FM. The MMP was analysed by measuring the intensity of TMRE and MitoTracker green FM and calculation of the intensity of TMRE in relation to MitoTracker intensity. The resulting values indicate MMP with regard to mitochondrial mass.

Treatment with Valinomycin significantly reduced the MMP in all cell lines. In Miro1-R272Q and Miro1-R450C fibroblasts the MMP was significantly increased to ~2 fold under baseline conditions compared to Ctrl 1. (Figure 38 A). The difference between the reduced MMP after Valinomycin treatment and baseline MMP in untreated cells was not altered in Miro1 mutant fibroblasts compared to Ctrl 1, indicating that Miro1 mutant fibroblasts are equally susceptible to Valinomycin than the Ctrl 1 fibroblast line (Figure 38 B).

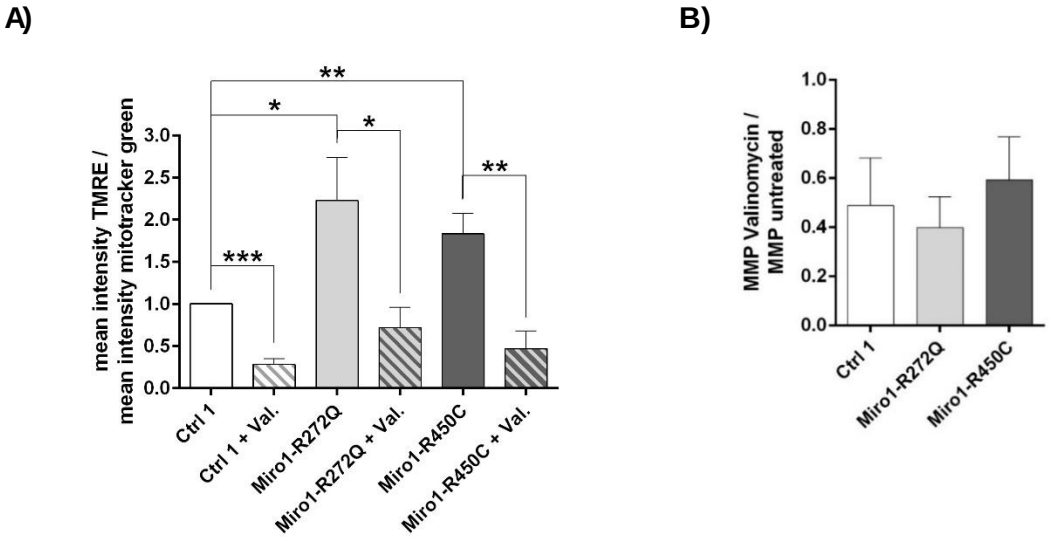

Figure 38: Mitochondrial membrane potential of immortalized fibroblasts

Mitochondrial membrane potential was measured by FACS analysis. **A)** Immortalized fibroblasts were treated with 5 nM Valinomycin for 14 hours and afterwards stained with TMRE and MitoTracker green FM. Valnimomycin treatment significantly reduced the MMP. MMP was significantly increased in Miro1-R272Q and in Miro1-R450C fibroblasts. Data indicated as mean ± SEM. **B)** Evaluation of the delta between baseline MMP and reduced MMP after Valinomycin treatment. The reduction of the MMP induced by Valinomycin was comparable in all fibroblast lines. Data indicated as mean ± SEM. * $p \leq 0.05$ ** $p \leq 0.01$ *** $p \leq 0.001$ by multiple t-test, Holm-Sidak multiple comparison correction. n = 6

3.12.1 Knockdown of RhoT1 causes mitochondrial hyperpolarisation in M17 cells

The mitochondrial membrane potential (MMP) was measured in M17 cells with stable knockdown of endogenous *RhoT1* (*RhoT1*-KD) with FACS analysis. Cells with stable knockdown of *RhoT1* were transfected with Miro1/V5 constructs Miro1-WT, Miro1-R272Q, Miro1-R450C or Miro1-F676V, respectively. M17 cells were treated with 10 µM CCCP for 20 min to decrease MMP and afterwards stained with TMRE. Treatment with CCCP reduced the MMP.

M17 cells with stable *RhoT1*-KD showed a significant increase of MMP to ~1,5 fold compared to M17 cells without knockdown of *RhoT1* (M17 + miRNA-Ctrl). M17 cells with knockdown of endogenous *RhoT1* overexpressing Miro1-WT, Miro1-R272Q, Miro1-R450C or Miro1-F676V constructs, respectively, also showed an increase of MMP, which was only significant in cells expressing Miro1-WT when compared to M17 + miRNA-Ctrl (Figure 39).

Thus, the M17 *RhoT1*-KD cell model resembles the phenotype of increased MMP that was observed in Miro1 mutant immortalized fibroblasts (Figure 38).

The remaining cells left over from FACS analysis were used to verify the expression of V5-tagged Miro1 protein. Expression of Miro1-WT/V5, Miro1-R272Q/V5, Miro1-R450C/V5 and Miro1-F676V/V5 was verified in all three experiments, although Miro1-WT/V5 was hardly detectable in experiment 1 due to insufficient cell amount left as can be seen by the also faint band for β-Actin (Figure 40).

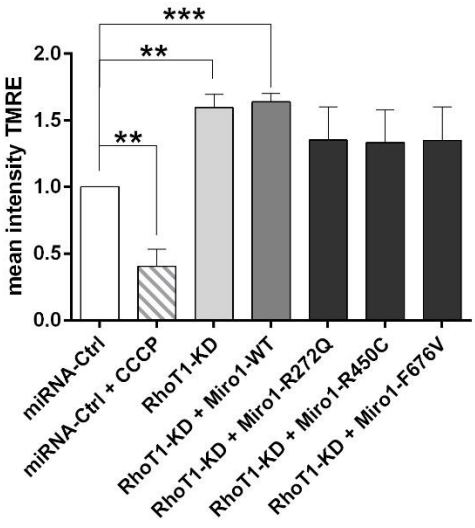

Figure 39: Mitochondrial membrane potential of M17 cells with RhoT1-KD

Mitochondrial membrane potential was measured by FACS analysis. M17 cells with stable knockdown of *RhoT1* and retransfection with *RhoT1* constructs. Cells were treated with 10 µM CCCP for 20 min and stained with TMRE. FACS data showed an increase of MMP in the *RhoT1*-KD cell line and in cells with *RhoT1*-KD + Miro1-WT/V5 compared to M17 + miRNA-Ctrl. MMP was slightly increased in cells with *RhoT1*-KD expressing Miro1-R272Q/V5, Miro1-R450C/V5 or Miro1-F676V/V5, respectively. Data indicated as mean ± SEM. * $p \leq 0.05$ ** $p \leq 0.01$ *** $p \leq 0.001$ by multiple t-test, Holm-Sidak multiple comparison correction. n = 3

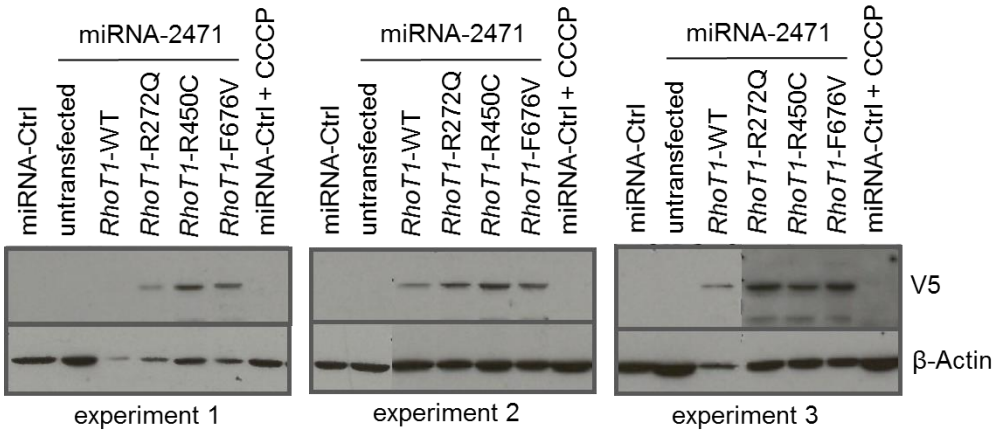

Figure 40: Expression of RhoT1-V5 in M17+miRNA used for FACS measurement

Western Blot showing expression of *RhoT1*-V5 constructs in M17 cells with stable knockdown of endogenous *RhoT1*. All four constructs containing either wild type *RhoT1* (*RhoT1*-WT/V5), *RhoT1*-R272Q/V5, *RhoT1*-R450C/V5 or *RhoT1*-F676V/V5 were expressed in all three experiments.

3.13 Mitochondrial reactive oxygen species (ROS) level was not changed in Miro1 mutant fibroblasts

Mitochondrial superoxide is a by-product of oxidative phosphorylation and is produced by reduction of molecular oxygen. Impaired function of the respiratory chain increases production of superoxide by complex I and complex III. Superoxide levels were measured by FACS analysis in immortalized fibroblasts stained with MitoSOX and MitoTracker.

Miro1 mutant fibroblasts showed no alteration of mitochondrial superoxide level compared to Ctrl 1 fibroblasts. Treatment with 20 nM of Piericidin A for 14 h significantly increased mitochondrial superoxide levels in all fibroblast cell lines (Figure 41 A). The difference between increased superoxide level after Piericidin A treatment and baseline superoxide level in untreated cells was also not altered in Miro1 mutant fibroblasts compared to Ctrl 1 fibroblasts, indicating that Miro1 fibroblasts are equally prone to produce superoxide during complex I inhibition than Ctrl 1 fibroblasts (Figure 41 B).

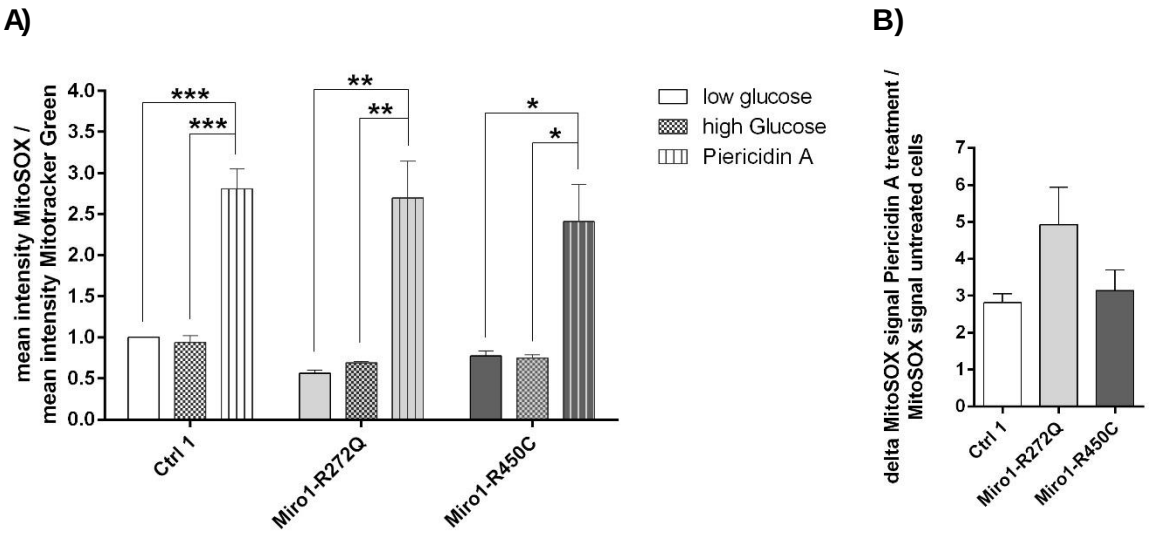

Figure 41: Mitochondrial ROS production in immortalized fibroblasts

A) Immortalized fibroblasts were treated with 20 nM Piericidin A and afterwards stained with MitoSOX-Red and MitoTracker green FM. Mitochondrial superoxide level was measured by FACS analysis. MitoSOX signal was normalized to MitoTracker signal. Under baseline conditions mitochondrial superoxide level was not changed in Miro1-R272Q and Miro1-R450C compared to Ctrl 1 fibroblasts. Treatment with Piericidin A increases mitochondrial superoxide production significantly in all fibroblast lines. **B)** The delta of increased mitochondrial ROS signal induced by Piericidin A and the baseline ROS signal in untreated cells was indistinguishable in all fibroblast lines. Data indicated as mean ± SEM. * $p \leq 0.05$ ** $p \leq 0.01$ *** $p \leq 0.001$ by multiple t-test, Holm-Sidak multiple comparison correction. n = 4

3.13.1 mtDNA damage was not increased in Miro1 mutant fibroblasts

Analysing mtDNA damage in the patient-derived fibroblasts was used as additional approach to investigate the possible load of oxidative stress, because high levels of ROS can damage mtDNA by inducing lesions.

Under basal conditions mtDNA damage load of Miro1-R272Q and Miro1R450C was indistinguishable from the mtDNA damage load of three different age matched control fibroblast lines (Ctrl 1, Ctrl 2, Ctrl 3). Induction of oxidative stress by treatment with H_2O_2, Rotenone or a combination of both induced a slight, yet not significant increase of mtDNA damage in Ctrl 1, Ctrl 3 and Miro1-R450C native fibroblast lines, but not in Ctrl 2 and Miro1-R272Q fibroblasts.

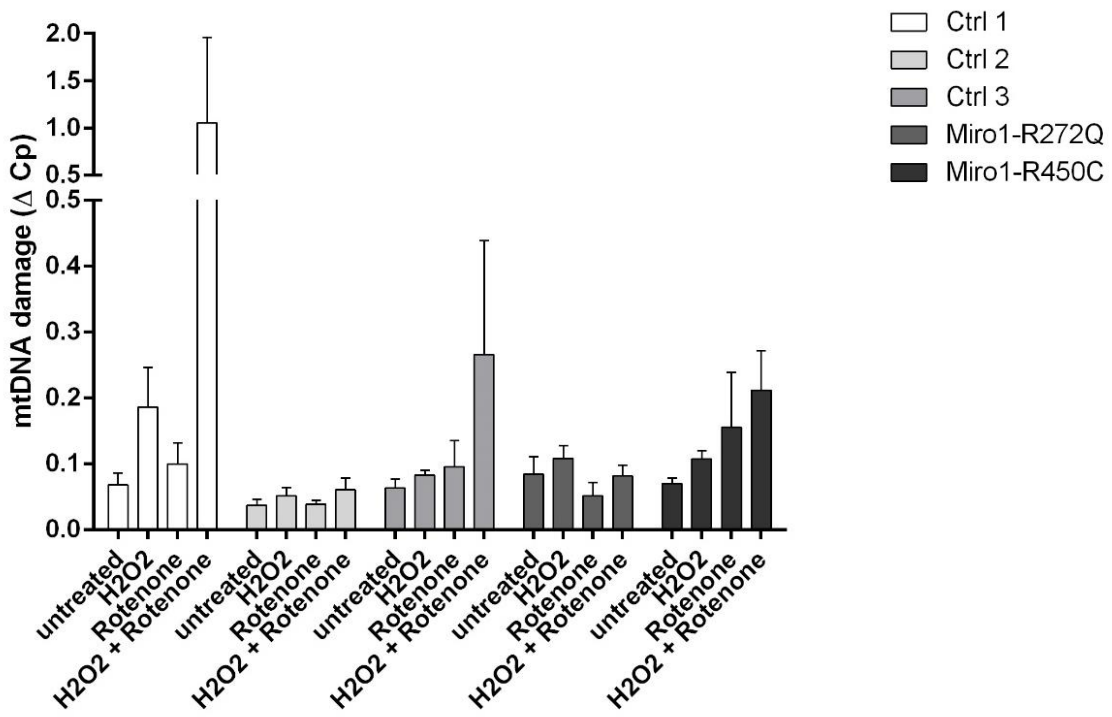

Figure 42: mtDNA damage in native fibroblasts

Analysis of mtDNA damage in native fibroblasts under standard growth conditions and after treatment with H_2O_2 and Rotenone to induce oxidative stress. Treatment with H_2O_2 and Rotenone induced an increase of mtDNA damage load in fibroblasts, but mtDNA damage was not higher in Miro1-R272Q or Miro1-R450C fibroblasts compared to the three control lines. Data indicated as mean ± SEM. n = 2 - 3

3.13.2 Miro1-R272Q and Miro1-R450C cause reduction of Manganese superoxide dismutase (MnSOD) protein level

Because mitochondrial superoxide levels were not increased in Miro1 mutant fibroblasts (Figure 41 A) the question was raised whether ROS levels were successfully quenched by antioxidant enzymes. MnSOD is a key enzyme that quenches reactive oxygen species in mitochondria.

3.13.2.1 MnSOD protein is reduced in Miro1-R450C fibroblasts

Western Blot analysis revealed that MnSOD protein level was reduced to 0.1 fold in Miro1-R450C fibroblasts compared to Ctrl 1 (Figure 43 B), indicating that the unchanged superoxide levels in those fibroblasts measured by FACS (Figure 41 A) are not a result of increased MnSOD protein. In Miro1-R272Q fibroblasts MnSOD protein level was not significantly changed.

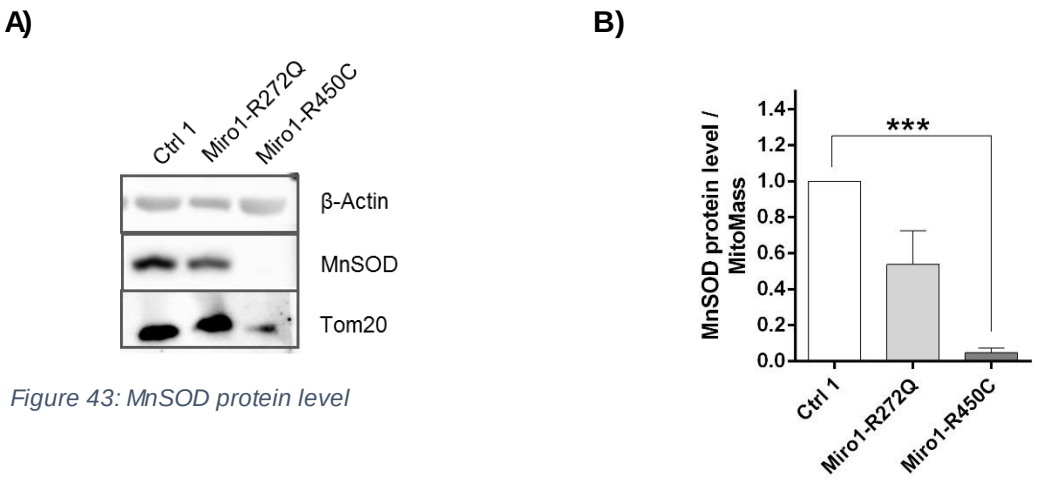

Figure 43: MnSOD protein level

A) Representative image of Western Blot showing MnSOD and Tom20 protein. **B)** Densitometry evaluation of Western Blot for MnSOD. MnSOD protein was normalized to mitochondrial mass, indicated by Tom20 protein level. Miro1-R272Q showed a slightly reduced MnSOD protein level, whereas MnSOD was significantly redcued in Miro1-R450C fibroblasts. Data indicated as mean ± SEM. * $p \leq 0.05$ ** $p \leq 0.01$ *** $p \leq 0.001$ by multiple t-test, Holm-Sidak multiple comparison correction. n = 3

3.13.2.2 *MnSOD protein was reduced in M17 cells with RhoT1 knockdown, overexpressing Miro1-R272Q or Miro1-R450C*

M17 cells with stable knockdown of endogenous *RhoT1*, overexpressing Miro1-WT/V5, Miro1-R272Q/V5, Miro1-R450C/V5 or Miro1-F676V/V5 protein were analysed for MnSOD protein levels. In M17 cells with knockdown of *RhoT1* (*RhoT1*-KD; Figure 19) MnSOD protein level were not changed, which was also true for M17 cells with *RhoT1*-KD over-expressing wild type Miro1 protein (*RhoT1*-KD + Miro1-WT-myc; *RhoT1*-KD + Miro1-WT-V5). On the other hand, M17 cells with *RhoT1*-KD over-expressing Miro1-R272Q/V5 or Miro1-R450C/V5 showed significantly less MnSOD protein level to ~0.6 fold compared to M17 cells without knockdown of endogenous *RhoT1* (Figure 44 B).

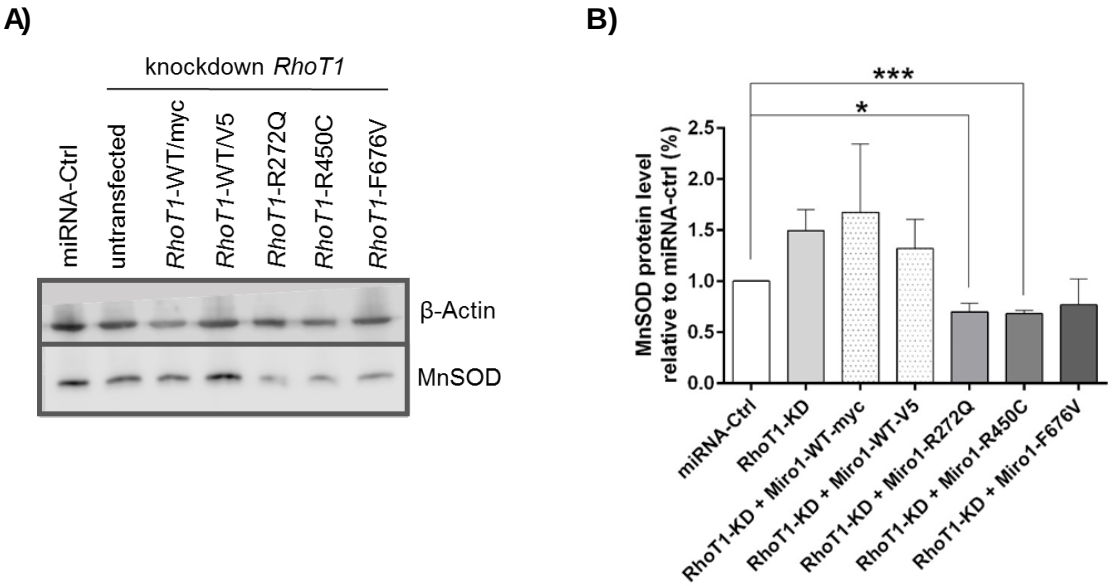

Figure 44: MnSOD protein level in M17 cells with stable knockdown of RhoT1

A) Representative image of Western Blot showing MnSOD protein. **B)** Densitometry evaluation of Western Blot for MnSOD protein level. M17 cells with stable knockdown of endogenous *RhoT1* (*RhoT1*-KD), over-expressing Miro1-R272Q/V5 or Miro1-R450C/V5 showed significantly less levels of MnSOD protein compared to M17 without knockdown of *RhoT1* (miRNA-Ctrl). Data indicated as mean ± SEM. * $p \leq 0.05$ ** $p \leq 0.01$ *** $p \leq 0.001$ by multiple t-test, Holm-Sidak multiple comparison correction. n = 3

3.14 Calcium buffering capacity is altered in Miro1 mutant fibroblasts

Apart from the ER, mitochondria provide the major capacity for intracellular calcium buffering. This function in taking up and accumulating calcium from the cytosol is most important to maintain cellular calcium homeostasis (Szabadkai and Duchen 2008). Miro was found to be involved in the regulation of calcium uptake by the mitochondria via it's EF hand motifs (Chang, Niescier et al. 2011). Also it was found that the functionality of both GTPase domains is required for proper calcium homeostasis (Saotome, Safiulina et al. 2008) (Kornmann, Osman et al. 2011). The mutation R272Q is located within the first EF hand domain and the mutation R450C within the C-terminal GTPase domain (Figure 6). Hence, investigation of the calcium buffering ability of the Miro1 mutant fibroblasts contributes to get further insight in the pathogenic mechanisms of the mutations.

Fluo-4 fluorescence intensity, which is proportional to the cytosolic calcium concentration, was used to visualize the cytosolic calcium flux. Treatment with 30 µM histamine induced the release of calcium from intracellular stores, like the ER and mitochondria, and subsequently increased cytosolic calcium concentration in all applied fibroblast lines. The increase in calcium concentration after histamine treatment was not significantly elevated in Ctrl 1 and Miro1-R450C fibroblasts (Figure 45 A, C), but in Miro1-R272Q fibroblasts cytosolic calcium concentration after histamine treatment was significantly increased (Figure 45 B). Elevation of cytosolic calcium concentration after histamine treatment was significantly lower in Miro1-R450C fibroblasts compared to Miro1-R272Q fibroblasts ($p = 0.0046$) (Figure 45 B, C).

Time laps microscopy after histamine treatment revealed the subsequent buffering of calcium by the ER and mitochondria. In Ctrl 1 fibroblasts cytosolic calcium concentration after Histamine treatment decreased during the 5 min imaging and by the end of the imaging nearly reaches the initial level (Figure 45 A). In Miro1-R272Q fibroblasts. The following time laps imaging revealed that cytosolic calcium concentration was decreased rapidly and finally reached the base line level (Figure 45 B). Interestingly, Miro1-R450C fibroblasts did not display a great release of calcium after histamine treatment (significantly lower than calcium release in Miro1-R272Q, $p = 0.0046$) and cytosolic calcium concentration did not decrease after the initial release during 5 min of imaging (Figure 45 C).

A)

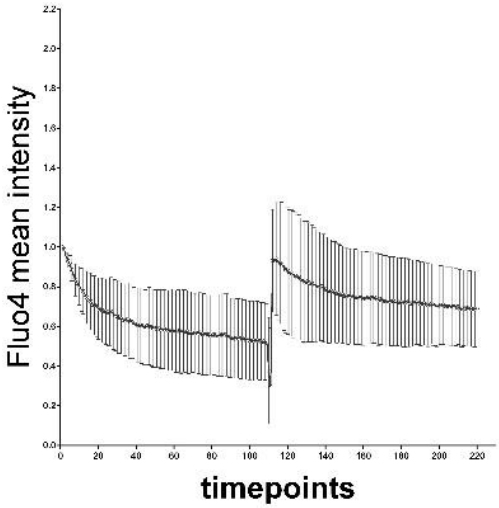

B)

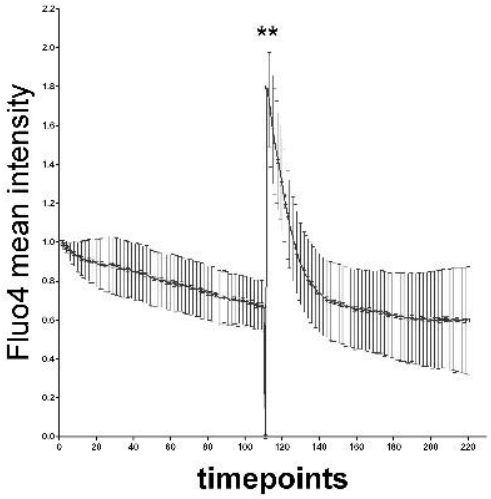

C)

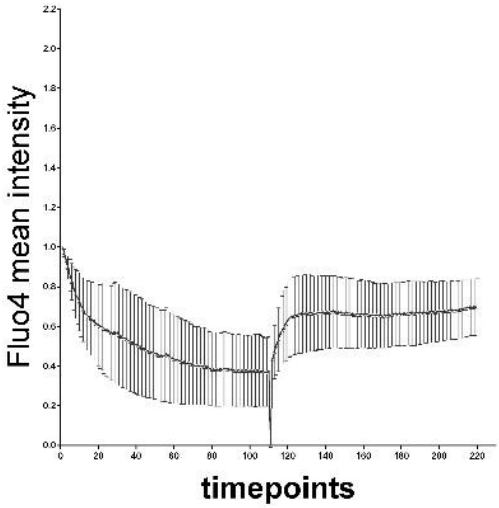

Figure 45: Cytosolic calcium flux

Cytosolic calcium was measured in immortalized fibroblasts stained with Fluo-4 Direct Calcium assay Kit. Time laps microscopy imaging was done in living immortalised fibroblasts. Treatment with 30 µM histamine was used to release calcium from intracellular calcium storage. The resulting increase of Fluo-4 intensity and the following decrease was measured with time laps microscopy in **A)** Ctrl 1 fibroblasts, **B)** Miro1-R272Q and **C)** Miro1-R450C fibroblasts. Evaluation of Fluo-4 intensity indicates that histamine induces the highest elevation in cytosolic calcium concentration in Miro1-R272Q fibroblasts (**B**).

Data indicated as mean ± SEM. * $p \leq 0.05$ ** $p \leq 0.01$ *** $p \leq 0.001$ by Students t-Test. n = 3

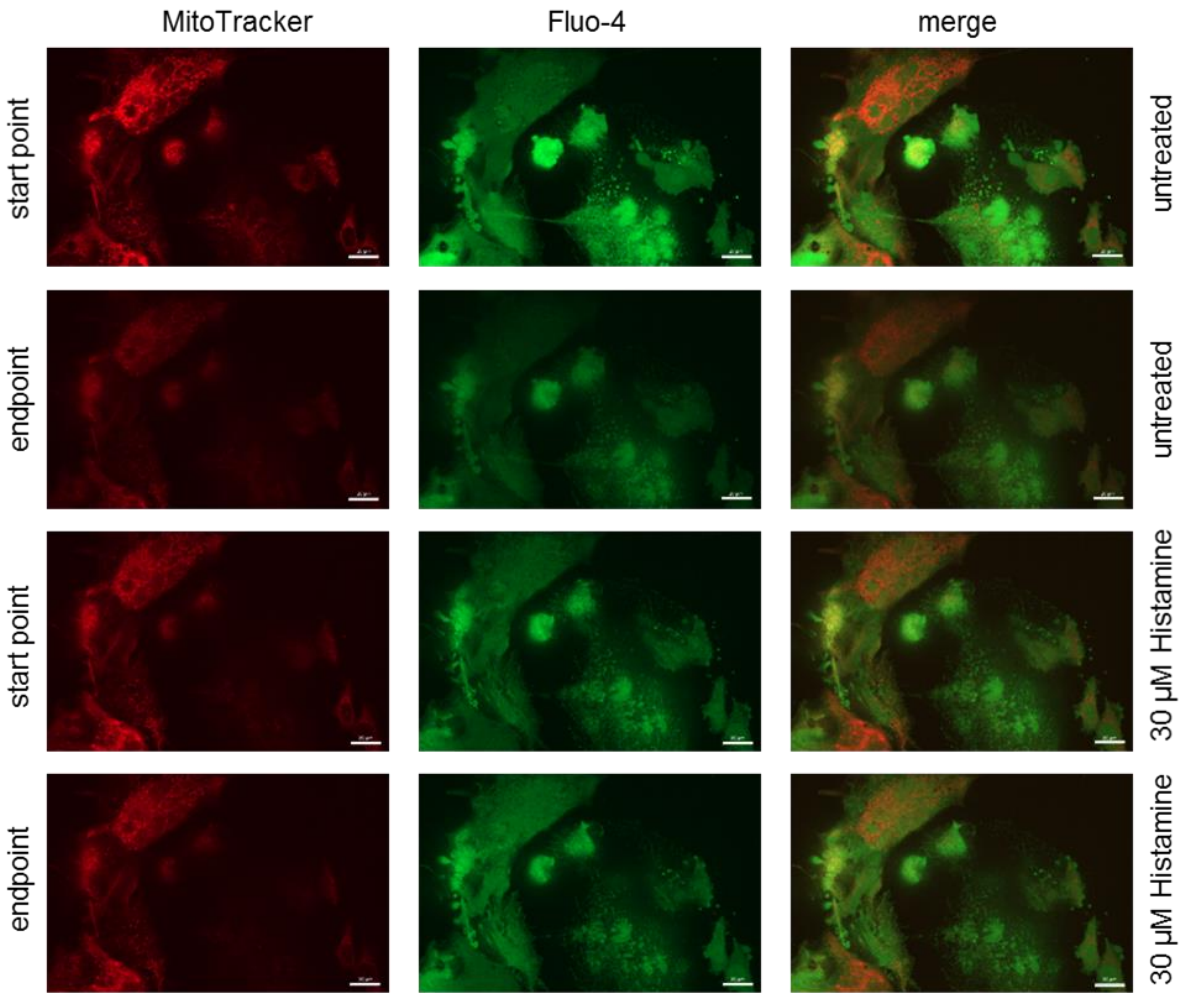

Ctrl 1 fibroblasts: Representative images for live cell microscopy of immortalized fibroblasts stained with MitoTracker DeepRed and Fluo-4. Cells were imaged for 5 min (untreated start point – end point). Calcium release from intracellular calcium stores was triggerd by treatment with 30 µM histamine (30 µM histamine start point). Cells were imaged for 5 min after adding histamine (30 µM histamine end point). Images taken at x40 magnification. Scale bars indicate 20 µm.

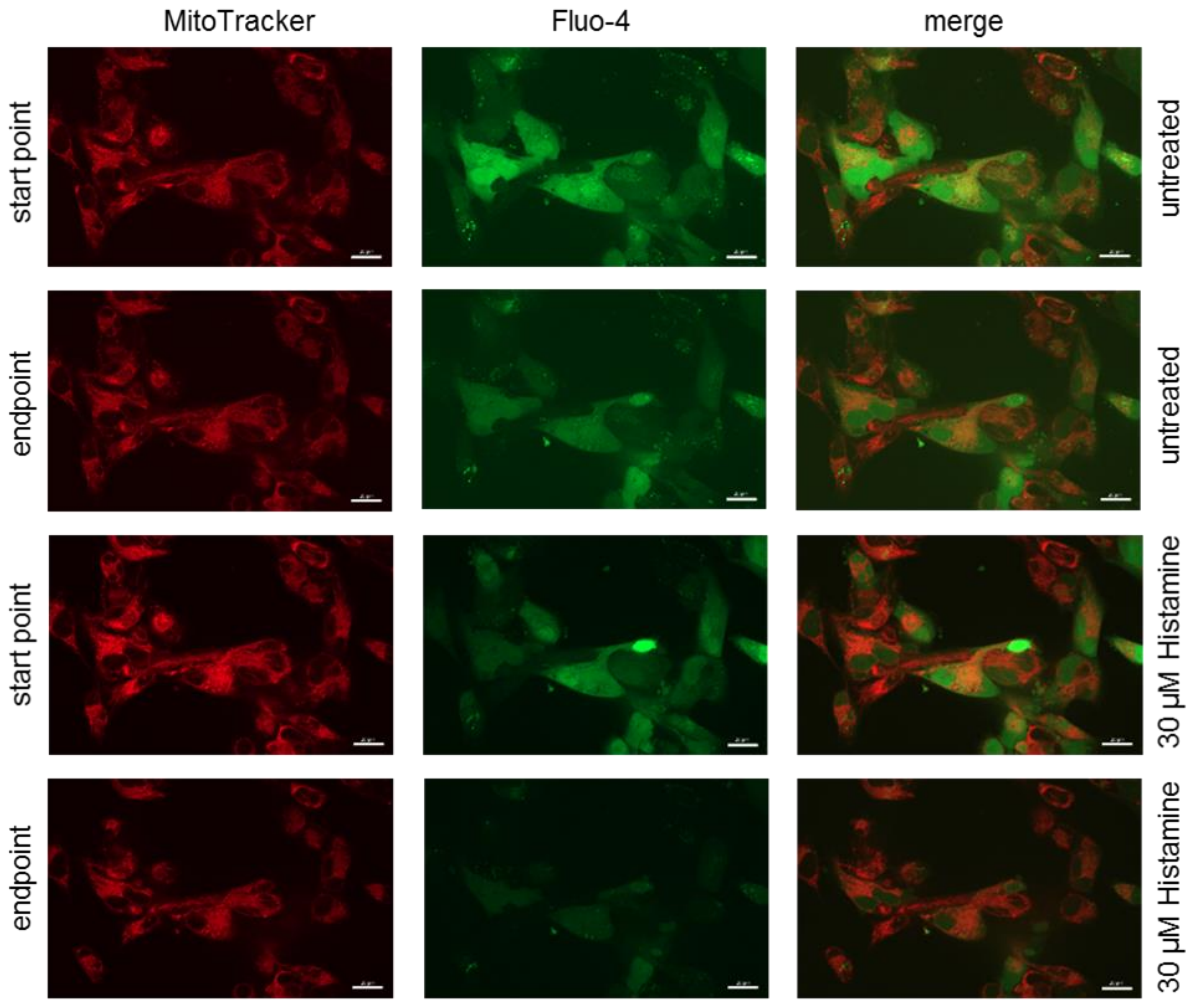

Miro1-R272Q fibroblasts: Representative images for live cell microscopy of immortalized fibroblasts stained with MitoTracker DeepRed and Fluo-4. Cells were imaged for 5 min (untreated start point – end point). Calcium release from intracellular calcium stores was triggerd by treatment with 30 µM histamine (30 µM histamine start point). Cells were imaged for 5 min after adding histamine (30 µM histamine end point). Images taken at x40 magnification. Scale bars indicate 20 µm.

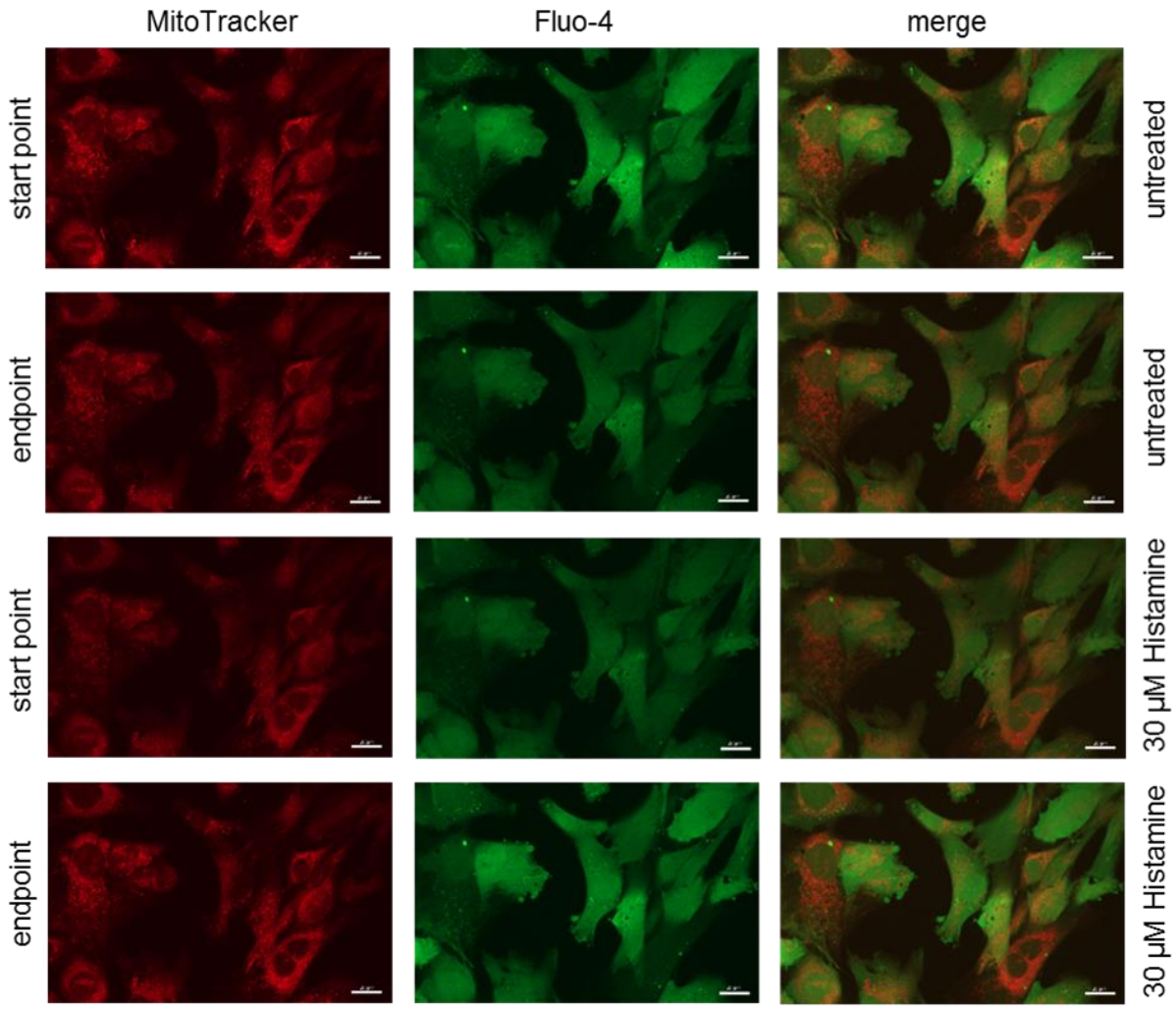

Miro1-R450C fibroblasts: Representative images for live cell microscopy of immortalized fibroblasts stained with MitoTracker DeepRed and Fluo-4. Cells were imaged for 5 min (untreated start point – end point). Calcium release from intracellular calcium stores was triggerd by treatment with 30 µM histamine (30 µM histamine start point). Cells were imaged for 5 min after adding histamine (30 µM histamine end point). Images taken at x40 magnification. Scale bars indicate 20 µm.

3.15 Staurosporine-induced apoptosis was increased in Miro1-R272Q mutant fibroblasts

Fransson et al. found an increased apoptosis rate in COS 7 cells transfected with constitutively active Miro1 or Miro2 mutants (Fransson, Ruusala et al. 2003). Amongst other important functions mitochondria also induce apoptosis cascades when mitochondrial function is irreversibly impaired (McBride, Neuspiel et al. 2006) (Tatton, Chalmers-Redman et al. 2003). As mitochondrial dysfunction was observed in Miro1 mutant fibroblast, e.g. decreased mitochondrial mass (Figure 17) and altered mitochondrial respiration (Figure 37), cells were also analysed for early apoptosis using FACS analysis. Therefore, immortalized fibroblasts were stained with Annexin V Alexa Fluor 568 conjugate and DAPI to discriminate living and dead cells from cells that undergo early apoptosis. Treatment with 1 µM Staurosporine for 2 hours was used to induce apoptosis.

Untreated immortalized Miro1-R272Q and Miro1-R450C mutant fibroblasts showed no increase in early apoptosis rate or number of dead cells compared to Ctrl 1 fibroblasts. Staurosporine treatment significantly increased apoptosis in all fibroblast lines compared to the respective untreated cells. Staurosporine-induced apoptosis was significantly higher in Miro1-R272Q fibroblasts compared to Ctrl 1 and Miro1-R450C fibroblasts (Figure 46).

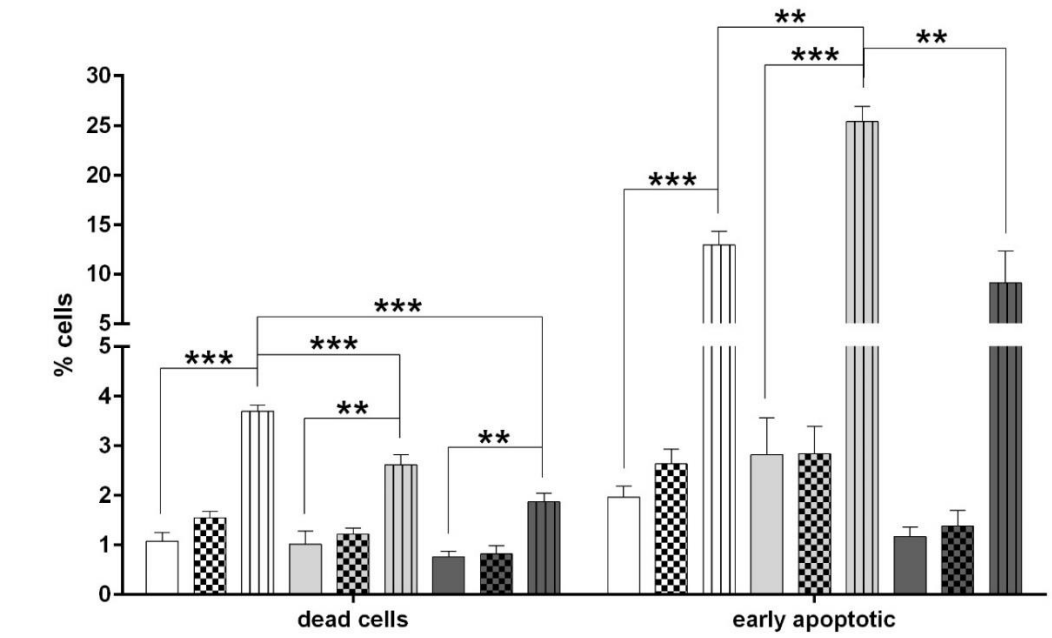

Figure 46: Early apoptosis in immortalized fibroblasts

Early apoptosis and cell death was measured in immortalized fibroblasts by FACS analysis. Cells were treated with 1 µM Staurosporine for 2 hours to induce apoptosis and afterwards stained with Annexin V Alexa Fluor 568 conjugate and DAPI.

Under baseline conditions Miro1 mutant fibroblasts neither showed increased apoptosis, nor increased cell death. Staurosporine treatment induced apoptosis in all fibroblast lines. Staurosporine-induced apoptosis was significantly higher in Miro1-R272Q fibroblasts compared to Ctrl 1 and Miro1-R450C fibroblasts. Data indicated as mean ± SEM. * $p \leq 0.05$ ** $p \leq 0.01$ *** $p \leq 0.001$ by multiple t-test, Holm-Sidak multiple comparison correction. n = 3

4 Discussion

4.1 Mutations in Miro1 are rare causes for PD

Miro proteins have multiple functions on mitochondrial maintenance and their function in distributing mitochondria is crucial for the organization of the mitochondrial network (Fransson, Ruusala et al. 2003) (Fransson, Ruusala et al. 2006) as well as for cellular calcium homeostasis (Wang and Schwarz 2009) (Chang, Niescier et al. 2011). Proper mitochondrial function is especially important for DA neurons, which are predominantly lost in PD. Interestingly, it was reported that overexpression of Miro caused significant loss of DA neurons in drosophila (Liu, Sawada et al. 2012) and a knockout resulted in absence of mitochondria from axons and synapses, thereby severely impairing neuronal function (Guo, Macleod et al. 2005) (Tsai, Course et al. 2014). As a consequence, it was assumed that dysfunction of Miro can cause PD. However, a first attempt to correlate SNPs in *RhoT1* with PD or the age of onset of PD was not successful (Anvret, Ran et al. 2012). SNPs are common variants with a frequency of >5 %. Rare variants with a stronger effect and a frequency of <0.5 % cannot be detected by this approach (Pritchard 2001) (McCarthy and Hirschhorn 2008) but can be captured e.g. by sequencing [reviewed by (Manolio, Collins et al. 2009)]. Accordingly, exome sequencing of the promising candidate gene *RhoT1* enabled us to identify the first disease-associated Miro1 mutations in PD patients from a German cohort of PD patients and age matched healthy controls. Co-segregation analysis could not be conducted due to the fact that the affected fathers of the patients harbouring the Miro1-R272Q and Miro1-R450C mutations are deceased and the brother of the Miro1-F676V mutation carrier was not available for the present study. The identified three PD patients displayed a similar clinical phenotype of tremor dominant symptoms.

In order to determine the potential pathological relevance of the mutations genetic databases have been searched. In different databases containing information about 67486 unrelated individuals only one individual was identified harbouring the R450C mutation. This individual was included in the somatic cancer database cosmic70 (Table 30). In contrast to germline mutations, somatic mutations only affect a small fraction of cells, possibly leading to cancer. Therefore, we considered the identified carrier of the somatic Miro1-R450C mutation as not relevant for the present study. Furthermore, an additional cohort of 1238 German PD patients and 662 healthy controls (KORA cohort) was screened for mutations in *RhoT1*, but only one healthy control person was identified carrying the F676V mutation (Table 30). This result makes a PD causing effect of Miro1-F676V unlikely.

Taken together, these findings suggest that the identified PD-associated mutations in *RhoT1* are rare *de novo* mutations, which is in line with the unsuccessful genetic screen for PD-associated SNP's in *RhoT1* done by Anvret and colleagues (Anvret, Ran et al. 2012). As the identified PD patients harbour heterozygous mutations in *RhoT1*, we hypothesize that these rare variants have a significant impact on health, as reviewed by Manolio (Manolio, Collins et al. 2009).

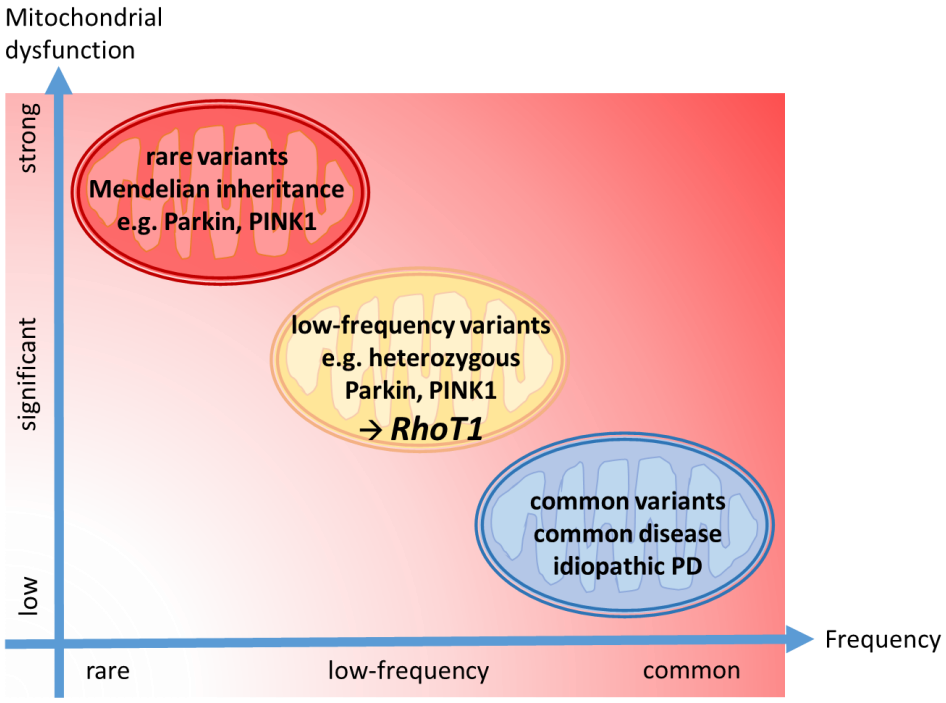

Figure 47: Risk allele frequency and effect size

Schematic overview of allele frequency and effect size of the variant. Rare variants with a strong impact on health typically have a Mendelian inheritance pattern and can therefore be identified by co-segregation studies. Low-frequency variants with a less strong, but significant impact do not show a Mendelian inheritance and are neither detectable by linkage analysis because the effect is not strong enough, nor by genome-wide association studies (GWAS) because these variants are too rare. These variants account for the missing heritability in PD. We propose that the identified PD-associated variants of *RhoT1* are low-frequency variants with significant effect on health. Common variants with a low effect are typically detected by GWAS.

A multiple set of bioinformatical prediction tools have been applied to predict possible pathogenic effects of the identified Miro1 mutations (2.2). These *in silico* analyses revealed that especially Miro1-R272Q, the mutation located in the EF hand domain, has a high likelihood for negative effects on the protein function, with eight of the nine applied analysis

tools predicting a disease causing effect. For Miro1-R450C four of the nine tools predicted a disease causing effect, and for Miro1-F676V two (Figure 7).

Taken both into consideration, the bioinformatical prediction and the genetic data, we hypothesize, that the mutations Miro1-R272Q and Miro1-R450C have a significant impact on the functionality of Miro1 protein, whereas the effect of Miro1-F676V seemed to be less deleterious.

4.1.1 Impact of Miro1 mutations on Miro1 protein structure and functionality

The identified mutations are located within highly conserved protein domains, R272Q within the ligand mimic motif of the first EF hand domain (Klosowiak, Focia et al. 2013), R450C within the C-terminal GTPase domain and F676V within the TMD (Figure 6). Surprisingly, calcium binding to the EF hand domains or nucleotide binding to the GTPase domains did not significantly change the structural conformation of Miro (Klosowiak, Focia et al. 2013). Although the mutations R272Q and R450C are not likely to cause major alterations of the protein structure, still subtle influences could have a significant impact on the functionality of Miro1 as apparently major conformational shifts are not present in the wild type protein.

As the homology model of human Miro1 was based on the 3D structure of dMiro F676V could not be included because the amino acid is not conserved in dMiro.

The amino acids R272 and R450 are located at the surface of Miro1, being exposed to the cytosol. Both amino acids are not located in immediate proximity to predicted phosphorylation sites T298 and Y463 (PhosphoSitePlus analysis), nor to the published possible phosphorylation site Ser156 of PINK1 (Wang, Winter et al. 2011) (Tsai, Course et al. 2014). Therefore, the phosphorylation of Miro1 at known sites, e.g. by PINK1 at Ser156 for subsequent proteasomal degradation was predicted to be not affected. The possible target site for PINK1, Ser156 was under debate because another study failed to verify an influence of this amino acid on Miro1 degradation by the PINK1/Parkin pathway (Birsa, Norkett et al. 2014). Instead, it was proposed that PINK1 phosphorylates and thereby activates Parkin (Kondapalli, Kazlauskaite et al. 2012) and that Parkin in turn ubiquitinates Miro for subsequent degradation. Parkin ubiquitinates Miro1 at highly conserved amino acids Lys153, Lys230, Lys235, Lys330 and Lys572 (Kazlauskaite, Kelly et al. 2014). These amino acids are not in close proximity to R272 or R450. But interestingly, Miro1 undergoes a rather unusual mono-ubiquitylation at the mentioned amino acids, which are located in the N-terminal GTPase domain (Lys153), the second EF hand domain (Lys330) or close to the TMD (Lys572), raising the possibility that mono-ubiquitylation by Parkin could alter

GTPase activity, calcium binding ability and/ or translocation of Miro1 to mitochondria under certain conditions (Kazlauskaite, Kelly et al. 2014). However, the identified mutations R272Q and R450C are not likely to affect the proposed phosphorylation by PINK1, nor the ubiquitylation by Parkin, but the question remained whether the respective mutations affect calcium binding, GTP hydrolysis or mitochondrial localization.

4.2 Reduction of total Miro1 protein and Miro1 mutations both contribute to mitochondrial dysfunction in PD patients

In the present study, results obtained from patient-derived fibroblasts were supported by results from an independent cell model in M17 cells with stable knockdown of endogenous *RhoT1* and transiently overexpression of Miro1-R272Q, Miro1-R450C or Miro1-F676V mutant protein. Although the M17 cells partially resemble the phenotypes observed in fibroblasts, there were also differences (Table 31):

In M17 cells with stable knockdown of endogenous *RhoT1* Tom20 protein amount was comparable to M17 cells without knockdown of *RhoT1*. In contrast, overexpression of Miro1-R272Q, Miro1-R450C or Miro1-F676V protein in M17 with *RhoT1*-KD caused a significant reduction of mitochondrial mass, indicated by reduced Tom20 protein amount (Figure 23). In M17 cells with *RhoT1*-KD overexpressing Miro1-R272Q or Miro1-R450C protein, MnSOD protein level was significantly decreased compared to wild type M17 cells (Figure 44), which means that overexpression of Miro1-R272Q in M17 cells caused reduction of Tom20 and MnSOD protein level, which could not be observed in Miro1-R272Q fibroblasts (Table 31). The observation that Tom20 and MnSOD protein amount were also significantly decreased in M17 cells with *RhoT1*-KD overexpressing Miro1 mutant protein supports the idea that Miro1 mutants directly cause mitochondrial dysfunction, indicating that the mitochondrial phenotypes observed in Miro1 mutant fibroblasts were not caused by additional mutations in the PD-patients harbouring the Miro1-R272Q or Miro1-R450C mutation. Furthermore, the knockdown of *RhoT1* in M17 cells also induced a significant elevation of MMP compared to cells without knockdown of *RhoT1* (Figure 39) like was observed in Miro1-R272Q and Miro1-R450C fibroblasts. Overexpression of Miro1-WT did not rescue the mitochondrial hyperpolarization. Several previous studies reported that overexpression of wild type Miro also induces mitochondrial dysfunction (Russo, Louie et al. 2009) (Fransson, Ruusala et al. 2006) that was even sufficient to cause loss of neurons (Liu, Sawada et al. 2012). Overexpression of Miro1-R272Q, Miro1-R450C or Miro1-F676V slightly increased MMP, but without reaching statistical significance. Given these results, it is possible that a change of Miro1 protein level in general (either by knockdown or

overexpression) leads to mitochondrial dysfunction that subsequently causes mitochondrial hyperpolarization.

Table 31: Summary of phenotypes obtained from fibroblasts and M17 cells

immortalized fibroblasts		**M17 cells**			
Miro1-R272Q	**Miro1-R450C**	***RhoT1*-KD**	***RhoT1*-KD + overexpression**		**phenotype**
			Miro1-WT	**Miro1-mutants**	
not changed	reduced	not changed	not changed	reduced	**mitochondrial mass (Tom20)**
not changed	reduced	not changed	not changed	reduced	**MnSOD protein**
increased	increased	increased	increased	not significantly increased	**MMP**

The M17 cell model with knockdown of endogenous *RhoT1* and transiently overexpression of Miro1 protein is an artificial model, which does not fully resemble the situation in patient-derived fibroblasts. The knockdown of endogenous *RhoT1* corresponds to the reduction of total Miro1 protein amount observed in Miro1-R272Q and Miro1-R450C fibroblasts (Figure 13), but the patients are heterozygous, thus expressing Miro1-WT and Miro1 mutant proteins. Because overall Miro1 protein (wild type and mutant protein) is reduced in both patient-derived fibroblasts lines, overexpression of mutant Miro1 protein in cells with knockdown of endogenous Miro1 does not exactly reflect the *in vivo* situation. Overexpression of wild type Miro1 was reported to induce mitochondrial phenotypes in several studies (Russo, Louie et al. 2009) (Fransson, Ruusala et al. 2006) (Liu, Sawada et al. 2012). Therefore it is possible that an artificial overexpression of Miro1-WT, Miro1-R272Q or Miro1-R450C induces mitochondrial phenotypes in M17 cells, which cannot be observed in Miro1 mutant fibroblasts. Still, mitochondrial phenotypes observed in fibroblasts could be successfully replicated in the M17 cell model, e.g. MMP hyperpolarization, reduction of mitochondrial mass and reduced MnSOD protein level, which is in line with the

hypothesis that Miro1 mutations as well as reduction of total Miro1 protein amount causes mitochondrial dysfunction.

4.3 Miro1-R272Q and Miro1-R450C cause distinct mitochondrial phenotypes

Although both fibroblast lines obtained from PD-patients harbour mutations in the same gene, the cell lines display different mitochondrial phenotypes. A similar observation was made for LRRK2. Different mutations in this gene have different consequences for LRRK2 function, but cause the same disease. The mutation G2019S in the kinase domain of LRRK2 is the most common pathogenic mutation in LRRK2 (Singleton, Farrer et al. 2013) and causes a detrimental increase of LRRK2 kinase activity (West, Moore et al. 2007). The mutations R1441C, R1441G and R1441H in the GTPase domain of LRRK2 interfere with the GTP hydrolysis ability of LRRK2 (Lewis, Greggio et al. 2007) (Liao, Wu et al. 2014), thereby inducing cellular toxicity (Chan, Chua et al. 2014) (West, Moore et al. 2005). Still, all the identified mutation carriers suffer from PD.

The Miro1 mutations R272Q and R450C likewise cause distinct mitochondrial phenotypes, interestingly despite the fact that overall Miro1 protein amount was significantly reduced in both mutant fibroblasts lines. The reason for the reduction of Miro1 protein seems to be different in both fibroblast lines as *RhoT1* mRNA level was only observed to be reduced in Miro1-R450C fibroblasts, but not in Miro1-R272Q fibroblasts.

Miro1-R450C fibroblasts showed a number of alterations, which were not observed in Miro1-R272Q fibroblasts. Miro1-R450C specific alterations were reduction of mitochondrial mass, increased mitochondrial biogenesis, while MnSOD protein was reduced, reduced citrate synthase enzyme activity, increased citrate synthase protein level and decreased calcium buffering capability. Miro1-R272Q fibroblasts also displayed an impaired cytosolic calcium homeostasis, but distinct from the disrupted calcium-buffering observed in Miro1-R450C fibroblasts. We hypothesize that the mutation R272Q disrupts calcium binding to Miro1 and therefore the calcium homeostasis by mitochondria, as observed by (Stephen, Higgs et al. 2015) and (Chang, Niescier et al. 2011), in turn probably making cells more susceptible to calcium-induced apoptosis (Figure 46). The R450C mutation in contrast could interfere with the ER-mitochondrial contact regulation, which is regulated by the C-terminal GTPase domain of Miro1 (Saotome, Safiulina et al. 2008) (Kornmann, Osman et al. 2011) and therefore disrupt cytosolic calcium buffering.

Mitochondrial spare respiratory capacity was significantly lower in Miro1-R272Q compared to Ctrl 1 fibroblasts, whereas OCR was significantly increased in Miro1-R450C fibroblasts,

but still both phenotypes cause MMP hyperpolarization. We hypothesize that alteration of respiration caused the changes of the MMP, which in turn evokes certain cell responses for compensation or quality control. Considering the results from *gem1*Δ yeast displaying a severe growth defect on medium containing glycerol as non-fermentable carbon source and the insufficient rescue of the growth defect by Gem1-R298Q (the yeast orthologue of Miro1-R272Q), at least Miro1-R272Q was classified as loss-of-function mutation. Because the heterozygous fibroblast lines Miro1-R272Q and Miro1-R450C display significant different phenotypes both mutations were considered to have dominant negative effects, which will be further discussed in detail in the following sections.

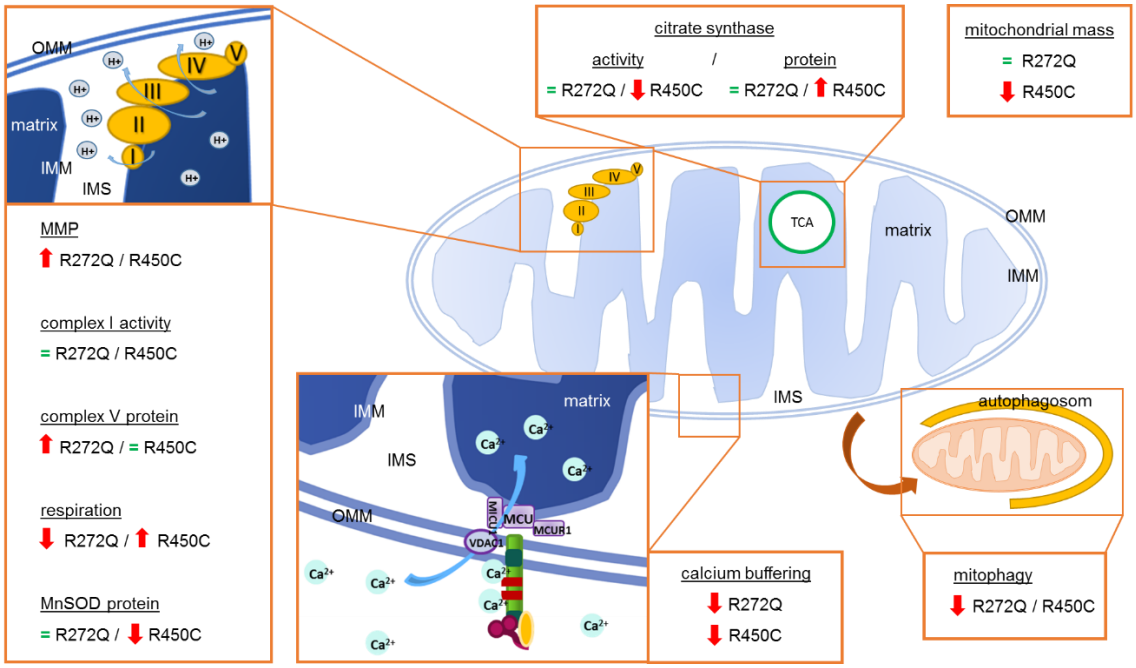

Figure 48: Overview of mitochondrial phenotypes in patient-derived fibroblasts

Overview of mitochondrial phenotypes observed in Miro1-R272Q and Miro1-R450C fibroblasts. Mitochondrial membrane potential was increased in Miro1-R272Q and Miro1-R450C fibroblasts. Complex V protein amount was increased in Miro1-R272Q fibroblasts. Mitochondrial respiration was significant lower in Miro1-R272Q fibroblasts compared to Miro1-R450C fibroblasts. MnSOD protein level was reduced in Miro1-R450C fibroblasts. Citrate synthase activity was decreased in Miro1-R450C fibroblasts, whereas protein level was increased. Mitochondrial mass was reduced in Miro1-R450C fibroblasts. Calcium buffering was impaired in Miro1-R272Q and in Miro1-R450C fibroblasts. Mitophagy was impaired in Miro1-R272Q and Miro1-R450C fibroblasts. **MMP**: mitochondrial membrane potential. **OMM**: outer mitochondrial membrane. **IMM**: inner mitochondrial membrane. **IMS**: intermembrane space. **TCA**: tricarboxylic acid cycle. **MICU**: mitochondrial calcium uptake. (Perocchi, Gohil et al. 2010) **MCU**: mitochondrial calcium uniporter. (Baughman, Perocchi et al. 2011) (De Stefani, Raffaello et al. 2011) **MCUR1**: mitochondrial calcium uniporter regulator 1. (Mallilankaraman, Cardenas et al. 2012).

4.4 Functional implications for the mutation Miro1-R272Q

Fibroblasts were obtained from a female PD patient carrying the heterozygous point mutation c.815 G>A in the *RhoT1* gene, leading to the amino acid change R to Q at position 272 in the amino acid chain. This mutation is located within the highly conserved N-terminal EF hand domain of Miro1, which is one of two calcium binding domains of the protein. From the obtained results of the present study we hypothesize that Miro1-R272Q is a loss-of-function mutation.

4.4.1 Miro1 protein stability

Compared to control fibroblasts (Ctrl 1) the total protein amount of Miro1 was reduced to less than half in Miro1-R272Q fibroblasts (Figure 13). Because *RhoT1* is biallelic expressed (Gimelbrant, Hutchinson et al. 2007) and the fact that the PD patients were heterozygous for the *RhoT1* mutations, it was justified to analyse the mRNA level of *RhoT1*, because reduced protein level could arise from reduced transcription of the mutant allele, but apparently mRNA level were not reduced in Miro1-R272Q fibroblasts (Figure 14) and sequencing of *RhoT1* cDNA revealed that wild type and mutant alleles are expressed on RNA level (Figure 15). Therefore mechanisms for reduction of Miro1 protein are likely different from mRNA levels.

In silico analysis predicted that the mutation R272Q had only a minor impact on protein stability [0,32 Kcal/mol (NeEMO) and 0,4 Kcal/mol (I-MUTANT)] (3.3). Still, these minor effects on predicted protein stability *in silico* can have unexpected high impact on protein stability *in vivo*, as was also recently reported in a study about DJ-1-M26I mutant protein. This mutation was also predicted to have only minor effects on protein stability, but *in vivo* the protein amount was significantly reduced (Milkovic, Catazaro et al. 2015). Milkovic and colleagues found that despite the pico- to nanosecond dynamics of DJ-1 wild type and DJ-1-M26I were similar, the mutant DJ-1-M26I was thermodynamically more flexible on longer time-scales, consequently generating transiently instable protein conformations, which resulted in loss of mutant protein *in vivo* (Milkovic, Catazaro et al. 2015).

Another study reported that the ability of the first EF hand domain of Miro1 to bind calcium is crucial for protein stability. A loss of function mutation in the N-terminal EF hand domain, which interfered with calcium binding, caused a complete loss of the mutant Miro1 protein *in vivo* (Koshiba, Holman et al. 2011). This finding suggests that protein stability of Miro1-R272Q was impaired due to a loss-of-function-character of the mutation. This finding further indicates that also minor changes on protein structure and thermal stability can have a

relevant impact *in vivo* and was further substantiated by the successful rescue of Miro1 protein by inhibition of the proteasome. Blocking the proteasomal protein degradation by MG132 increased total Miro1 protein levels by ~1.6 fold more than in Ctrl 1 fibroblasts. Previous studies reported that Miro1 is predominantly degraded by the proteasome before mitophagy occurs (Birsa, Norkett et al. 2014) (Wang, Winter et al. 2011). However, *RhoT1* is biallelic expressed (Gimelbrant, Hutchinson et al. 2007), meaning that the wild-type and the mutant alleles are expressed in the heterozygous patient-derived fibroblasts, which could be confirmed by sequencing *RhoT1* cDNA (Figure 15). Therefore, it can be assumed that the accumulated Miro1 protein after inhibition of the proteasome consists of Miro1-WT and Miro1-R272Q, supported by the observation that *RhoT1* mRNA level was not decreased in Miro1-R272Q fibroblasts. We conclude that the mutation R272Q disrupts calcium binding to Miro1, which leads to protein instability and subsequent degradation, further leading us to investigate the relevance of Miro1-R272Q for mitochondrial calcium homeostasis.

4.4.2 Calcium homeostasis

The calcium binding ability of Miro is not only relevant for mitochondrial transport, but also for influx of calcium from the cytosol into the mitochondrial matrix (Chang, Niescier et al. 2011). The exposed localisation of the amino acid R272 within the N-terminal EF hand domain (Figure 8) raises the possibility that the mutation R272Q affects the calcium binding ability and subsequent operation of Miro1.

In Miro1-R272Q fibroblasts cytosolic calcium concentration raised significantly after histamine treatment, whereas in Ctrl 1 fibroblasts the calcium peak was much lower (Figure 45). In Ctrl 1 and Miro1-R272Q fibroblasts calcium concentration in the cytosol decreased during the 5 min imaging after histamine-evoked calcium release and nearly reached the initial level, indicating that the cells are able to somehow buffer cytosolic calcium under these conditions, either by mitochondria and/ or by the ER.

In a recent study, primary rat astrocytes with endogenous Miro1 and overexpression of Miro1 with mutant EF hand domains ($Miro1^{\Delta EF}$) showed a similar phenotype: upon stimulation with ATP calcium release from internal stores was significantly increased compared to control astrocytes, in terms of amplitude, frequency and duration of the calcium peaks (Stephen, Higgs et al. 2015). The authors conclude, that disruption of the EF hand domains of Miro1 might alter the regulation of intracellular calcium concentration, which could result in higher vulnerability to calcium overload (Stephen, Higgs et al. 2015).

Furthermore, the disruption of EF hand domains in this study also had a dominant negative effect, like was observed in Miro1-R272Q fibroblasts.

The hypothesis of disrupted mitochondrial calcium homeostasis caused by Miro1-R272Q was also supported by another study in 2011, showing that loss of function mutations of Gem1 EF hand domains in yeast resulted in failed localization of Gem1 to ERMES, consequently leading to impairment of phospholipid and calcium exchange between mitochondria and the ER (Kornmann, Osman et al. 2011). Furthermore, it was shown, that loss of function mutations of the EF hand domains significantly impaired calcium uptake into the mitochondrial matrix in *drosophila* neurons (Chang, Niescier et al. 2011).

We conclude that Miro1-R272Q interferes with intracellular calcium homeostasis, possibly increasing the risk of calcium overload.

4.4.3 Mitochondrial respiration and MMP

Calcium influx into mitochondria is also important to enhance the activity of calcium-induced enzymes of the TCA cycle and the respiratory chain to increase mitochondrial ATP production (Wan, LaNoue et al. 1989) (McCormack, Halestrap et al. 1990) (Chan, Gertler et al. 2009). It was reported that Miro is involved in the regulation of calcium influx into mitochondria (Chang, Niescier et al. 2011). Gem1 is the yeast orthologue of Miro1 and Miro2. Previous studies reported that *gem1*Δ yeast display a significant growth defect on non-fermentable carbon source (Frederick, McCaffery et al. 2004) (Kornmann, Osman et al. 2011). A phenotype with impaired growth was not only observed in yeast, but also in *gemA* deficient *Dictyostelium discoideum* (Vlahou, Elias et al. 2011). In the present study the same severe phenotype was observed in yeast growing on medium containing a non-fermentable carbon source, where energy metabolism and therefore growth relies on mitochondrial function (Figure 12).

The hypothesis that mitochondrial calcium homeostasis is involved in the growth defect of *gem1*Δ yeast was supported by observations in yeast devoid of VDAC. VDAC was previously suggested as member of the protein complex facilitating ER-mitochondrial contact sites, where VDAC is required for mitochondrial calcium uptake (Szabadkai, Bianchi et al. 2006). Yeast without VDAC expression also display severe growth defects when growing on medium containing a non-fermentable carbon source (Wu, Sampson et al. 1999) (Xu, Decker et al. 1999), thereby indicating that impaired mitochondrial calcium homeostasis could be involved in the phenotype.

Interestingly, knockdown of DISC1 or its interaction partner Mitofilin resulted in similar disruption of mitochondrial metabolism, as published by (Park, Jeong et al. 2010). DISC1 was described to interact with the Miro/Milton complex for regulation of mitochondrial transport (Ogawa, Malavasi et al. 2014). The knockdown of DISC1 or Mitofilin led to reduced activity of NADH dehydrogenase of the electron transport chain with subsequent reduction of ATP production in murine CNS-tumour CAD cells and in primary mouse neurons. Ionomycin was used to rise cytosolic calcium levels in CAD cells. Time laps imaging revealed a disruption of mitochondrial calcium buffering when DISC1 or Mitofilin was knocked down (Park, Jeong et al. 2010). These findings suggest that DISC1/ Mitofilin might not only be involved in the mitochondrial transport-involved function of Miro, but also in Miro1-mediated mitochondrial calcium homeostasis, which makes sense when considering the localization of DISC1 in the mitochondrial intermembrane space and of Mitofilin in the IMM (see Figure 2). Apparently, disruption of the protein complex around Miro1 affects mitochondrial metabolism, probably by disruption of mitochondrial calcium homeostasis.

The exact reason for the growth defect of *gem1*Δ yeast on non-fermentable carbon source is not finally clarified yet, but existing publications provide multiple hints that *gem1*/ *gemA* deficiency impairs mitochondrial respiration (Frederick, McCaffery et al. 2004) (Vlahou, Elias et al. 2011). Another explanation was provided by the observation that *gem1*Δ yeast have a problem to pass mtDNA to the next generation of daughter cells (Frederick, McCaffery et al. 2004) (Frederick, Okamoto et al. 2008), likely because distribution of newly replicated mtDNA relies on Gem1 (Murley, Lackner et al. 2013). Decreased mtDNA content in daughter yeast cells results in decreased respiratory activity, thereby probably impairing energy metabolism on non-fermentable carbon source. However, measurement of total mtDNA copy number in Miro1-R272Q fibroblasts under baseline conditions, as well as under oxidative stress induced by H_2O_2 or rotenone treatment, revealed no decrease of mtDNA copy number (Figure 30). The contribution of decreased mtDNA copy numbers in the growth defect was therefore considered to be unlikely.

Growth on non-fermentable carbon source could be restored by expression of Gem1-WT in *gem1*Δ yeast, but not by expression of Gem1-R298Q. The amino acid R272 is conserved in yeast as amino acid R298. As the mutation R298Q is located in the first EF hand domain of Gem1, it is tempting to speculate that Gem1-R298Q (or Miro1-R272Q respectively) could affect mitochondrial respiration by insufficient mitochondrial calcium concentration, thereby indicating that R298Q, and likely its human counterpart R272Q as well, is a loss of function mutation.

In Miro1-R272Q immortalized fibroblasts basal respiration, capacity for ATP production and maximal respiration were indistinguishable compared to Ctrl 1 fibroblasts, whereas spare respiratory capacity was significantly lower in Miro1-R272Q fibroblasts compared to Ctrl 1 fibroblasts (Figure 37). These results are in line with the results obtained from *gem1*Δ yeast expressing Gem1-R298Q and led us to the hypothesis that Miro1-R272Q impairs mitochondrial respiration by impaired mitochondrial calcium homeostasis.

It has long been noticed that under normal conditions cells are able to provide the necessary energy at a basal respiratory activity, which is below the maximal possible respiratory activity. The difference is defined as spare respiratory capacity and is important to provide higher levels of ATP in case of higher demand [reviewed by (Desler, Hansen et al. 2012)]. A long-lasting overstressing of spare respiratory capacity was linked to aging (Desler, Hansen et al. 2012) and neurodegeneration (Nicholls 2008) (Yadava and Nicholls 2007). This was particularly interesting in a model of primary rat neurons treated with low concentrations of rotenone (5 nM or 20 nM). Increased calcium entry via NMDA receptors demanded so much ATP for the maintenance of calcium homeostasis that the diminished spare respiratory capacity (induced by rotenone) caused increased susceptibility towards glutamate excitotoxicity (Yadava and Nicholls 2007). However, complex I activity was not decreased in Miro1-R272Q and therefore likely not the cause for the observed diminished spare respiratory capacity. Spare respiratory capacity can also be regulated by different factors, e.g. inhibition of complex IV by ATP (Ramzan, Staniek et al. 2010) (Kadenbach, Ramzan et al. 2010) as well as by the membrane potential, with a high MMP usually reflecting a high spare respiratory capacity (Piccoli, Scrima et al. 2006) (Dalmonte, Forte et al. 2009), or by nitric oxide (NO) (Poderoso, Carreras et al. 1996) (Riobo, Clementi et al. 2001) (Diers, Broniowska et al. 2011). A high MMP induces NO production by the mitochondrial enzyme nitric oxide synthase (mtNOS) and in turn leads to inhibition of complex III and IV (Valdez, Zaobornyj et al. 2006). A chronic decrease of spare respiratory capacity was therefore linked to aging and neurodegeneration as neurons are predominantly depending on the ability to cope with increased ATP demand under stress conditions [reviewed by (Desler, Hansen et al. 2012). We therefore propose that the observed reduction of spare respiratory capacity in Miro1-R272Q cause an increased vulnerability towards stress and subsequently can cause a crisis of energy metabolism under demanding conditions.

Despite the fact that complex V protein amount was significantly increased in Miro1-R272Q compared to Ctrl 1 fibroblasts (Figure 33), capacity for ATP production was not increased

in Miro1-R272Q fibroblasts, but spare respiratory capacity was significantly lower compared to Ctrl 1 fibroblasts (Figure 37). These results indicate that the ATPase (complex V) might be not be working sufficiently in Miro1-R272Q fibroblasts.

Under physiological conditions the reflux of protons through complex V, which is the force that provides the energy for ATP production, prevents pathological membrane hyperpolarization. An impaired reflux of protons into the mitochondrial matrix could consequently cause mitochondrial hyperpolarization. This hypothesis was supported by the observation that the complex V inhibitor oligomycin induces mitochondrial hyperpolarization (Di Lisa and Bernardi 1998). Under physiological conditions the MMP has a mean value of -139 mV and fluctuates between -108 and -159 mV, depending on respiratory activity (Li, Fang et al. 2013) (Valko, Leibfritz et al. 2007) (Radak, Chung et al. 2008). Usually MMP values are high when the respiratory function, ATP production and oxygen consumption are low. The MMP gets discharged to increase ATP production, reflected by increased oxygen consumption. To recharge the MMP the electron transport chain activity is increased to pump protons across the inner mitochondrial membrane back into the intermembrane space (Arvier, Lagoutte et al. 2007) (Bagkos, Koufopoulos et al. 2014). Our observation of consistently increased MMP in Miro1-R272Q fibroblasts further supports the hypothesis that Miro1-R272Q cells display a problem with energy metabolism. As measurement of OCR only allowed to assess the theoretical capacity for ATP production, it will be necessary to measure the actual ATP content in the cells, e.g. by a luminescent method, to draw conclusions for energy supply in the cells.

In cancer development mitochondrial hyperpolarization seems to protect cells against apoptosis (Hardonniere, Huc et al. 2015). Nevertheless, hyperpolarization within a certain range can also induce apoptosis. Mitochondrial damage induced in CHO-K1, MRC-5 or HeLa cells caused mitochondrial hyperpolarization-triggered cell death even without increased ROS production (Leal, de Queiroz et al. 2015). In cultured rat hippocampal neurons treatment with Staurosporine induced mitochondrial hyperpolarization and subsequent cytochrome c release, thereby inducing apoptosis (Poppe, Reimertz et al. 2001). The authors of the study hypothesized that Staurosporine leads to a calcium-dependent increase of mitochondrial respiration that causes mitochondrial membrane hyperpolarization (Poppe, Reimertz et al. 2001). Other studies also observed calcium-dependent apoptosis induced by Staurosporine treatment (Kruman and Mattson 1999) (Prehn, Jordan et al. 1997), while another study showed that hyperpolarization of mitochondria does not always cause apoptosis (Iijima 2006). Taken together, it seems that

Staurosporine induces an increase of cytosolic calcium concentration, which in turn leads to increased calcium influx into mitochondria that stimulates activity of mitochondrial respiration, thereby inducing hyperpolarization of the mitochondrial membrane and in turn activating mitochondrial membrane permeability transition and subsequent release of cytochrome c (Kruman and Mattson 1999). Mitochondrial hyperpolarization that is not induced by Staurosporine likewise increases influx of calcium into mitochondrial matrix, which triggers release of cytochrome c (Kruman and Mattson 1999).

Considering the calcium-depending action of Staurosporine on MMP and the observed mitochondrial dysfunction and MMP hyperpolarization in Miro1 mutant fibroblasts, it was reasonable to use this compound to induce apoptosis, as Miro1 is critically involved in calcium homeostasis and mitochondrial maintenance.

Under baseline conditions, the apoptosis rate was comparable between Ctrl 1 and Miro1 mutant fibroblasts (Figure 46). This certainly means that the observed hyperpolarization of Miro1 mutant fibroblasts (Figure 38) alone was not sufficient to induce apoptosis in fibroblasts. Staurosporine significantly induced apoptosis in all three fibroblast lines (Figure 46), likely by further increasing MMP hyperpolarization. In Miro1-R272Q fibroblasts apoptosis induced by Staurosporine was significantly higher compared to Ctrl 1 (and to Miro1-R450C) fibroblasts (Figure 46). In combination with the observed impaired calcium homeostasis in Miro1-R272Q fibroblasts, we conclude that Miro1-R272Q fibroblasts are more susceptible to calcium overload and subsequent apoptosis.

4.4.4 Mitophagy

Given the observed alterations of mitochondrial function in Miro1-R272Q fibroblasts, like calcium homeostasis, mitochondrial respiration and membrane potential, we wondered whether these phenotypes induce clearance of dysfunctional mitochondria as means of mitochondrial quality control.

Previous studies identified the stop of mitochondrial movement by reduction of Miro protein levels as initiation step for mitophagy, either by knockdown of Miro in neurons (Liu, Sawada et al. 2012) or by increased PINK1/ Parkin-mediated degradation of Miro in rat hippocampal neurons (Wang, Winter et al. 2011). Reduced Miro1 protein levels in Miro1-R272Q fibroblasts were apparently not linked to a decrease of total mitochondrial mass under baseline conditions. Still, as Miro1 degradation was increased in Miro1-R272Q fibroblasts and this was previously implicated as initial step for mitophagy (Liu, Sawada et al. 2012) (Wang, Winter et al. 2011), we wondered if mitophagy was either induced or affected.

Fragmentation of the mitochondrial network was considered as prerequisite for degradation of mitochondria as uptake of mitochondria by autophagosomes requires distinct single organelles. An increased overlap of mitochondria and lysosomes consequently indicates mitochondrial degradation. In Miro1-R272Q fibroblasts mitochondrial morphology was not changed compared to two control fibroblast lines from healthy age matched donors, meaning that the mitochondrial network was not fragmented and consistently, co-localization of lysosomes and mitochondria was not increased under baseline growth conditions (Figure 25).

A similar observation was recently made by Stephen and colleagues, who used astrocytes overexpressing EF hand mutant Miro1 (Miro1$^{\Delta EF}$). Under baseline conditions, overexpression of Miro1$^{\Delta EF}$ had no influence on mitochondrial morphology, but when astrocytes were stimulated with glutamate, mitochondrial length was increased in Miro1$^{\Delta EF}$ overexpressing cells, whereas mitochondrial size was decreased in control cells, indicating that mitochondrial morphology is depending on the functionality of the EF hands under certain conditions (Stephen, Higgs et al. 2015). A similar observation was also made in a previous study by Saotome et al. Overexpression of EF hand mutant Miro1 in primary cortical neurons from rats led to increased mitochondrial length in processes upon neuronal stimulation with 90 mM KCl (Saotome, Safiulina et al. 2008).

Both EF hand domains of Miro1 mediate the stop of mitochondrial transport upon calcium binding (Wang and Schwarz 2009) (MacAskill, Brickley et al. 2009). Disruption of calcium binding by mutation of one EF hand impairs the calcium-mediated stop of mitochondria, resulting in mobile mitochondria, that are more likely to fuse with other mitochondria and therefore probably causing enlarged mitochondria (Liu, Weaver et al. 2009). Enlarged mitochondria in turn could interfere with mitophagy, as was indicated in studies where overexpression of Miro1 lead to enlarged mitochondria and loss of DA neurons (Liu, Sawada et al. 2012), a similar phenotype like observed in PINK1 or Parkin knockout flies (Park, Lee et al. 2006) (Clark, Dodson et al. 2006). The observations of these studies suggest, that stimulation of Miro1-R272Q fibroblasts, e.g. by using histamine could reveal a phenotype of altered mitochondrial morphology that was not observed under baseline conditions. Further analysis under stress conditions (e.g. inhibition of complex I with Piericidin A to increase ROS production or decreasing MMP with Valinomycin) could reveal alterations of mitochondrial quality control and turn over induced by impaired Miro1 function.

To further investigate whether mitophagy was affected in Miro1-R272Q fibroblasts the autophagy marker LC3 II was investigated. The results indicate that autophagic flux was impaired in Miro1-R272Q fibroblasts, because upon inhibition of autophagy using

Bafilomycin A_1 LC3 II did not accumulate significantly. Moreover, also FBS starvation did not induce the formation of LC3 II, thereby indicating that formation of the autophagosome is affected. As mitophagy is a special form of autophagy to degrade mitochondria, we propose that mitophagy is impaired in Miro1-R272Q fibroblasts.

Recently, it was shown that autophagosomes preferentially form at ER-mitochondrial contact sites (Hamasaki, Furuta et al. 2013). The so called omegasome was identified to be the origin of the isolation membrane, which is derived from the ER to form autophagosomes (Axe, Walker et al. 2008). Hamasaki and colleagues proposed that the ER is the origin of autophagosome formation and the close contact to mitochondria ensures supply of components and energy for the process. Disruption of the ER-mitochondria contact by knockdown of Mfn2, which was shown to facilitate the contact of both organelles (de Brito and Scorrano 2008), led to impaired autophagosome formation (Hamasaki, Furuta et al. 2013). Mfn2 was found to interact with Miro1 in the same complex, not only to facilitate mitochondrial transport, but also to regulate mitochondrial calcium uptake (Misko, Jiang et al. 2010) at ER-mitochondrial contact sites (de Brito and Scorrano 2008) (Kornmann, Osman et al. 2011) (Chang, Niescier et al. 2011). For this reason we speculate that the mutation of the calcium binding domain of Miro1-R272Q impairs calcium binding and therewith disrupts the function of ER-mitochondria contact sites, subsequently impairing autophagosome formation and probably autophagy in general.

In summary, we propose that the mutation R272Q disrupts the calcium binding ability of Miro1 and therewith cellular calcium homeostasis and Miro1 protein stability. This dysfunction likely impairs mitochondrial respiration. As a consequence mitochondrial membrane is hyperpolarized and cells become more vulnerable to calcium overload and calcium-mediated apoptosis. Furthermore, insufficient mitochondrial quality control via mitophagy adds to mitochondrial dysfunction.

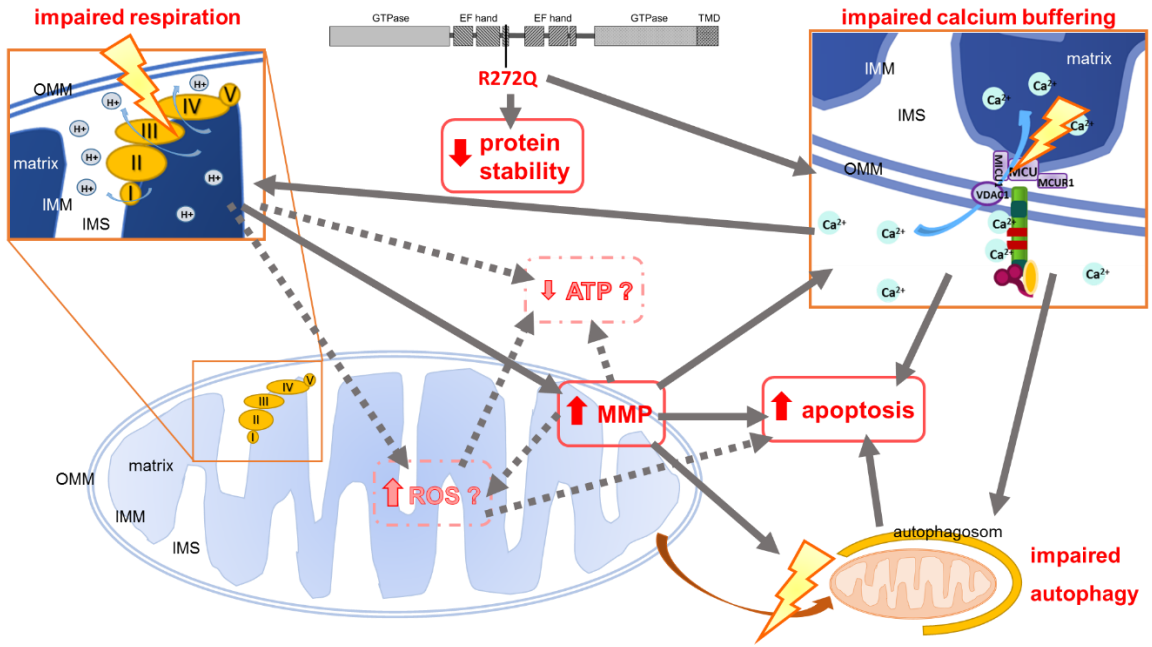

Figure 49: Overview of mitochondrial phenotype found in Miro1-R272Q fibroblasts

We hypothesize that the mutation R272Q in the EF hand interferes with calcium binding, which in turn impairs protein stability and mitochondrial calcium buffering ability, which also impairs respiratory activity. Impaired respiration leads to hyperpolarization of mitochondrial membrane. Autophagic flux is impaired by the increased MMP and the impaired calcium buffering. Mitochondrial hyperpolarization, impaired autophagy and calcium buffering leads to increased vulnerability to apoptosis.

OMM: outer mitochondrial membrane. **IMM**: inner mitochondrial membrane. **IMS**: intermembrane space. **MMP**: mitochondrial membrane potential.

4.5 Functional implications for the mutation Miro1-R450C

The second investigated mutation in the *RhoT1* gene described in this study is the heterozygous point mutation c.1348 C>T, causing the amino acid change R to C at position 450 of the amino acid chain of Miro1. This mutation lies within the C-terminal GTPase domain, which is highly conserved across different species and modulates not only anterograde transport of mitochondria (Babic, Russo et al. 2015) and the calcium binding ability of Miro1 (Klosowiak, Focia et al. 2013) (Saotome, Safiulina et al. 2008) (Kornmann, Osman et al. 2011), but also the interaction of Miro with other proteins.

4.5.1 Calcium buffering

Whilst the mutation R450C is not located within the calcium binding EF hand domains, it was shown that the EF hand domains (including R272Q) and the C-terminal GTPase domain (including R450C) form a unique side-by-side 3D structure that facilitates a close interplay of the domains (Klosowiak, Focia et al. 2013). Therefore it is possible that both mutations independently affect calcium homeostasis. Indeed, we were able to define a phenotype related to disrupted calcium homeostasis in Miro1-R450C fibroblasts.

Histamine was used to release calcium from mitochondria and the ER, resulting in slightly elevated cytosolic calcium concentrations compared to the calcium peak in Ctrl 1 fibroblasts. During 5 min of imaging following the histamine treatment cytosolic calcium concentration decreased in Ctrl 1 and in Miro1-R272Q fibroblasts, but in Miro1-R450C fibroblasts cytosolic calcium concentration did not decrease at all within the same time frame (Figure 45). This observation suggests that buffering of cytosolic calcium is impaired in this cell line.

Previous studies found that functionality of both GTPase domains of Miro1 are required for calcium-mediated function of Miro in H9c2 cells and in primary cortical neurons of rats (Saotome, Safiulina et al. 2008). Similar observations were made in a *gem1*Δ yeast strain expressing different mutant forms of Gem1, displaying impaired metabolite and calcium exchange between ER and mitochondria: Disruption of the N-terminal GTPase domain of Gem1 disturbed localization of mutant Gem1 to the ERMES complex, which connects the ER and mitochondria and facilitates exchange between both organelles, whereas loss of function mutants of the C-terminal GTPase domain localized properly to ERMES, but also failed to rescue the *gem1*Δ phenotype (Kornmann, Osman et al. 2011). These results further substantiated our hypothesis, that also the mutation R450C located in the C-terminal GTPase domain is able to affect mitochondrial calcium homeostasis.

As a next step to validate our hypothesis, we suggest to investigate how mitochondria in Miro1-R450C mutant cells are able to cope with repeated stimuli, e.g. by triggering calcium release from ER and mitochondria using histamine or ATP and inhibition of calcium uptake by the ER using Thapsigargin, a commonly used specific inhibitor of sarco-endoplasmic reticulum calcium-ATPases [(SERCA), reviewed by (Treiman, Caspersen et al. 1998)]. Due to the observed diminished calcium buffering capacity of Miro1-R450C fibroblasts, it is possible that these cells are more vulnerable to excitotoxicity, caused by disrupted cytosolic calcium homeostasis.

4.5.2 Mitochondrial mass

Regarding Miro1 protein level, Miro1-R450C fibroblasts displayed the same effect on overall Miro1 protein levels like observed in Miro1-R272Q fibroblasts. Miro1 protein level was reduced to approximately half of the protein amount compared to Ctrl 1 fibroblasts (Figure 13).

Inhibition of the proteasome using MG132 elevated total Miro1 protein level in Miro1-R450C fibroblasts. Given the fact, that the same observation was made in Ctrl fibroblasts, this was not surprising, as it was shown that also Miro1-WT gets constantly degraded by the proteasome (Wang, Winter et al. 2011) (Birsa, Norkett et al. 2014). As *RhoT1* is bi-allelic expressed (Gimelbrant, Hutchinson et al. 2007), it cannot be ruled out, that the reduced *RhoT1* mRNA level observed in Miro1-R450C fibroblasts result from decreased expression of the mutant allele. Sequencing of *RhoT1* cDNA showed that wild type and mutant alleles of *RhoT1* are expressed in Miro1-R272Q fibroblasts (Figure 15), thereby suggesting that Miro1-R450C protein is expressed in Miro1-R450C fibroblasts. Mitochondrial mass was also reduced by approximately half of the amount in Miro1-R450C fibroblasts compared to Ctrl 1 fibroblasts (Figure 17).

This result was in line with previous studies, which reported that knockdown of Miro1 and Miro2 in CHO, HeLa or HEK293T cells (Suzuki, Danilchanka et al. 2014) or knockout of GemA in *D. discoideum* (Vlahou, Elias et al. 2011) resulted in decreased mitochondrial mass. However, in the M17 cell model with stable *RhoT1*-KD Tom20 and MnSOD protein were not reduced, but overexpression of Miro1-R450C lead to significant decrease of Tom20 and MnSOD protein levels, like was also observed in Miro1-R450C fibroblasts. These results indicate that the mutant protein Miro1-R450C is expressed to some extent in Miro1-R450C fibroblasts and has a dominant negative effect.

As mitochondrial mass was reduced in Miro1-R450C mutant fibroblasts mitochondrial biogenesis was investigated. PPARγ coactivator-1α (PGC1α) is a coactivator of transcription, e.g. for genes related to ROS defence (like SOD1, MnSOD, catalase and glutathione peroxidase-1) (St-Pierre, Drori et al. 2006) and the main driver for mitochondrial biogenesis and mitochondrial respiration [reviewed by (Corona and Duchen 2015)]. PGC1α is induced, amongst others, by energy deficit (Nemoto, Fergusson et al. 2005) (Jeninga, Schoonjans et al. 2010), which can be a result of reduced mitochondrial mass. In Miro1-R450C fibroblasts PGC1α protein level was increased to ~3.5 fold compared to Ctrl 1 fibroblasts (Figure 29). Expression of nuclear-encoded genes for complexes of the respiratory chain is also activated by PGC1α (Zheng, Liao et al. 2010). In line with this report, indeed the protein amount of complex IV of the respiratory chain was slightly increased in Miro1-R450C fibroblasts (Figure 33) and citrate synthase protein amount was significantly increased in Miro1-R450C (Figure 31). We speculate that PGC1α is upregulated to compensate the reduction of mitochondrial mass in Miro1-R450C fibroblasts.

Mitochondrial biogenesis requires synthesis of mtDNA. Therefore an increase of mtDNA copy number points to induced biogenesis. However, in Miro1-R450C mutant fibroblasts mtDNA copy number was not increased under baseline conditions and oxidative stress induced by treatment with H_2O_2, Rotenone or a combination of H_2O_2 and Rotenone caused minor elevation of mtDNA copy number, which did not reach statistical significance compared to three age matched control lines (Figure 30). These results have not been normalized to mitochondrial mass. So it is possible that mtDNA copy number is elevated when the reduced mitochondrial mass was considered. The observation of slightly increased mtDNA copy number despite severely reduced mitochondrial mass (Figure 17) in Miro1-R450C fibroblasts argues for induced mitochondrial biogenesis as well.

Surprisingly, at the same time protein level of MnSOD, which is one protein induced by PGC1α (St-Pierre, Drori et al. 2006), was significantly reduced in Miro1-R450C, compared to Ctrl 1 fibroblasts (Figure 43). MnSOD is a homotetrameric enzyme located in the mitochondrial matrix (Borgstahl, Parge et al. 1992) (Wispe, Clark et al. 1989) at the site of superoxide production. MnSOD catalyzes the dismutation of superoxide to hydrogen peroxide and oxygen ($2O_2^{\bullet-} + 2H^+ \rightarrow H_2O_2 + O_2$) (Abreu and Cabelli 2010).

In Miro1-R272Q fibroblasts MnSOD protein level were comparable to Ctrl 1 fibroblasts and both cell lines showed clear, easily detectable protein bands on Western Blots from three independent experiments (Figure 43). Measurement of mitochondrial superoxide levels

showed that superoxide was not elevated in Miro1 mutant fibroblast lines. In contrast to Ctrl 1 and Miro1-R272Q fibroblasts, MnSOD protein was hardly detectible in Miro1-R450C in three independent experiments. This result allows the conclusion that MnSOD protein is present in cells although ROS level seems not to be pathologically increased. The significant reduction of MnSOD protein was also not explained by the reduced mitochondrial mass in Miro1-R450C fibroblasts, because MnSOD protein level was normalized to Tom20 protein level.

A similar observation was made in another study in fibroblasts of PD-patients with mutations in *parkin*. PGC1α was significantly increased in the parkin-mutant fibroblasts, but the downstream genes for mitochondrial biogenesis NRF1, NRF2, TFAM, ATPaseβ were unchanged and the target genes GPX1 and MnSOD were even significantly lower expressed (Pacelli, De Rasmo et al. 2011). Another study reported that under ischemic conditions PGC1α was upregulated as well without subsequent upregulation of mitochondrial genes (Shoag and Arany 2010). The reason for the failed induction of target genes despite upregulation of PGC1α remained elusive in both studies. An explanation was suggested by another study, which reported that transcription of MnSOD can be disturbed by mitochondrial oxidative stress. In this study DJ-1 was described to inhibit the SUMOylation of protein-associated splicing factor (PSF) and thereby preventing the interaction of PSF with PGC1α, which in turn leaves PGC1α free to induce the transcription of MnSOD. Under oxidative stress conditions DJ-1 gets oxidized and consequently is not able to inhibit the SUMOylation of PSF anymore. SUMOylated PSF then binds to PGC1α and thereby inhibits activation of MnSOD transcription (Zhong and Xu 2008).

Interestingly, another workgroup recently observed a different connection between reduction of MnSOD protein amount and increase of biogenesis: in rat kidney cells siRNA-induced knockdown of MnSOD caused increased ROS levels, subsequently leading to induction of mitochondrial biogenesis, as indicated by increased PGC1α protein levels (Marine, Krager et al. 2014). These observations raise the question of cause and effect in the Miro1-R450C fibroblasts: mitochondrial dysfunction in Miro1-R450C fibroblasts could increase ROS levels, which in turn could impair MnSOD expression despite increased PGC1α, like was observed by Zhong and colleagues. Or MnSOD protein is reduced by another, yet unknown reason, leading to increased ROS levels, which induces PGC1α and thereby mitochondrial biogenesis, like observed in the study by Marine et al. Further investigations will be needed to dissect cause and effect in Miro1-R450C cells.

To further enlighten the reason for the reduction of mitochondrial mass in Miro1-R450C fibroblasts mitochondrial morphology and co-localization of mitochondria and lysosomes were assessed in native fibroblasts (2.10.2, 2.10.3). Mitophagy requires isolation of dysfunctional mitochondria from the mitochondrial network to allow the single mitochondria to be engulfed by autophagosome, meaning that increased mitophagy is accompanied by fragmentation of the mitochondrial network. However, the same observation like in Miro1-R272Q fibroblasts was made: mitochondrial morphology was not changed (Figure 25), and co-localization of mitochondria and lysosomes was not increased in Miro1-R450C fibroblasts under standard growth conditions (Figure 27).

Knockout of *gemA* in *D. discoideum* also did not affect mitochondrial morphology, although mitochondrial respiration was increased, but apparently working insufficiently, as indicated by reduced ATP production (Vlahou, Elias et al. 2011), thereby suggesting that mitochondrial dysfunction must not be accompanied by significant changes of mitochondrial morphology.

The fact that mitochondrial dysfunction in Miro1-R450C fibroblasts did not affect mitochondrial morphology nor co-localization of mitochondria and lysosomes lead us to further investigate the autophagy marker LC3 II. Analysis revealed that autophagic flux was impaired in Miro1-R450C fibroblasts, because in contrast to Ctrl 1 fibroblasts, LC3 II did not accumulate in Miro1-R450C fibroblasts upon inhibition of the lysosomal degradation pathway, while FBS starvation was not sufficient to induce LC3 II accumulation, either. As Miro1-R450C showed a possible problem of calcium buffering, one could speculate that disruption of ER-mitochondrial contact sites might also be involved in disturbance of autophagosome formation, like was discussed for Miro1-R272Q fibroblasts.

Mitophagy is more complex than previously described and consists of at least three different types. The different types vary on whether or not mitochondrial membrane depolarization occurs, the involvement of the PINK1/Parkin pathway and on the action of LC3. But the final step for mitochondrial degradation within lysosomes is the same in all three types of mitophagy. Bafilomycin A_1 is an inhibitor of the vacuolar proton ATPase, thereby preventing the fusion of autophagosomes with lysosomes (Yamamoto, Tagawa et al. 1998). Consequently, using Bafilomycin A_1 seems to inhibit all three types of mitophagy as well as all other types of autophagy. LC3 is involved in Type 1 and Type 2 mitophagy and in other types of organellar autophagy, but apparently not in Type 3 mitophagy.

Type 1 mitophagy occurs upon nutrient starvation, leading to fission of damaged mitochondria for subsequent engulfment by LC3 II-labeled autophagosomes (Tanida, Ueno et al. 2008) and finally lysosomal degradation. In this pathway it seems that damaged

mitochondria only depolarize when they are engulfed by the acidified autophagosome, meaning that mitochondrial membrane depolarization is not required for initiation of mitophagy [reviewed in (Lemasters 2014)] and therefore Type 1 mitophagy occurs in a PINK1/Parkin-independent manner (McLelland, Soubannier et al. 2014).

In contrast, Type 2 mitophagy is induced by mitochondrial membrane depolarization and therefore involves the PINK1/Parkin pathway (Nieminen, Saylor et al. 1995) (Narendra, Tanaka et al. 2008). Interestingly, microscopy experiments revealed that mitochondrial fission was not detectable and also no formation of cup-shaped isolation membranes, which normally occur upon engulfment by autophagosomes (Lemasters 2014). Instead, single LC3 aggregates surround the mitochondria and fuse together to form a LC3-membrane around the mitochondria (Lemasters 2014). The finally enclosed mitochondria are then fused with lysosomes for degradation.

Type 3 mitophagy is the so called micromitophagy. Oxidized or otherwise damaged proteins and lipids are sequestered from the mitochondria into mitochondria-derived vesicles (MDV), without involving mitochondrial fission (Soubannier, Rippstein et al. 2012). The mitochondrial membrane is not depolarized, but it seems that the MDV's are depolarized, thus involving the PINK1/Parkin pathway (McLelland, Soubannier et al. 2014). MDV's then are incorporated into multivesicular bodies and subsequently degraded by the lysosomal pathway (Soubannier, McLelland et al. 2012).

The involvement of the PINK1/Parkin pathway should be considered when investigating mitophagy in Miro1 mutant cells. It was reported that upon depolarization of the mitochondrial membrane, PINK1 accumulates at mitochondria and recruits Parkin (Geisler, Holmstrom et al. 2010). PINK1 apparently phosphorylates Parkin to activate its E3 ligase activity (Kazlauskaite, Kelly et al. 2014). Then, Parkin ubiquitinates Miro1 for proteasomal degradation (Birsa, Norkett et al. 2014) (Sarraf, Raman et al. 2013), which was proposed to be the initial step for mitophagy by isolating damaged mitochondria from the healthy mitochondrial network (Liu, Sawada et al. 2012). Also Sarraf et al. identified Miro1/2 as targets of Parkin depending on mitochondrial membrane depolarization (Sarraf, Raman et al. 2013). However, in Miro1-R450C fibroblasts (and Miro1-R272Q fibroblasts as well) mitochondrial membrane was rather hyperpolarized and Miro1 protein levels were already decreased. Probably this phenotype interferes with initiation of mitophagy via PINK1/Parkin. Further investigations will be necessary to assess the impact of Miro1-R450C (and Miro1-R272Q) on PINK1/Parkin mediated mitochondrial quality control, e.g. by further co-localization analysis of mitochondria and lysosomes under stress conditions, or e.g. by analysing the ability of mutant Miro1 to interact with PINK1 and Parkin, because although

PINK1 is likely not phosphorylating Miro1 (Birsa, Norkett et al. 2014) it was still found to interact with the Miro/Milton complex (Weihofen, Thomas et al. 2009).

4.5.3 Mitochondrial respiration, ROS and MMP

The observed severe reduction of mitochondrial mass in Miro1-R450C fibroblasts justified the question whether this phenotype could cause a shortcoming of energy supply and therefore evoke compensatory mechanisms.

Analysis of mitochondrial functionality revealed that both Miro1 mutant fibroblast lines showed very different phenotypes in terms of mitochondrial respiration. Overall, Miro1-R450C showed a significant higher mitochondrial OCR, compared to Miro1-R272Q fibroblasts. In Miro1-R450C fibroblasts basal respiration, capacity of ATP production, proton leak and maximal respiration were slightly, but not significantly higher compared to Ctrl 1 fibroblasts. The values of the parameters spare respiratory capacity and non-mitochondrial respiration were significantly elevated compared to Ctrl 1 fibroblasts (Figure 37). In combination with the data of citrate synthase activity (Figure 31) it is possible that the respiratory chain is hyperactive in Miro1-R450C fibroblasts to ensure energy supply despite the decreased mitochondrial mass, but at the same time the respiratory chain is not working efficiently.

The key enzyme of the TCA cycle providing NADH and $FADH_2$ as proton donors for the enzymes of the respiratory chain is citrate synthase. Biochemical measurement of citrate synthase activity showed that enzyme activity was significantly reduced in Miro1-R450C fibroblasts compared to Ctrl 1 fibroblasts (Figure 31). The activity data were normalized to mitochondrial protein amount used for the measurement, such resembling citrate synthase activity on mitochondrial level. Therefore, it can be concluded that activity was not reduced due to the reduction of mitochondrial mass observed in Miro1-R450C fibroblasts. It is likely to speculate that the diminished activity of citrate synthase is even more severe on cellular level due to the decreased mitochondrial mass observed in Miro1-R450C fibroblasts.

The reason for the reduced activity of citrate synthase remained obscure in the present study. Yet, it is possible that oxidative damage can decrease enzyme activity. In a mouse model with heterozygous knockout of MnSOD, oxidative damage caused inhibition of aconitase, which is another enzyme of the TCA (Williams, Van Remmen et al. 1998). Furthermore, a recent study in neuron-like NSC-34 cells with overexpression of a loss-of-function mutant SOD1 displayed malfunction of the TCA upon oxidative stress, as assessed by chromatography coupled with mass spectrometry (Veyrat-Durebex, Corcia et al. 2015).

The direct inhibition of citrate synthase enzyme activity was shown in isolated mitochondria exposed to 2,2'-azobis(2-amidinopropane)dihydrochloride (AAPH). AAPH generates peroxyl and alkoxyl radicals and thereby oxidative stress, which led to inhibition of citrate synthase enzyme activity by changing biochemical properties of the protein (Chepelev, Bennitz et al. 2009). Taken together, the findings of these studies led us to the hypothesis that oxidative damage could reduce activity of citrate synthase in Miro1-R450C fibroblasts, as significant reduction of MnSOD was also observed. Because ROS is damaging several enzymes in an unspecific manner, also measurement of aconitase enzyme activity should be considered for future analysis to investigate whether the TCA functionality is more generally affected in Miro1-R450C fibroblasts.

Aside from the results of diminished MnSOD protein amount and decreased citrate synthase enzyme activity, also the observed increase of non-mitochondrial respiration in Miro1-R450C fibroblasts could point to increased load of ROS. Non-mitochondrial respiration can arise from free radicals, which are produced by oxidases like NAD(P)H oxidase (Stokes 2007) (Frazziano, Champion et al. 2012) or xanthine oxidase (Chambers, Parks et al. 1985). It was furthermore shown that intracellular superoxide and hydrogen peroxide increase non-mitochondrial respiration (Chacko, Zhi et al. 2015). However, we did not find an increase of mitochondrial superoxide levels using the mitochondria specific superoxide indicator MitoSOX. The fluorescent probe called MitoSOX consists of mitochondrial-targeted dihydroethidium (Robinson, Janes et al. 2008). It is believed that superoxide reacts with MitoSOX to 2-hydroxymitoethidium (2-OH-Mito-E+). But MitoSOX can also form mito-ethidium (Mito-E+) as product of nonspecific oxidation. The fluorescence spectra of 2-OH-Mito-E+ and Mito-E+ are not distinguishable, making MitoSOX an unreliable superoxide marker (Kalyanaraman, Darley-Usmar et al. 2012). HPLC-fluorescence or mass spectrometry have been recommended to directly identify 2-OH-Mito-E+ (Kalyanaraman, Darley-Usmar et al. 2012). Beyond that, the stoichiometry of the reaction between dihydroethidium and superoxide is not clear, making the quantification of superoxide by measuring fluorescence impossible (Zielonka and Kalyanaraman 2010). Even the correct localization of superoxide production is challenging as superoxide has a short half-live and can diffuse away or into a compartment. For more reliable localization of superoxide production it will be necessary to assess probe oxidation in the cytosol and in mitochondria at the same time, to determine in which compartment the probe undergoes more oxidation compared to the other compartment (Winterbourn 2014). Given the limitations of our approach to detect superoxide production, further investigations will be necessary and results (decreased MnSOD protein, decreased citrate synthase activity,

increased MMP, increased non-mitochondrial respiration) point to increased ROS levels in Miro1-R450C fibroblasts, although we were not able to substantiate this hypothesis.

Despite the decreased citrate synthase enzyme activity in Miro1-R450C fibroblasts, the protein amount of citrate synthase was significantly increased compared to Ctrl 1 fibroblasts (Figure 31). Citrate synthase protein level was also normalized to mitochondrial mass, such resembling protein amount on mitochondrial level. The data indicate that citrate synthase protein was significantly increased likely as compensatory effect in order to maintain the energy metabolism despite greatly reduced mitochondrial mass.

Given these results, we propose to assess NADH and FAD ratio in Miro1 fibroblasts [e.g. by measuring the auto fluorescence of NADH at 360 nm and the auto fluorescence of FAD with an excitation at 454 nm (Bartolome and Abramov 2015)]. The results of this measurement will allow to assess the amount of substrate, which is provided by the TCA for oxidative phosphorylation.

Complex I activity was biochemically measured in Miro1-R450C fibroblasts. When normalized to citrate synthase protein, complex I activity was unchanged in Miro1-R450C fibroblasts compared to Ctrl 1 fibroblasts (Figure 32). The normalization to citrate synthase protein allowed to assess complex I activity on mitochondrial level. This means that complex I activity could be lower on total cell level in Miro1-R450C fibroblasts due to the decreased mitochondrial mass. Indeed, in Miro1-R450C fibroblasts the protein amount of complexes I, II, III, IV and V were not significantly increased compared to Ctrl 1 fibroblasts (Figure 33), thus indicating that in Miro1-R450C fibroblasts the reduction of mitochondrial mass was not compensated by elevation of the respiratory complexes to maintain energy supply.

It was previously reported, that PGC1α increases mitochondrial respiration. This effect was reported to be beneficial in cellular models of mutant α-synuclein by preventing cell death of DA neurons (Zheng, Liao et al. 2010), whereas overexpression of PGC1α in the nigrostriatal system of rats leads to loss of DA neurons (Ciron, Lengacher et al. 2012), probably because the mitochondrial hyperactivity was accompanied by increased production of ROS (Corona and Duchen 2015). Most characteristic was the increase of spare respiratory capacity in Miro1-R450C fibroblasts compared to Ctrl 1 fibroblasts. Long-term regulation of spare respiratory capacity is mediated by PGC1α. Whereas NO produced by mtNOS in mitochondria decreases the activity of mitochondrial respiration (as we proposed for Miro1-R272Q fibroblasts), interestingly, NO production by the nuclear NO synthase was shown to increase respiratory activity and thereby spare respiratory capacity

by activation of PGC1α (Cerqueira, Cunha et al. 2012). Whether the elevation of PGC1α is beneficial or harmful for DA neurons in the Miro1-R450C model remains elusive in this study and will be addressed in future investigations.

In *Dictyostelium discoideum* with knockout of *gemA* (the orthologue of Miro; *gemA*Δ) a strikingly similar phenotype compared to Miro1-R450C fibroblasts was observed: i) *gemA* deficiency did not changed mitochondrial size or morphology, ii) overall mitochondrial mass was significantly reduced, iii) OCR was significantly increased. Although OCR was increased, the actual ATP level was much lower in *gemA*Δ, a finding, which could not be explained by the reduction of mitochondrial mass (Vlahou, Elias et al. 2011). This raises the possibility that also in Miro1-R450C cells increase of OCR might not be sufficient to sustain ATP production. Measuring OCR with the Extracellular flux analyzer only allowed to assess the capacity for ATP production, but ATP content of the cells was not measured directly. Therefore measurement of the actual ATP content of the cells, e.g. using a luminescent assay, will be necessary to complete the results for assessing mitochondrial respiration and energy production.

We hypothesize that the alteration of mitochondrial respiration observed in Miro1-R450C fibroblasts leads to hyperpolarization of the MMP. The MMP was increased by 2 fold compared to Ctrl 1 fibroblasts (Figure 38). The MMP is generated by protons that are pumped out of the mitochondrial matrix into the intermembrane space by complexes of the respiratory chain. The resulting proton gradient provides the energy to convert ADP into ATP when protons re-enter the matrix through complex V. Functionality of the respiratory chain and the MMP are therefore tightly linked and mutually dependent. In Miro1-R450C fibroblasts the respiratory function is rather hyperactive (Figure 37). This means that mitochondrial hyperpolarization could be generated by a large amount of protons, which are pumped out of the mitochondrial matrix into the intermembrane space. Consequently oxygen consumption and capacity of ATP production are increased, as was observed when measuring OCR (Figure 36, Figure 37). As previously described, the capacity of ATP production measured by OCR does not reflect the actual ATP content in the cell. In contrast, it was shown that even small changes of MMP of about 10 % reduces ATP production by 90 %, at the same time increasing ROS production by 90 % (Ma, Cao et al. 2010). This observation further supports the hypothesis that the actual ATP production could be decreased in Miro1-R450C cells.

Mitochondrial hyperpolarization is often observed in cancer cells and seems to increase cell survival by inhibition of apoptosis (Heerdt, Houston et al. 2006) (Hardonniere, Huc et al.

2015). Badgkos et al. recently proposed that the high MMP observed in cancer cells is the factor driving mitochondrial retrograde signalling that induces expression of nuclear encoded genes required for tumor development and survival (Bagkos, Koufopoulos et al. 2015). In contrast, an elevation of MMP still in the physiological range of non-cancer cells, seems to induce mitochondrial biogenesis, e.g. by activation of PGC1α, to ensure mitochondrial energy metabolism (Bagkos, Koufopoulos et al. 2015), thus providing a possible link between MMP hyperpolarization and increase of PGC1α in Miro1-R450C fibroblasts. Mitochondrial retrograde signalling activates or inhibits expression of nuclear encoded genes depending on the wavelength of the electromagnetic field generated by the MMP. Therefore the level of MMP increase determines the outcome of cell metabolism and cell fate, either by driving cancer development, inducing mitochondrial biogenesis or by inducing or preventing apoptosis [reviewed by (Bagkos, Koufopoulos et al. 2015)].

As increased MMP is often observed in cancer cells (Heerdt, Houston et al. 2006) (Holme, Gorria et al. 2007) (Huc, Gilot et al. 2003), the concern was raised that the immortalization of fibroblasts with the pLenti-III-SV40 construct (Applied Biological Materials Inc., Richmond, Canada), expressing the Large T Antigen of SV40 (2.5.1.2) could induce a cancer-like phenotype leading to mitochondrial hyperpolarization. However, this was rather unlikely as a significant difference in MMP was observed between Ctrl 1 and mutant fibroblasts, which all have been immortalized in the same way (2.5.1.2) and knockdown of *RhoT1* in M17 cells also lead to significant hyperpolarization of the mitochondrial membrane compared to M17 without knockdown of *RhoT1*.

We hypothesize that the Miro1-R450C mutation also interferes with calcium binding and thereby impairs mitochondrial calcium buffering capability. This could also disrupt mitochondrial respiration, subsequently leading to hyperpolarization of the mitochondrial membrane. This phenotype induces mitochondrial biogenesis via PGC1α. Disruption of mitochondrial respiration and elevation of the MMP could increase oxidative stress, which could explain the observed reduction of citrate synthase activity and reduced expression of MnSOD protein. However, mitochondrial superoxide levels were not elevated in our hands. Furthermore, mitochondrial mass was reduced despite increased PGC1α and impaired autophagic flux.

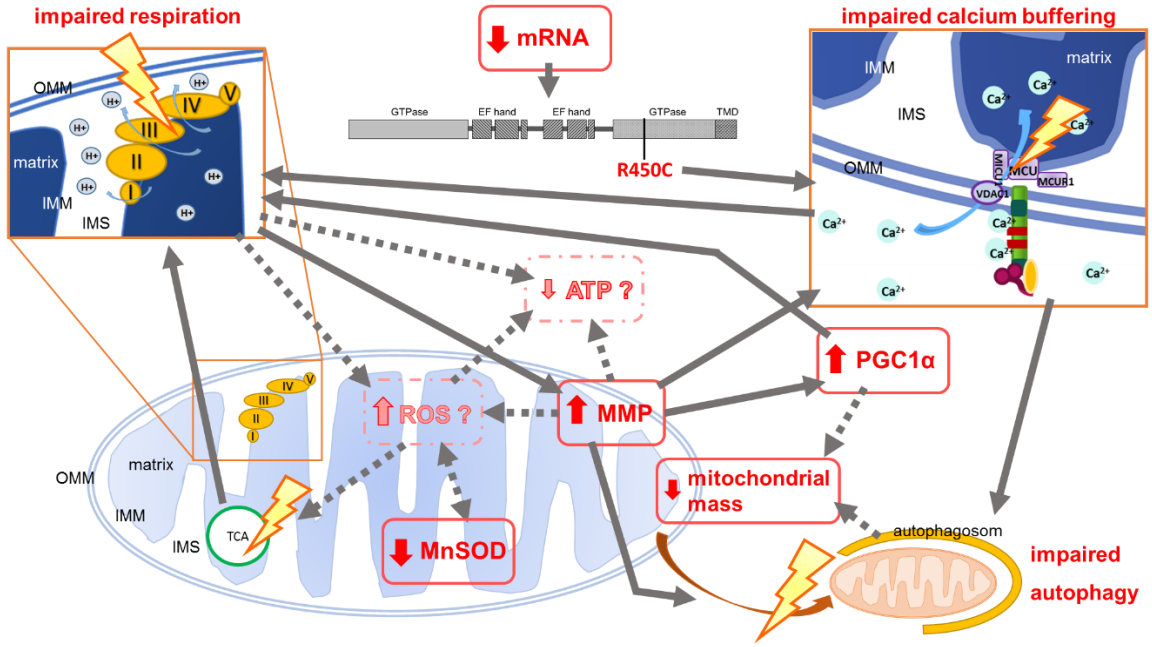

Figure 50: Overview on mitochondrial phenotype found in Miro1-R450C fibroblasts

We hypothesize that the mutation R450C in the GTPase domain interferes with calcium binding, which in turn also impairs respiratory activity. Impaired respiration leads to hyperpolarization of mitochondrial membrane. Autophagic flux is impaired by the increased MMP and the impaired calcium buffering. We further hypothesize that increased MMP, decreased MnSOD protein levels and impaired respiration could increase oxidative stress, which could lead to the observed decreased activity of citrate synthase and the decreased amount of MnSOD protein. Mitochondrial membrane hyperpolarization leads to increased PGC1α protein level, which increases mitochondrial respiration. Mitochondrial mass could be decreased due to an imbalance of autophagy and mitochondrial biogenesis.

OMM: outer mitochondrial membrane. **IMM**: inner mitochondrial membrane. **IMS**: intermembrane space. **MMP**: mitochondrial membrane potential. **TCA**: tricarboxylic acid cycle

4.6 Outlook and perspectives

4.6.1 Future investigations to further dissect the pathogenic mechanisms of Miro1 mutations in PD

The present study left some questions unanswered regarding calcium homeostasis, mitophagy, oxidative stress and mitochondrial transport.

With the applied method it was not possible to distinguish the contribution of mitochondria and the ER to the decrease of cytosolic calcium levels. More investigations are needed to estimate the calcium buffering ability of mitochondria in Miro1-R272Q and Miro1-R450C cells, e.g. by inhibiting calcium uptake by the ER by using Thapsigargin. Inhibition of calcium uptake by the ER makes calcium buffering rely more on mitochondrial calcium uptake and therefore enables to assessed mitochondrial calcium buffering separately from ER calcium uptake.

In future studies, we propose to investigate the impact of Miro1-R272Q and Miro1-R450C on ER-mitochondria contact sites, e.g. by live cell imaging of cells stained with MitoTracker and the ER specific live cell imaging dye ER-tracker (e.g. by Thermo Fisher Scientific, Braunschweig, Germany). Simultaneous staining of ATG5, which served as marker for early stages of autophagosome formation (Hamasaki, Furuta et al. 2013), enables to investigate the impact of the ER-mitochondria interaction on autophagy initiation at the same time. Furthermore, using the time-sensitive mitochondria-targeted fluorescent protein MitoTimer enables to assess the age profile of mitochondria by live cell imaging (Ferree, Trudeau et al. 2013). This approach will help to simultaneously dissect the impact of Miro1 mutations on mitochondrial biogenesis and mitochondrial turnover.

Our first attempt to assess the impact of Miro1 mutants on oxidative stress by measurement of mitochondrial superoxide production revealed no alteration in Miro1-R272Q or Miro1-R450C fibroblasts. However, due to the observed reduction of MnSOD protein levels in Miro1-R450C fibroblasts and the alteration of cytosolic calcium buffering as well as alteration of mitochondrial respiration in Miro1-R272Q and Miro1-R450C fibroblasts with subsequent mitochondrial membrane hyperpolarization, we still wonder whether oxidative stress could play a role in mitochondrial dysfunction in these cells. As mentioned before, measuring ROS levels is not trivial and therefore needs further backup by an independent method. Therefore, cytosolic superoxide levels will be measured using the superoxide indicator dihydroethidium (e.g. by Thermo Fisher Scientific, Braunschweig, Germany) and by assessing the amount of oxidized proteins in cytosolic and mitochondrial fractions using

the OxyBlot Protein Oxidation Detection Kit (e.g. by Millipore Corporation, Darmstadt, Germany). The optimal growth conditions of immortalized fibroblasts in high glucose DMEM containing 15 % FBS could prevent pathogenic superoxide formation because under these conditions energy metabolism could rely more on glycolysis than on mitochondrial respiration. Using low glucose medium (1 g/ L instead of 4.5 g/ L glucose) was also not sufficient to increase superoxide production in the present study. For future analysis it could be applicable to use DMEM without glucose (containing galactose as carbon source) for a longer period of time to force fibroblasts to switch their metabolism from glycolysis to mitochondrial respiration and therefore drive ROS formation.

Furthermore, mtDNA did not accumulate significant amounts of lesions upon oxidative stress under the applied conditions (Figure 42). The applied treatment of fibroblasts with H_2O_2 for 5 min or rotenone for 20 min could be insufficient to induce a significant amount of mtDNA damage in fibroblasts. A longer treatment could reveal whether compensatory mechanisms in Miro1 mutant cells might be overpowered faster than in control cells.

In the present study, we investigated the impact of Miro1 mutants on mitochondrial function and homeostasis. But another important aspect of Miro1 function is the regulation of mitochondrial transport, which was not analysed in fibroblasts. For future studies Miro1 mutant fibroblasts will be reprogrammed into induced pluripotent stem cells (iPSC) for further differentiation into DA neurons. These cells will be used to address the question of whether Miro1-R272Q or Miro1-R450C impair mitochondrial transport in neurons.

4.6.2 Implications for Miro1 mutant neurons

In neurons Miro plays an important role not only for mitochondrial maintenance but also for distribution of mitochondria to active synapses. There, mitochondria are important for calcium buffering and APT synthesis (Macaskill, Rinholm et al. 2009) (Chang, Niescier et al. 2011). Furthermore, Miro-dependent transport of mitochondria into dendrites and synapses allows the delivery of proteins synthesized in the soma to distant parts of the cell and maintenance of peripheral mitochondria (Amiri and Hollenbeck 2008). As a result, it is not surprising that different studies reported on impaired neuronal functions in Miro deficient models: Flies expressing mutant dMiro displayed impaired neuronal signalling due to defective vesicle release and abnormal synaptic morphology (Guo, Macleod et al. 2005), which was attributed to mitochondrial depletion in synapses caused by impaired mitochondrial transport (Guo, Macleod et al. 2005) (Babic, Russo et al. 2015). Interestingly, overexpression and knockout/ knockdown of dMiro resulted in a similar decrease of mitochondria in distal parts of axons; in neurons overexpressing dMiro this phenotype was

caused by alteration of mitochondrial movement kinetics (Russo, Louie et al. 2009). Impaired mitochondrial transport into axons and synapses was sufficient to cause loss of DA neurons in *drosophila* (Liu, Sawada et al. 2012) and loss of motor neurons in mice, even when mitochondrial respiration was not impaired (Nguyen, Oh et al. 2014). In mice (Nguyen, Oh et al. 2014) and *drosophila* (Russo, Louie et al. 2009) even heterozygous Miro depletion was sufficient to cause loss of neurons.

These findings strongly support the hypothesis that Miro1 mutations identified in PD patients cause mitochondrial dysfunction that is sufficient to induce loss of DA neurons, subsequently leading to neurodegeneration in PD. Mitochondrial transport was not assessed in Miro1 mutant fibroblasts, but given the neuronal phenotypes induced by knockdown of Miro in *drosophila* (Babic, Russo et al. 2015) (Russo, Louie et al. 2009) (Guo, Macleod et al. 2005) (Liu, Sawada et al. 2012) and mice (Nguyen, Oh et al. 2014), it can be speculated that the observed reduction of total Miro1 protein levels in Miro1-R272Q and Miro1-R450C cells (Figure 13) alone is sufficient to cause neuronal impairment. Additionally, the mutations in Miro1 most likely contribute to mitochondrial dysfunction and therefore further decrease neuronal survival: the reduction of mitochondrial mass (Figure 17) and reduction of MnSOD protein (Figure 43) observed in Miro1-R450C cells could cause insufficient ATP production and increase of oxidative stress, respectively, whereas results suggest an increased sensitivity of Miro1-R272Q fibroblasts towards elevated calcium concentration.

DA neurons are especially prone to oxidative damage and naturally possess higher levels of ROS (Slivka and Cohen 1985) (Fasano, Bergamasco et al. 2006) (Sulzer and Zecca 2000). The crucial function of MnSOD is well established. Knockout of MnSOD in *drosophila* led to early death 1 day after eclosion and heterozygous knockout flies showed a higher vulnerability to paraquat-induced oxidative stress, resulting in decreased viability (Duttaroy, Paul et al. 2003). Homozygous MnSOD knockout mice displayed severe cardiomyopathy, rapid fatigue during exercise and early death only 10 days after birth (Li, Huang et al. 1995). In contrast, heterozygous knockout mice survived longer, but accumulated oxidative damage of mitochondria over time, e.g. oxidative damage of the enzymes aconitase and NADH oxidoreductase, as well as mtDNA damage, while oxidative damage to proteins in the cytosol was not observed (Williams, Van Remmen et al. 1998) (Van Remmen, Ikeno et al. 2003). In the light of these results the decreased levels of MnSOD observed in Miro1-R450C fibroblasts could lead to increased oxidative stress and subsequent loss of DA neurons. Furthermore, it is possible that due to the observed alterations of mitochondrial respiration in Miro1 mutant cells and the high energy demand of neurons, ROS production could be elevated in Miro1 mutant neurons, leading to oxidative stress.

We further speculate that the observed alterations in mitochondrial respiration (Figure 37), impaired calcium homeostasis and MMP hyperpolarization (Figure 38) additionally impairs neuronal cell survival. It is delicate to draw conclusions from the results of MMP and apoptosis obtained from immortalized fibroblasts for neurons, because the metabolism is very different in both cell types and with it consequently also ROS production, MMP, vulnerability to stress and stress response.

Summarizing the results of impaired mitochondrial function in Miro1 mutant fibroblasts and in M17 cells with knockdown of *RhoT1* overexpressing Miro1 mutant proteins, it can be concluded from this study, that the mutations R272Q and R450C in Miro1 are sufficient to cause neurodegeneration in PD. Beyond that, the results of this study emphasize the importance of Miro1 for mitochondrial homeostasis and maintenance. To our knowledge, this is the first study describing PD-associated mutations of *RhoT1* and the resulting mitochondrial phenotypes.

5 Literature

Abou-Sleiman, P. M., M. M. Muqit, N. Q. McDonald, Y. X. Yang, S. Gandhi, D. G. Healy, K. Harvey, R. J. Harvey, E. Deas, K. Bhatia, N. Quinn, A. Lees, D. S. Latchman and N. W. Wood (2006). "A heterozygous effect for PINK1 mutations in Parkinson's disease?" Ann Neurol **60**(4): 414-419.

Abreu, I. A. and D. E. Cabelli (2010). "Superoxide dismutases-a review of the metal-associated mechanistic variations." Biochim Biophys Acta **1804**(2): 263-274.

Aktories, K., G. Schmidt and I. Just (2000). "Rho GTPases as targets of bacterial protein toxins." Biol Chem **381**(5-6): 421-426.

Alam, A., K. A. Miller, M. Chaand, J. S. Butler and M. Dziejman (2011). "Identification of Vibrio cholerae type III secretion system effector proteins." Infect Immun **79**(4): 1728-1740.

Alexeyev, M. F. (2009). "Is there more to aging than mitochondrial DNA and reactive oxygen species?" FEBS J **276**(20): 5768-5787.

Amiri, M. and P. J. Hollenbeck (2008). "Mitochondrial biogenesis in the axons of vertebrate peripheral neurons." Dev Neurobiol **68**(11): 1348-1361.

Ammerer, G., C. P. Hunter, J. H. Rothman, G. C. Saari, L. A. Valls and T. H. Stevens (1986). "PEP4 gene of Saccharomyces cerevisiae encodes proteinase A, a vacuolar enzyme required for processing of vacuolar precursors." Mol Cell Biol **6**(7): 2490-2499.

Anderson, J. P., D. E. Walker, J. M. Goldstein, R. de Laat, K. Banducci, R. J. Caccavello, R. Barbour, J. Huang, K. Kling, M. Lee, L. Diep, P. S. Keim, X. Shen, T. Chataway, M. G. Schlossmacher, P. Seubert, D. Schenk, S. Sinha, W. P. Gai and T. J. Chilcote (2006). "Phosphorylation of Ser-129 is the dominant pathological modification of alpha-synuclein in familial and sporadic Lewy body disease." J Biol Chem **281**(40): 29739-29752.

Andres-Mateos, E., C. Perier, L. Zhang, B. Blanchard-Fillion, T. M. Greco, B. Thomas, H. S. Ko, M. Sasaki, H. Ischiropoulos, S. Przedborski, T. M. Dawson and V. L. Dawson (2007). "DJ-1 gene deletion reveals that DJ-1 is an atypical peroxiredoxin-like peroxidase." Proc Natl Acad Sci U S A **104**(37): 14807-14812.

Andreyev, A. Y., B. Fahy and G. Fiskum (1998). "Cytochrome c release from brain mitochondria is independent of the mitochondrial permeability transition." FEBS Lett **439**(3): 373-376.

Anvret, A., C. Ran, M. Westerlund, O. Sydow, T. Willows, L. Olson, D. Galter and A. C. Belin (2012). "Genetic Screening of the Mitochondrial Rho GTPases MIRO1 and MIRO2 in Parkinson's Disease." Open Neurol J **6**: 1-5.

Aoyama, K., K. Matsubara, Y. Fujikawa, Y. Nagahiro, K. Shimizu, N. Umegae, N. Hayase, H. Shiono and S. Kobayashi (2000). "Nitration of manganese superoxide dismutase in cerebrospinal fluids is a marker for peroxynitrite-mediated oxidative stress in neurodegenerative diseases." Ann Neurol **47**(4): 524-527.

Arnoult, D., L. Carneiro, I. Tattoli and S. E. Girardin (2009). "The role of mitochondria in cellular defense against microbial infection." Semin Immunol **21**(4): 223-232.

Arvier, M., L. Lagoutte, G. Johnson, J. F. Dumas, B. Sion, G. Grizard, Y. Malthiery, G. Simard and P. Ritz (2007). "Adenine nucleotide translocator promotes oxidative phosphorylation and mild uncoupling in mitochondria after dexamethasone treatment." Am J Physiol Endocrinol Metab **293**(5): E1320-1324.

Ashkenazy, H., E. Erez, E. Martz, T. Pupko and N. Ben-Tal (2010). "ConSurf 2010: calculating evolutionary conservation in sequence and structure of proteins and nucleic acids." Nucleic Acids Res **38**(Web Server issue): W529-533.

Ashrafi, G., J. S. Schlehe, M. J. LaVoie and T. L. Schwarz (2014). "Mitophagy of damaged mitochondria occurs locally in distal neuronal axons and requires PINK1 and Parkin." J Cell Biol **206**(5): 655-670.

Aspenstrom, P., A. Fransson and J. Saras (2004). "Rho GTPases have diverse effects on the organization of the actin filament system." Biochem J **377**(Pt 2): 327-337.

Atkin, T. A., A. F. MacAskill, N. J. Brandon and J. T. Kittler (2011). "Disrupted in Schizophrenia-1 regulates intracellular trafficking of mitochondria in neurons." Mol Psychiatry **16**(2): 122-124, 121.

Attwell, D. and S. B. Laughlin (2001). "An energy budget for signaling in the grey matter of the brain." J Cereb Blood Flow Metab **21**(10): 1133-1145.

Axe, E. L., S. A. Walker, M. Manifava, P. Chandra, H. L. Roderick, A. Habermann, G. Griffiths and N. T. Ktistakis (2008). "Autophagosome formation from membrane compartments enriched in phosphatidylinositol 3-phosphate and dynamically connected to the endoplasmic reticulum." J Cell Biol **182**(4): 685-701.

Babic, M., G. J. Russo, A. J. Wellington, R. M. Sangston, M. Gonzalez and K. E. Zinsmaier (2015). "Miro's N-terminal GTPase domain is required for transport of mitochondria into axons and dendrites." J Neurosci **35**(14): 5754-5771.

Bagkos, G., K. Koufopoulos and C. Piperi (2014). "A new model for mitochondrial membrane potential production and storage." Med Hypotheses **83**(2): 175-181.

Bagkos, G., K. Koufopoulos and C. Piperi (2015). "Mitochondrial emitted electromagnetic signals mediate retrograde signaling." Med Hypotheses **85**(6): 810-818.

Baloh, R. H. (2008). "Mitochondrial dynamics and peripheral neuropathy." Neuroscientist **14**(1): 12-18.

Baloh, R. H., R. E. Schmidt, A. Pestronk and J. Milbrandt (2007). "Altered axonal mitochondrial transport in the pathogenesis of Charcot-Marie-Tooth disease from mitofusin 2 mutations." J Neurosci **27**(2): 422-430.

Bartolome, F. and A. Y. Abramov (2015). "Measurement of mitochondrial NADH and FAD autofluorescence in live cells." Methods Mol Biol **1264**: 263-270.

Baughman, J. M., F. Perocchi, H. S. Girgis, M. Plovanich, C. A. Belcher-Timme, Y. Sancak, X. R. Bao, L. Strittmatter, O. Goldberger, R. L. Bogorad, V. Koteliansky and V. K. Mootha (2011). "Integrative genomics identifies MCU as an essential component of the mitochondrial calcium uniporter." Nature **476**(7360): 341-345.

Beck, M., K. Brickley, H. L. Wilkinson, S. Sharma, M. Smith, P. L. Chazot, S. Pollard and F. A. Stephenson (2002). "Identification, molecular cloning, and characterization of a novel GABAA receptor-associated protein, GRIF-1." J Biol Chem **277**(33): 30079-30090.

Ben-Shachar, D. and D. Laifenfeld (2004). "Mitochondria, synaptic plasticity, and schizophrenia." Int Rev Neurobiol **59**: 273-296.

Bender, A., K. J. Krishnan, C. M. Morris, G. A. Taylor, A. K. Reeve, R. H. Perry, E. Jaros, J. S. Hersheson, J. Betts, T. Klopstock, R. W. Taylor and D. M. Turnbull (2006). "High levels of mitochondrial DNA deletions in substantia nigra neurons in aging and Parkinson disease." Nat Genet **38**(5): 515-517.

Berger, A. K., G. P. Cortese, K. D. Amodeo, A. Weihofen, A. Letai and M. J. LaVoie (2009). "Parkin selectively alters the intrinsic threshold for mitochondrial cytochrome c release." Hum Mol Genet **18**(22): 4317-4328.

Bernheimer, H., W. Birkmayer, O. Hornykiewicz, K. Jellinger and F. Seitelberger (1973). "Brain dopamine and the syndromes of Parkinson and Huntington. Clinical, morphological and neurochemical correlations." J Neurol Sci **20**(4): 415-455.

Betarbet, R., T. B. Sherer, G. MacKenzie, M. Garcia-Osuna, A. V. Panov and J. T. Greenamyre (2000). "Chronic systemic pesticide exposure reproduces features of Parkinson's disease." Nat Neurosci **3**(12): 1301-1306.

Bhat, A. H., K. B. Dar, S. Anees, M. A. Zargar, A. Masood, M. A. Sofi and S. A. Ganie (2015). "Oxidative stress, mitochondrial dysfunction and neurodegenerative diseases; a mechanistic insight." Biomed Pharmacother **74**: 101-110.

Birsa, N., R. Norkett, T. Wauer, T. E. Mevissen, H. C. Wu, T. Foltynie, K. Bhatia, W. D. Hirst, D. Komander, H. Plun-Favreau and J. T. Kittler (2014). "Lysine 27 ubiquitination of the mitochondrial transport protein Miro is dependent on serine 65 of the Parkin ubiquitin ligase." J Biol Chem **289**(21): 14569-14582.

Bogaerts, V., K. Nuytemans, J. Reumers, P. Pals, S. Engelborghs, B. Pickut, E. Corsmit, K. Peeters, J. Schymkowitz, P. P. De Deyn, P. Cras, F. Rousseau, J. Theuns and C. Van Broeckhoven (2008). "Genetic variability in the mitochondrial serine protease HTRA2 contributes to risk for Parkinson disease." Hum Mutat **29**(6): 832-840.

Bonifati, V., P. Rizzu, M. J. van Baren, O. Schaap, G. J. Breedveld, E. Krieger, M. C. Dekker, F. Squitieri, P. Ibanez, M. Joosse, J. W. van Dongen, N. Vanacore, J. C. van Swieten, A. Brice, G. Meco, C. M. van Duijn, B. A. Oostra and P. Heutink (2003). "Mutations in the DJ-1 gene associated with autosomal recessive early-onset parkinsonism." Science **299**(5604): 256-259.

Borgstahl, G. E., H. E. Parge, M. J. Hickey, W. F. Beyer, Jr., R. A. Hallewell and J. A. Tainer (1992). "The structure of human mitochondrial manganese superoxide dismutase reveals a novel tetrameric interface of two 4-helix bundles." Cell **71**(1): 107-118.

Bosco, D. A., D. M. Fowler, Q. Zhang, J. Nieva, E. T. Powers, P. Wentworth, Jr., R. A. Lerner and J. W. Kelly (2006). "Elevated levels of oxidized cholesterol metabolites in Lewy body disease brains accelerate alpha-synuclein fibrilization." Nat Chem Biol **2**(5): 249-253.

Bowling, A. C. and M. F. Beal (1995). "Bioenergetic and oxidative stress in neurodegenerative diseases." Life Sci **56**(14): 1151-1171.

Braak, H., E. Ghebremedhin, U. Rub, H. Bratzke and K. Del Tredici (2004). "Stages in the development of Parkinson's disease-related pathology." Cell Tissue Res **318**(1): 121-134.

Breen, K. C. and G. Drutyte (2013). "Non-motor symptoms of Parkinson's disease: the patient's perspective." J Neural Transm **120**(4): 531-535.

Briones, T. L., E. Suh, L. Jozsa, M. Rogozinska, J. Woods and M. Wadowska (2005). "Changes in number of synapses and mitochondria in presynaptic terminals in the dentate gyrus following cerebral ischemia and rehabilitation training." Brain Res **1033**(1): 51-57.

Bussey, H., D. B. Kaback, W. Zhong, D. T. Vo, M. W. Clark, N. Fortin, J. Hall, B. F. Ouellette, T. Keng, A. B. Barton and et al. (1995). "The nucleotide sequence of chromosome I from Saccharomyces cerevisiae." Proc Natl Acad Sci U S A **92**(9): 3809-3813.

Butterfield, D. A., A. Castegna, C. M. Lauderback and J. Drake (2002). "Evidence that amyloid beta-peptide-induced lipid peroxidation and its sequelae in Alzheimer's disease brain contribute to neuronal death." Neurobiol Aging **23**(5): 655-664.

Cai, Q., H. M. Zakaria, A. Simone and Z. H. Sheng (2012). "Spatial parkin translocation and degradation of damaged mitochondria via mitophagy in live cortical neurons." Curr Biol **22**(6): 545-552.

Canet-Aviles, R. M., M. A. Wilson, D. W. Miller, R. Ahmad, C. McLendon, S. Bandyopadhyay, M. J. Baptista, D. Ringe, G. A. Petsko and M. R. Cookson (2004). "The Parkinson's disease protein DJ-1 is neuroprotective due to cysteine-sulfinic acid-driven mitochondrial localization." Proc Natl Acad Sci U S A **101**(24): 9103-9108.

Capriotti, E., P. Fariselli and R. Casadio (2005). "I-Mutant2.0: predicting stability changes upon mutation from the protein sequence or structure." Nucleic Acids Res **33**(Web Server issue): W306-310.

Cardno, A. G. and Gottesman, II (2000). "Twin studies of schizophrenia: from bow-and-arrow concordances to star wars Mx and functional genomics." Am J Med Genet **97**(1): 12-17.

Carmichael, S. T. (2003). "Plasticity of cortical projections after stroke." Neuroscientist **9**(1): 64-75.

Castilho, R. F., O. Hansson, M. W. Ward, S. L. Budd and D. G. Nicholls (1998). "Mitochondrial control of acute glutamate excitotoxicity in cultured cerebellar granule cells." J Neurosci **18**(24): 10277-10286.

Caughey, B. and P. T. Lansbury (2003). "Protofibrils, pores, fibrils, and neurodegeneration: separating the responsible protein aggregates from the innocent bystanders." Annu Rev Neurosci **26**: 267-298.

Cerqueira, F. M., F. M. Cunha, F. R. Laurindo and A. J. Kowaltowski (2012). "Calorie restriction increases cerebral mitochondrial respiratory capacity in a NO*-mediated mechanism: impact on neuronal survival." Free Radic Biol Med **52**(7): 1236-1241.

Chacko, B. K., D. Zhi, V. M. Darley-Usmar and T. Mitchell (2015). "The Bioenergetic Health Index is a sensitive measure of oxidative stress in human monocytes." Redox Biol **8**: 43-50.

Chambers, D. E., D. A. Parks, G. Patterson, R. Roy, J. M. McCord, S. Yoshida, L. F. Parmley and J. M. Downey (1985). "Xanthine oxidase as a source of free radical damage in myocardial ischemia." J Mol Cell Cardiol **17**(2): 145-152.

Chan, C. S., T. S. Gertler and D. J. Surmeier (2009). "Calcium homeostasis, selective vulnerability and Parkinson's disease." Trends Neurosci **32**(5): 249-256.

Chan, S. L., L. L. Chua, D. C. Angeles and E. K. Tan (2014). "MAP1B rescues LRRK2 mutant-mediated cytotoxicity." Mol Brain **7**: 29.

Chang, D. T., A. S. Honick and I. J. Reynolds (2006). "Mitochondrial trafficking to synapses in cultured primary cortical neurons." J Neurosci **26**(26): 7035-7045.

Chang, K. T., R. F. Niescier and K. T. Min (2011). "Mitochondrial matrix Ca2+ as an intrinsic signal regulating mitochondrial motility in axons." Proc Natl Acad Sci U S A **108**(37): 15456-15461.

Chen, H., S. A. Detmer, A. J. Ewald, E. E. Griffin, S. E. Fraser and D. C. Chan (2003). "Mitofusins Mfn1 and Mfn2 coordinately regulate mitochondrial fusion and are essential for embryonic development." J Cell Biol **160**(2): 189-200.

Chen, H., J. M. McCaffery and D. C. Chan (2007). "Mitochondrial fusion protects against neurodegeneration in the cerebellum." Cell **130**(3): 548-562.

Chepelev, N. L., J. D. Bennitz, J. S. Wright, J. C. Smith and W. G. Willmore (2009). "Oxidative modification of citrate synthase by peroxyl radicals and protection with novel antioxidants." J Enzyme Inhib Med Chem **24**(6): 1319-1331.

Cherra, S. J., 3rd, E. Steer, A. M. Gusdon, K. Kiselyov and C. T. Chu (2013). "Mutant LRRK2 elicits calcium imbalance and depletion of dendritic mitochondria in neurons." Am J Pathol **182**(2): 474-484.

Chun, S. and J. C. Fay (2009). "Identification of deleterious mutations within three human genomes." Genome Res **19**(9): 1553-1561.

Cipolat, S., O. Martins de Brito, B. Dal Zilio and L. Scorrano (2004). "OPA1 requires mitofusin 1 to promote mitochondrial fusion." Proc Natl Acad Sci U S A **101**(45): 15927-15932.

Ciron, C., S. Lengacher, J. Dusonchet, P. Aebischer and B. L. Schneider (2012). "Sustained expression of PGC-1alpha in the rat nigrostriatal system selectively impairs dopaminergic function." Hum Mol Genet **21**(8): 1861-1876.

Clark, I. E., M. W. Dodson, C. Jiang, J. H. Cao, J. R. Huh, J. H. Seol, S. J. Yoo, B. A. Hay and M. Guo (2006). "Drosophila pink1 is required for mitochondrial function and interacts genetically with parkin." Nature **441**(7097): 1162-1166.

Clayton, D. F. and J. M. George (1998). "The synucleins: a family of proteins involved in synaptic function, plasticity, neurodegeneration and disease." Trends Neurosci **21**(6): 249-254.

Cloonan, S. M. and A. M. Choi (2013). "Mitochondria: sensors and mediators of innate immune receptor signaling." Curr Opin Microbiol **16**(3): 327-338.

Conway, K. A., J. C. Rochet, R. M. Bieganski and P. T. Lansbury, Jr. (2001). "Kinetic stabilization of the alpha-synuclein protofibril by a dopamine-alpha-synuclein adduct." Science **294**(5545): 1346-1349.

Corona, J. C. and M. R. Duchen (2015). "PPARgamma and PGC-1alpha as therapeutic targets in Parkinson's." Neurochem Res **40**(2): 308-316.

d'Ischia, M. and G. Prota (1997). "Biosynthesis, structure, and function of neuromelanin and its relation to Parkinson's disease: a critical update." Pigment Cell Res **10**(6): 370-376.

Dagda, R. K. and C. T. Chu (2009). "Mitochondrial quality control: insights on how Parkinson's disease related genes PINK1, parkin, and Omi/HtrA2 interact to maintain mitochondrial homeostasis." J Bioenerg Biomembr **41**(6): 473-479.

Dalmonte, M. E., E. Forte, M. L. Genova, A. Giuffre, P. Sarti and G. Lenaz (2009). "Control of respiration by cytochrome c oxidase in intact cells: role of the membrane potential." J Biol Chem **284**(47): 32331-32335.

de Brito, O. M. and L. Scorrano (2008). "Mitofusin 2 tethers endoplasmic reticulum to mitochondria." Nature **456**(7222): 605-610.

de Rijk, M. C., L. J. Launer, K. Berger, M. M. Breteler, J. F. Dartigues, M. Baldereschi, L. Fratiglioni, A. Lobo, J. Martinez-Lage, C. Trenkwalder and A. Hofman (2000). "Prevalence of Parkinson's disease in Europe: A collaborative study of population-based cohorts. Neurologic Diseases in the Elderly Research Group." Neurology **54**(11 Suppl 5): S21-23.

De Stefani, D., A. Raffaello, E. Teardo, I. Szabo and R. Rizzuto (2011). "A forty-kilodalton protein of the inner membrane is the mitochondrial calcium uniporter." Nature **476**(7360): 336-340.

De Vos, K. J., A. J. Grierson, S. Ackerley and C. C. Miller (2008). "Role of axonal transport in neurodegenerative diseases." Annu Rev Neurosci **31**: 151-173.

Desler, C., T. L. Hansen, J. B. Frederiksen, M. L. Marcker, K. K. Singh and L. Juel Rasmussen (2012). "Is There a Link between Mitochondrial Reserve Respiratory Capacity and Aging?" J Aging Res **2012**: 192503.

Detmer, S. A., C. Vande Velde, D. W. Cleveland and D. C. Chan (2008). "Hindlimb gait defects due to motor axon loss and reduced distal muscles in a transgenic mouse model of Charcot-Marie-Tooth type 2A." Hum Mol Genet **17**(3): 367-375.

Dexter, D. T., C. J. Carter, F. R. Wells, F. Javoy-Agid, Y. Agid, A. Lees, P. Jenner and C. D. Marsden (1989). "Basal lipid peroxidation in substantia nigra is increased in Parkinson's disease." J Neurochem **52**(2): 381-389.

Di Lisa, F. and P. Bernardi (1998). "Mitochondrial function as a determinant of recovery or death in cell response to injury." Mol Cell Biochem **184**(1-2): 379-391.

Diers, A. R., K. A. Broniowska, V. M. Darley-Usmar and N. Hogg (2011). "Differential regulation of metabolism by nitric oxide and S-nitrosothiols in endothelial cells." Am J Physiol Heart Circ Physiol **301**(3): H803-812.

DiMauro, S. (2004). "Mitochondrial diseases." Biochim Biophys Acta **1658**(1-2): 80-88.

Dong, C., P. Wei, X. Jian, R. Gibbs, E. Boerwinkle, K. Wang and X. Liu (2015). "Comparison and integration of deleteriousness prediction methods for nonsynonymous SNVs in whole exome sequencing studies." Hum Mol Genet **24**(8): 2125-2137.

Duan, X., J. H. Chang, S. Ge, R. L. Faulkner, J. Y. Kim, Y. Kitabatake, X. B. Liu, C. H. Yang, J. D. Jordan, D. K. Ma, C. Y. Liu, S. Ganesan, H. J. Cheng, G. L. Ming, B. Lu and H. Song (2007). "Disrupted-In-Schizophrenia 1 regulates integration of newly generated neurons in the adult brain." Cell **130**(6): 1146-1158.

Duttaroy, A., A. Paul, M. Kundu and A. Belton (2003). "A Sod2 null mutation confers severely reduced adult life span in Drosophila." Genetics **165**(4): 2295-2299.

Eura, Y., N. Ishihara, S. Yokota and K. Mihara (2003). "Two mitofusin proteins, mammalian homologues of FZO, with distinct functions are both required for mitochondrial fusion." J Biochem **134**(3): 333-344.

Fasano, M., B. Bergamasco and L. Lopiano (2006). "Modifications of the iron-neuromelanin system in Parkinson's disease." J Neurochem **96**(4): 909-916.

Ferree, A. W., K. Trudeau, E. Zik, I. Y. Benador, G. Twig, R. A. Gottlieb and O. S. Shirihai (2013). "MitoTimer probe reveals the impact of autophagy, fusion, and motility on subcellular distribution of young and old mitochondrial protein and on relative mitochondrial protein age." Autophagy **9**(11): 1887-1896.

Finn, R. D., J. Mistry, J. Tate, P. Coggill, A. Heger, J. E. Pollington, O. L. Gavin, P. Gunasekaran, G. Ceric, K. Forslund, L. Holm, E. L. Sonnhammer, S. R. Eddy and A. Bateman (2010). "The Pfam protein families database." Nucleic Acids Res **38**(Database issue): D211-222.

Fiskum, G., A. Starkov, B. M. Polster and C. Chinopoulos (2003). "Mitochondrial mechanisms of neural cell death and neuroprotective interventions in Parkinson's disease." Ann N Y Acad Sci **991**: 111-119.

Foppoli, C., R. Coccia, C. Cini and M. A. Rosei (1997). "Catecholamines oxidation by xanthine oxidase." Biochim Biophys Acta **1334**(2-3): 200-206.

Fransson, A., A. Ruusala and P. Aspenstrom (2003). "Atypical Rho GTPases have roles in mitochondrial homeostasis and apoptosis." J Biol Chem **278**(8): 6495-6502.

Fransson, S., A. Ruusala and P. Aspenstrom (2006). "The atypical Rho GTPases Miro-1 and Miro-2 have essential roles in mitochondrial trafficking." Biochem Biophys Res Commun **344**(2): 500-510.

Frazziano, G., H. C. Champion and P. J. Pagano (2012). "NADPH oxidase-derived ROS and the regulation of pulmonary vessel tone." Am J Physiol Heart Circ Physiol **302**(11): H2166-2177.

Frederick, R. L., J. M. McCaffery, K. W. Cunningham, K. Okamoto and J. M. Shaw (2004). "Yeast Miro GTPase, Gem1p, regulates mitochondrial morphology via a novel pathway." J Cell Biol **167**(1): 87-98.

Frederick, R. L., K. Okamoto and J. M. Shaw (2008). "Multiple pathways influence mitochondrial inheritance in budding yeast." Genetics **178**(2): 825-837.

Fujiwara, H., M. Hasegawa, N. Dohmae, A. Kawashima, E. Masliah, M. S. Goldberg, J. Shen, K. Takio and T. Iwatsubo (2002). "alpha-Synuclein is phosphorylated in synucleinopathy lesions." Nat Cell Biol **4**(2): 160-164.

Fukuda, R., H. Zhang, J. W. Kim, L. Shimoda, C. V. Dang and G. L. Semenza (2007). "HIF-1 regulates cytochrome oxidase subunits to optimize efficiency of respiration in hypoxic cells." Cell **129**(1): 111-122.

Gandhi, S., A. Wood-Kaczmar, Z. Yao, H. Plun-Favreau, E. Deas, K. Klupsch, J. Downward, D. S. Latchman, S. J. Tabrizi, N. W. Wood, M. R. Duchen and A. Y. Abramov (2009). "PINK1-associated Parkinson's disease is caused by neuronal vulnerability to calcium-induced cell death." Mol Cell **33**(5): 627-638.

Geisler, S., K. M. Holmstrom, D. Skujat, F. C. Fiesel, O. C. Rothfuss, P. J. Kahle and W. Springer (2010). "PINK1/Parkin-mediated mitophagy is dependent on VDAC1 and p62/SQSTM1." Nat Cell Biol **12**(2): 119-131.

Ghezzi, D. and M. Zeviani (2012). "Assembly factors of human mitochondrial respiratory chain complexes: physiology and pathophysiology." Adv Exp Med Biol **748**: 65-106.

Gifford, J. L., M. P. Walsh and H. J. Vogel (2007). "Structures and metal-ion-binding properties of the Ca2+-binding helix-loop-helix EF-hand motifs." Biochem J **405**(2): 199-221.

Gilks, W. P., P. M. Abou-Sleiman, S. Gandhi, S. Jain, A. Singleton, A. J. Lees, K. Shaw, K. P. Bhatia, V. Bonifati, N. P. Quinn, J. Lynch, D. G. Healy, J. L. Holton, T. Revesz and N. W. Wood (2005). "A common LRRK2 mutation in idiopathic Parkinson's disease." Lancet **365**(9457): 415-416.

Gimelbrant, A., J. N. Hutchinson, B. R. Thompson and A. Chess (2007). "Widespread monoallelic expression on human autosomes." Science **318**(5853): 1136-1140.

Giollo, M., A. J. Martin, I. Walsh, C. Ferrari and S. C. Tosatto (2014). "NeEMO: a method using residue interaction networks to improve prediction of protein stability upon mutation." BMC Genomics **15 Suppl 4**: S7.

Gloeckner, C. J., A. Schumacher, K. Boldt and M. Ueffing (2009). "The Parkinson disease-associated protein kinase LRRK2 exhibits MAPKKK activity and phosphorylates MKK3/6 and MKK4/7, in vitro." J Neurochem **109**(4): 959-968.

Goldberg, M. S., A. Pisani, M. Haburcak, T. A. Vortherms, T. Kitada, C. Costa, Y. Tong, G. Martella, A. Tscherter, A. Martins, G. Bernardi, B. L. Roth, E. N. Pothos, P. Calabresi and

J. Shen (2005). "Nigrostriatal dopaminergic deficits and hypokinesia caused by inactivation of the familial Parkinsonism-linked gene DJ-1." Neuron **45**(4): 489-496.

Good, P. F., A. Hsu, P. Werner, D. P. Perl and C. W. Olanow (1998). "Protein nitration in Parkinson's disease." J Neuropathol Exp Neurol **57**(4): 338-342.

Greene, A. W., K. Grenier, M. A. Aguileta, S. Muise, R. Farazifard, M. E. Haque, H. M. McBride, D. S. Park and E. A. Fon (2012). "Mitochondrial processing peptidase regulates PINK1 processing, import and Parkin recruitment." EMBO Rep **13**(4): 378-385.

Greten-Harrison, B., M. Polydoro, M. Morimoto-Tomita, L. Diao, A. M. Williams, E. H. Nie, S. Makani, N. Tian, P. E. Castillo, V. L. Buchman and S. S. Chandra (2010). "alphabetagamma-Synuclein triple knockout mice reveal age-dependent neuronal dysfunction." Proc Natl Acad Sci U S A **107**(45): 19573-19578.

Grunewald, A., M. E. Gegg, J. W. Taanman, R. H. King, N. Kock, C. Klein and A. H. Schapira (2009). "Differential effects of PINK1 nonsense and missense mutations on mitochondrial function and morphology." Exp Neurol **219**(1): 266-273.

Guo, X., G. T. Macleod, A. Wellington, F. Hu, S. Panchumarthi, M. Schoenfield, L. Marin, M. P. Charlton, H. L. Atwood and K. E. Zinsmaier (2005). "The GTPase dMiro is required for axonal transport of mitochondria to Drosophila synapses." Neuron **47**(3): 379-393.

Hamasaki, M., N. Furuta, A. Matsuda, A. Nezu, A. Yamamoto, N. Fujita, H. Oomori, T. Noda, T. Haraguchi, Y. Hiraoka, A. Amano and T. Yoshimori (2013). "Autophagosomes form at ER-mitochondria contact sites." Nature **495**(7441): 389-393.

Hanekamp, T., M. K. Thorsness, I. Rebbapragada, E. M. Fisher, C. Seebart, M. R. Darland, J. A. Coxbill, D. L. Updike and P. E. Thorsness (2002). "Maintenance of mitochondrial morphology is linked to maintenance of the mitochondrial genome in Saccharomyces cerevisiae." Genetics **162**(3): 1147-1156.

Hardonniere, K., L. Huc, N. Podechard, M. Fernier, X. Tekpli, I. Gallais, O. Sergent and D. Lagadic-Gossmann (2015). "Benzo[a]pyrene-induced nitric oxide production acts as a survival signal targeting mitochondrial membrane potential." Toxicol In Vitro **29**(7): 1597-1608.

Hastings, T. G. (1995). "Enzymatic oxidation of dopamine: the role of prostaglandin H synthase." J Neurochem **64**(2): 919-924.

Hayashi, T., C. Ishimori, K. Takahashi-Niki, T. Taira, Y. C. Kim, H. Maita, C. Maita, H. Ariga and S. M. Iguchi-Ariga (2009). "DJ-1 binds to mitochondrial complex I and maintains its activity." Biochem Biophys Res Commun **390**(3): 667-672.

Hedrich, K., M. Kann, A. J. Lanthaler, A. Dalski, C. Eskelson, O. Landt, E. Schwinger, P. Vieregge, A. E. Lang, X. O. Breakefield, L. J. Ozelius, P. P. Pramstaller and C. Klein (2001). "The importance of gene dosage studies: mutational analysis of the parkin gene in early-onset parkinsonism." Hum Mol Genet **10**(16): 1649-1656.

Heerdt, B. G., M. A. Houston and L. H. Augenlicht (2006). "Growth properties of colonic tumor cells are a function of the intrinsic mitochondrial membrane potential." Cancer Res **66**(3): 1591-1596.

Hegde, R., S. M. Srinivasula, Z. Zhang, R. Wassell, R. Mukattash, L. Cilenti, G. DuBois, Y. Lazebnik, A. S. Zervos, T. Fernandes-Alnemri and E. S. Alnemri (2002). "Identification of Omi/HtrA2 as a mitochondrial apoptotic serine protease that disrupts inhibitor of apoptosis protein-caspase interaction." J Biol Chem **277**(1): 432-438.

Hensley, K., M. L. Maidt, Z. Yu, H. Sang, W. R. Markesbery and R. A. Floyd (1998). "Electrochemical analysis of protein nitrotyrosine and dityrosine in the Alzheimer brain indicates region-specific accumulation." J Neurosci **18**(20): 8126-8132.

Hobbs, A. E., M. Srinivasan, J. M. McCaffery and R. E. Jensen (2001). "Mmm1p, a mitochondrial outer membrane protein, is connected to mitochondrial DNA (mtDNA) nucleoids and required for mtDNA stability." J Cell Biol **152**(2): 401-410.

Hoeflich, K. P. and M. Ikura (2002). "Calmodulin in action: diversity in target recognition and activation mechanisms." Cell **108**(6): 739-742.

Hoglinger, G. U., G. Carrard, P. P. Michel, F. Medja, A. Lombes, M. Ruberg, B. Friguet and E. C. Hirsch (2003). "Dysfunction of mitochondrial complex I and the proteasome: interactions between two biochemical deficits in a cellular model of Parkinson's disease." J Neurochem **86**(5): 1297-1307.

Hollenbeck, P. J. (2005). "Mitochondria and neurotransmission: evacuating the synapse." Neuron **47**(3): 331-333.

Hollenbeck, P. J. and W. M. Saxton (2005). "The axonal transport of mitochondria." J Cell Sci **118**(Pt 23): 5411-5419.

Holme, J. A., M. Gorria, V. M. Arlt, S. Ovrebo, A. Solhaug, X. Tekpli, N. E. Landvik, L. Huc, O. Fardel and D. Lagadic-Gossmann (2007). "Different mechanisms involved in apoptosis following exposure to benzo[a]pyrene in F258 and Hepa1c1c7 cells." Chem Biol Interact **167**(1): 41-55.

Honbou, K., N. N. Suzuki, M. Horiuchi, T. Niki, T. Taira, H. Ariga and F. Inagaki (2003). "The crystal structure of DJ-1, a protein related to male fertility and Parkinson's disease." J Biol Chem **278**(33): 31380-31384.

Hsu, C. H., D. Chan, E. Greggio, S. Saha, M. D. Guillily, A. Ferree, K. Raghavan, G. C. Shen, L. Segal, H. Ryu, M. R. Cookson and B. Wolozin (2010). "MKK6 binds and regulates expression of Parkinson's disease-related protein LRRK2." J Neurochem **112**(6): 1593-1604.

Huc, L., D. Gilot, C. Gardyn, M. Rissel, M. T. Dimanche-Boitrel, A. Guillouzo, O. Fardel and D. Lagadic-Gossmann (2003). "Apoptotic mitochondrial dysfunction induced by benzo(a)pyrene in liver epithelial cells: role of p53 and pHi changes." Ann N Y Acad Sci **1010**: 167-170.

Iijima, T. (2006). "Mitochondrial membrane potential and ischemic neuronal death." Neurosci Res **55**(3): 234-243.

Iyer, S. P., Y. Akimoto and G. W. Hart (2003). "Identification and cloning of a novel family of coiled-coil domain proteins that interact with O-GlcNAc transferase." J Biol Chem **278**(7): 5399-5409.

Jankovic, J. (2008). "Parkinson's disease: clinical features and diagnosis." J Neurol Neurosurg Psychiatry **79**(4): 368-376.

Janssen, A. J., F. J. Trijbels, R. C. Sengers, J. A. Smeitink, L. P. van den Heuvel, L. T. Wintjes, B. J. Stoltenborg-Hogenkamp and R. J. Rodenburg (2007). "Spectrophotometric assay for complex I of the respiratory chain in tissue samples and cultured fibroblasts." Clin Chem **53**(4): 729-734.

Jeninga, E. H., K. Schoonjans and J. Auwerx (2010). "Reversible acetylation of PGC-1: connecting energy sensors and effectors to guarantee metabolic flexibility." Oncogene **29**(33): 4617-4624.

Jesenberger, V. and S. Jentsch (2002). "Deadly encounter: ubiquitin meets apoptosis." Nat Rev Mol Cell Biol **3**(2): 112-121.

Johnson, B. N., A. K. Berger, G. P. Cortese and M. J. Lavoie (2012). "The ubiquitin E3 ligase parkin regulates the proapoptotic function of Bax." Proc Natl Acad Sci U S A **109**(16): 6283-6288.

Jones, J. M., P. Datta, S. M. Srinivasula, W. Ji, S. Gupta, Z. Zhang, E. Davies, G. Hajnoczky, T. L. Saunders, M. L. Van Keuren, T. Fernandes-Alnemri, M. H. Meisler and E. S. Alnemri (2003). "Loss of Omi mitochondrial protease activity causes the neuromuscular disorder of mnd2 mutant mice." Nature **425**(6959): 721-727.

Junn, E., H. Taniguchi, B. S. Jeong, X. Zhao, H. Ichijo and M. M. Mouradian (2005). "Interaction of DJ-1 with Daxx inhibits apoptosis signal-regulating kinase 1 activity and cell death." Proc Natl Acad Sci U S A **102**(27): 9691-9696.

Kadenbach, B., R. Ramzan, L. Wen and S. Vogt (2010). "New extension of the Mitchell Theory for oxidative phosphorylation in mitochondria of living organisms." Biochim Biophys Acta **1800**(3): 205-212.

Kalyanaraman, B., V. Darley-Usmar, K. J. Davies, P. A. Dennery, H. J. Forman, M. B. Grisham, G. E. Mann, K. Moore, L. J. Roberts, 2nd and H. Ischiropoulos (2012). "Measuring reactive oxygen and nitrogen species with fluorescent probes: challenges and limitations." Free Radic Biol Med **52**(1): 1-6.

Kamiya, A., K. Kubo, T. Tomoda, M. Takaki, R. Youn, Y. Ozeki, N. Sawamura, U. Park, C. Kudo, M. Okawa, C. A. Ross, M. E. Hatten, K. Nakajima and A. Sawa (2005). "A schizophrenia-associated mutation of DISC1 perturbs cerebral cortex development." Nat Cell Biol **7**(12): 1167-1178.

Karbowski, M. and R. J. Youle (2003). "Dynamics of mitochondrial morphology in healthy cells and during apoptosis." Cell Death Differ **10**(8): 870-880.

Kazlauskaite, A., V. Kelly, C. Johnson, C. Baillie, C. J. Hastie, M. Peggie, T. Macartney, H. I. Woodroof, D. R. Alessi, P. G. Pedrioli and M. M. Muqit (2014). "Phosphorylation of Parkin at Serine65 is essential for activation: elaboration of a Miro1 substrate-based assay of Parkin E3 ligase activity." Open Biol **4**: 130213.

Kelly, D. P. and R. C. Scarpulla (2004). "Transcriptional regulatory circuits controlling mitochondrial biogenesis and function." Genes Dev **18**(4): 357-368.

Kim, J. W., I. Tchernyshyov, G. L. Semenza and C. V. Dang (2006). "HIF-1-mediated expression of pyruvate dehydrogenase kinase: a metabolic switch required for cellular adaptation to hypoxia." Cell Metab **3**(3): 177-185.

Kim, R. H., M. Peters, Y. Jang, W. Shi, M. Pintilie, G. C. Fletcher, C. DeLuca, J. Liepa, L. Zhou, B. Snow, R. C. Binari, A. S. Manoukian, M. R. Bray, F. F. Liu, M. S. Tsao and T. W. Mak (2005). "DJ-1, a novel regulator of the tumor suppressor PTEN." Cancer Cell **7**(3): 263-273.

Kim, R. H., P. D. Smith, H. Aleyasin, S. Hayley, M. P. Mount, S. Pownall, A. Wakeham, A. J. You-Ten, S. K. Kalia, P. Horne, D. Westaway, A. M. Lozano, H. Anisman, D. S. Park and T. W. Mak (2005). "Hypersensitivity of DJ-1-deficient mice to 1-methyl-4-phenyl-1,2,3,6-tetrahydropyrindine (MPTP) and oxidative stress." Proc Natl Acad Sci U S A **102**(14): 5215-5220.

Kinouchi, R., T. Kinouchi, T. Hamamoto, T. Saito, A. Tavares, T. Tsuru and S. Yamagami (2006). "Distribution of CESP-1 protein in the corneal endothelium and other tissues." Invest Ophthalmol Vis Sci **47**(4): 1397-1403.

Klein, C., K. Lohmann-Hedrich, E. Rogaeva, M. G. Schlossmacher and A. E. Lang (2007). "Deciphering the role of heterozygous mutations in genes associated with parkinsonism." Lancet Neurol **6**(7): 652-662.

Klosowiak, J. L., P. J. Focia, S. Chakravarthy, E. C. Landahl, D. M. Freymann and S. E. Rice (2013). "Structural coupling of the EF hand and C-terminal GTPase domains in the mitochondrial protein Miro." EMBO Rep **14**(11): 968-974.

Koide-Yoshida, S., T. Niki, M. Ueda, S. Himeno, T. Taira, S. M. Iguchi-Ariga, Y. Ando and H. Ariga (2007). "DJ-1 degrades transthyretin and an inactive form of DJ-1 is secreted in familial amyloidotic polyneuropathy." Int J Mol Med **19**(6): 885-893.

Kondapalli, C., A. Kazlauskaite, N. Zhang, H. I. Woodroof, D. G. Campbell, R. Gourlay, L. Burchell, H. Walden, T. J. Macartney, M. Deak, A. Knebel, D. R. Alessi and M. M. Muqit (2012). "PINK1 is activated by mitochondrial membrane potential depolarization and stimulates Parkin E3 ligase activity by phosphorylating Serine 65." Open Biol **2**(5): 120080.

Koopman, G., C. P. Reutelingsperger, G. A. Kuijten, R. M. Keehnen, S. T. Pals and M. H. van Oers (1994). "Annexin V for flow cytometric detection of phosphatidylserine expression on B cells undergoing apoptosis." Blood **84**(5): 1415-1420.

Kornmann, B., C. Osman and P. Walter (2011). "The conserved GTPase Gem1 regulates endoplasmic reticulum-mitochondria connections." Proc Natl Acad Sci U S A **108**(34): 14151-14156.

Kornmann, B. and P. Walter (2010). "ERMES-mediated ER-mitochondria contacts: molecular hubs for the regulation of mitochondrial biology." J Cell Sci **123**(Pt 9): 1389-1393.

Koshiba, T., H. A. Holman, K. Kubara, K. Yasukawa, S. Kawabata, K. Okamoto, J. MacFarlane and J. M. Shaw (2011). "Structure-function analysis of the yeast mitochondrial Rho GTPase, Gem1p: implications for mitochondrial inheritance." J Biol Chem **286**(1): 354-362.

Koutsopoulos, O. S., D. Laine, L. Osellame, D. M. Chudakov, R. G. Parton, A. E. Frazier and M. T. Ryan (2010). "Human Miltons associate with mitochondria and induce microtubule-dependent remodeling of mitochondrial networks." Biochim Biophys Acta **1803**(5): 564-574.

Kraytsberg, Y., E. Kudryavtseva, A. C. McKee, C. Geula, N. W. Kowall and K. Khrapko (2006). "Mitochondrial DNA deletions are abundant and cause functional impairment in aged human substantia nigra neurons." Nat Genet **38**(5): 518-520.

Krebiehl, G., S. Ruckerbauer, L. F. Burbulla, N. Kieper, B. Maurer, J. Waak, H. Wolburg, Z. Gizatullina, F. N. Gellerich, D. Woitalla, O. Riess, P. J. Kahle, T. Proikas-Cezanne and R. Kruger (2010). "Reduced basal autophagy and impaired mitochondrial dynamics due to loss of Parkinson's disease-associated protein DJ-1." PLoS One **5**(2): e9367.

Kruman, II and M. P. Mattson (1999). "Pivotal role of mitochondrial calcium uptake in neural cell apoptosis and necrosis." J Neurochem **72**(2): 529-540.

Kung, L. and R. C. Roberts (1999). "Mitochondrial pathology in human schizophrenic striatum: a postmortem ultrastructural study." Synapse **31**(1): 67-75.

Kuroda, Y., T. Mitsui, M. Kunishige and T. Matsumoto (2006). "Parkin affects mitochondrial function and apoptosis in neuronal and myogenic cells." Biochem Biophys Res Commun **348**(3): 787-793.

Langston, J. W., P. Ballard, J. W. Tetrud and I. Irwin (1983). "Chronic Parkinsonism in humans due to a product of meperidine-analog synthesis." Science **219**(4587): 979-980.

Lashuel, H. A., D. Hartley, B. M. Petre, T. Walz and P. T. Lansbury, Jr. (2002). "Neurodegenerative disease: amyloid pores from pathogenic mutations." Nature **418**(6895): 291.

Leal, A. M., J. D. de Queiroz, S. R. de Medeiros, T. K. Lima and L. F. Agnez-Lima (2015). "Violacein induces cell death by triggering mitochondrial membrane hyperpolarization in vitro." BMC Microbiol **15**: 115.

Lee, S., Y. Sato and R. A. Nixon (2011). "Lysosomal proteolysis inhibition selectively disrupts axonal transport of degradative organelles and causes an Alzheimer's-like axonal dystrophy." J Neurosci **31**(21): 7817-7830.

Lee, S. J., S. J. Kim, I. K. Kim, J. Ko, C. S. Jeong, G. H. Kim, C. Park, S. O. Kang, P. G. Suh, H. S. Lee and S. S. Cha (2003). "Crystal structures of human DJ-1 and Escherichia coli Hsp31, which share an evolutionarily conserved domain." J Biol Chem **278**(45): 44552-44559.

Lehle, S., D. G. Hildebrand, B. Merz, P. N. Malak, M. S. Becker, P. Schmezer, F. Essmann, K. Schulze-Osthoff and O. Rothfuss (2014). "LORD-Q: a long-run real-time PCR-based DNA-damage quantification method for nuclear and mitochondrial genome analysis." Nucleic Acids Res **42**(6): e41.

Lemasters, J. J. (2014). "Variants of mitochondrial autophagy: Types 1 and 2 mitophagy and micromitophagy (Type 3)." Redox Biol **2**: 749-754.

Lemasters, J. J., A. L. Nieminen, T. Qian, L. C. Trost, S. P. Elmore, Y. Nishimura, R. A. Crowe, W. E. Cascio, C. A. Bradham, D. A. Brenner and B. Herman (1998). "The mitochondrial permeability transition in cell death: a common mechanism in necrosis, apoptosis and autophagy." Biochim Biophys Acta **1366**(1-2): 177-196.

Lewis, P. A., E. Greggio, A. Beilina, S. Jain, A. Baker and M. R. Cookson (2007). "The R1441C mutation of LRRK2 disrupts GTP hydrolysis." Biochem Biophys Res Commun **357**(3): 668-671.

Li, W. W., R. Yang, J. C. Guo, H. M. Ren, X. L. Zha, J. S. Cheng and D. F. Cai (2007). "Localization of alpha-synuclein to mitochondria within midbrain of mice." Neuroreport **18**(15): 1543-1546.

Li, X., P. Fang, J. Mai, E. T. Choi, H. Wang and X. F. Yang (2013). "Targeting mitochondrial reactive oxygen species as novel therapy for inflammatory diseases and cancers." J Hematol Oncol **6**: 19.

Li, Y., T. T. Huang, E. J. Carlson, S. Melov, P. C. Ursell, J. L. Olson, L. J. Noble, M. P. Yoshimura, C. Berger, P. H. Chan, D. C. Wallace and C. J. Epstein (1995). "Dilated cardiomyopathy and neonatal lethality in mutant mice lacking manganese superoxide dismutase." Nat Genet **11**(4): 376-381.

Li, Y., S. Lim, D. Hoffman, P. Aspenstrom, H. J. Federoff and D. A. Rempe (2009). "HUMMR, a hypoxia- and HIF-1alpha-inducible protein, alters mitochondrial distribution and transport." J Cell Biol **185**(6): 1065-1081.

Liao, J., C. X. Wu, C. Burlak, S. Zhang, H. Sahm, M. Wang, Z. Y. Zhang, K. W. Vogel, M. Federici, S. M. Riddle, R. J. Nichols, D. Liu, M. R. Cookson, T. A. Stone and Q. Q. Hoang (2014). "Parkinson disease-associated mutation R1441H in LRRK2 prolongs the "active state" of its GTPase domain." Proc Natl Acad Sci U S A **111**(11): 4055-4060.

Lin, J., C. Handschin and B. M. Spiegelman (2005). "Metabolic control through the PGC-1 family of transcription coactivators." Cell Metab **1**(6): 361-370.

Liou, A. K., R. K. Leak, L. Li and M. J. Zigmond (2008). "Wild-type LRRK2 but not its mutant attenuates stress-induced cell death via ERK pathway." Neurobiol Dis **32**(1): 116-124.

Liu, S., T. Sawada, S. Lee, W. Yu, G. Silverio, P. Alapatt, I. Millan, A. Shen, W. Saxton, T. Kanao, R. Takahashi, N. Hattori, Y. Imai and B. Lu (2012). "Parkinson's disease-associated kinase PINK1 regulates Miro protein level and axonal transport of mitochondria." PLoS Genet **8**(3): e1002537.

Liu, X., D. Weaver, O. Shirihai and G. Hajnoczky (2009). "Mitochondrial 'kiss-and-run': interplay between mitochondrial motility and fusion-fission dynamics." EMBO J **28**(20): 3074-3089.

Lopez-Domenech, G., R. Serrat, S. Mirra, S. D'Aniello, I. Somorjai, A. Abad, N. Vitureira, E. Garcia-Arumi, M. T. Alonso, M. Rodriguez-Prados, F. Burgaya, A. L. Andreu, J. Garcia-Sancho, R. Trullas, J. Garcia-Fernandez and E. Soriano (2012). "The Eutherian Armcx genes regulate mitochondrial trafficking in neurons and interact with Miro and Trak2." Nat Commun **3**: 814.

Ma, Z., M. Cao, Y. Liu, Y. He, Y. Wang, C. Yang, W. Wang, Y. Du, M. Zhou and F. Gao (2010). "Mitochondrial F1Fo-ATP synthase translocates to cell surface in hepatocytes and has high activity in tumor-like acidic and hypoxic environment." Acta Biochim Biophys Sin (Shanghai) **42**(8): 530-537.

MacAskill, A. F., K. Brickley, F. A. Stephenson and J. T. Kittler (2009). "GTPase dependent recruitment of Grif-1 by Miro1 regulates mitochondrial trafficking in hippocampal neurons." Mol Cell Neurosci **40**(3): 301-312.

Macaskill, A. F., J. E. Rinholm, A. E. Twelvetrees, I. L. Arancibia-Carcamo, J. Muir, A. Fransson, P. Aspenstrom, D. Attwell and J. T. Kittler (2009). "Miro1 is a calcium sensor for glutamate receptor-dependent localization of mitochondria at synapses." Neuron **61**(4): 541-555.

Mackie, S., J. K. Millar and D. J. Porteous (2007). "Role of DISC1 in neural development and schizophrenia." Curr Opin Neurobiol **17**(1): 95-102.

Maday, S., K. E. Wallace and E. L. Holzbaur (2012). "Autophagosomes initiate distally and mature during transport toward the cell soma in primary neurons." J Cell Biol **196**(4): 407-417.

Mallilankaraman, K., C. Cardenas, P. J. Doonan, H. C. Chandramoorthy, K. M. Irrinki, T. Golenar, G. Csordas, P. Madireddi, J. Yang, M. Muller, R. Miller, J. E. Kolesar, J. Molgo, B. Kaufman, G. Hajnoczky, J. K. Foskett and M. Madesh (2012). "MCUR1 is an essential component of mitochondrial Ca2+ uptake that regulates cellular metabolism." Nat Cell Biol **14**(12): 1336-1343.

Mandemakers, W., V. A. Morais and B. De Strooper (2007). "A cell biological perspective on mitochondrial dysfunction in Parkinson disease and other neurodegenerative diseases." J Cell Sci **120**(Pt 10): 1707-1716.

Manolio, T. A., F. S. Collins, N. J. Cox, D. B. Goldstein, L. A. Hindorff, D. J. Hunter, M. I. McCarthy, E. M. Ramos, L. R. Cardon, A. Chakravarti, J. H. Cho, A. E. Guttmacher, A. Kong, L. Kruglyak, E. Mardis, C. N. Rotimi, M. Slatkin, D. Valle, A. S. Whittemore, M. Boehnke, A. G. Clark, E. E. Eichler, G. Gibson, J. L. Haines, T. F. Mackay, S. A. McCarroll and P. M. Visscher (2009). "Finding the missing heritability of complex diseases." Nature **461**(7265): 747-753.

Mao, Y., X. Ge, C. L. Frank, J. M. Madison, A. N. Koehler, M. K. Doud, C. Tassa, E. M. Berry, T. Soda, K. K. Singh, T. Biechele, T. L. Petryshen, R. T. Moon, S. J. Haggarty and

L. H. Tsai (2009). "Disrupted in schizophrenia 1 regulates neuronal progenitor proliferation via modulation of GSK3beta/beta-catenin signaling." Cell **136**(6): 1017-1031.

Marine, A., K. J. Krager, N. Aykin-Burns and L. A. Macmillan-Crow (2014). "Peroxynitrite induced mitochondrial biogenesis following MnSOD knockdown in normal rat kidney (NRK) cells." Redox Biol **2**: 348-357.

Markham, A., I. Cameron, P. Franklin and M. Spedding (2004). "BDNF increases rat brain mitochondrial respiratory coupling at complex I, but not complex II." Eur J Neurosci **20**(5): 1189-1196.

Martins, L. M., A. Morrison, K. Klupsch, V. Fedele, N. Moisoi, P. Teismann, A. Abuin, E. Grau, M. Geppert, G. P. Livi, C. L. Creasy, A. Martin, I. Hargreaves, S. J. Heales, H. Okada, S. Brandner, J. B. Schulz, T. Mak and J. Downward (2004). "Neuroprotective role of the Reaper-related serine protease HtrA2/Omi revealed by targeted deletion in mice." Mol Cell Biol **24**(22): 9848-9862.

Maurer, I., S. Zierz and H. Moller (2001). "Evidence for a mitochondrial oxidative phosphorylation defect in brains from patients with schizophrenia." Schizophr Res **48**(1): 125-136.

McBride, H. M., M. Neuspiel and S. Wasiak (2006). "Mitochondria: more than just a powerhouse." Curr Biol **16**(14): R551-560.

McCarthy, M. I. and J. N. Hirschhorn (2008). "Genome-wide association studies: potential next steps on a genetic journey." Hum Mol Genet **17**(R2): R156-165.

McCormack, J. G., A. P. Halestrap and R. M. Denton (1990). "Role of calcium ions in regulation of mammalian intramitochondrial metabolism." Physiol Rev **70**(2): 391-425.

McLelland, G. L., V. Soubannier, C. X. Chen, H. M. McBride and E. A. Fon (2014). "Parkin and PINK1 function in a vesicular trafficking pathway regulating mitochondrial quality control." EMBO J **33**(4): 282-295.

McTaggart, S. J. (2006). "Isoprenylated proteins." Cell Mol Life Sci **63**(3): 255-267.

Meulener, M. C., K. Xu, L. Thomson, H. Ischiropoulos and N. M. Bonini (2006). "Mutational analysis of DJ-1 in Drosophila implicates functional inactivation by oxidative damage and aging." Proc Natl Acad Sci U S A **103**(33): 12517-12522.

Milkovic, N. M., J. Catazaro, J. Lin, S. Halouska, J. L. Kizziah, S. Basiaga, R. L. Cerny, R. Powers and M. A. Wilson (2015). "Transient sampling of aggregation-prone conformations causes pathogenic instability of a parkinsonian mutant of DJ-1 at physiological temperature." Protein Sci **24**(10): 1671-1685.

Millar, J. K., B. S. Pickard, S. Mackie, R. James, S. Christie, S. R. Buchanan, M. P. Malloy, J. E. Chubb, E. Huston, G. S. Baillie, P. A. Thomson, E. V. Hill, N. J. Brandon, J. C. Rain, L. M. Camargo, P. J. Whiting, M. D. Houslay, D. H. Blackwood, W. J. Muir and D. J. Porteous (2005). "DISC1 and PDE4B are interacting genetic factors in schizophrenia that regulate cAMP signaling." Science **310**(5751): 1187-1191.

Miller, K. E. and M. P. Sheetz (2004). "Axonal mitochondrial transport and potential are correlated." J Cell Sci **117**(Pt 13): 2791-2804.

Milosevic, I., S. Giovedi, X. Lou, A. Raimondi, C. Collesi, H. Shen, S. Paradise, E. O'Toole, S. Ferguson, O. Cremona and P. De Camilli (2011). "Recruitment of endophilin to clathrin-coated pit necks is required for efficient vesicle uncoating after fission." Neuron **72**(4): 587-601.

Misko, A., S. Jiang, I. Wegorzewska, J. Milbrandt and R. H. Baloh (2010). "Mitofusin 2 is necessary for transport of axonal mitochondria and interacts with the Miro/Milton complex." J Neurosci **30**(12): 4232-4240.

Mizuno, Y., S. Ohta, M. Tanaka, S. Takamiya, K. Suzuki, T. Sato, H. Oya, T. Ozawa and Y. Kagawa (1989). "Deficiencies in complex I subunits of the respiratory chain in Parkinson's disease." Biochem Biophys Res Commun **163**(3): 1450-1455.

Moore, D. J., L. Zhang, J. Troncoso, M. K. Lee, N. Hattori, Y. Mizuno, T. M. Dawson and V. L. Dawson (2005). "Association of DJ-1 and parkin mediated by pathogenic DJ-1 mutations and oxidative stress." Hum Mol Genet **14**(1): 71-84.

Morlino, G., O. Barreiro, F. Baixauli, J. Robles-Valero, J. M. Gonzalez-Granado, R. Villa-Bellosta, J. Cuenca, C. O. Sanchez-Sorzano, E. Veiga, N. B. Martin-Cofreces and F. Sanchez-Madrid (2014). "Miro-1 links mitochondria and microtubule Dynein motors to control lymphocyte migration and polarity." Mol Cell Biol **34**(8): 1412-1426.

Mortiboys, H., J. Aasly and O. Bandmann (2013). "Ursocholanic acid rescues mitochondrial function in common forms of familial Parkinson's disease." Brain **136**(Pt 10): 3038-3050.

Mortiboys, H., K. J. Thomas, W. J. Koopman, S. Klaffke, P. Abou-Sleiman, S. Olpin, N. W. Wood, P. H. Willems, J. A. Smeitink, M. R. Cookson and O. Bandmann (2008). "Mitochondrial function and morphology are impaired in parkin-mutant fibroblasts." Ann Neurol **64**(5): 555-565.

Mou, Z., A. R. Tapper and P. D. Gardner (2009). "The armadillo repeat-containing protein, ARMCX3, physically and functionally interacts with the developmental regulatory factor Sox10." J Biol Chem **284**(20): 13629-13640.

Murley, A., L. L. Lackner, C. Osman, M. West, G. K. Voeltz, P. Walter and J. Nunnari (2013). "ER-associated mitochondrial division links the distribution of mitochondria and mitochondrial DNA in yeast." Elife **2**: e00422.

Nakabeppu, Y., D. Tsuchimoto, H. Yamaguchi and K. Sakumi (2007). "Oxidative damage in nucleic acids and Parkinson's disease." J Neurosci Res **85**(5): 919-934.

Nakamura, K., V. M. Nemani, F. Azarbal, G. Skibinski, J. M. Levy, K. Egami, L. Munishkina, J. Zhang, B. Gardner, J. Wakabayashi, H. Sesaki, Y. Cheng, S. Finkbeiner, R. L. Nussbaum, E. Masliah and R. H. Edwards (2011). "Direct membrane association drives mitochondrial fission by the Parkinson disease-associated protein alpha-synuclein." J Biol Chem **286**(23): 20710-20726.

Nakamura, K., V. M. Nemani, E. K. Wallender, K. Kaehlcke, M. Ott and R. H. Edwards (2008). "Optical reporters for the conformation of alpha-synuclein reveal a specific interaction with mitochondria." J Neurosci **28**(47): 12305-12317.

Nalls, M. A., N. Pankratz, C. M. Lill, C. B. Do, D. G. Hernandez, M. Saad, A. L. DeStefano, E. Kara, J. Bras, M. Sharma, C. Schulte, M. F. Keller, S. Arepalli, C. Letson, C. Edsall, H. Stefansson, X. Liu, H. Pliner, J. H. Lee, R. Cheng, C. International Parkinson's Disease Genomics, G. I. Parkinson's Study Group Parkinson's Research: The Organized, andMe, GenePd, C. NeuroGenetics Research, G. Hussman Institute of Human, I. Ashkenazi Jewish Dataset, H. Cohorts for, E. Aging Research in Genetic, C. North American Brain Expression, C. United Kingdom Brain Expression, C. Greek Parkinson's Disease, G. Alzheimer Genetic Analysis, M. A. Ikram, J. P. Ioannidis, G. M. Hadjigeorgiou, J. C. Bis, M. Martinez, J. S. Perlmutter, A. Goate, K. Marder, B. Fiske, M. Sutherland, G. Xiromerisiou, R. H. Myers, L. N. Clark, K. Stefansson, J. A. Hardy, P. Heutink, H. Chen, N. W. Wood, H. Houlden, H. Payami, A. Brice, W. K. Scott, T. Gasser, L. Bertram, N. Eriksson, T. Foroud and A. B. Singleton (2014). "Large-scale meta-analysis of genome-wide association data identifies six new risk loci for Parkinson's disease." Nat Genet **46**(9): 989-993.

Narendra, D., A. Tanaka, D. F. Suen and R. J. Youle (2008). "Parkin is recruited selectively to impaired mitochondria and promotes their autophagy." J Cell Biol **183**(5): 795-803.

Nemani, V. M., W. Lu, V. Berge, K. Nakamura, B. Onoa, M. K. Lee, F. A. Chaudhry, R. A. Nicoll and R. H. Edwards (2010). "Increased expression of alpha-synuclein reduces neurotransmitter release by inhibiting synaptic vesicle reclustering after endocytosis." Neuron **65**(1): 66-79.

Nemoto, S., M. M. Fergusson and T. Finkel (2005). "SIRT1 functionally interacts with the metabolic regulator and transcriptional coactivator PGC-1{alpha}." J Biol Chem **280**(16): 16456-16460.

Nguyen, T. T., S. S. Oh, D. Weaver, A. Lewandowska, D. Maxfield, M. H. Schuler, N. K. Smith, J. Macfarlane, G. Saunders, C. A. Palmer, V. Debattisti, T. Koshiba, S. Pulst, E. L. Feldman, G. Hajnoczky and J. M. Shaw (2014). "Loss of Miro1-directed mitochondrial movement results in a novel murine model for neuron disease." Proc Natl Acad Sci U S A **111**(35): E3631-3640.

Nicholls, D. and K. Akerman (1982). "Mitochondrial calcium transport." Biochim Biophys Acta **683**(1): 57-88.

Nicholls, D. G. (2008). "Oxidative stress and energy crises in neuronal dysfunction." Ann N Y Acad Sci **1147**: 53-60.

Nicklas, W. J., I. Vyas and R. E. Heikkila (1985). "Inhibition of NADH-linked oxidation in brain mitochondria by 1-methyl-4-phenyl-pyridine, a metabolite of the neurotoxin, 1-methyl-4-phenyl-1,2,5,6-tetrahydropyridine." Life Sci **36**(26): 2503-2508.

Nieminen, A. L., A. K. Saylor, S. A. Tesfai, B. Herman and J. J. Lemasters (1995). "Contribution of the mitochondrial permeability transition to lethal injury after exposure of hepatocytes to t-butylhydroperoxide." Biochem J **307 (Pt 1)**: 99-106.

Niu, J., M. Yu, C. Wang and Z. Xu (2012). "Leucine-rich repeat kinase 2 disturbs mitochondrial dynamics via Dynamin-like protein." J Neurochem **122**(3): 650-658.

Noguchi, J., M. Matsuzaki, G. C. Ellis-Davies and H. Kasai (2005). "Spine-neck geometry determines NMDA receptor-dependent Ca2+ signaling in dendrites." Neuron **46**(4): 609-622.

Numakawa, T., S. Suzuki, E. Kumamaru, N. Adachi, M. Richards and H. Kunugi (2010). "BDNF function and intracellular signaling in neurons." Histol Histopathol **25**(2): 237-258.

Obeso, J. A., M. C. Rodriguez-Oroz, M. Rodriguez, J. L. Lanciego, J. Artieda, N. Gonzalo and C. W. Olanow (2000). "Pathophysiology of the basal ganglia in Parkinson's disease." Trends Neurosci **23**(10 Suppl): S8-19.

Ogawa, F., E. L. Malavasi, D. K. Crummie, J. E. Eykelenboom, D. C. Soares, S. Mackie, D. J. Porteous and J. K. Millar (2014). "DISC1 complexes with TRAK1 and Miro1 to modulate anterograde axonal mitochondrial trafficking." Hum Mol Genet **23**(4): 906-919.

Olzmann, J. A., K. Brown, K. D. Wilkinson, H. D. Rees, Q. Huai, H. Ke, A. I. Levey, L. Li and L. S. Chin (2004). "Familial Parkinson's disease-associated L166P mutation disrupts DJ-1 protein folding and function." J Biol Chem **279**(9): 8506-8515.

Orth, M. and A. H. Schapira (2002). "Mitochondrial involvement in Parkinson's disease." Neurochem Int **40**(6): 533-541.

Orth, M. and S. J. Tabrizi (2003). "Models of Parkinson's disease." Mov Disord **18**(7): 729-737.

Ozeki, Y., T. Tomoda, J. Kleiderlein, A. Kamiya, L. Bord, K. Fujii, M. Okawa, N. Yamada, M. E. Hatten, S. H. Snyder, C. A. Ross and A. Sawa (2003). "Disrupted-in-Schizophrenia-1 (DISC-1): mutant truncation prevents binding to NudE-like (NUDEL) and inhibits neurite outgrowth." Proc Natl Acad Sci U S A **100**(1): 289-294.

Pacelli, C., D. De Rasmo, A. Signorile, I. Grattagliano, G. di Tullio, A. D'Orazio, B. Nico, G. P. Comi, D. Ronchi, E. Ferranini, D. Pirolo, P. Seibel, S. Schubert, A. Gaballo, G. Villani and T. Cocco (2011). "Mitochondrial defect and PGC-1alpha dysfunction in parkin-associated familial Parkinson's disease." Biochim Biophys Acta **1812**(8): 1041-1053.

Palacino, J. J., D. Sagi, M. S. Goldberg, S. Krauss, C. Motz, M. Wacker, J. Klose and J. Shen (2004). "Mitochondrial dysfunction and oxidative damage in parkin-deficient mice." J Biol Chem **279**(18): 18614-18622.

Papandreou, I., R. A. Cairns, L. Fontana, A. L. Lim and N. C. Denko (2006). "HIF-1 mediates adaptation to hypoxia by actively downregulating mitochondrial oxygen consumption." Cell Metab **3**(3): 187-197.

Papkovskaia, T. D., K. Y. Chau, F. Inesta-Vaquera, D. B. Papkovsky, D. G. Healy, K. Nishio, J. Staddon, M. R. Duchen, J. Hardy, A. H. Schapira and J. M. Cooper (2012). "G2019S leucine-rich repeat kinase 2 causes uncoupling protein-mediated mitochondrial depolarization." Hum Mol Genet **21**(19): 4201-4213.

Park, J., S. B. Lee, S. Lee, Y. Kim, S. Song, S. Kim, E. Bae, J. Kim, M. Shong, J. M. Kim and J. Chung (2006). "Mitochondrial dysfunction in Drosophila PINK1 mutants is complemented by parkin." Nature **441**(7097): 1157-1161.

Park, Y. U., J. Jeong, H. Lee, J. Y. Mun, J. H. Kim, J. S. Lee, M. D. Nguyen, S. S. Han, P. G. Suh and S. K. Park (2010). "Disrupted-in-schizophrenia 1 (DISC1) plays essential roles in mitochondria in collaboration with Mitofilin." Proc Natl Acad Sci U S A **107**(41): 17785-17790.

Parker, W. D., Jr., S. J. Boyson and J. K. Parks (1989). "Abnormalities of the electron transport chain in idiopathic Parkinson's disease." Ann Neurol **26**(6): 719-723.

Perez, R. G., J. C. Waymire, E. Lin, J. J. Liu, F. Guo and M. J. Zigmond (2002). "A role for alpha-synuclein in the regulation of dopamine biosynthesis." J Neurosci **22**(8): 3090-3099.

Perocchi, F., V. M. Gohil, H. S. Girgis, X. R. Bao, J. E. McCombs, A. E. Palmer and V. K. Mootha (2010). "MICU1 encodes a mitochondrial EF hand protein required for Ca(2+) uptake." Nature **467**(7313): 291-296.

Piccoli, C., A. Sardanelli, R. Scrima, M. Ripoli, G. Quarato, A. D'Aprile, F. Bellomo, S. Scacco, G. De Michele, A. Filla, A. Iuso, D. Boffoli, N. Capitanio and S. Papa (2008). "Mitochondrial respiratory dysfunction in familiar parkinsonism associated with PINK1 mutation." Neurochem Res **33**(12): 2565-2574.

Piccoli, C., R. Scrima, D. Boffoli and N. Capitanio (2006). "Control by cytochrome c oxidase of the cellular oxidative phosphorylation system depends on the mitochondrial energy state." Biochem J **396**(3): 573-583.

Pilling, A. D., D. Horiuchi, C. M. Lively and W. M. Saxton (2006). "Kinesin-1 and Dynein are the primary motors for fast transport of mitochondria in Drosophila motor axons." Mol Biol Cell **17**(4): 2057-2068.

Poderoso, J. J., M. C. Carreras, C. Lisdero, N. Riobo, F. Schopfer and A. Boveris (1996). "Nitric oxide inhibits electron transfer and increases superoxide radical production in rat heart mitochondria and submitochondrial particles." Arch Biochem Biophys **328**(1): 85-92.

Poppe, M., C. Reimertz, H. Dussmann, A. J. Krohn, C. M. Luetjens, D. Bockelmann, A. L. Nieminen, D. Kogel and J. H. Prehn (2001). "Dissipation of potassium and proton gradients inhibits mitochondrial hyperpolarization and cytochrome c release during neural apoptosis." J Neurosci **21**(13): 4551-4563.

Prehn, J. H., J. Jordan, G. D. Ghadge, E. Preis, M. F. Galindo, R. P. Roos, J. Krieglstein and R. J. Miller (1997). "Ca2+ and reactive oxygen species in staurosporine-induced neuronal apoptosis." J Neurochem **68**(4): 1679-1685.

Pritchard, J. K. (2001). "Are rare variants responsible for susceptibility to complex diseases?" Am J Hum Genet **69**(1): 124-137.

Qiu, J. H., A. Asai, S. Chi, N. Saito, H. Hamada and T. Kirino (2000). "Proteasome inhibitors induce cytochrome c-caspase-3-like protease-mediated apoptosis in cultured cortical neurons." J Neurosci **20**(1): 259-265.

Radak, Z., H. Y. Chung, E. Koltai, A. W. Taylor and S. Goto (2008). "Exercise, oxidative stress and hormesis." Ageing Res Rev **7**(1): 34-42.

Ramzan, R., K. Staniek, B. Kadenbach and S. Vogt (2010). "Mitochondrial respiration and membrane potential are regulated by the allosteric ATP-inhibition of cytochrome c oxidase." Biochim Biophys Acta **1797**(9): 1672-1680.

Rapizzi, E., P. Pinton, G. Szabadkai, M. R. Wieckowski, G. Vandecasteele, G. Baird, R. A. Tuft, K. E. Fogarty and R. Rizzuto (2002). "Recombinant expression of the voltage-dependent anion channel enhances the transfer of Ca2+ microdomains to mitochondria." J Cell Biol **159**(4): 613-624.

Riobo, N. A., E. Clementi, M. Melani, A. Boveris, E. Cadenas, S. Moncada and J. J. Poderoso (2001). "Nitric oxide inhibits mitochondrial NADH:ubiquinone reductase activity through peroxynitrite formation." Biochem J **359**(Pt 1): 139-145.

Rizzuto, R., D. De Stefani, A. Raffaello and C. Mammucari (2012). "Mitochondria as sensors and regulators of calcium signalling." Nat Rev Mol Cell Biol **13**(9): 566-578.

Robinson, K. M., M. S. Janes and J. S. Beckman (2008). "The selective detection of mitochondrial superoxide by live cell imaging." Nat Protoc **3**(6): 941-947.

Rojo, M., F. Legros, D. Chateau and A. Lombes (2002). "Membrane topology and mitochondrial targeting of mitofusins, ubiquitous mammalian homologs of the transmembrane GTPase Fzo." J Cell Sci **115**(Pt 8): 1663-1674.

Rosei, M. A., C. Blarzino, R. Coccia, C. Foppoli, L. Mosca and C. Cini (1998). "Production of melanin pigments by cytochrome c/H2O2 system." Int J Biochem Cell Biol **30**(4): 457-463.

Rossignol, R., B. Faustin, C. Rocher, M. Malgat, J. P. Mazat and T. Letellier (2003). "Mitochondrial threshold effects." Biochem J **370**(Pt 3): 751-762.

Russo, G. J., K. Louie, A. Wellington, G. T. Macleod, F. Hu, S. Panchumarthi and K. E. Zinsmaier (2009). "Drosophila Miro is required for both anterograde and retrograde axonal mitochondrial transport." J Neurosci **29**(17): 5443-5455.

Saotome, M., D. Safiulina, G. Szabadkai, S. Das, A. Fransson, P. Aspenstrom, R. Rizzuto and G. Hajnoczky (2008). "Bidirectional Ca2+-dependent control of mitochondrial dynamics by the Miro GTPase." Proc Natl Acad Sci U S A **105**(52): 20728-20733.

Sarraf, S. A., M. Raman, V. Guarani-Pereira, M. E. Sowa, E. L. Huttlin, S. P. Gygi and J. W. Harper (2013). "Landscape of the PARKIN-dependent ubiquitylome in response to mitochondrial depolarization." Nature **496**(7445): 372-376.

Schapira, A. H., J. M. Cooper, D. Dexter, P. Jenner, J. B. Clark and C. D. Marsden (1989). "Mitochondrial complex I deficiency in Parkinson's disease." Lancet **1**(8649): 1269.

Sekito, A., S. Koide-Yoshida, T. Niki, T. Taira, S. M. Iguchi-Ariga and H. Ariga (2006). "DJ-1 interacts with HIPK1 and affects H2O2-induced cell death." Free Radic Res **40**(2): 155-165.

Semenza, G. L. (2000). "HIF-1: mediator of physiological and pathophysiological responses to hypoxia." J Appl Physiol (1985) **88**(4): 1474-1480.

Shamoto-Nagai, M., W. Maruyama, Y. Kato, K. Isobe, M. Tanaka, M. Naoi and T. Osawa (2003). "An inhibitor of mitochondrial complex I, rotenone, inactivates proteasome by oxidative modification and induces aggregation of oxidized proteins in SH-SY5Y cells." J Neurosci Res **74**(4): 589-597.

Shendelman, S., A. Jonason, C. Martinat, T. Leete and A. Abeliovich (2004). "DJ-1 is a redox-dependent molecular chaperone that inhibits alpha-synuclein aggregate formation." PLoS Biol **2**(11): e362.

Shinbo, Y., T. Taira, T. Niki, S. M. Iguchi-Ariga and H. Ariga (2005). "DJ-1 restores p53 transcription activity inhibited by Topors/p53BP3." Int J Oncol **26**(3): 641-648.

Shino, M. Y., V. McGuire, S. K. Van Den Eeden, C. M. Tanner, R. Popat, A. Leimpeter, A. L. Bernstein and L. M. Nelson (2010). "Familial aggregation of Parkinson's disease in a multiethnic community-based case-control study." Mov Disord **25**(15): 2587-2594.

Shoag, J. and Z. Arany (2010). "Regulation of hypoxia-inducible genes by PGC-1 alpha." Arterioscler Thromb Vasc Biol **30**(4): 662-666.

Sievers, F., A. Wilm, D. Dineen, T. J. Gibson, K. Karplus, W. Li, R. Lopez, H. McWilliam, M. Remmert, J. Soding, J. D. Thompson and D. G. Higgins (2011). "Fast, scalable generation of high-quality protein multiple sequence alignments using Clustal Omega." Mol Syst Biol **7**: 539.

Singleton, A. B., M. J. Farrer and V. Bonifati (2013). "The genetics of Parkinson's disease: progress and therapeutic implications." Mov Disord **28**(1): 14-23.

Slivka, A. and G. Cohen (1985). "Hydroxyl radical attack on dopamine." J Biol Chem **260**(29): 15466-15472.

Smith, W. W., Z. Pei, H. Jiang, D. J. Moore, Y. Liang, A. B. West, V. L. Dawson, T. M. Dawson and C. A. Ross (2005). "Leucine-rich repeat kinase 2 (LRRK2) interacts with parkin, and mutant LRRK2 induces neuronal degeneration." Proc Natl Acad Sci U S A **102**(51): 18676-18681.

Soubannier, V., G. L. McLelland, R. Zunino, E. Braschi, P. Rippstein, E. A. Fon and H. M. McBride (2012). "A vesicular transport pathway shuttles cargo from mitochondria to lysosomes." Curr Biol **22**(2): 135-141.

Soubannier, V., P. Rippstein, B. A. Kaufman, E. A. Shoubridge and H. M. McBride (2012). "Reconstitution of mitochondria derived vesicle formation demonstrates selective enrichment of oxidized cargo." PLoS One **7**(12): e52830.

Soucek, T., R. Cumming, R. Dargusch, P. Maher and D. Schubert (2003). "The regulation of glucose metabolism by HIF-1 mediates a neuroprotective response to amyloid beta peptide." Neuron **39**(1): 43-56.

Spillantini, M. G., M. L. Schmidt, V. M. Lee, J. Q. Trojanowski, R. Jakes and M. Goedert (1997). "Alpha-synuclein in Lewy bodies." Nature **388**(6645): 839-840.

St-Pierre, J., S. Drori, M. Uldry, J. M. Silvaggi, J. Rhee, S. Jager, C. Handschin, K. Zheng, J. Lin, W. Yang, D. K. Simon, R. Bachoo and B. M. Spiegelman (2006). "Suppression of reactive oxygen species and neurodegeneration by the PGC-1 transcriptional coactivators." Cell **127**(2): 397-408.

Starkov, A. A. (2010). "The molecular identity of the mitochondrial Ca2+ sequestration system." FEBS J **277**(18): 3652-3663.

Stephen, T. L., N. F. Higgs, D. F. Sheehan, S. Al Awabdh, G. Lopez-Domenech, I. L. Arancibia-Carcamo and J. T. Kittler (2015). "Miro1 Regulates Activity-Driven Positioning of Mitochondria within Astrocytic Processes Apposed to Synapses to Regulate Intracellular Calcium Signaling." J Neurosci **35**(48): 15996-16011.

Stokes, K. Y. (2007). "NAD(P)H oxidase: where there's smoke, there's fire." Am J Physiol Heart Circ Physiol **292**(1): H119-120.

Stout, A. K., H. M. Raphael, B. I. Kanterewicz, E. Klann and I. J. Reynolds (1998). "Glutamate-induced neuron death requires mitochondrial calcium uptake." Nat Neurosci **1**(5): 366-373.

Strauss, K. M., L. M. Martins, H. Plun-Favreau, F. P. Marx, S. Kautzmann, D. Berg, T. Gasser, Z. Wszolek, T. Muller, A. Bornemann, H. Wolburg, J. Downward, O. Riess, J. B. Schulz and R. Kruger (2005). "Loss of function mutations in the gene encoding Omi/HtrA2 in Parkinson's disease." Hum Mol Genet **14**(15): 2099-2111.

Su, B., Y. S. Ji, X. L. Sun, X. H. Liu and Z. Y. Chen (2014). "Brain-derived neurotrophic factor (BDNF)-induced mitochondrial motility arrest and presynaptic docking contribute to BDNF-enhanced synaptic transmission." J Biol Chem **289**(3): 1213-1226.

Su, Y. C. and X. Qi (2013). "Inhibition of excessive mitochondrial fission reduced aberrant autophagy and neuronal damage caused by LRRK2 G2019S mutation." Hum Mol Genet **22**(22): 4545-4561.

Sullivan, P. G., N. B. Dragicevic, J. H. Deng, Y. Bai, E. Dimayuga, Q. Ding, Q. Chen, A. J. Bruce-Keller and J. N. Keller (2004). "Proteasome inhibition alters neural mitochondrial homeostasis and mitochondria turnover." J Biol Chem **279**(20): 20699-20707.

Sulzer, D. and L. Zecca (2000). "Intraneuronal dopamine-quinone synthesis: a review." Neurotox Res **1**(3): 181-195.

Suzuki, M., O. Danilchanka and J. J. Mekalanos (2014). "Vibrio cholerae T3SS effector VopE modulates mitochondrial dynamics and innate immune signaling by targeting Miro GTPases." Cell Host Microbe **16**(5): 581-591.

Szabadkai, G., K. Bianchi, P. Varnai, D. De Stefani, M. R. Wieckowski, D. Cavagna, A. I. Nagy, T. Balla and R. Rizzuto (2006). "Chaperone-mediated coupling of endoplasmic reticulum and mitochondrial Ca2+ channels." J Cell Biol **175**(6): 901-911.

Szabadkai, G. and M. R. Duchen (2008). "Mitochondria: the hub of cellular Ca2+ signaling." Physiology (Bethesda) **23**: 84-94.

Szabadkai, G., A. M. Simoni, K. Bianchi, D. De Stefani, S. Leo, M. R. Wieckowski and R. Rizzuto (2006). "Mitochondrial dynamics and Ca2+ signaling." Biochim Biophys Acta **1763**(5-6): 442-449.

Tabrizi, S. J., M. Orth, J. M. Wilkinson, J. W. Taanman, T. T. Warner, J. M. Cooper and A. H. Schapira (2000). "Expression of mutant alpha-synuclein causes increased susceptibility to dopamine toxicity." Hum Mol Genet **9**(18): 2683-2689.

Taira, T., S. M. Iguchi-Ariga and H. Ariga (2004). "Co-localization with DJ-1 is essential for the androgen receptor to exert its transcription activity that has been impaired by androgen antagonists." Biol Pharm Bull **27**(4): 574-577.

Takai, Y., T. Sasaki and T. Matozaki (2001). "Small GTP-binding proteins." Physiol Rev **81**(1): 153-208.

Tang, B., H. Xiong, P. Sun, Y. Zhang, D. Wang, Z. Hu, Z. Zhu, H. Ma, Q. Pan, J. H. Xia, K. Xia and Z. Zhang (2006). "Association of PINK1 and DJ-1 confers digenic inheritance of early-onset Parkinson's disease." Hum Mol Genet **15**(11): 1816-1825.

Tanida, I., T. Ueno and E. Kominami (2008). "LC3 and Autophagy." Methods Mol Biol **445**: 77-88.

Tatton, W. G., R. Chalmers-Redman, D. Brown and N. Tatton (2003). "Apoptosis in Parkinson's disease: signals for neuronal degradation." Ann Neurol **53 Suppl 3**: S61-70; discussion S70-62.

Thomas, K. J., M. K. McCoy, J. Blackinton, A. Beilina, M. van der Brug, A. Sandebring, D. Miller, D. Maric, A. Cedazo-Minguez and M. R. Cookson (2011). "DJ-1 acts in parallel to the PINK1/parkin pathway to control mitochondrial function and autophagy." Hum Mol Genet **20**(1): 40-50.

Thyagarajan, D., S. Bressman, C. Bruno, S. Przedborski, S. Shanske, T. Lynch, S. Fahn and S. DiMauro (2000). "A novel mitochondrial 12SrRNA point mutation in parkinsonism, deafness, and neuropathy." Ann Neurol **48**(5): 730-736.

Tompa, P. (2005). "The interplay between structure and function in intrinsically unstructured proteins." FEBS Lett **579**(15): 3346-3354.

Treiman, M., C. Caspersen and S. B. Christensen (1998). "A tool coming of age: thapsigargin as an inhibitor of sarco-endoplasmic reticulum Ca(2+)-ATPases." Trends Pharmacol Sci **19**(4): 131-135.

Tsai, P. I., M. M. Course, J. R. Lovas, C. H. Hsieh, M. Babic, K. E. Zinsmaier and X. Wang (2014). "PINK1-mediated phosphorylation of Miro inhibits synaptic growth and protects dopaminergic neurons in Drosophila." Sci Rep **4**: 6962.

Unal Gulsuner, H., S. Gulsuner, F. N. Mercan, O. E. Onat, T. Walsh, H. Shahin, M. K. Lee, O. Dogu, T. Kansu, H. Topaloglu, B. Elibol, C. Akbostanci, M. C. King, T. Ozcelik and A. B. Tekinay (2014). "Mitochondrial serine protease HTRA2 p.G399S in a kindred with essential tremor and Parkinson disease." Proc Natl Acad Sci U S A **111**(51): 18285-18290.

Valdez, L. B., T. Zaobornyj and A. Boveris (2006). "Mitochondrial metabolic states and membrane potential modulate mtNOS activity." Biochim Biophys Acta **1757**(3): 166-172.

Valente, E. M., P. M. Abou-Sleiman, V. Caputo, M. M. Muqit, K. Harvey, S. Gispert, Z. Ali, D. Del Turco, A. R. Bentivoglio, D. G. Healy, A. Albanese, R. Nussbaum, R. Gonzalez-Maldonado, T. Deller, S. Salvi, P. Cortelli, W. P. Gilks, D. S. Latchman, R. J. Harvey, B. Dallapiccola, G. Auburger and N. W. Wood (2004). "Hereditary early-onset Parkinson's disease caused by mutations in PINK1." Science **304**(5674): 1158-1160.

Valente, E. M., S. Salvi, T. Ialongo, R. Marongiu, A. E. Elia, V. Caputo, L. Romito, A. Albanese, B. Dallapiccola and A. R. Bentivoglio (2004). "PINK1 mutations are associated with sporadic early-onset parkinsonism." Ann Neurol **56**(3): 336-341.

Valko, M., D. Leibfritz, J. Moncol, M. T. Cronin, M. Mazur and J. Telser (2007). "Free radicals and antioxidants in normal physiological functions and human disease." Int J Biochem Cell Biol **39**(1): 44-84.

van Duijn, C. M., M. C. Dekker, V. Bonifati, R. J. Galjaard, J. J. Houwing-Duistermaat, P. J. Snijders, L. Testers, G. J. Breedveld, M. Horstink, L. A. Sandkuijl, J. C. van Swieten, B. A. Oostra and P. Heutink (2001). "Park7, a novel locus for autosomal recessive early-onset parkinsonism, on chromosome 1p36." Am J Hum Genet **69**(3): 629-634.

Van Houten, B., V. Woshner and J. H. Santos (2006). "Role of mitochondrial DNA in toxic responses to oxidative stress." DNA Repair (Amst) **5**(2): 145-152.

van Loo, G., M. van Gurp, B. Depuydt, S. M. Srinivasula, I. Rodriguez, E. S. Alnemri, K. Gevaert, J. Vandekerckhove, W. Declercq and P. Vandenabeele (2002). "The serine protease Omi/HtrA2 is released from mitochondria during apoptosis. Omi interacts with caspase-inhibitor XIAP and induces enhanced caspase activity." Cell Death Differ **9**(1): 20-26.

Van Remmen, H., Y. Ikeno, M. Hamilton, M. Pahlavani, N. Wolf, S. R. Thorpe, N. L. Alderson, J. W. Baynes, C. J. Epstein, T. T. Huang, J. Nelson, R. Strong and A. Richardson (2003). "Life-long reduction in MnSOD activity results in increased DNA damage and higher incidence of cancer but does not accelerate aging." Physiol Genomics **16**(1): 29-37.

van Spronsen, M., M. Mikhaylova, J. Lipka, M. A. Schlager, D. J. van den Heuvel, M. Kuijpers, P. S. Wulf, N. Keijzer, J. Demmers, L. C. Kapitein, D. Jaarsma, H. C. Gerritsen, A. Akhmanova and C. C. Hoogenraad (2013). "TRAK/Milton motor-adaptor proteins steer mitochondrial trafficking to axons and dendrites." Neuron **77**(3): 485-502.

Vander Heiden, M. G., N. S. Chandel, E. K. Williamson, P. T. Schumacker and C. B. Thompson (1997). "Bcl-xL regulates the membrane potential and volume homeostasis of mitochondria." Cell **91**(5): 627-637.

Verburg, J. and P. J. Hollenbeck (2008). "Mitochondrial membrane potential in axons increases with local nerve growth factor or semaphorin signaling." J Neurosci **28**(33): 8306-8315.

Veyrat-Durebex, C., P. Corcia, E. Piver, D. Devos, A. Dangoumau, F. Gouel, P. Vourc'h, P. Emond, F. Laumonnier, L. Nadal-Desbarats, P. H. Gordon, C. R. Andres and H. Blasco (2015). "Disruption of TCA Cycle and Glutamate Metabolism Identified by Metabolomics in an In Vitro Model of Amyotrophic Lateral Sclerosis." Mol Neurobiol.

Vlahou, G., M. Elias, J. C. von Kleist-Retzow, R. J. Wiesner and F. Rivero (2011). "The Ras related GTPase Miro is not required for mitochondrial transport in Dictyostelium discoideum." Eur J Cell Biol **90**(4): 342-355.

Voets, A. M., M. Huigsloot, P. J. Lindsey, A. M. Leenders, W. J. Koopman, P. H. Willems, R. J. Rodenburg, J. A. Smeitink and H. J. Smeets (2012). "Transcriptional changes in OXPHOS complex I deficiency are related to anti-oxidant pathways and could explain the disturbed calcium homeostasis." Biochim Biophys Acta **1822**(7): 1161-1168.

von Campenhausen, S., B. Bornschein, R. Wick, K. Botzel, C. Sampaio, W. Poewe, W. Oertel, U. Siebert, K. Berger and R. Dodel (2005). "Prevalence and incidence of Parkinson's disease in Europe." Eur Neuropsychopharmacol **15**(4): 473-490.

Wan, B., K. F. LaNoue, J. Y. Cheung and R. C. Scaduto, Jr. (1989). "Regulation of citric acid cycle by calcium." J Biol Chem **264**(23): 13430-13439.

Wang, X. and T. L. Schwarz (2009). "The mechanism of Ca2+ -dependent regulation of kinesin-mediated mitochondrial motility." Cell **136**(1): 163-174.

Wang, X., D. Winter, G. Ashrafi, J. Schlehe, Y. L. Wong, D. Selkoe, S. Rice, J. Steen, M. J. LaVoie and T. L. Schwarz (2011). "PINK1 and Parkin target Miro for phosphorylation and degradation to arrest mitochondrial motility." Cell **147**(4): 893-906.

Wang, X., M. H. Yan, H. Fujioka, J. Liu, A. Wilson-Delfosse, S. G. Chen, G. Perry, G. Casadesus and X. Zhu (2012). "LRRK2 regulates mitochondrial dynamics and function through direct interaction with DLP1." Hum Mol Genet **21**(9): 1931-1944.

Wattenberg, B. and T. Lithgow (2001). "Targeting of C-terminal (tail)-anchored proteins: understanding how cytoplasmic activities are anchored to intracellular membranes." Traffic **2**(1): 66-71.

Weihofen, A., K. J. Thomas, B. L. Ostaszewski, M. R. Cookson and D. J. Selkoe (2009). "Pink1 forms a multiprotein complex with Miro and Milton, linking Pink1 function to mitochondrial trafficking." Biochemistry **48**(9): 2045-2052.

West, A. B., D. Maraganore, J. Crook, T. Lesnick, P. J. Lockhart, K. M. Wilkes, G. Kapatos, J. A. Hardy and M. J. Farrer (2002). "Functional association of the parkin gene promoter with idiopathic Parkinson's disease." Hum Mol Genet **11**(22): 2787-2792.

West, A. B., D. J. Moore, S. Biskup, A. Bugayenko, W. W. Smith, C. A. Ross, V. L. Dawson and T. M. Dawson (2005). "Parkinson's disease-associated mutations in leucine-rich repeat kinase 2 augment kinase activity." Proc Natl Acad Sci U S A **102**(46): 16842-16847.

West, A. B., D. J. Moore, C. Choi, S. A. Andrabi, X. Li, D. Dikeman, S. Biskup, Z. Zhang, K. L. Lim, V. L. Dawson and T. M. Dawson (2007). "Parkinson's disease-associated mutations in LRRK2 link enhanced GTP-binding and kinase activities to neuronal toxicity." Hum Mol Genet **16**(2): 223-232.

Williams, M. D., H. Van Remmen, C. C. Conrad, T. T. Huang, C. J. Epstein and A. Richardson (1998). "Increased oxidative damage is correlated to altered mitochondrial function in heterozygous manganese superoxide dismutase knockout mice." J Biol Chem **273**(43): 28510-28515.

Wilson, M. A., J. L. Collins, Y. Hod, D. Ringe and G. A. Petsko (2003). "The 1.1-A resolution crystal structure of DJ-1, the protein mutated in autosomal recessive early onset Parkinson's disease." Proc Natl Acad Sci U S A **100**(16): 9256-9261.

Winterbourn, C. C. (2014). "The challenges of using fluorescent probes to detect and quantify specific reactive oxygen species in living cells." Biochim Biophys Acta **1840**(2): 730-738.

Wispe, J. R., J. C. Clark, M. S. Burhans, K. E. Kropp, T. R. Korfhagen and J. A. Whitsett (1989). "Synthesis and processing of the precursor for human mangano-superoxide dismutase." Biochim Biophys Acta **994**(1): 30-36.

Wood-Kaczmar, A., S. Gandhi, Z. Yao, A. Y. Abramov, E. A. Miljan, G. Keen, L. Stanyer, I. Hargreaves, K. Klupsch, E. Deas, J. Downward, L. Mansfield, P. Jat, J. Taylor, S. Heales, M. R. Duchen, D. Latchman, S. J. Tabrizi and N. W. Wood (2008). "PINK1 is necessary for long term survival and mitochondrial function in human dopaminergic neurons." PLoS One **3**(6): e2455.

Woolford, C. A., L. B. Daniels, F. J. Park, E. W. Jones, J. N. Van Arsdell and M. A. Innis (1986). "The PEP4 gene encodes an aspartyl protease implicated in the posttranslational regulation of Saccharomyces cerevisiae vacuolar hydrolases." Mol Cell Biol **6**(7): 2500-2510.

Wu, S., M. J. Sampson, W. K. Decker and W. J. Craigen (1999). "Each mammalian mitochondrial outer membrane porin protein is dispensable: effects on cellular respiration." Biochim Biophys Acta **1452**(1): 68-78.

Xu, J., N. Zhong, H. Wang, J. E. Elias, C. Y. Kim, I. Woldman, C. Pifl, S. P. Gygi, C. Geula and B. A. Yankner (2005). "The Parkinson's disease-associated DJ-1 protein is a

transcriptional co-activator that protects against neuronal apoptosis." Hum Mol Genet **14**(9): 1231-1241.

Xu, X., W. Decker, M. J. Sampson, W. J. Craigen and M. Colombini (1999). "Mouse VDAC isoforms expressed in yeast: channel properties and their roles in mitochondrial outer membrane permeability." J Membr Biol **170**(2): 89-102.

Yadava, N. and D. G. Nicholls (2007). "Spare respiratory capacity rather than oxidative stress regulates glutamate excitotoxicity after partial respiratory inhibition of mitochondrial complex I with rotenone." J Neurosci **27**(27): 7310-7317.

Yamamoto, A., Y. Tagawa, T. Yoshimori, Y. Moriyama, R. Masaki and Y. Tashiro (1998). "Bafilomycin A1 prevents maturation of autophagic vacuoles by inhibiting fusion between autophagosomes and lysosomes in rat hepatoma cell line, H-4-II-E cells." Cell Struct Funct **23**(1): 33-42.

Yamaoka, S. and C. J. Leaver (2008). "EMB2473/MIRO1, an Arabidopsis Miro GTPase, is required for embryogenesis and influences mitochondrial morphology in pollen." Plant Cell **20**(3): 589-601.

Yokota, T., K. Sugawara, K. Ito, R. Takahashi, H. Ariga and H. Mizusawa (2003). "Down regulation of DJ-1 enhances cell death by oxidative stress, ER stress, and proteasome inhibition." Biochem Biophys Res Commun **312**(4): 1342-1348.

Zamzami, N., S. A. Susin, P. Marchetti, T. Hirsch, I. Gomez-Monterrey, M. Castedo and G. Kroemer (1996). "Mitochondrial control of nuclear apoptosis." J Exp Med **183**(4): 1533-1544.

Zeevalk, G. D., R. Razmpour and L. P. Bernard (2008). "Glutathione and Parkinson's disease: is this the elephant in the room?" Biomed Pharmacother **62**(4): 236-249.

Zhang, L., M. Shimoji, B. Thomas, D. J. Moore, S. W. Yu, N. I. Marupudi, R. Torp, I. A. Torgner, O. P. Ottersen, T. M. Dawson and V. L. Dawson (2005). "Mitochondrial localization of the Parkinson's disease related protein DJ-1: implications for pathogenesis." Hum Mol Genet **14**(14): 2063-2073.

Zhang, Y. (2008). "I-TASSER server for protein 3D structure prediction." BMC Bioinformatics **9**: 40.

Zheng, B., Z. Liao, J. J. Locascio, K. A. Lesniak, S. S. Roderick, M. L. Watt, A. C. Eklund, Y. Zhang-James, P. D. Kim, M. A. Hauser, E. Grunblatt, L. B. Moran, S. A. Mandel, P. Riederer, R. M. Miller, H. J. Federoff, U. Wullner, S. Papapetropoulos, M. B. Youdim, I. Cantuti-Castelvetri, A. B. Young, J. M. Vance, R. L. Davis, J. C. Hedreen, C. H. Adler, T. G. Beach, M. B. Graeber, F. A. Middleton, J. C. Rochet, C. R. Scherzer and P. D. G. E. C. Global (2010). "PGC-1alpha, a potential therapeutic target for early intervention in Parkinson's disease." Sci Transl Med **2**(52): 52ra73.

Zhong, N. and J. Xu (2008). "Synergistic activation of the human MnSOD promoter by DJ-1 and PGC-1alpha: regulation by SUMOylation and oxidation." Hum Mol Genet **17**(21): 3357-3367.

Zielonka, J. and B. Kalyanaraman (2010). "Hydroethidine- and MitoSOX-derived red fluorescence is not a reliable indicator of intracellular superoxide formation: another inconvenient truth." Free Radic Biol Med **48**(8): 983-1001.

Zoratti, M. and I. Szabo (1995). "The mitochondrial permeability transition." Biochim Biophys Acta **1241**(2): 139-176.

Zuchner, S., I. V. Mersiyanova, M. Muglia, N. Bissar-Tadmouri, J. Rochelle, E. L. Dadali, M. Zappia, E. Nelis, A. Patitucci, J. Senderek, Y. Parman, O. Evgrafov, P. D. Jonghe, Y.

Takahashi, S. Tsuji, M. A. Pericak-Vance, A. Quattrone, E. Battaloglu, A. V. Polyakov, V. Timmerman, J. M. Schroder and J. M. Vance (2004). "Mutations in the mitochondrial GTPase mitofusin 2 cause Charcot-Marie-Tooth neuropathy type 2A." Nat Genet **36**(5): 449-451.

6 Appendix

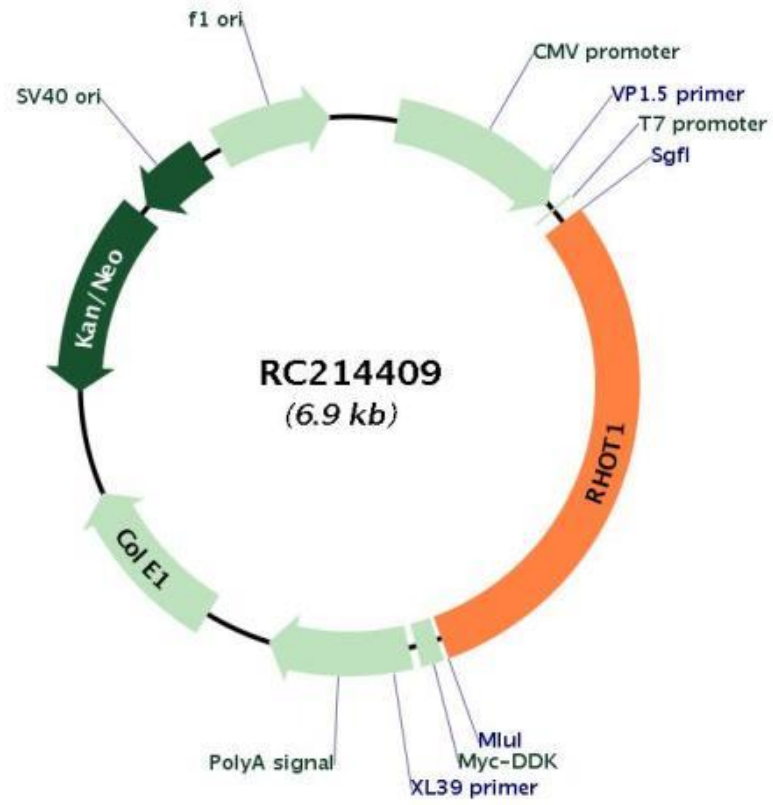

Figure 51: Vector map of pCMV6-Entry

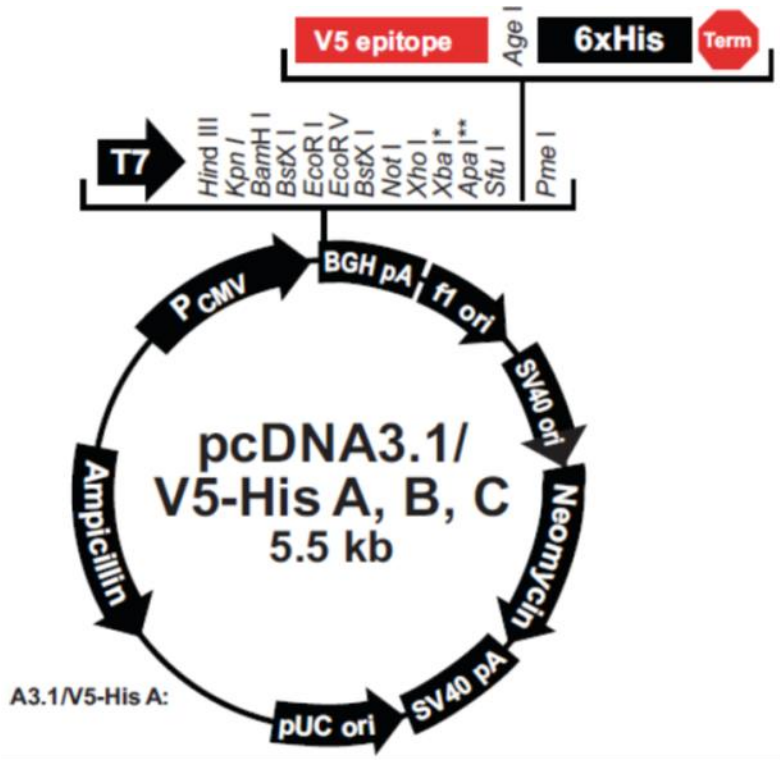

Figure 52: Vector map of pcDNA3.1/V5-His A

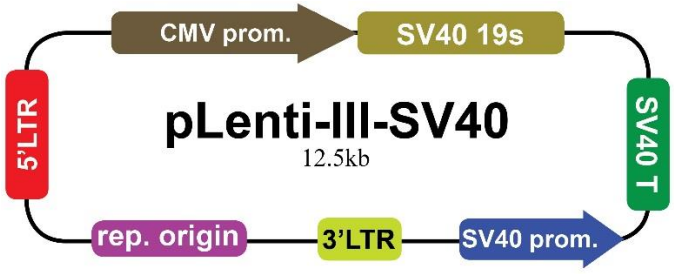

Figure 53: Vector map of pLenti-III-SV40

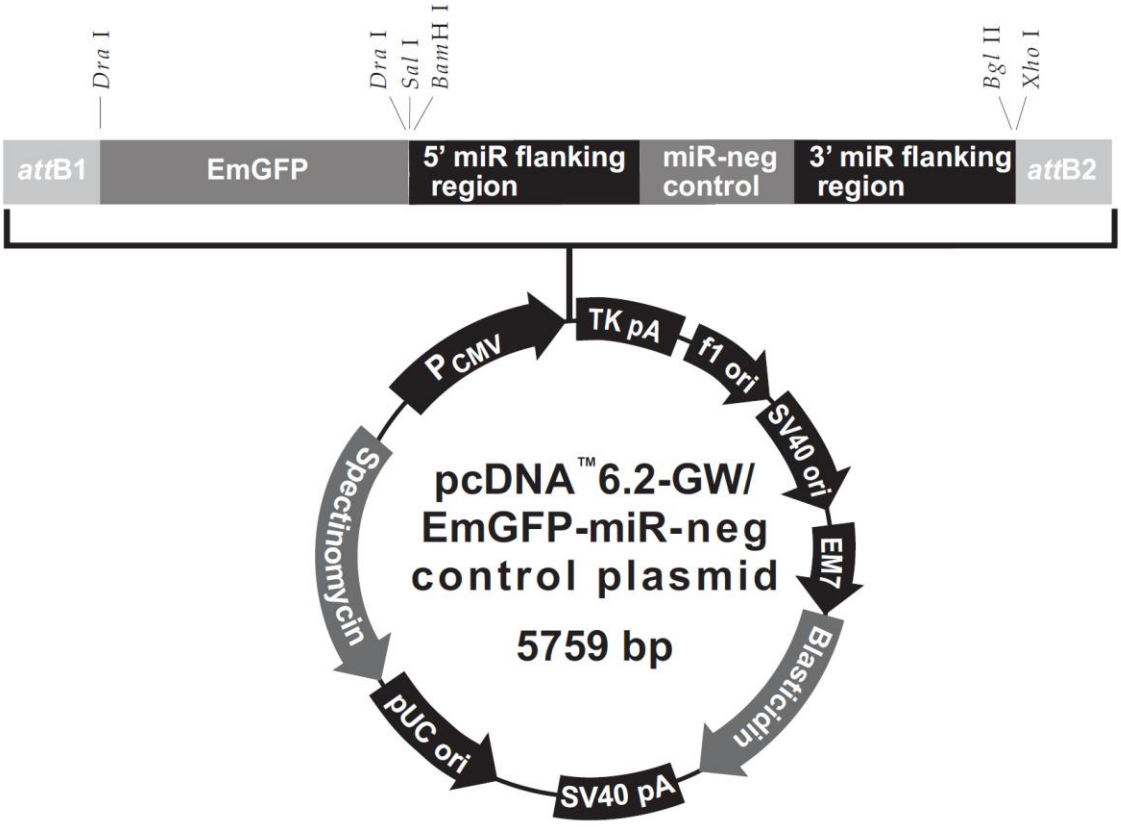

Figure 54: Vector map of pcDNA6.2-GW/EmGFP-miR-neg control plasmid

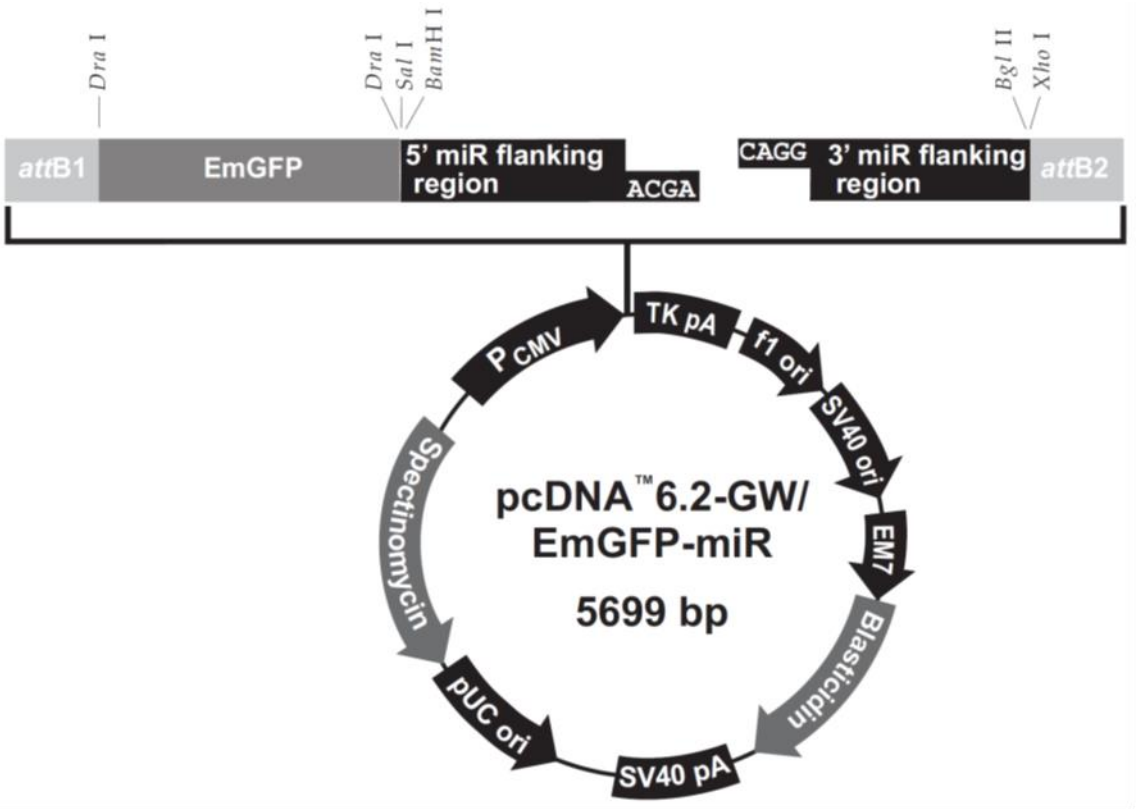

Figure 55: Vector map of pcDNA6.2-GW/EmGFP-miR

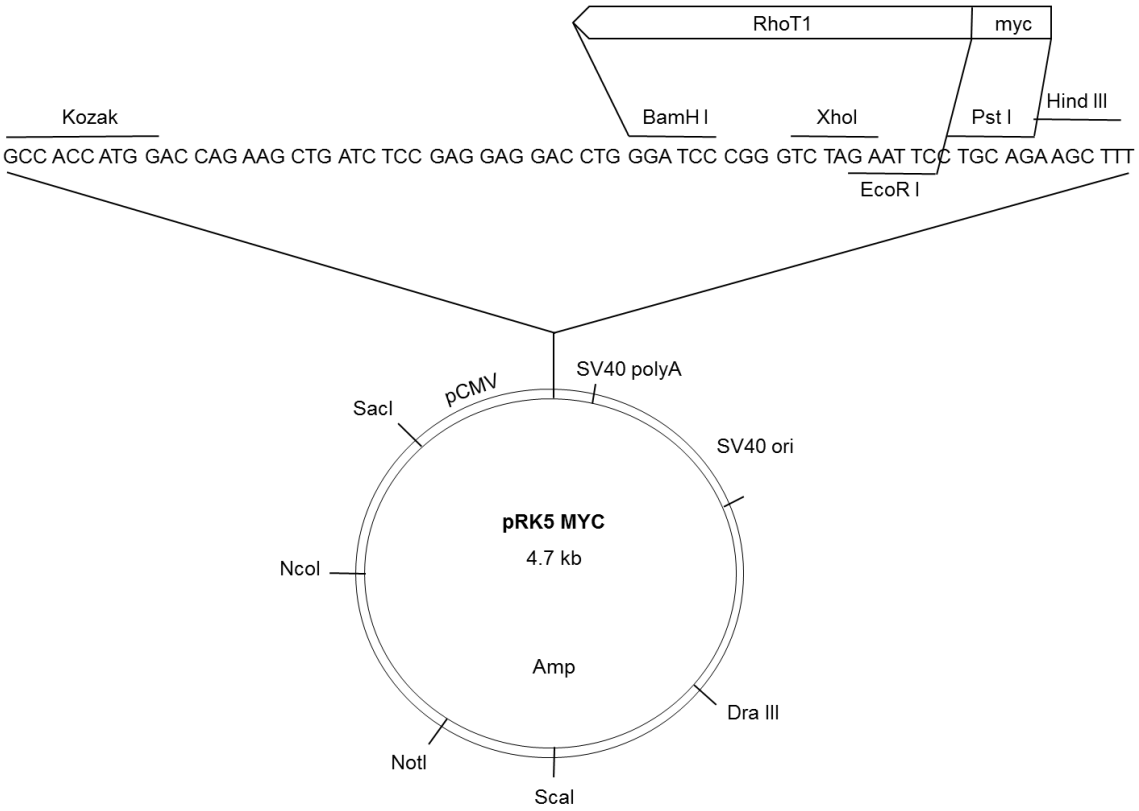

Figure 56: Vector map of pRK-5 myc/ RhoT1

Constructed by: D. Dieckmann, MRC-LMCB, UCL, UK

kind gift by P. Aspenström, karolinska-Institute, Upsalla, Schweden